CR 114464
AVAILABLE TO
THE PUBLIC

FINAL REPORT

TASK II

LARGE SCALE WIND TUNNEL INVESTIGATION OF A FOLDING TILT ROTOR

(NASA CONTRACT NAS 2-5461)

(NASA-CR-114464) LARGE SCALE WIND TUNNEL INVESTIGATION OF A FOLDING TILT ROTOR Final Report (Bell Helicopter Co.) May 1972 195 p

N72-30013

CSCL 01B

Unclas

G3/C2 40030

REPORT D272-099-002



BELL HELICOPTER COMPANY
POST OFFICE BOX 482 · FORT WORTH, TEXAS 76101 A textron COMPANY

CR 114464
AVAILABLE TO
THE PUBLIC

FINAL REPORT

TASK II

LARGE SCALE WIND TUNNEL INVESTIGATION OF A FOLDING TILT ROTOR

(NASA CONTRACT NAS 2-5461)

REPORT D272-099-002

MAY 1972

BELL HELICOPTER COMPANY
POST OFFICE BOX 482 · FORT WORTH TEXAS 76101 A textron COMPANY

BELL HELICOPTER COMPANY
POST OFFICE BOX 482 • FORT WORTH, TEXAS

PROPRIETARY RIGHTS NOTICE

This data is furnished with unlimited data rights to the U.S. Government in accordance with the provisions of Contract No. NAS2-5461.

D272-099-002

7851 88256 REV 1070

TABLE OF CONTENTS

		Page
I.	SUMMARY	I-1
II.	INTRODUCTION	II-1
	A. THE CONCEPT	II-1
	B. BACKGROUND	II-2
	C. TECHNICAL RISK AREAS	II-3
	D. OBJECTIVE OF THE LARGE-SCALE WIND-TUNNEL INVESTIGATION	II-4
III.	THE FOLDING PROPROTOR CONVERSION SEQUENCE	III-1
	A. THE SEQUENCE STEPS	III-1
	B. THE AIRCRAFT CONVERSION	III-1
	C. INVESTIGATIONS OF THE CONVERSION SEQUENCE	III-2
	D. THE RATIONALE OF THE CONVERSION SEQUENCE	III-2
IV.	HELICOPTER TO AIRPLANE MODE CONVERSION SEQUENCE	IV-1
	A. GENERAL	IV-1
	B. HOVER FLIGHT MODE (α_{MAST} = +75 DEGREES)	IV-1
	C. HELICOPTER CONVERSION FLIGHT MODE (α_{MAST} = +60, +30, AND +15 DEGREES)	IV-1
	D. AIRPLANE FLIGHT MODE (α_{MAST} = 0 DEGREES)	IV-1
V.	DESCRIPTION OF THE FOLDING PROPROTOR TEST HARDWARE	V-1
	A. FOLDING PROPROTOR	V-1
	1. Basic Design	V-1
	2. Blade Mass Balance	V-3
	3. Full Pitch Range	V-3
	4. Fold Mechanism	V-5
	5. Fold Link Safety Lock	V-6
	6. Fold Interconnect System	V-6
	7. Pitch Change Lockout	V-6
	8. Rotor Index and Lock	v-6
	9. Hub Flapping Lockout	V-7

Use or disclosure of data on this page is subject to the restriction on the title page.

TABLE OF CONTENTS - Continued

	Page
B. CONTROLS	V-7
1. Collective	V-7
2. Cyclic	V-8
3. Hub Spring	V-8
4. Folding Sequence Control System	V-8
C. HYDRAULIC POWER SYSTEM	V-9
D. WING AND POD DYNAMIC TEST STAND	V-9
1. Wing Description	V-9
2. Test Stand Dynamics	V-10
3. Rotor Pod	V-10
4. Fold Stow Lock	V-14
5. Rotor and Spinner Fairing	V-14
E. INSTRUMENTATION	V-15
VI. CONVERSION SEQUENCE DYNAMICS--TEST DATA AND CORRELATION WITH THEORY	VI-1
A. TEST PROGRAM	VI-1
B. DESCRIPTION OF THEORY USED TO PREDICT DYNAMIC CHARACTERISTICS	VI-1
C. DYNAMIC RESPONSE CHARACTERISTICS DURING THE FEATHER-FOLD SEQUENCE	VI-4
D. DYNAMIC STABILITY CHARACTERISTICS	VI-5
1. Test Procedure	VI-5
2. Measured Stability Characteristics	VI-6
3. Correlation of Theory with Measured Characteristics	VI-7
E. PROPROTOR AND CONTROL LOAD CHARACTERISTICS	VI-7
1. Test Procedure	
2. Measured Blade and Control Loads	VI-8
3. Correlation of Theory with Measured Loads	VI-9

TABLE OF CONTENTS - Continued

		Page
F.	WING LOAD AND PYLON VIBRATION CHARACTERISTICS	VI-9
	1. Test Procedures	VI-9
	2. Measured Wing Loads and Pylon Vibration	VI-10
	3. Correlation of Theory with Measured	VI-10
G.	COMPARISON WITH RESULTS OF SMALL-SCALE MODEL TEST	VI-11
H.	CALCULATED TIME HISTORY OF FEATHER-FOLD SEQUENCE	VI-11
I.	ACTUAL FEATHER-FOLD SEQUENCE TIME HISTORY AT 175 KNOTS	VI-11
J.	CONCLUSIONS FROM THE DYNAMIC TEST PROGRAM	VI-11
	1. Stability	VI-11
	2. Loads	VI-14
	3. Dynamic Response	VI-14
	4. Optimum Feather/Unfeather Time	VI-15
	5. Computer Program Correlation	VI-15
VII.	FOLDING PROPROTOR CONVERSION CRITERIA CONSIDERATIONS	VII-1
	A. SEQUENCE PROBLEMS INVESTIGATED	VII-1
	1. Rotor Speed Programming	VII-1
	2. Mast Index and Lock	VII-1
	B. RESULTING CRITERIA FOR AIRCRAFT DESIGN	VII-2
	1. Rotor Speed Control	VII-2
	2. Mast Index and Lock	VII-2
	3. Rotor Stop/Start Rate	VII-2
	4. Hub Flapping Lockout	VII-3
	5. Angle of Attack	VII-4
	6. Airspeed	VII-5
VIII.	RECOMMENDED FUTURE WORK	VIII-1
	A. GENERAL	VIII-1
	B. FULL-SCALE LIFT AND DRAG INVESTIGATION	VIII-1
	C. AUTOMATIC CONVERSION SEQUENCE CONTROL	VIII-1
	D. ROTOR FATIGUE EVALUATION	VIII-1

TABLE OF CONTENTS - Concluded

		Page
	E. DESIGN IMPROVEMENT OF FOLDING PROPROTOR FOR FLIGHT	VIII-2
	1. Elimination of Hydraulics from Rotating System	VIII-2
	2. Full-Collective Pitch Range	VIII-2
	3. Mast Index and Lock	VIII-3
	4. Rotor Weight Reduction	VIII-3
IX	REFERENCES	IX-1
	APPENDIX	1

Use or disclosure of data on this page is subject to the restriction on the title page.

ILLUSTRATIONS

Figure		Page
I-1	Model 627 Folding Proprotor - Blades Unfolded	I-3
I-2	Model 627 Folding Proprotor - Blades Partially Folded	I-4
I-3	Model 627 Folding Proprotor - Blades Fully Folded	I-5
II-1	Folding-Proprotor Sequence of Operation	II-5
II-2	Folding Proprotor V/STOL Aircraft for Military Missions	II-6
II-3	Folding Proprotor Transport Civil Operations	II-7
II-4	Folding Proprotor Feasibility Model Tests	II-8
II-5	Stopping/Starting Transition Model	II-9
II-6	Folding Proprotor Flutter Model	II-9
II-7	Blade Stowing, Force Model	II-10
II-8	Folding Proprotor Force Model	II-10
II-9	Model 266 Dynamic Model with Foldable Blades	II-11
II-10	Model 627 One-Fifth-Scale Folding-Proprotor Model	II-11
II-11	Model D270A One-Tenth-Scale Powered Force Model	II-12
III-1	Conversion Requirements	III-4
III-2	Control Console for Wind-Tunnel Test	III-5
V-1	Schematic of Model 627 Folding Proprotor	V-17
V-2	25-Foot Folding Proprotor Blade Geometry	V-18
V-3	Model 627 Folding Proprotor Collective Mode Natural Frequencies	V-19
V-4	Model 627 Folding Proprotor Cyclic Mode Natural Frequencies	V-20
V-5	Model 627 Folding Proprotor Scissors Mode Natural Frequencies	V-21
V-6	Model 627 Blade Beamwise Limit Load Capability	V-22

Use or disclosure of data on this page is subject to the restriction on the title page.

ILLUSTRATIONS - Continued

Figure		Page
V-7	Model 627 Blade Chordwise Limit Load Capability	V-23
V-8	Model 627 Folding Proprotor Hub, Controls, and Fold Mechanism	V-24
V-9	Folding Moment at Hinge Centerline	V-25
V-10	Unfolding Moment at Hinge Centerline	V-26
V-11	Model 627 Folding Proprotor Mast Index Lock	V-27
V-12	Model 627 Folding Proprotor Collective Actuator and Boost Cylinder	V-28
V-13	Model 627 Folding Proprotor on Whirl Test Stand	V-29
V-14	Model 627 Folding Proprotor Actuation Control Diagram	V-30
V-15	Model 627 Test Hydraulic System, Blade Folding and Pitch Locking	V-31
V-16	Model 627 Test Hydraulic System, Hub Locking, Mast Locking, and Collective Actuator	V-32
V-17	NASTRAN Structural Model of Model 627 Rotor on Dynamic Test Stand	V-33
V-18	Model 627 Folding Proprotor Dynamic Test Stand with Pylon Yaw, Hub Flapping, and Mast Rotation Locked, Blade Root Collective of 126 Degrees	V-34
V-19	Test Aerodynamic Shaker Vane Position	V-35
V-20	Model 627 Folding Proprotor Pod with Fold Stow Slots	V-36
VI-1	Time History of Full-Scale Test Feather-Fold Sequence Dynamics, 150 Knots, $\alpha_{MAST} = 4^{o}$	VI-16
VI-2	Time History of Full-Scale Test Unfold-Unfeather Sequence Dynamics, 150 Knots, $\alpha_{MAST} = 4^{o}$	VI-17
VI-3	Method of Extracting Dynamic Stability Characteristics	VI-18
VI-4	Wing Beam and Chord Bending Modes Frequency and Damping Versus Airspeed Gimbal Locked Out	VI-19
VI-5	Wing Beam Bending Mode Frequency and Damping Versus RPM, Gimbal Locked Out	VI-20
VI-6	Wing Beam and Chord Mode Frequency and Damping Versus Blade Fold Angle, 150 Knots Airspeed	VI-21

ILLUSTRATIONS - Continued

Figure		Page
VI-7	Measured Wing Torsion Frequency and Damping and Measured Blade Beam Bending Frequency Versus Blade Fold Angle, 150 Knots Airspeed	VI-22
VI-8	Wing Beam and Chord Frequency and Damping Versus Airspeed for 30-Degree Blade Fold Angle	VI-23
VI-9	Blade and Control System Oscillatory Loads Versus Angle of Attack, Gimbal Free	VI-24
VI-10	Blade Flapping Versus Angle of Attack, Gimbal Free and Gimbal Locked Out	VI-25
VI-11	Blade Steady-State Oscillatory Loads Versus Angle of Attack, 425 RPM, Gimbal Locked Out	VI-26
VI-12	Blade Steady-State Oscillatory Loads Versus Airspeed, 425 RPM, Gimbal Locked Out and Gimbal Free	VI-27
VI-13	Peak Blade Oscillatory Loads During Proprotor Stop Sequence Versus Angle of Attack, 175 Knots Airspeed-Gimbal Locked Out	VI-28
VI-14	Peak Blade Oscillatory Loads During Proprotor Start Sequence Versus Angle of Attack, 175 Knots Airspeed	VI-29
VI-15	Peak Blade Oscillatory Loads During Stop/Start S quence Versus Airspeed-Gimbal Locked Out	VI-30
VI-16	Steady Blade Bending Moments and Mast Torque Versus Blade Fold Angle, 150 Knots Airspeed	VI-31
VI-17	Pitch Link Axial Load and Pitch Lockout Moment Versus Blade Fold Angle, 150 Knots Airspeed	VI-32
VI-18	Blade Station 52.5 Steady Beam Bending Moment Versus Angle of Attack for Several Blade Fold Angles	VI-33
VI-19	Mast Torque Variation with Mast Angle of Attack for Several Blade Fold Angles, 150 Knots Airspeed	VI-34
VI-20	Pitch Link Axial Load and Pitch Lockout Moment Versus Angle of Attack for 30-Degree Blade Fold Angle 150 Knots Airspeed	VI-35
VI-21	Comparison of Blade Steady Loads Versus Angle of Attack for Three Azimuth Positions	VI-36
VI-22	Steady Blade and Control Loads Versus Airspeed	VI-37

ILLUSTRATIONS - Continued

Figure		Page
VI-23	Pylon Vibration at Blade Passage Frequency Versus Rate of Feathering	VI-38
VI-24	Pylon Vibration at Blade Passage Frequency Versus Rate of Unfeathering	VI-39
VI-25	Pylon Vibration at Blade Passage Frequency Versus Mast Angle of Attack During Feathering	VI-40
VI-26	Pylon Vibration at Blade Passage Frequency Versus Mast Angle of Attack During Unfeathering	VI-41
VI-27	Pylon Vibration at Blade Passage Frequency Versus Airspeed During Feathering/Unfeathering	VI-42
VI-28	Wing Root Loads Versus Rate of Feathering	VI-43
VI-29	Wing Root Loads Versus Rate of Unfeathering	VI-44
VI-30	Wing Root Loads Versus Mast Angle of Attack During Feathering	VI-45
VI-31	Wing Root Loads Versus Mast Angle of Attack During Unfeathering	VI-46
VI-32	Wing Root Steady Bending Moment Versus Blade Fold Angle	VI-47
VI-33	Wing Root Steady Bending Moment Versus Mast Angle of Attack	VI-48
VI-34	Wing Root Steady Bending Moment Versus Airspeed	VI-49
VI-35	Comparison of Small-Scale and Full-Scale Measured Peak Blade Station 52.5 Oscillatory Loads During Feathering	VI-50
VI-36	Comparison of Small-Scale and Full-Scale Measured Pylon Acceleration During Blade Feathering	VI-51
VI-37	Time History of Dynamic Response During Feather-Fold Sequence at 175 Knots Full-Scale and Six Degrees Wing Angle of Attack, One-Fifth-Scale Model	VI-52
VI-38	Calculated Time History of Feather-Fold Sequence, 150 Knots Airspeed, Four Degrees Mast Angle of Attack	VI-53
VI-39	Calculated Time History of Unfeather Sequence, 150 Knots Airspeed, Four Degrees Mast Angle of Attack	VI-54

ILLUSTRATIONS - Continued

Figure		Page
VI-40	Hub Flapping Lockout Time History, 175 Knots, Mast Angle of Attack Minus One Degree (Run 16.7)	VI-53
VI-41	Hub Flapping Lockout Time History, 175 Knots, Mast Angle of Attack Two Degrees (Run 16.13)	VI-54
VI-42	Rotor Stopping and Mast Lockout Time History, 175 Knots, Mast Angle of Attack Minus Two Degrees (Run 29.2)	VI-55
VI-43	Rotor Stopping and Mast Lockout Time History, 175 Knots, Mast Angle of Attack Minus Two Degrees (Run 29.2)	VI-56
VI-44	Blade Folding Time History, 175 Knots, Mast Angle of Attack Minus Two Degrees (Run 29.2)	VI-57
VI-45	Blade Folding Time History, 175 Knots, Mast Angle of Attack Minus Two Degrees (Run 29.2)	VI-58
VI-46	Blade Unfolding Time History, 175 Knots, Mast Angle of Attack Minus Two Degrees (Run 29.3)	VI-59
VI-47	Blade Unfolding Time History, 175 Knots, Mast Angle of Attack Minus Two Degrees (Run 29.3)	VI-60
VI-48	Mast Unlock and Rotor Start Time History, 175 Knots, Mast Angle of Attack Minus Two Degrees (Run 29.3)	VI-61
VI-49	Mast Unlock and Rotor Start Time History, 175 Knots, Mast Angle of Attack Minus Two Degrees (Run 29.3)	VI-62
VI-50	Hub Flapping Unlock Time History, 175 Knots, Mast Angle of Attack Minus One Degree (Run 16.8)	VI-63
VI-51	Model 627 Predicted Proprotor Stability Boundaries with Gimbal Free/Gimbal Locked, Cantilevered Wing	VI-64
VI-52	Model 627 Folding Proprotor V-n Diagram Based on the Allowable Test Load Limit at Blade Fold Hinge	VI-65
VII-1	Mast Index and Lockout Loads	VII-6
VII-2	Rotor RPM Variations Prior to Mast Index	VII-7
VII-3	Rotor RPM Response to Collective Near Feather	VII-7
VII-4	Collective Pitch - Feather Schedule	VII-8
VII-5	Peak Vibration at Pylon Conversion Axis During Blade Feathering, Calculated	VII-9

Use or disclosure of data on this page is subject to the restriction on the title page.

ILLUSTRATIONS - Concluded

Figure		Page
VII-6	Peak Vibration at Crew Station During Blade Feathering, Calculated	VII-9
VII-7	Hub Flapping Lockout Moment	VII-10
VII-8	Flapping Reduction Caused by Hub Lockout Actuation	VII-10
1	Model 627 Folding Proprotor Lift Coefficient Versus Angle of Attack	4
2	Model 627 Folding Proprotor Lift Versus Drag Coefficient at Various Fold Angles	5
3	Model 627 Folding Proprotor Drag Summary	6

Use or disclosure of data on this page is subject to the restriction on the title page.

LIST OF TABLES

Table		Page
III-I	Model 627 Folding Proprotor Sequence Control Switch Arrangement	III-3
V-I	Design Parameters for Model 627 Folding Proprotor	V-1
V-II	Model 627 Rotor Stiffness and Mass Properties	V-4
V-III	Dynamic Test Stand Mass Properties	V-11
V-IV	Dynamic Test Stand Stiffness Properties	V-12
V-V	Model 627 Test Stand Wing/Pylon/Rotor Coupled Frequencies at 0-Degree Blade Fold, Blade Root Collective 126 Degrees	V-13
V-VI	Instrumentation for Model 627 Test Program	V-16
VI-I	Run Schedule of Model 627 Wind-Tunnel Test	VI-2
VI-II	Variation of Wing Chord Mode Frequency and Damping with Excitation Amplitude	VI-7

Use or disclosure of data on this page is subject to the restriction on the title page.

NOMENCLATURE

Symbol	Description
BLADE BEAM 33	Blade beamwise moment at 22-percent blade radius
BLADE BEAM 52.5	Blade beamwise moment at 35-percent blade radius
C_L, C_D	Wing lift and drag coefficients
C_l, C_d, C_m	Blade lift, drag, and pitching moment
$\mathcal{L}$	Centerline
IP	Inplane mode
K_H	Hub restraint spring rate
M_β	Blade beam moment at the fold hinge
n	Load factor
OP	Out of plane mode
PL	Pitch-link loads
S_W	Wing reference area
V	Airspeed
WING BEAM MOMENT	Wing beamwise moments at the wing root, 140 inches from the wingtip
WING CHORD MOMENT	Wing chordwise moments at the wing root, 140 inches from the wingtip
WING TORSION MOMENT	Wing torsional moments at the wing root, 140 inches from the wingtip
α	Tunnel yaw angle (angle of attack)
γ	Blade fold angle
ΔT	Time for feathering or unfeathering
ζ	Damping ratio
ρ	Density of air
ψ	Blade azimuth position, zero if blade is straight up in the tunnel (180 degrees from wing)

Use or disclosure of data on this page is subject to the restriction on the title page.

NOMENCLATURE - Concluded

Symbol	Description
Ω	Rotor rpm
Ω_o	Initial rotor rpm for blade feathering
Ω_{END}	Final rotor rpm for blade unfeathering

Use or disclosure of data on this page is subject to the restriction on the title page.

I. SUMMARY

An advanced design 25-foot-diameter folding tilt rotor was tested in the NASA-Ames Large-Scale Wind Tunnel under NASA Contract NAS2-5461 (Reference 1). Bell Helicopter Company designed and manufactured the folding proprotor which is designated the Bell Model 627, modified the existing wing semispan dynamic test stand, and supported the test under the above contract.

Figures I-1, -2, and -3 show the full-scale model installed in the 40- by 80-foot wind tunnel in the unfolded, partially folded, and fully folded positions during the February 1972 unpowered airplane-mode tests. During the tests, the rotor completed over 40 start/stop sequences. After completing the sequences in a stepwise manner, smooth stop/start transitions were made in approximately 2.0 seconds. Wind-tunnel speeds up through 175 knots were used, at which point the rotor mast angle of attack was increased to 4 degrees, corresponding to a maneuver condition of about 1.5g. Blade folding and unfolding was accomplished up to a rotor mast angle of attack of 8 degrees at 175 knots. With the blades in various fold positions, the rotor mast angle of attack was increased to 19 degrees at 125 knots and to 12 degrees at 150 knots.

Complete sequences including stop-index-fold-unfold and start up were completed up through 175 knots. Folding or unfolding each require between 8.5 and 9.0 seconds, and the full sequence is accomplished in about two minutes. During these tests, the model experienced simulated maneuver loads ranging from 0 to +2g. Dynamic characteristics were checked to the maximum wind-tunnel airspeed of 195 knots. The envelope of the wind-tunnel test program, in terms of mast angle of attack, airspeed, and equivalent gust loads is shown in Figure I-4. Also shown in Figure I-4 is the transition mode design maneuver load envelope.

Oscillatory rotor and control loads were about 30 percent less sensitive to angle of attack than predicted during all phases of the stop/fold sequence since the hub flapping lockout was not as stiff as assumed for analytical predictions. During stopping and starting, the rotor blade fold lug experiences about three to five cycles of high oscillatory load. The total damage fraction for the fold joint was 0.00276 which indicates less than one percent of the lug fatigue life was expanded during the wind-tunnel test. The remainder of the blade and hub did not exceed endurance limits at any time during the test.

These Task II tests were preceeded by extensive work accomplished under Task I of the contract, which included preliminary design studies to define the Model 627 folding proprotor, and a minimum-size research aircraft designated the D272A, that could perform flight research investigations. The studies, which are based on the Bell Model 300 proprotor design study and on prior work accomplished under Bell Helicopter Company Independent Research and Development, include aircraft and rotor layouts, weight estimations, performance calculations, and dynamic and stability analyses. This work is reported in Bell Report D272-099-001 (Reference 2) and was submitted in April 1970.

The successful conclusion of the test program presented herein, indicates that the folding tilt rotor is feasible and shows potential operational capability of performing under the range of conditions it would encounter in actual research flight. Future work in preparation for research flight is recommended (see Section VIII). This program also indicates expanded capabilities for the Bell Model 300 proprotor aircraft concept.

REPRODUCIBILITY OF THE ORIGINAL PAGE IS POOR.

Use or disclosure of data on this page is subject to the restriction on the title page.

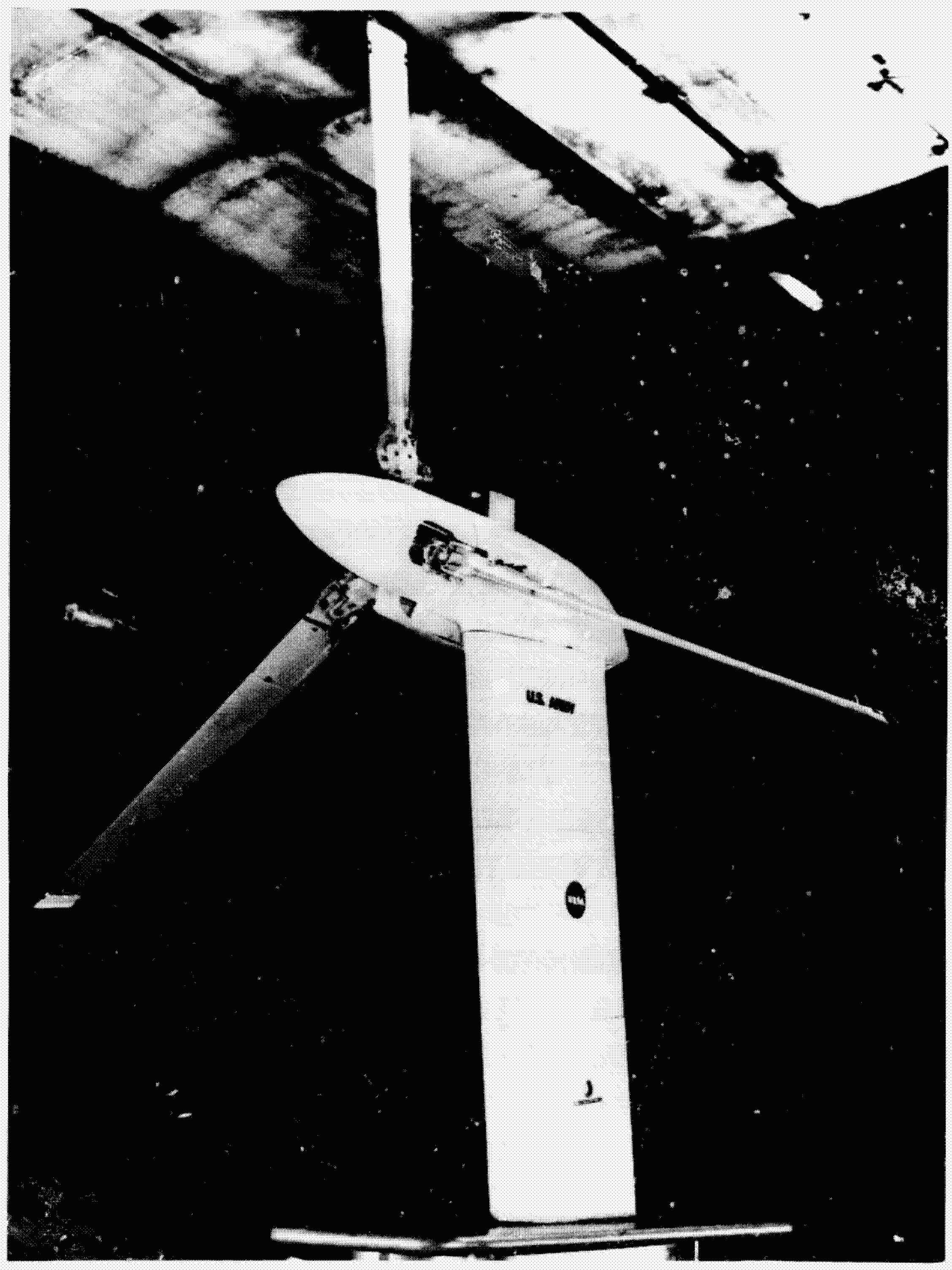


Figure I-1. Model 627 Folding Proprotor - Blades Unfolded.

REPRODUCIBILITY OF THE ORIGINAL PAGE IS POOR.

Use or disclosure of data on this page is subject to the restriction on the title page.

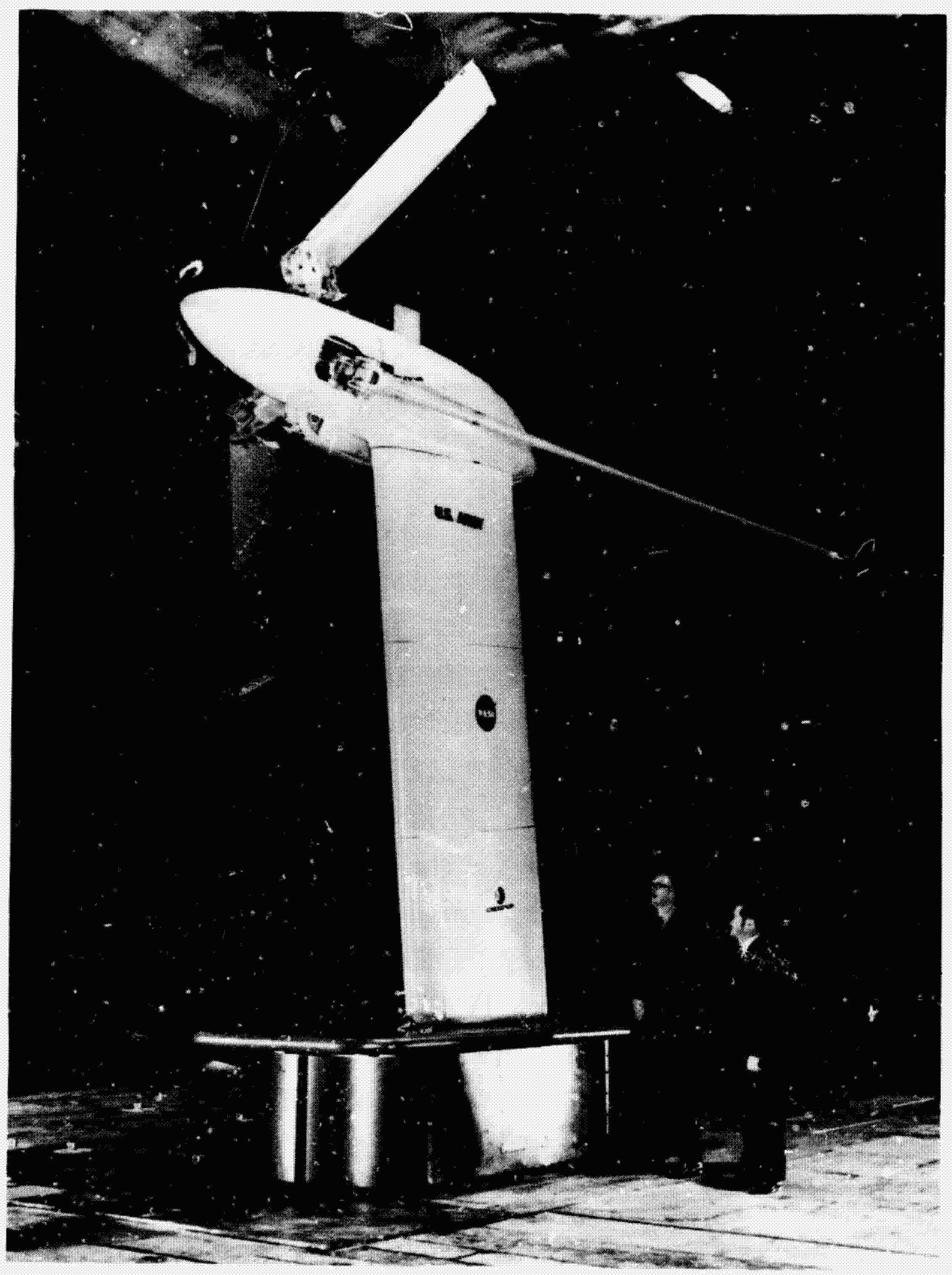


Figure I-2. Model 627 Folding Proprotor - Blades Partially Folded.

REPRODUCIBILITY OF THE ORIGINAL PAGE IS POOR.

Use or disclosure of data on this page is subject to the restriction on the title page

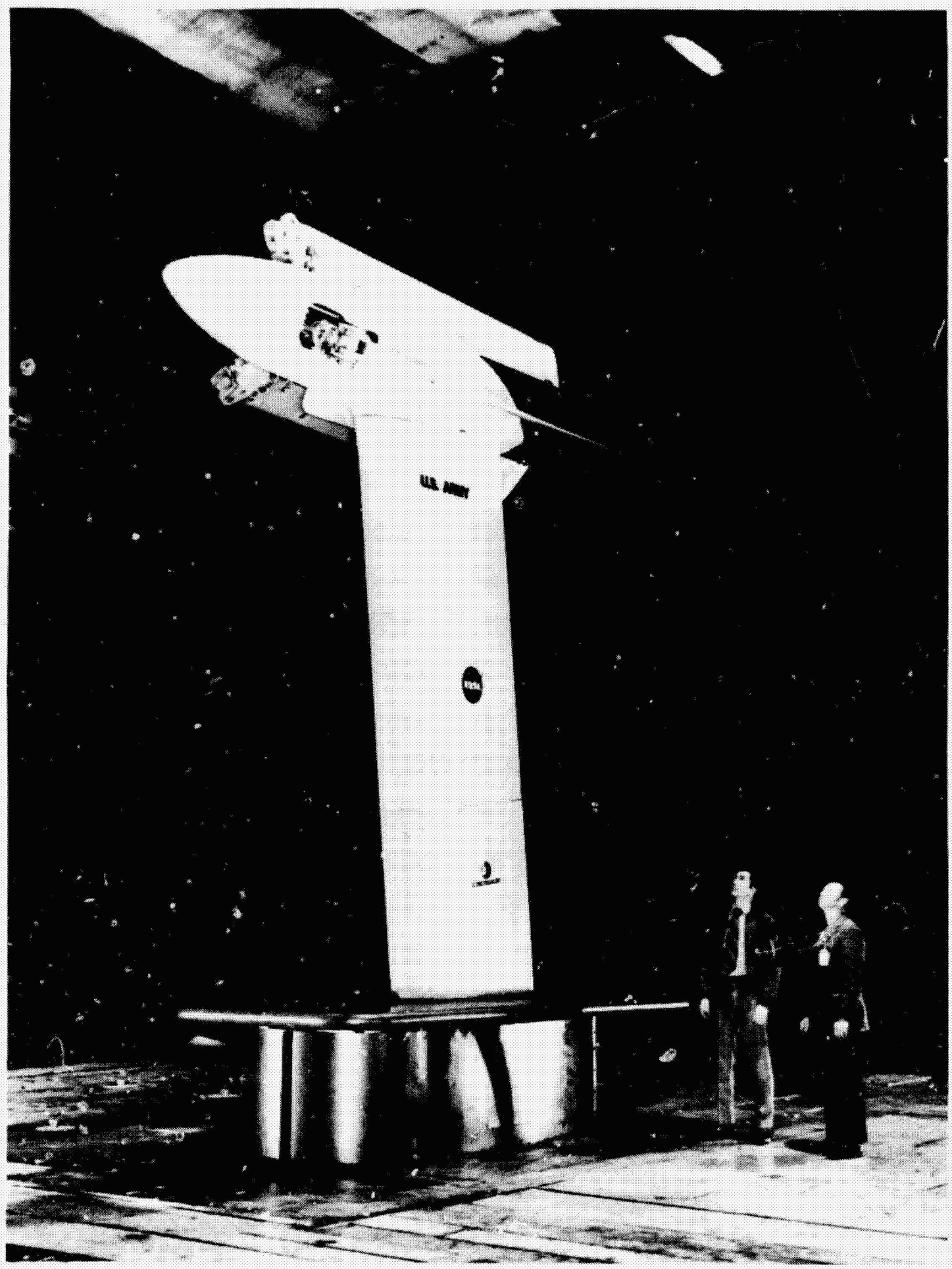


Figure I-3. Model 627 Folding Proprotor - Blades Fully Folded.

Use or disclosure of data on this page is subject to the restriction on the title page.

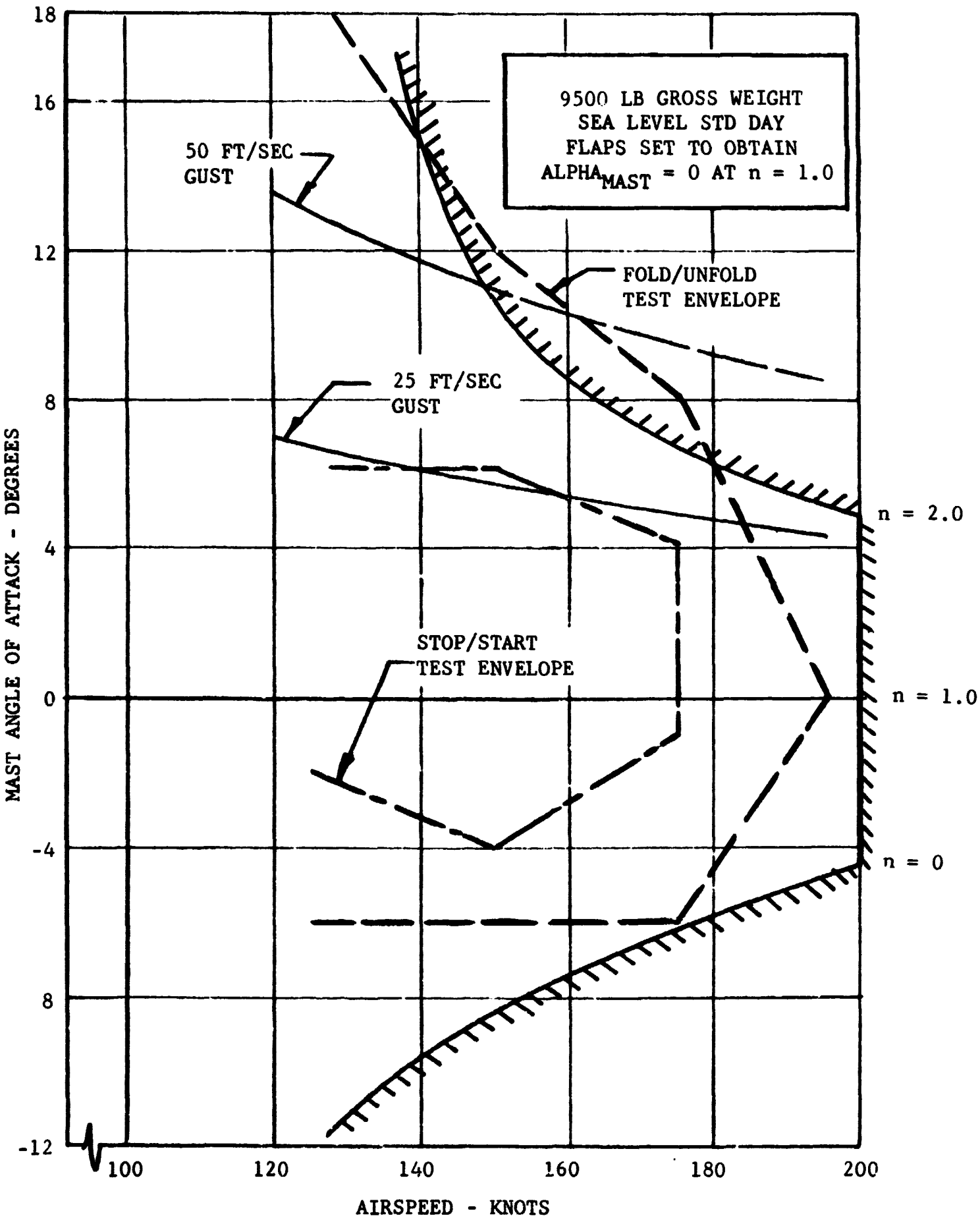


Figure I-4. Model 627 Folding Proprotor Stop/Start, Fold/Unfold To Angle of Attack Test Envelope.

Use or disclosure of data on this page is subject to the restriction on the title page.

II. INTRODUCTION

A. THE CONCEPT

The folding-proprotor VTOL concept combines the low-speed flight characteristics of the helicopter with the high subsonic cruise characteristics of the conventional turbojet airplane. Because of this highly desirable combination of flight characteristics, the folding-proprotor concept has been investigated for both military and commercial applications.

The folding-proprotor VTOL sequence of operation is illustrated in Figure II-1. Takeoff is accomplished in helicopter mode with the nacelles vertical. After takeoff, the folding proprotor aircraft is accelerated to an airspeed at which wing lift can support the aircraft. The nacelles are then mechanically tilted 90 degrees so that the proprotors act as propellers. During vertical and low-speed flight, control of the aircraft is by use of the helicopter collective and cyclic pitch controls. These controls are washed out as the nacelles are tilted forward, and at 90 degrees nacelle tilt, control is by a collective proprotor governor and by conventional fixed-wing controls. The nacelle-tilting process is operationally flexible; it can be accomplished over a wide range of airspeeds and maneuver conditions, and with or without power.

After the nacelles are tilted, flight can be continued with the proprotors acting as propellers or the proprotors can be feathered and folded, and fan engine thrust used for propulsion. The proprotor feathering process is accomplished by transferring power from the proprotors to high bypass ratio fans (compound engines capable of delivering shaft power or fan thrust). The windmilling proprotors are then declutched from the engines and the blades feathered. When stopped, the proprotors are indexed and the blades folded. With the blades folded, the folding proprotor aircraft is operated as a conventional jet aircraft. For landing, the tilt/feather/fold sequence described above is reversed. In an emergency, a conventional airplane landing could be made at an airfield with blades folded.

The folding-proprotor aircraft offers a combination of good hover efficiency, low-downwash characteristics, acceptable noise levels, and high cruise efficiency. Maximum speed capability, which can be specified in the design stage to meet the needs of the mission, is not restricted by constraints associated with proprotors or propellers. Military missions which could benefit from these characteristics include logistics support, airborne assault, armed escort, and search and rescue (see Figure II-2). Of the different approaches to low-disc-loading military VTOL, the folding proprotor is believed to hold considerable promise for transport-type missions where high enroute speed, extended hover time, and/or unrestricted approach are requirements.

The high cruise speed capability of the folding-proprotor VTOL concept increases productivity for logistics support missions, decreases vulnerability during air-assault and aircrew-rescue missions when penetrating a nonpermissive environment, and offers faster response for all missions--frequently the difference between success or failure of a military operation.

Use or disclosure of data on this page is subject to the restriction on the title page.

From the commercial standpoint, if present trends continue, airports will soon be saturated; VTOL aircraft development offers one of the most promising areas in alleviating this situation. In the commercial air transport field, the four U. S. high density air corridors (Northeast, Great Lakes, California, and Chicago) are already at or near saturation. Aircraft of this type offer one promising means of alleviating the problems of air traffic and airport access road congestion. The low noise level and minimal downwash, combined with jet transport cruise performance, will contribute greatly to the acceptance of V/STOL aircraft both by the communities from which they operate and by the passengers. A commercial transport folding-proprotor aircraft operation in a metropolitan area is depicted in Figure II-3.

B. BACKGROUND

An investigation of stoppable-rotor configurations was initiated in 1967 by the U. S. Air Force. Detail information was requested of industry relating to possible low-disc-loading VTOL configurations suitable for high-speed mission requirements. The Bell response considered trail rotor, edgewise stopped rotor, and folding-proprotor configurations. Based on exploratory model tests and analyses, together with future clarification of the Air Force requirements, the folding-proprotor configuration was subsequently recommended as the best technical approach.

The folding-proprotor configuration is a logical development of the proprotor configuration, the feasibility of which was proven during extensive flight and wind-tunnel tests of the Bell XV-3. Additional design studies and small-scale model tests of a transport size proprotor aircraft were performed during the Army Composite Aircraft Program. These studies and NASA/Army full-scale wind-tunnel tests of a 25-foot-diameter flightworthy proprotor, Reference 3, greatly extended the state of the art of proprotor technology, and provided a firm base for technology studies of the folding proprotor.

Research and development work to advance proprotor technology has been in process at Bell over the past quarter of a century, with greatly concentrated effort during the past eight years. Over the past four years, considerable studies and investigations of the folding proprotor have been made at Bell, including force, aeroelastic and flutter models, and full-scale mechanism laboratory tests. The work has included specific projects for Air Force, Army, and NASA, as well as Bell's Independent R&D Program. Some of these early program models are shown in Figures II-4 through II-8.

Results of the tests and studies, reported in References 4 through 11, showed that the folding-proprotor concept was feasible--in that small-scale models of the rotor were successfully tested, stopped, folded, and started in a wind tunnel at high-scale speeds. However, problems and risk areas related to the stop-fold-start sequence were encountered and identified. These included:

- Aeroelastic characteristics of the wing-rotor-pylon (particularly rotor stability and flapping response to external disturbances and aeroelastic behavior during proprotor feather and folding).

Use or disclosure of data on this page is subject to the restriction on the title page.

- Aircraft stability and control characteristics during the stopping and folding of the rotors.

- Aerodynamic interference between the wing and proprotor.

These well-identified dynamic areas were initially investigated in January 1970 with a one-sixth-scale semispan model of the Bell 266 with dynamically-scaled blades and pylon which could be fixed in the various blade fold positions as shown in Figure II-9. Later, wind-tunnel tests were made in February 1971 with a one-fifth-scale aeroelastic semispan model of the 25-foot-diameter Model 627 folding proprotor, Figure II-10.

During design studies, aircraft size selection and sensitivity analyses were made and design criteria were developed for folding proprotor rescue and transport missions as given in References 12 and 13. Following the design studies, a one-tenth-scale powered force model of the operational rescue folding-proprotor aircraft, Figure II-11, was fabricated and checked out at Bell under Air Force contract (Reference 10). Final results of the Air Force studies and model programs are summarized in Reference 14.

C. TECHNICAL RISK AREAS

Proprotor instability, similar in nature to propeller whirl flutter, was encountered during tests of the XV-3 convertiplane. Subsequent investigations have led to an understanding of proprotor instability and have provided design approaches which can provide an adequate margin of stability for tilting-proprotor VTOL aircraft. In the case of the folding proprotor aircraft, the proprotor stability requirements are somewhat relaxed since the blades are folded prior to operation at high speed.

The XV-3 flight tests showed that provision of adequate flapping clearance between the proprotor blades and the wing leading edge in the airplane mode is required for tilting-proprotor aircraft. In general, the required clearance is proportional to the square of the proprotor advance ratio, $V/\Omega R$, and can be reduced if the blade flapping natural frequency is detuned from one per rev by using flapping restraint and/or pitch-flap coupling. For the folding proprotor aircraft, the large advance ratios occurring during blade feathering will cause excessive flapping unless flapping is restrained. However, restrained flapping or the use of very stiff hingeless blades increases one-per-rev loads in the rotor (since flapping acts to alleviate one-per-rev airloads). The use of high flapping restraint only during stopping and starting appeared feasible since only a limited number of cycles is incurred during a stop/start cycle.

Initially it was thought that the dynamic response during proprotor feathering would be negligible. This was based on the assumption that the axial flow condition of the proprotor would not induce significant oscillatory excitation. However, during wind-tunnel tests of small-scale dynamic models, relatively high vibrations of the wing and pylon were recorded. These occurred at the blade passage frequency with peak vibrations occurring when the proprotor angular velocity was one-third of the wing/pylon natural frequency. The source of this vibration was determined to be wing-blade aerodynamic interference, principally the change in the blade airloads as it passed immediately in front

Use or disclosure of data on this page is subject to the restriction on the title page.

of the wing. In the preliminary tests, only very slow rates of feathering were possible because of mechanical limitations. A fast rate of feathering appears to be desirable since it will reduce resonance buildup.

In addition to the above risk areas, it was found that the mechanisms associated with the folding-proprotor concept are a significant design problem from the standpoint of achieving a reliable mechanism at a reasonable weight. These risks were investigated during the subject test program, and are discussed in Section VI of this report.

D. OBJECTIVE OF THE LARGE-SCALE WIND-TUNNEL INVESTIGATION

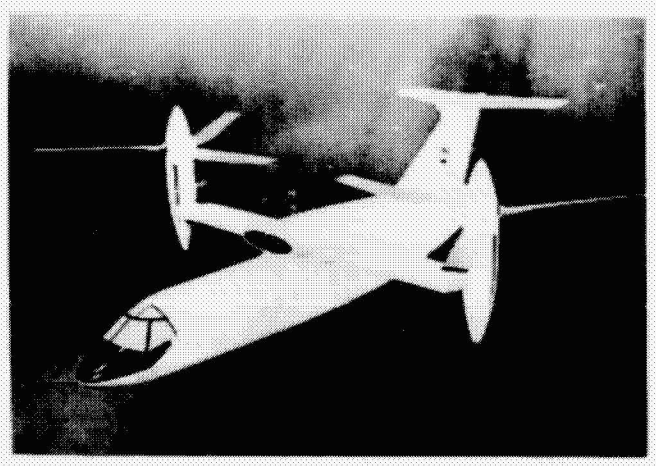
Various small-scale model tests conducted earlier indicated the folding proprotor to be feasible and practical. However, no suitable evidence was available to prove the small-scale data to be directly applicable to full-scale hardware. Also, design solutions to the critical component of folding, indexing, and locking needed to be worked out in full scale to determine functional characteristics, weight penalty, and real-time operating procedures. A full-scale folding-proprotor program became a definite possibility due to the prior Bell IR&D development of the 25-foot-diameter Model 300 proprotor. In May 1969, the NASA-Ames Research Center and the Army Aeronautical Research Laboratory contracted with Bell for design studies of a tilt-rotor proof-of concept aircraft.

In July 1969, Bell Helicopter Company was awarded the contract for the full-scale folding-proprotor design, fabrication, and large-scale wind-tunnel investigation; and for preliminary design studies of minimum-size folding-proprotor research aircraft. This is the subject of this report and of the the Task I design studies report of Reference 2.

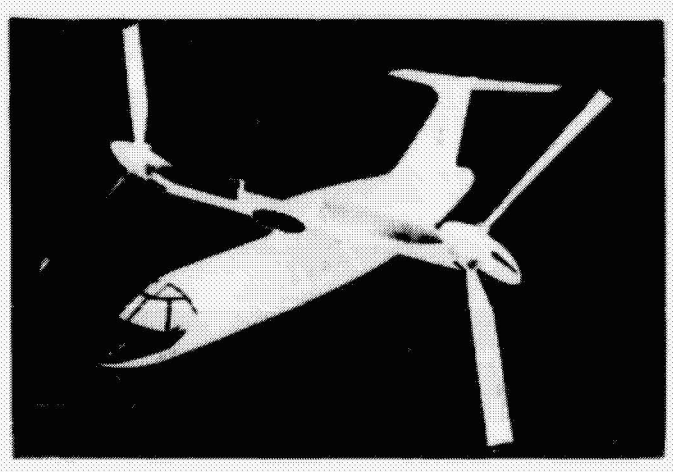
The stated objectives of the program were: "To achieve a practical flight-worthy folding tilt-rotor design with blades that can be stopped, indexed, folded (and unfolded), and stowed into the wingtip pylon so that the final folded blade pylon configuration will have low drag in cruise configuration. The full-scale folding tilt rotor shall be for a medium-size flight research vehicle which can be scaled with certainty to an operational-size aircraft, and the rotor design shall be representative of a flight application for which the stop-fold cycle is activated at airspeeds of 170 to 180 knots in gusty air. Structurally, the tilt rotor shall be designed to operate in propeller mode, and to perform the stop-fold and unfold cycle at maximum wind-tunnel airspeed of 200 knots and to a rotor shaft angle-of-attack objective of 20 degrees."

The intent of these objectives was met in the program as described in detail in Sections V and VI of this report.

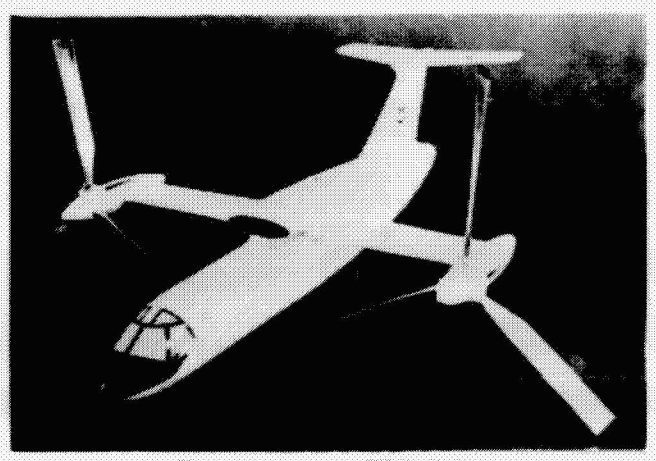
Use or disclosure of data on this page is subject to the restriction on the title page.



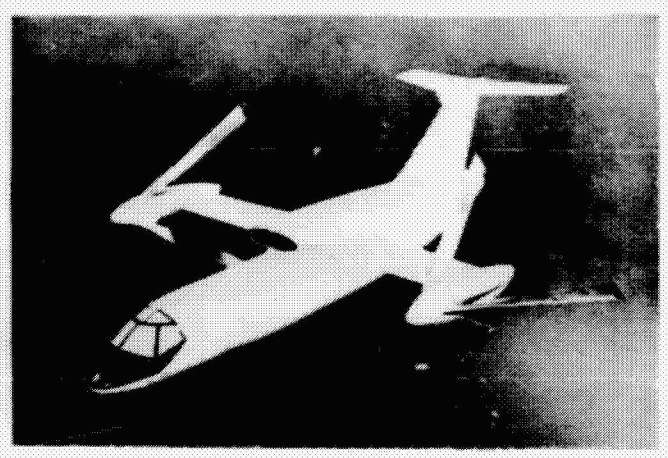
Helicopter Flight



Conversion



Proprotor Flight



Feather, Stop, and Fold



High-Speed Cruise

Figure II-1. Folding-Proprotor Sequence of Operation.

Use or disclosure of data on this page is subject to the restriction on the title page

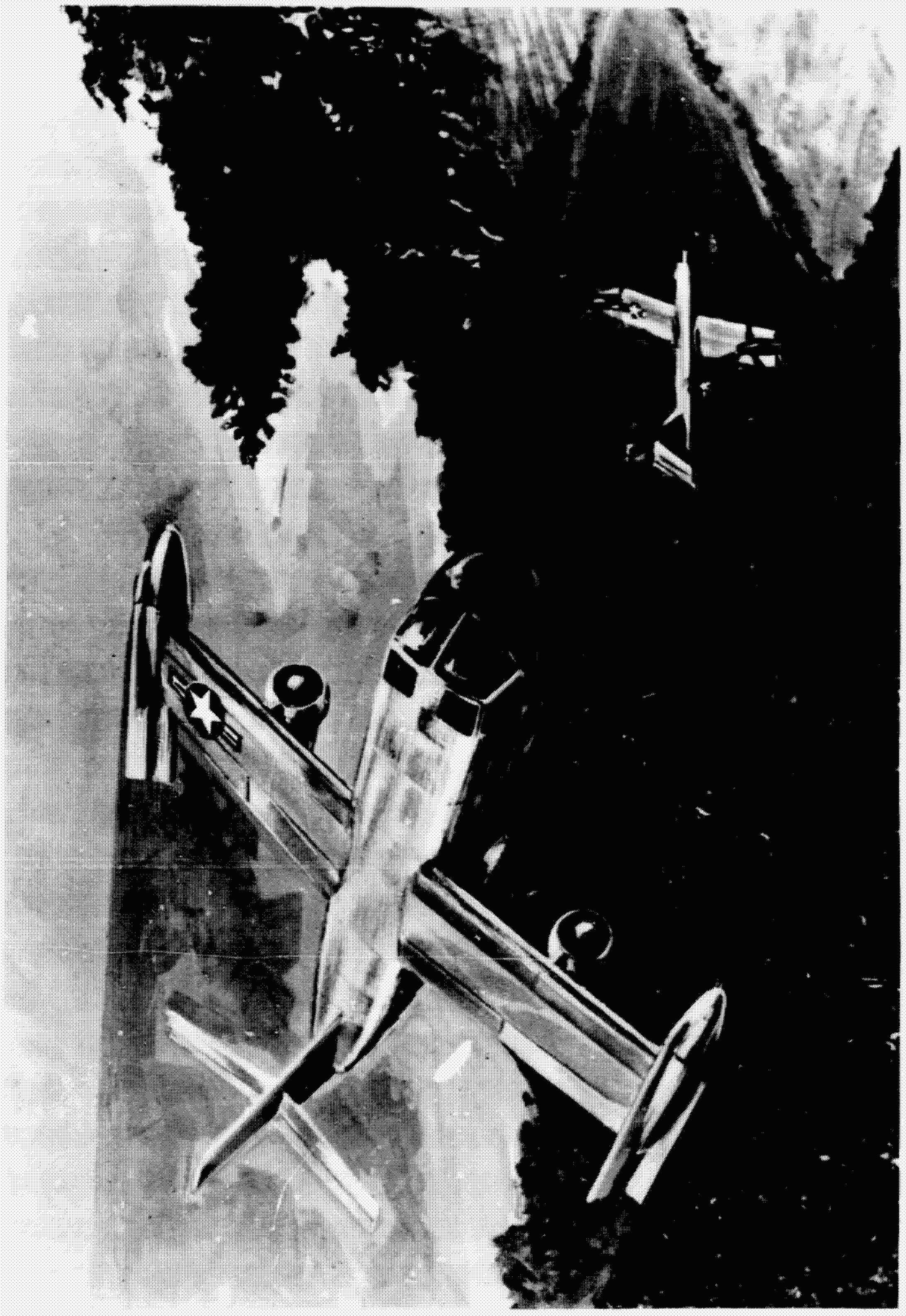


Figure II-2. Folding Proprotor V/STOL Aircraft for Military Missions.

Use or disclosure of data on this page is subject to the restriction on the title page.

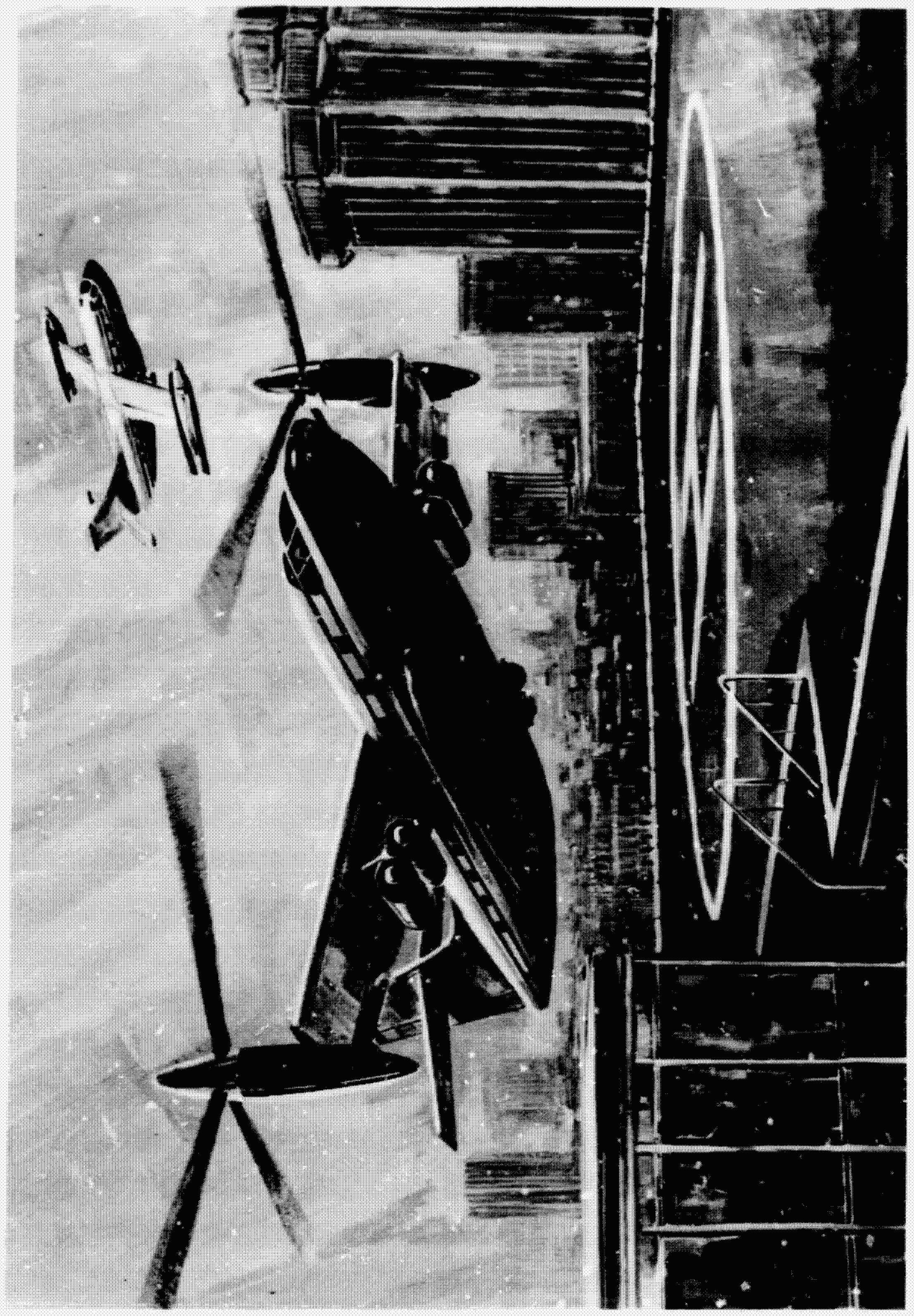


Figure II-3. Folding Proprotor Transport Civil Operations.

Use or disclosure of data on this page is subject to the restriction on the title page.

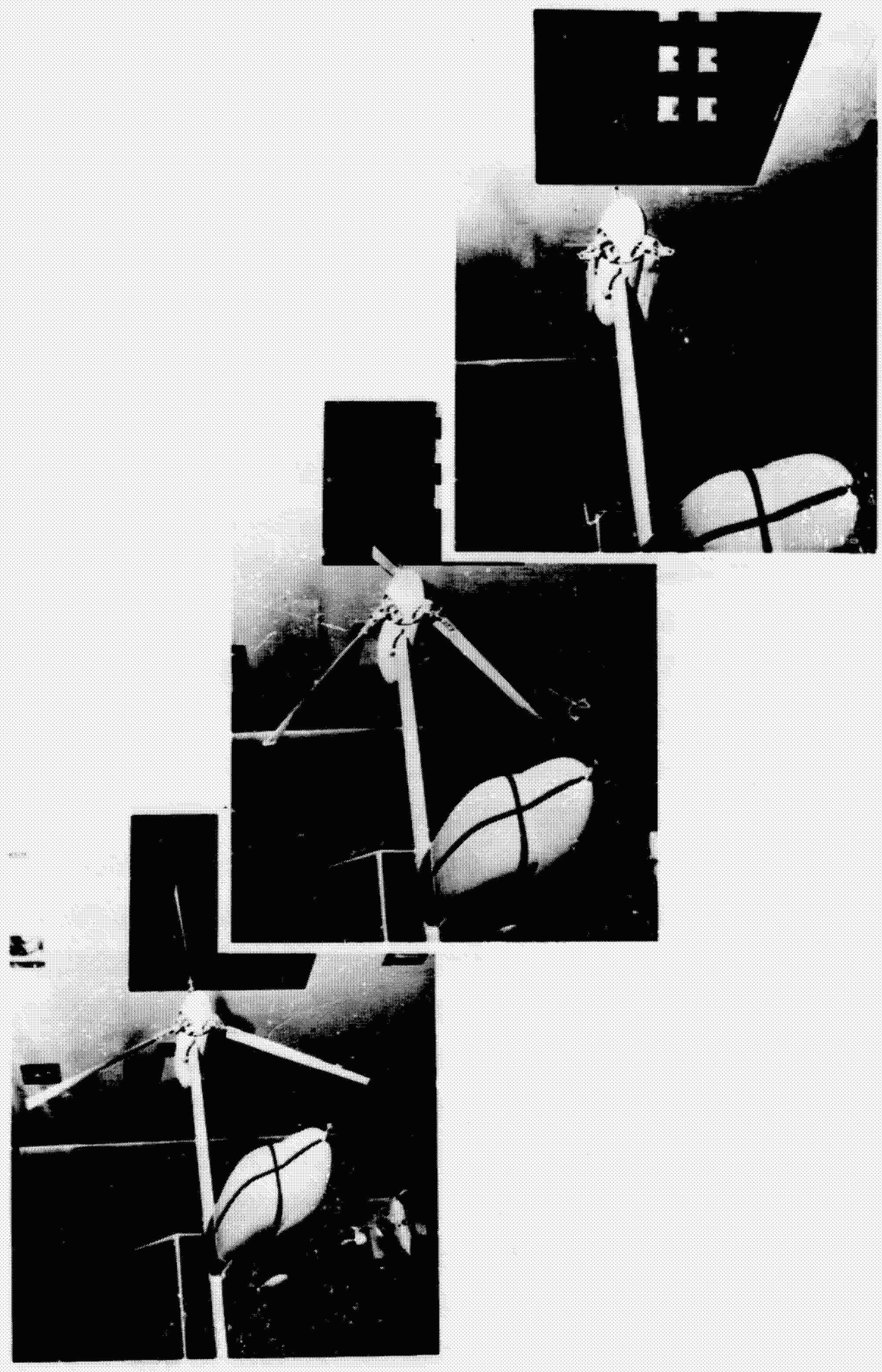


Figure II-4. Folding Proprotor Feasibility Model Tests.

Use or disclosure of data on this page is subject to the restriction on the title page.

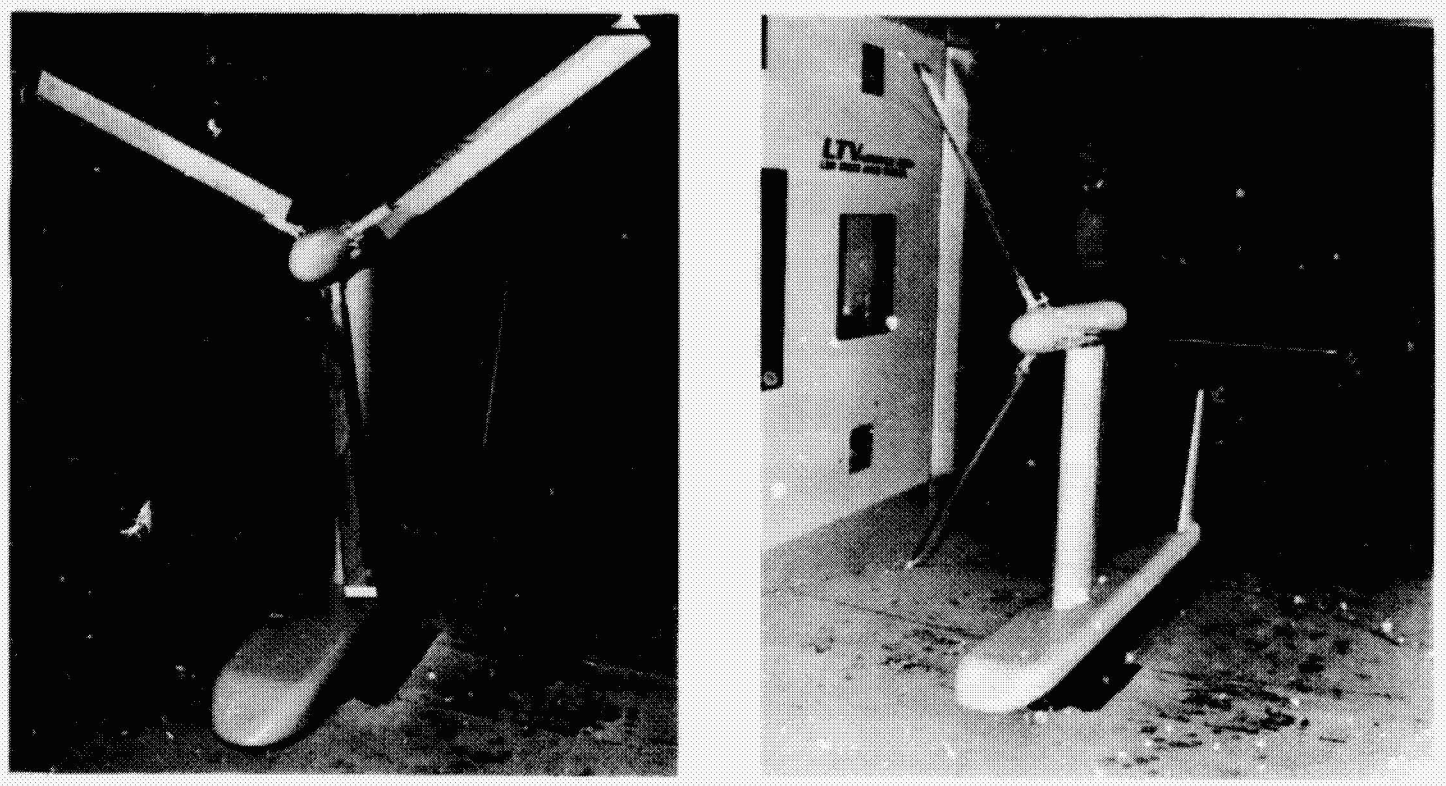


Figure II-5. Stopping/Starting Transition Model.

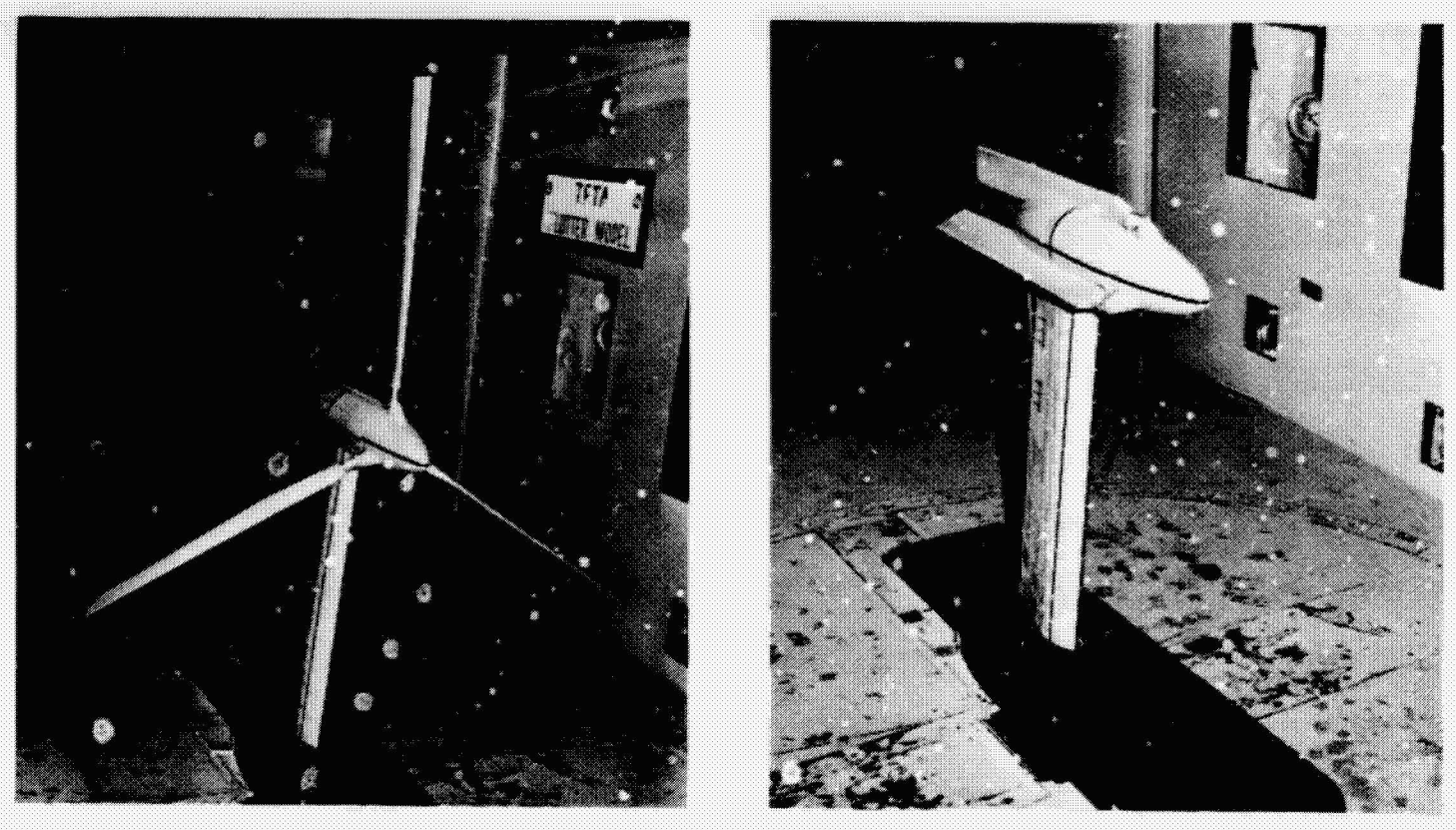
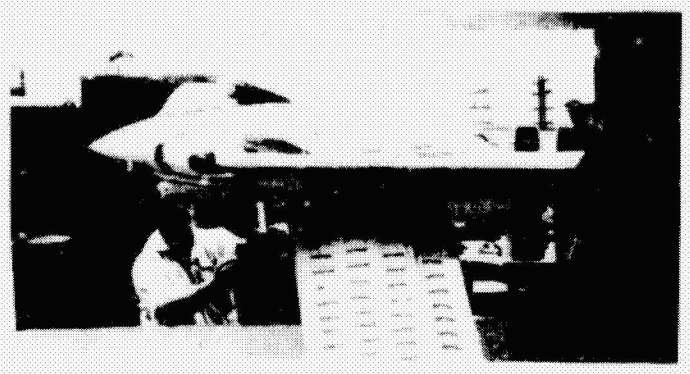


Figure II-6. Folding Proprotor Flutter Model.

REPRODUCIBILITY OF THE ORIGINAL PAGE IS POOR.

Use or disclosure of data on this page is subject to the restriction on the title page.

Edgewise



Flatwise

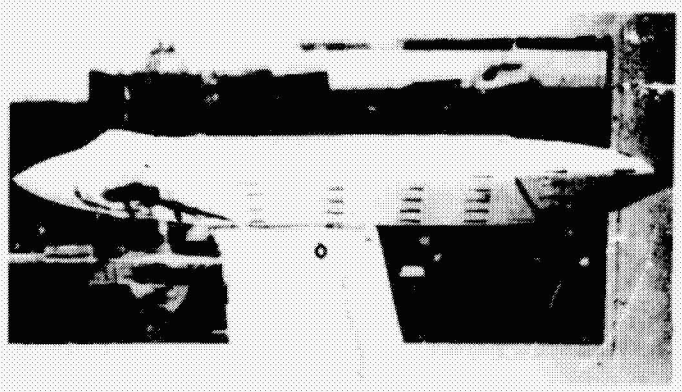


Figure II-7. Blade Stowing, Force Model.

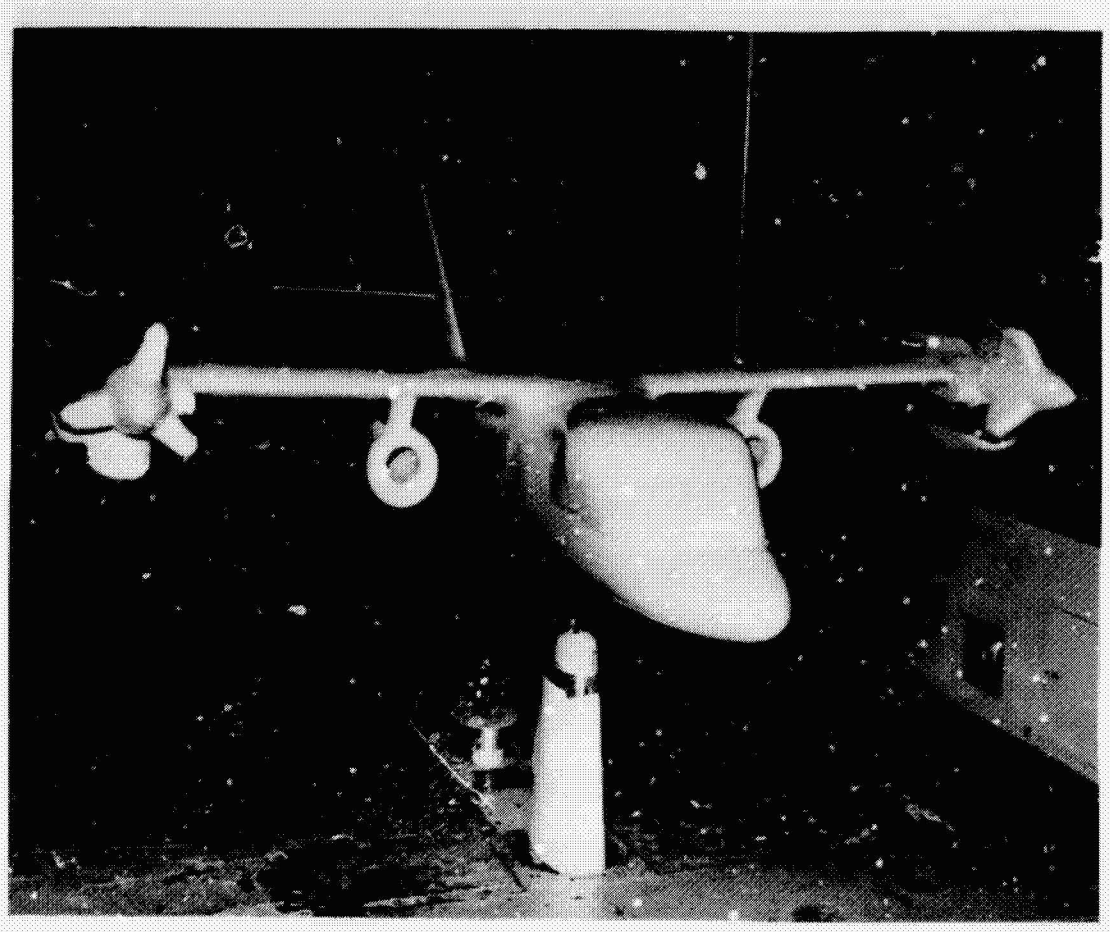


Figure II-8. Folding Proprotor Force Model.

REPRODUCIBILITY OF THE ORIGINAL PAGE IS POOR.

Use or disclosure of data on this page is subject to the restriction on the title page

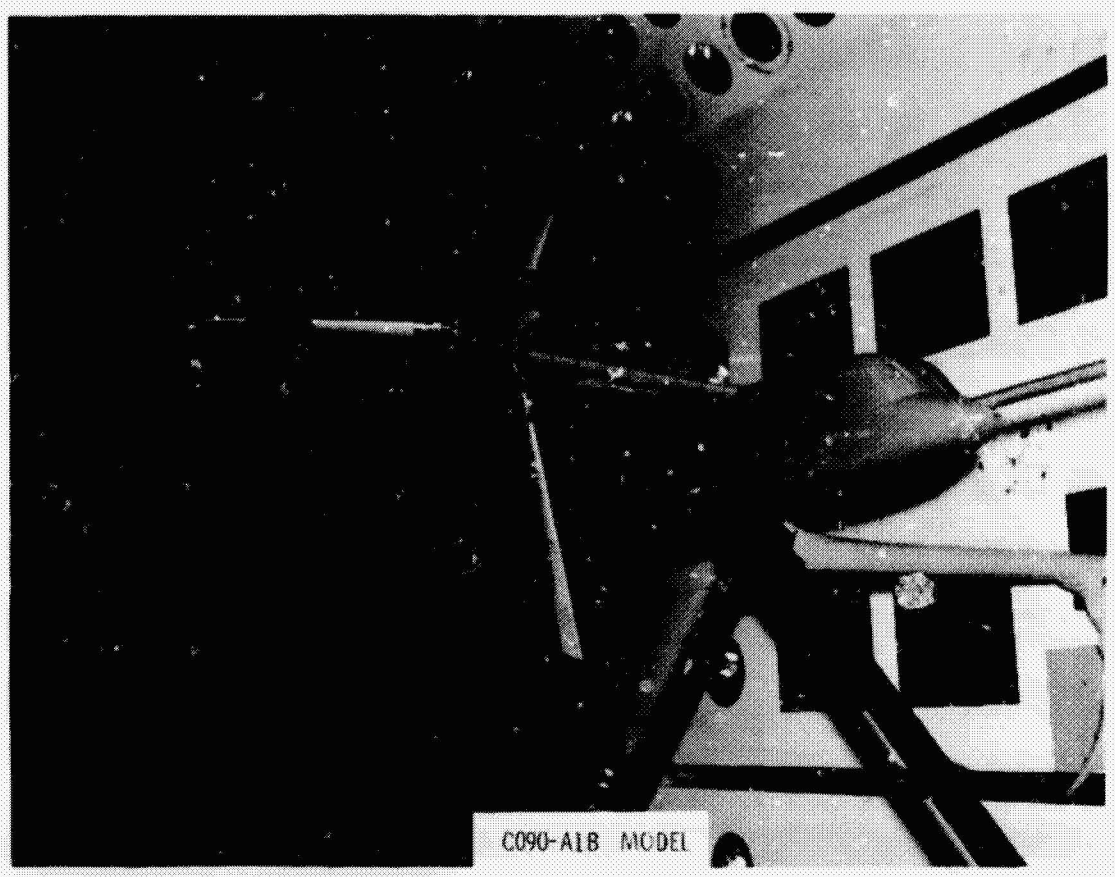


Figure II-9. Model 266 Dynamic Model with Foldable Blades.

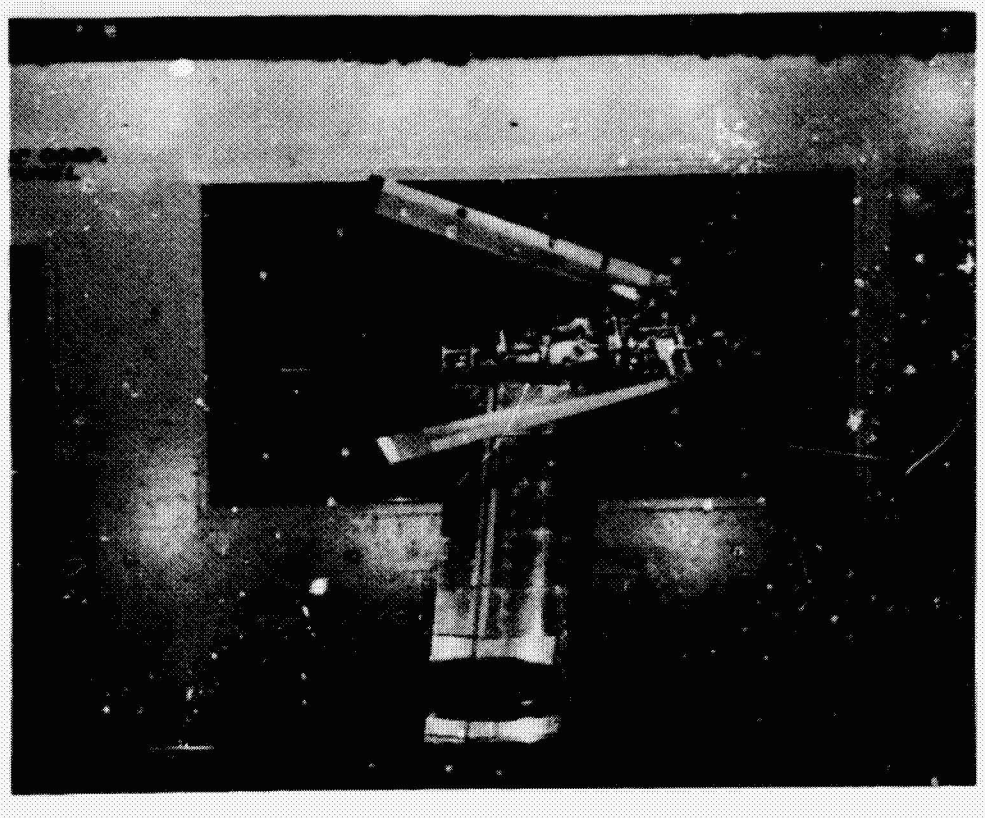


Figure II-10. Model 627 One-Fifth-Scale Folding-Proprotor Model.

REPRODUCIBILITY OF THE ORIGINAL PAGE IS POOR.

Use or disclosure of data on this page is subject to the restriction on the title page.

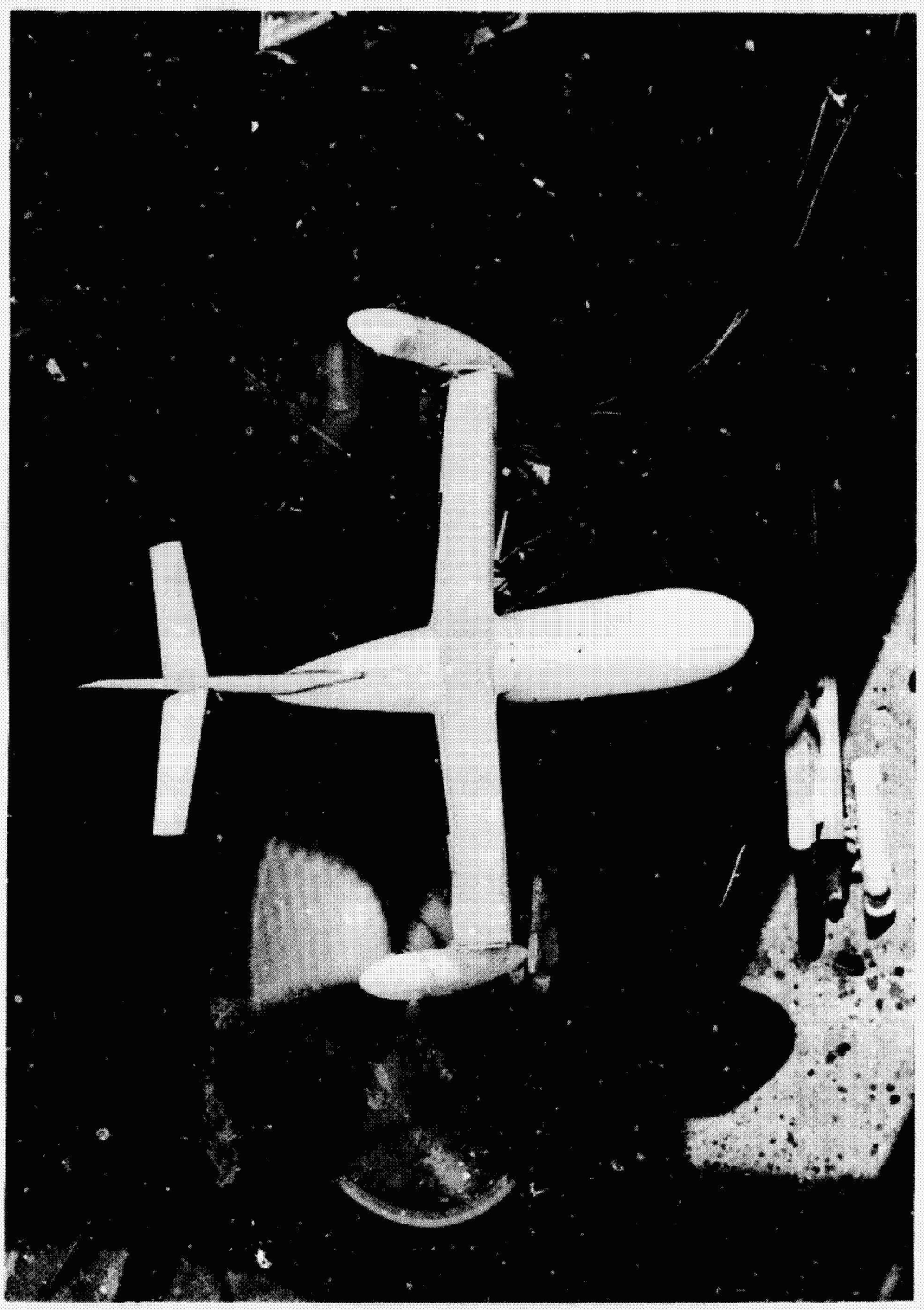


Figure II-11. Model D270A One-Tenth-Scale Powered Force Model.

Use or disclosure of data on this page is subject to the restriction on the title page.

III. THE FOLDING PROPROTOR CONVERSION SEQUENCE

A. THE SEQUENCE STEPS

The folding proprotor aircraft is designed to attain smooth transition from helicopter to airplane mode of flight using proprotor thrust, and finally to jet thrust with the proprotors stopped and stowed. The proprotor and the folding proprotor aircraft perform the same conversion sequence from helicopter to airplane mode flight. However, the sequence segments from flight with proprotor thrust to jet thrust are peculiar to the folding proprotor aircraft and are the principal configuration variables of this investigation. The sequence segments required to go from helicopter to airplane mode flight with jet thrust are as follows:

(1) Helicopter mode operation

(2) Convert pylons

(3) Airplane mode operation (proprotor thrust)

(4) Increase jet thrust, reduce rotor torque

(5) Declutch rotor (windmilling rotor)

(6) Reduce rpm to 70-80-percent hover

(7) Lock out flapping

(8) Feather rotor to obtain 0-3 rpm

(9) Index and lock mast

(10) Lock out collective pitch

(11) Fold and stow blades

B. THE AIRCRAFT CONVERSION

A typical transition (at 140 to 170 knots) of the folding proprotor aircraft with convertible fan/shaft engines is shown in Figure III-1. The sequence is initiated with pylon conversion which is controlled by the pilot from a transition "beep" switch on the cyclic stick. The governor select lever then changes from (N_{II}) rotor power turbine speed governing to (N_I) gas generator at 15 degrees of mast conversion. Proprotor rpm will be controlled by proprotor pitch at this point in the conversion from helicopter to proprotor mode. The transition process may then be continued by further use of the transition control "beep" switch. After pylon conversion, further "beeping" increases fan mass flow by either increasing pitch of the fan rotor or opening the fan flow valve (depending on the design concept of the engine). The increased demand on power tends to reduce power turbine speed which is offset by the proprotor governor reduction of proprotor pitch. The drop in proprotor thrust is almost fully compensated for by the increase in fan thrust. Fan thrust is then trimmed to maintain the desired rate of climb or airspeed. This trimming

Use or disclosure of data on this page is subject to the restriction on the title page.

is the only additional pilot control input required during the sequence. When the proprotor torque is essentially zero, the rotor may be decoupled from the drive train, the rotor speed decreased to 70 80 percent of hover rpm, the hub (flapping) locked, the rotor feathered to a stop, the mast indexed and locked, the blade pitch locked, and then the blades folded back and restrained in stow position. These steps can be stopped and reversed at any point by forward or reverse "beeping" of the transition switch. With the blades folded, the aircraft can be accelerated to its cruise speed. This sequence concept is also discussed in References 4, 5, and 14.

C. INVESTIGATIONS OF THE CONVERSION SEQUENCE

The transition sequence described above for Steps 1 through 3 was investigated during the Model 300 proprotor dynamic and powered wind-tunnel test of contract NAS2-5386. The conversion steps of these tests are given in Section IV. The sequence for Steps 6 through 11 were the subject of the folding proprotor investigation. The test hardware, data, and correlation with predictions are presented in Sections V and VI. Demonstration of Steps 4 and 5 will await availability of convertible fan shaft engines.

D. THE RATIONALE OF THE CONVERSION SEQUENCE

The purpose of the conversion sequence is to set up a logic of smooth transition control functions and configuration changes for the aircraft In this way, a manual system, such as used in the wind-tunnel test, or an automatic system such as has been considered for the aircraft (Section VIII) could be implemented. The optimum sequence control provides the lowest level of loads, the least number of cycles of high oscillatory loads or vibrations, and avoids operation near rotor natural frequencies. One of the key tasks in the subject test program was to implement the control means for actually performing a continuous sequence then carrying out the real-time sequence test to assess operator workload and system performance.

The control console used in the wind-tunnel investigation is shown in Figure III-2 The sequence panel switch arrangement as shown in Table III-I provided a means of monitoring the rotor configuration changes during the sequence and also prompted the operator to apply properly timed control through the system-condition feedback provided by the indicator lights. This same sequence could be applied to a logic circuitry package for an aircraft. Reliable system feedback information would be mandatory for an automatic system which would control the sequence in response to pilot command.

TABLE III-I. MODEL 627 FOLDING PROPROTOR SEQUENCE CONTROL SWITCH ARRANGEMENT

Switch No.	Left Indicator Light		Switch Positions			Right Indicator Light	
	Meaning	Color	Left	Center	Right	Color	Meaning
1	Sequence unarmed	G	Proprotor safety	(none)	To fold-cruise sequence	Y	Sequence armed if No. 11 armed
2	Rotor near 458 rpm	B	Go to proprotor pitch**	Off*	Reduce to 425 rpm**	B	Rotor near 425 rpm
3	Flapping unlocked	B	Unlock flapping	Off	Lock flapping	B	Flapping locked
4	Rotor near 425 rpm	B	Go to pitch 425 rpm**	Off	Go to pitch stopped**	B	Rotor near 0 to 3 rpm
5	Rotation unlocked	B	Unlock mast rotation	Off	Lock mast rotation	B	Rotation locked
6	Mast torque below 1000 in-lb	B	Go to pitch stopped	Off*	Go to pitch fold	B	Fold-position pitch stop
7	Fold system disarmed	B	Disarm pitch/ fold system	Off	Fold system power	B	Fold system armed
8	Pitch unlocked and fold drive retracted	B	Unlock pitch/ shaft out	Off	Lock pitch/shaft in	B	Pitch locked/fold shaft engaged
9	All three blades unlocked and safety locked	B	Unfold blades*	Off*	Fold blades	B	All three blades folded
10	Stow unlocked (bladders de-flated)	B	Unlock stow	(none)	Lock stow	B	Stow locked (bladders inflated)
11	Sequence armed if No. 1 is armed	Y	To proprotor	(none)	Fold-cruise safety	G	Sequence unarmed

*Momentary

**rpm-sensitive switch (a) Sense 425 rpm (b) Sense 0 to 3 rpm (c) Sense 458 rpm

BELL HELICOPTER COMPANY

Use or disclosure of data on this page is subject to the restriction on the title page.

REPRODUCIBILITY OF THE ORIGINAL PAGE IS POOR

Use or disclosure of data on this page is subject to the restriction on the title page

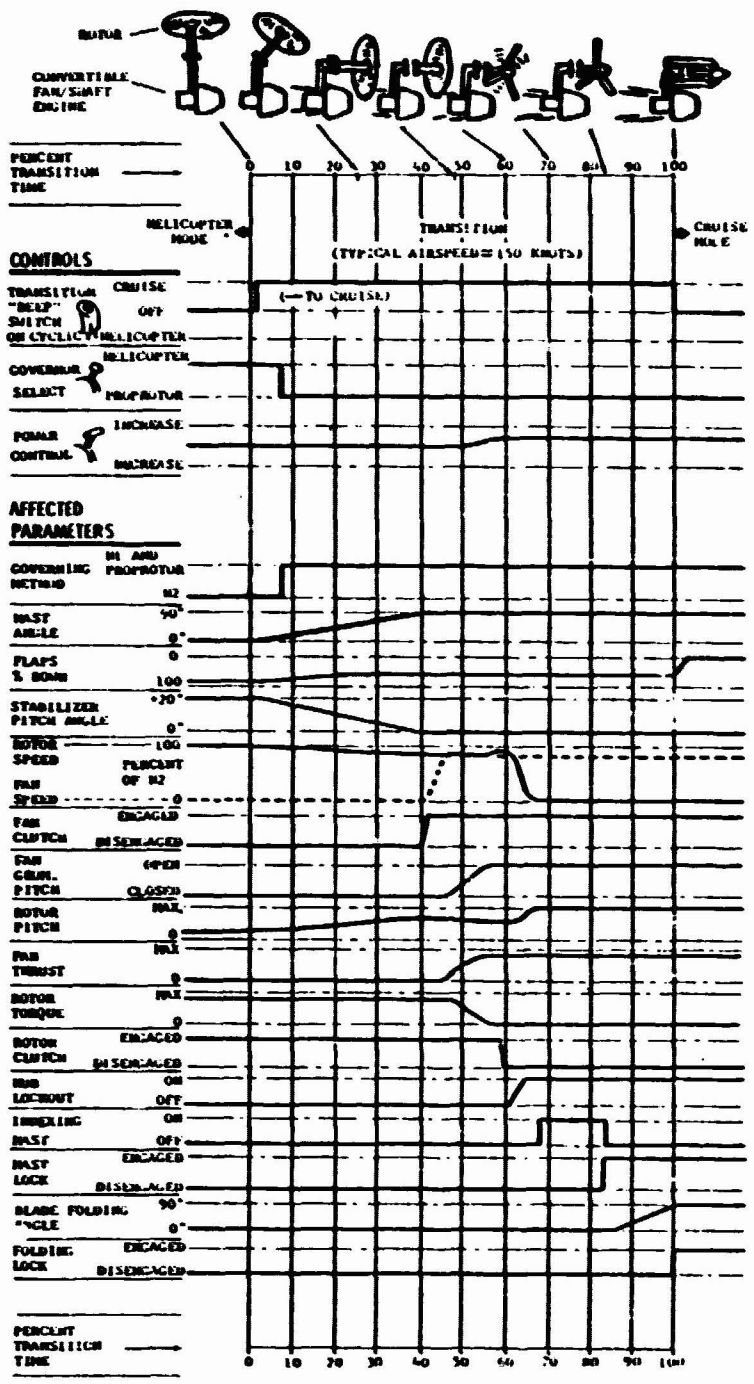


Figure III-1. Conversion Requirements.

Use or disclosure of data on this page is subject to the restriction on the title page.



Figure III-2. Control Console for Wind-Tunnel Test.

Use or disclosure of data on this page is subject to the restriction on the title page.

IV. HELICOPTER TO AIRPLANE MODE CONVERSION SEQUENCE

A. GENERAL

The BHC Model 300 25-foot-diameter proprotor was tested in the NASA-Ames 40- by 80-foot wind tunnel previously under the contract of Reference 16 to evaluate proprotor performance and loads in all three modes of flight: hover, helicopter-conversion, and airplane. The discussion with data and results are given in Reference 3. The following is a brief summary of the test configuration which is given only to complete the discussion of the conversion sequence.

B. HOVER FLIGHT MODE (α_{MAST} = +75 DEGREES)

Reference 3, Section IV, contains the results of the hover tests. Data were taken for proprotor tip speeds of 600 and 740 feet per second and for a mast angle of attack setting of 75 degrees. The proprotor provided lift efficiently in hover (at a typical operating condition, thrust was measured at 8.5 pounds per horsepower with the figure of merit of 0.78).

C. HELICOPTER CONVERSION FLIGHT MODE (α_{MAST} = +60, +30, AND +15 DEGREES)

Reference 3, Section IV, contains (nondimensionally) the variation of horsepower as a function of proprotor lift and propulsive force for mast angles of 15, 30, and 60 degrees, a tunnel speed range of 80 to 140 knots, and tip speeds of 700 and 740 feet per second.

Reference 3, Section VII, contains the measured blade and yoke bending moments and pitch link loads versus thrust for several conversion angles.

D. AIRPLANE FLIGHT MODE (α_{MAST} = 0 DEGREES)

Reference 3, Section IV, contains airplane mode (aixal) data and shows the propulsive force and efficiency data as a function of horsepower. Data are presented for tunnel speeds of 120, 160, and 185 knots, and tip speeds ranging from 400 to 740 feet per second.

The variation in blade and control oscillatory loads with airspeed and thrust is small. The steady pitch link loads are higher in airplane mode than they are in helicopter and conversion modes because the collective pitch is higher. The influence of thrust on the steady load is small. Oscillatory loads are also very low.

Use or disclosure of data on this page is subject to the restriction on the title page.

V. DESCRIPTION OF THE FOLDING PROPROTOR TEST HARDWARE

A. FOLDING PROPROTOR

The design of the folding proprotor is based on the 25-foot-diameter Bell Model 300 proprotor with stop-index-lock and fold provisions incorporated. The rotor has been designated the Model 627 folding proprotor with basic components as shown in Figure V-1. The design parameters are given in Table V-I.

1. Basic Design

The 25-foot three-bladed (folding) proprotor used for these tests evolved from the design studies of Reference 2 and is semirigid with the hub gimbal mounted to the mast to provide blade flapping freedom. The hub yoke is of forged titanium. The stiff titanium yoke aids in keeping all blade bending frequencies above rotor one per rev. Blade pitch motion and retention are provided by needle bearings and wire straps. Stainless steel liners, bonded to the titanium yoke, prevent fretting. The blades are fabricated of 17-7PH stainless steel using all bonded construction. The blade root, grip, and fold lug are made of 2014 forged aluminum. The geometry of the blades was developed for the Model 300 with the help of two-dimensional tests in subsonic and transonic wind tunnels. The blades have an NACA 64-208 airfoil at the tip and a highly cambered, relatively thick section at the root. A combination of twist and camber was chosen to meet the aerodynamic requirements for both helicopter and airplane flight, and to permit the blade spar structure to have a uniform twist rate, see Figure V-2.

The provision of feather/fold capability for the Model 627 rotor required several changes to the basic proprotor design which had a potential effect on blade natural frequencies. The net effect of the changes, including pitch change bearing spacing and size, spindle diameter, and the introduction of a hinge was held to a minimum. Because the inboard area stiffness was main tained and because the stiffness and mass properties of the outboard portion of the blade are not significantly changed, the Model 627 frequencies are nearly the same as those of the Model 300 as shown in Figures V-3 and V-4. Figure V-5 is for a mode for hub lockout only. The 627 stiffness and mass properties are shown in Table V-II. The Model 627 blade beamwise and chordwise limit load capability is shown in Figures V-6 and V-7 respectively. Drawings of the rotor design are enclosed at the end of the report.

TABLE V-I. DESIGN PARAMETERS FOR MODEL 627 FOLDING PROPROTOR

Diameter	25 ft
Number of blades	3
Blade chord	14 in.
Solidity	0.089
Aircraft design gross weight	9500 lb
Disc area	491 ft^2
Disc loading	10.4 lb/sq ft

Use or disclosure of data on this page is subject to the restriction on the title page.

TABLE V-I. Continued

Rotor tip speed	
Helicopter mode	700 fps, 534 rpm
Fixed-wing mode	600 fps, 458 rpm
Design overspeed	770 fps, 587 rpm (10 percent overspeed)
Mast index lock engage speed	
Normal operating	3 rpm
Design limit	10 rpm
Blade twist (see Figure V-2 for distribution)	33 deg
Thickness distribution (see Figure V-2 for distribution)	32 to 8 percent
Hub precone	2½ deg
Pitch flap coupling	δ_3 = -15 deg (increased pitch with up flapping)
Flapping clearance	10 deg
Cyclic pitch	
Helicopter mode	±8 deg
Fixed wing mode	none
Collective pitch at 0.75 radius	
Low range	-2 deg, +26 deg
High range	+26 deg, +88 deg
Blade feather	Chordline at 66 percent radius aligned with airstream
Hub spring stiffness (per rotor)	225 ft-lb/deg flapping
Hub lockout stiffness (per rotor)	4500 ft-lb/deg flapping (test value)
Hub lockout time	2 to 3 sec
Fold rate	10.2 deg/sec
Fold time	8-9 sec
Pitch rate to feather	25-30 deg/sec
Design airspeeds	
Helicopter mode	0-156 kt
Pylon conversion	40-189 kt
Proprotor mode	130-200 kt
Blade folding	130-200 kt
Rotors folded and stowed	150-400 kt
Design load factors (at design gross weight)	
Helicopter mode	+2.0 -0.5g
Pylon conversion mode	+3.0 -0.5g
Stop/fold sequence	+2.0 -0.0g

Use or disclosure of data on this page is subject to the restriction on the title page.

TABLE V-I. Concluded

Design gust velocity	
Infinite life	25 ft/sec at 1 g
Static limit (stopped rotor)	50 ft/sec at 1 g
Blade first inplane frequency	
Helicopter mode	1.25-1.6 per rev
Fixed wing mode	1.25-1.46 per rev
Blade first flapping frequency	
Helicopter mode - hub free	0.94 per rev
- hub locked	1.17 per rev
Fixed wing mode - hub free	0.95 per rev
- hub locked	1.27 per rev
Limit collective load (at boost cylinder)	6000 lb
Limit pitch link load	900 ± 600 lb

Design Torque Values

Mode	rpm	shp	Torque (in-lb)	Adjustment For Power Distribution (Torque x 1.1)	Limit Torque (Torque x 1.5)	Ultimate Load (Limit x 1.5)
Helicopter	565	820	91400	100600	151000	228000
Fixed wing	458	755	104000	114400	171000	258000

2. Blade Mass Balance

The Model 627 proprotor blades' mass balance was closely monitored to ensure that the design changes did not introduce blade flutter or weaving. The chordwise location of the 627 blades' effective center of gravity is 2 percent aft and 8 percent inboard of that of the Model 300 blade; however, this is considered satisfactory since the effective center of gravity is moved aft only 0.5 percent. The effective aerodynamic center is unchanged.

3. Full Pitch Range

The increased pitch range of the 627 proprotor was initially provided by a planetary gear pitch change horn with a gear ratio of 1.75:1. This had two major effects in addition to increasing the control travel: (1) it increased the effective pitch-flap coupling, δ_3, to -26 degrees and made the feathering of a given blade a function of the flapping of the tip-path plane at an azimuth 90 degrees removed from the original blade (flat tracking), and (2) it increased the downstream control system loads by 75 percent. The increased δ_3 reduced flapping and increased the blade flap-lag stability; however, the flat-tracking feature reduced the flapping stability. To accommodate increased control loads from the planetary gear ratio, the control system strength was increased by 75 percent over the Model 300.

Use or disclosure of data on this page is subject to the restriction on the title page.

TABLE V-II. MODEL 627 ROTOR STIFFNESS AND MASS PROPERTIES

HUB SEC	TORSO	VMASS	HMASS	VSOFT(E+6)	HSOFT(E+6)	RSOFT(E+6)
1.0	1.0	0.0	0.0	0.0	0.0	0.0
	A (E+6)	EIB (E-6)	G (E+6)	EIC (E-6)	WT/IN	FCENT
	0.0	-1.00	0.0	-1.00	2.380	0.19035
	0.10045	280.00	0.12390	227.00	4.010	0.18492
	0.17578	160.00	0.16642	169.00	3.750	0.17257
	0.12228	230.00	0.08549	329.00	1.440	0.16059
	0.14063	200.00	0.04687	600.00	2.940	0.15051
	0.26285	107.00	0.03750	750.00	1.300	0.13718
	0.38110	73.80	0.03125	900.00	0.690	0.12619
	0.51605	54.50	0.03750	750.00	0.606	0.11896
	0.65407	43.00	0.04327	650.00	0.625	0.11109
	0.76014	37.00	0.04687	600.00	0.541	0.10272
	0.88443	31.80	0.04900	574.00	0.515	0.09429
	1.06132	26.50	0.05189	542.00	0.491	0.08545
	1.27262	22.10	0.05536	508.00	0.457	0.07637
	1.54533	18.20	0.05934	474.00	0.442	0.06703
	1.88758	14.90	0.06334	444.00	0.419	0.05741
	2.34375	12.00	0.06745	417.00	0.396	0.04764
	2.96053	9.50	0.07156	393.00	0.372	0.03783
	3.85274	7.30	0.07581	371.00	0.347	0.02807
	5.02232	5.60	0.08036	350.00	0.324	0.01842
	6.85976	4.10	0.08446	333.00	0.300	0.00895
	9.56633	2.94	0.08844	318.00	1.000	0.0

PARAMETER SUMMARY

RADIUS	140 IN.		
DIAMETER	25 FT		
		FREQ RANGE	CPS
NO. BLADES	3	START	10
ROTOR RPM	458, 565, 0	DPMAX	30
		PLAST	5600

ROOT COLL 20.000, 45.000, 60.000 DEG
TWIST -25.000 DEG
NO. HUB SEC 1
TEETERING HUB GEOMETRY

BHC PROG DR1701 (C02), ROTOR AND CONTROL LOADS

IPSN = -627014
KWH = 6958
LOOP = 0

APPROX TENNIS-RACKET MOMENT = 5.95 IN-LB/DEG/BLADE AT 100 RPM
(ASSUMES SYMMETRICAL SECTIONS, NO DEFLECTIONS, NO OFFSETS)

Use or disclosure of data on this page is subject to the restriction on the title page.

The full collective pitch range mechanism was evaluated during the contractor's whirl test of the Model 627 folding proprotor at Bell Helicopter Company. Although the planetary pitch change mechanism produced satisfactory pitch change motion from helicopter flat pitch to full feather, the dynamic flapping characteristics were not satisfactory because of the flat-tracking feature of the planetary. A decision was made to lock out the planetary for the remainder of the test following the completion of an analysis that indicated that the rotor would be unstable above about 100 knots.

The available collective pitch range, after lock out of the planetary, is 62-1/2 degrees, which was sufficient to accomplish the wind-tunnel test without reindexing and did not in any way compromise the test program.

4. Fold Mechanism

This mechanism consists of a safety-locked nonover-center toggle linkage and a hydraulic gear-driven actuator. Three hydraulic motors are mounted to a gearbox on the hub yoke. These power a central ring gear of the interconnect gearbox which drives a shaft to each blade fold actuator. The mechanism of each blade contains four rotating joints with moly-coated steel sleeves rotating on bronze bushings. The fit is carefully controlled to reduce joint friction. The mechanism was designed so that the fold mechanism was adequate for the wind-tunnel test program and also will be satisfactory for possible future research flight tests. The rotor hub with fold mechanism is shown in Figure V-8.

Fold mechanism power input can be approximated from fold link load data recorded during the wind-tunnel test at 150 and 175 knots wind speed. These data are shown in Figure V-9 and V-10 for folding and unfolding moments at the fold lug hinge centerlines respectively. In these figures, positive moments indicate the fold linkage in tension (pulling the blade about the hinge), and negative moments indicate the fold linkage in compression (pushing the blade about the hinge). Frictional resistance at the joints make up part of the total folding moment. However, air loads contribute to the total moment when the blades are near the full open (unfolded) position. The moments also vary depending on the blade attitude of folding in a vertical or horizontal position although the trend is about the same. The power input may be approximated from the following relationship based on the maximum moment for the blade between 5 and 30 degrees of fold angle:

$$\text{Input hp} = \frac{\left(\begin{matrix}\text{Fold}\\ \text{Moment}\end{matrix}\right)\left(\begin{matrix}\text{Power Hinge}\\ \text{Arm}\end{matrix}\right)\left(\begin{matrix}\text{No. of}\\ \text{Blades}\end{matrix}\right)\left(\begin{matrix}\text{Motor Input}\\ \text{rpm}\end{matrix}\right)}{\left(\begin{matrix}\text{Fold Link}\\ \text{Arm}\end{matrix}\right)\left(\begin{matrix}\text{Power Hinge}\\ \text{Gear Ratio x Eff.}\end{matrix}\right)\left(\begin{matrix}\text{Worm Gearbox}\\ \text{Ratio x Eff.}\end{matrix}\right)\left(\begin{matrix}\text{Interconnect}\\ \text{Drive Eff.}\end{matrix}\right)(63025)}$$

$$= \frac{(20000)(10.7)(3)(3200)}{(13)(48 \times 0.67)(18.5 \times 0.62)(0.90)(63025)} = 7.5$$

For safety reasons the total fold motor power provided (16 horsepower) is 100 percent in excess of the power required per rotor.

Use or disclosure of data on this page is subject to the restriction on the title page.

5. Fold Link Safety Lock

The toggle fold linkage is designed with a mechanical safety lock pin which automatically engages when the blade is in the fully open position. The lock pin secures the fold drive arm to the drag link. A safety lock for the fold linkage is provided in the event of an actuator gear failure which might result in a blade azimuth shift. The lock pin is disengaged by the fold actuator driving through a cam slot to unlock the pin during the initial few degrees of actuator travel of the folding sequence. Locking is achieved at the last few degrees of actuator travel of the unfolding sequence.

6. Fold Interconnect System

The mechanism selected for blade folding, as previously discussed, provides for three hydraulic motors to drive a central ring gear on the hub yoke with drive shafts to each blade folding actuator. This drive system provides for interconnecting without the use of flexible drive shafts and will allow the power from each motor to be equally distributed. The drive design also allows for the individual blade weight inertia loads, friction, and airloads to be equalized at the hub and provides for a smooth actuation cycle.

7. Pitch Change Lockout

The static strength of the rotor yoke and blade for the high angle-of-attack folding condition is considerably greater than required for the rotating controls for all other design conditions. Investigation of the rotor indicates that lockout of the rotating controls during the folding sequence would improve the overall rotor strength and obtain a more balanced design structurally. The basic loads problems are the lift and drag due to mast angle and/or gust loads on the blade tending to twist the rotor about the pitch change axis in the same manner as a swept-wing aircraft applies lift loads to the fuselage. This twist load is resisted by the pitch horn. The solution is to lock the pitch horn securely to the hub yoke prior to folding. In the Model 627 design, this is accomplished by incorporating the hydraulic pitch lock cylinders into the same mechanism used to fold the blades so that the hydraulic locking pin motion also engages the fold drive shaft to each blade.

8. Rotor Index and Lock

The method of locking the rotor mast during the folding sequence is incorporated in a simple straightforward mechanism which will also keep it from being effective if it is engaged inadvertently during rotation or prematurely during stopping. Rotor stopping is obtained by feathering the blades with collective control. When the rotor is stopped, or up to ten rpm, the index hydraulic cylinder actuator is engaged which stops the rotor at one of the three possible index positions for folding. Three index positions are used so that rotor index can be accomplished in minimum time. When the rotor is stopped and indexed, the index actuator is automatically locked. This lock positively secures the rotor at the index position. The lockout mechanism is designed for the torque due to the blade pitch angle for fold with respect to the feather (zero rpm) angle being rigged, plus three degrees. This will produce up to 9000 foot-pounds of mast torque during folding.

The mechanism is fabricated from steel and was mounted to the pylon structure of the dynamic test stand. For the aircraft, it would be mounted to the transmission case. The mast includes a wheel with index position slots at the three equally spaced locations as shown in Figure V-11. (Recommended future improvements for this mechanism are discussed in Section VIII, paragraph E.3).

9. Hub Flapping Lockout

Flapping lockout for the rotor during stopping and starting is necessary to prevent the rotor from contacting the stops and moving close to the wing due to large flapping excursions with mast angle of attack and low rpm. During the helicopter and proprotor mode, the combination of the elastomeric hub restraint and the δ_3 provides adequate flapping control and good control power. During the rotor stopping sequence, at approximately 70 percent of hover rpm, a lockout is engaged, bringing the rotor to near a zero flapping condition. This condition is held throughout the fold/unfold sequence until the rotor is back to 70 percent of hover rpm. The mechanism consists of a hydraulic motor driving a gear actuator. This rotates an Acme power screw which in turn raises and lowers a conical lockout ring against a nonrotating centering ring on the hub. The input hydraulic power required to lock out the flapping within three seconds is six horsepower. The flapping moment actuator design limit is 85,000 inch-pounds and the lockout motor rate, due to gear ratios, provides lockout from up to ten degrees of flapping in 2.7 seconds. Ample torque capability is available for maneuvers and for 50 feet per second gusts.

B. CONTROLS

The Model 627 control system is patterned directly from the Model 300 to retain similarity with the proprotor for reduced engineering cost.

1. Collective

The primary control for the rotor for the wind-tunnel test is the collective system. The collective system consists of; (1) an electric linear actuator, (2) a hydraulic boost cylinder, (3) a servo valve and linkage to the electric actuator and boost cylinder, (4) a collective tube inside the mast connecting the boost system and the collective head, (5) pitch links and horns, and (6) control tubes to swashplate. Figure V-12 shows the collective control actuator and linkage.

A rise-and-fall collective head assembly above the proprotor moves three walking beams, thereby providing collective control. The hydraulic actuator positions the collective controls. The servo valve of the 3000 psi hydraulic actuator is positioned by a 28-volt electro-mechanical actuator to provide remote control. In the event of hydraulic pressure loss, the electric actuator provides a mechanical back up to carry the control loads until the tunnel speed is reduced. Also a check valve in the hydraulic pressure line will retain pressure to hold the control position at the time of a pressure loss in the system. The electrical power for the collective actuator is provided from a DC power supply in which the voltage is varied from 24 to 34 volts to provide a collective rate change.

Use or disclosure of data on this page is subject to the restriction on the title page.

2. Cyclic

Cyclic control is achieved through a monocyclic (fore and aft) swashplate below the proprotor. This system was operated during the contractor whirl test at BHC but was rigidly positioned at zero cyclic for the wind-tunnel test. This is to conform to the proprotor aircraft control system which will "washout" cyclic to zero during pylon conversion to the propeller flight mode.

3. Hub Spring

An elastomeric hub spring is utilized to increase the control moment capability of the proprotor. The hub spring is located in the nonrotating system to eliminate fatigue loading on this component. The spring is attached directly to the hub lockout actuator mounted to the top case of the transmission, and the upper attachment is to the hub yoke through a bearing set. Figure V-13 shows the rotor controls on the whirl test stand at BHC.

4. Folding Sequence Control System

a. System Requirements

The folding sequence control system requirements for the wind-tunnel test program are not as demanding as for the flight aircraft. In the tunnel, the sequence of control functions are manual so that the operator can stop and hold any part of the sequence as desired. The method used for the wind-tunnel test program involves the use of functional limit switches from a 28 volt DC power supply to initiate each step of the sequence, and indicator lights to show that each step has been accomplished satisfactorily. The controls allow stopping and reversal of any step in the sequence. For the D272A research aircraft it is desirable to provide an automatic sequence control system which relieves the pilot of the duties of programming the functions of a pylon conversion, stopping and folding. However, this automatic feature is only to relieve the pilot of excessive work load and must also be capable of stopping, holding or reversing the sequence at the pilots command, or of being quickly switched to manual control. This is discussed in the recommended future work in Section VIII, paragraph C.

b. Circuit Requirements

Electric circuits for the five solenoid control valves and eight position switches with indicator lights extend through the wing. This results in an approximately 32-wire bundle through the wing. From this bundle, five circuits go through the instrumentation slipring for the folding and locking controls in the rotating system. The circuit layout for functions like pitch lock, blade folding, and unfolding were provided with the limit switches in series for each of the three blades to provide indication that the function is complete for all blades. A diagram of the control system for the wind-tunnel test is shown in Figure V-14.

C. HYDRAULIC POWER SYSTEM

The hydraulic system for the Model 627 folding proprotor is a 3000 psig maximum operating pressure system with MIL-H-5606 fluid. The minimum operating pressure is 2000 psig. The flow requirement is 6 gpm for fold/unfold cycle and 4.5 gpm for hub lock/unlock. The mast lock or the collective boost cylinder each require about 2 gpm flow, but only one control functions at a time. The system supply lines in the wing and pod were sized to provide a maximum of 12 gpm to provide for a possible fold/unfold cycle rate increase. The fluid cleanness is assured by a 15 micron absolute filter in the pressure line at the base of the wing. The three-fourth-inch pressure and return connections at the base of the wing included quick disconnects. The hydraulic lines in the wing and pod are five-eights-inch diameter stainless steel to the solenoid control valves with one-half-inch diameter stainless steel lines for folding and a minimum of one-fourth-inch diameter stainless steel lines to the pitch lockout, hub lockout, mast lockout, and collective control. All the lines from a rigid member to a moveable component incorporate high pressure flex hoses, and all hoses on the rotor are protected with stainless steel wire braid covers. Four-way three-position solenoid valves provide control for each fold or lock function. During all rotor turning operations, a flow of 0.25 gpm at a pressure of 300 psig is provided to lubricate and cool the hydraulic slipring and to provide pressure to secure the pitch locks in the unlock position. This is provided by Lee jet restrictors in the lines.

The hydraulic system schematic for the fold and pitch lock system is shown in Figure V-15. The hydraulic schematic for hub lockout, mast lockout, and collective control is shown in Figure V-16.

The hydraulic system supply for the aerodynamic shaker vane is from the test stand system and incorporates a pressure regulator to drop the pressure to 1500 psig with a test-stand system pressure of 3000 psi. This is done to utilize an existing 1500 psi servo SCAS actuator from the Model 300 test system. The servo actuator controlled the frequency and amplitude of the oscillatory vane shaker motion. The response of the actuator is to 20-30 Hertz and ±15 degrees of feather motion from the remote control.

D. WING AND POD DYNAMIC TEST STAND

1. Wing Description

For dynamic stability testing, the Model 627 folding proprotor was mounted on a structure which simulated the Model 300 or the D272A semispan wing and nacelle without auxiliary thrust engines. Bell drawing 300-018-014, included at the end of the report, shows the test assembly. This wing was mounted vertically in the wind tunnel and attached directly to the tunnel balance. The wing angle of attack could be varied remotely and the limits were set at -10 and +20 degrees. Extensive use was made of the remote angle-of-attack variation capability during the test; however, all dynamic test-stand runs were made with the nacelle in the airplane mode. The wing angle of attack was coincident with the rotor mast angle of attack for the Model 627 test setup.

Use or disclosure of data on this page is subject to the restriction on the title page

The basic wing structure consists of a beam of rectangular cross section equal in bending and torsional stiffness to the actual Model 300 wing design. The wing airfoil is a simple aerodynamic fairing complete with light nonstructural components. All components of the beam and fairing are aluminum.

The airfoil section, however, is simplified to reduce manufacturing cost. Its thickness is 13.5 percent as compared to 23 percent for the Model 300 or D272A wing. The wing chord is 62 inches, and the spanwise length of the wing from the ground plane to the centerline of the rotor pod is 165 inches.

2. Test Stand Dynamics

The test stand parameters--wing chord, span, weight, stiffness, and sweep--are held as close to those of the Model 300 and D272A aircraft as possible.

The scaling factors of the test stand are 1:1 for Mach number, Froude number, and Lock number. The test stand natural frequencies were calculated prior to the dynamic stability test using a finite element structural model of the stand. Figure V-17 shows the layout of the structural model and the element properties, and node point masses are given in Tables V-III and V-IV.

A vibration survey of the test stand was conducted first at the contractor's facility and again when the stand was installed in the test section. A Lazan shaker was used to excite the system natural frequencies. Hand exictation of the fundamental modes was used to obtain modal damping ratios. The results of this survey are given in Table V-V.

The effect of locking out flapping and proprotor rotation on system natural frequencies was evaluated with the blades fully open. These data are also shown in Table V-V. The influence of the link attaching the pylon to the outboard rib, in the pylon yaw direction, and which controls the pylon yaw frequency, was evaluated and remained securely attached during the test. Prior to the shake test, the frequencies of the coupled wing/pylon/rotor system were calculated for several blade fold angles. The correlation is good in terms of trend. Minor modifications were made to the math model parameters to improve the absolute frequency correlation. The comparison of calculated to measured frequencies for various fold angles is shown in Figure V-18.

3. Rotor Pod

The tip pod includes the folding proprotor, with space provisions for the transmission and Pratt and Whitney PT6C-40 engine installation, and fold slots in the nacelle. The discussion of the folding proprotor, designated the Model 627 rotor, is given in Part A of this section.

Use or disclosure of data on this page is subject to the restriction on the title page.

TABLE V-III. DYNAMIC TEST STAND MASS PROPERTIES

	Mass and Inertia*					
Node	M_x	M_y	M_z	I_x	I_y	I_z
2	0.215	0.215	0.215	--	--	--
3	0.215	0.215	0.215	--	--	--
4	0.1	0.1	0.1	--	--	--
5	0.1	0.1	0.1	--	--	--
6	0.1	0.1	0.1	--	--	--
7	0.1	0.1	0.1	--	--	--
8	0.118	0.118	0.118	--	--	--
9	0.118	0.118	0.118	--	--	--
15	1.145	1.145	1.145	--	772	772
16	2.12	2.12	2.12	208	800	800
17	0.0026	0.0026	0.0026	--	--	--
18	0.0026	0.0026	0.0026	--	--	--
19	0.0026	0.0026	0.0026	--	--	--
20	1.453	1.453	1.453	--	--	--

*See Figure V-17 for element coordinate system.

All units in lb-in-sec system.

-- Indicates coordinate was not retained.

Use or disclosure of data on this page is subject to the restriction on the title page.

TABLE V-IV. DYNAMIC TEST STAND STIFFNESS PROPERTIES

Segment	Length (in)	EI_{BEAM} $(lb\text{-}in^2) \times 10^{-6}$	EI_{CHORD} $(lb\text{-}in^2) \times 10^{-1}$	GJ $(lb\text{-}in^2) \times 10^{-6}$
1	21.0	9570	19520	16870
2	21.0	2653	10410	2696
3	21.0	2653	10410	2696
4	21.0	2653	10410	2696
5	21.0	2653	10410	2696
6	21.0	2653	10410	2696
7	21.0	2653	10410	2696
8	18.4	2653	10410	2696
9	8.7	2760	10820	2690
10	8.7	2760	10820	2690
11	6.8	1722	129	340
12	6.8	1722	129	340
13	18.4	525	525	310
14	6.0	970	970	808
15	7.0	4000	4000	4200
16	16.8	10908	16991	10293
17	5.6	33292	23800	15277
18	1.7	9500	9500	7613
19	13.7	1142	821	725
20	13.7	600	600	466
21	18.5	171	171	90.5
22	2.0	171	171	90.5
23	1.0	10000	10000	10000
24	7.35	10000	10000	10000
25	2.0	$AE = 15 \times 10^6$ lb		
26	14.7	$AE = 5.7 \times 10^6$ lb		
27	7.35	10000	10000	10000
28	1.0	10000	10000	10000

TABLE V-V. MODEL 627 TEST STAND WING/PYLON/ROTOR COUPLED FREQUENCIES AT 0-DEGREE BLADE FOLD, BLADE ROOT COLLECTIVE 126 DEGREES

Mode Description		Gimbal Free Rotation Free Yaw Link In (cps) Calculated	Gimbal Free Rotation Free Yaw Link In (cps) Measured	Gimbal Free Rotation Free Yaw Link Out (cps) Calculated	Gimbal Free Rotation Free Yaw Link Out (cps) Measured	Flapping Locked Rotation Locked Yaw Link In (cps) Calculated	Flapping Locked Rotation Locked Yaw Link In (cps) Measured	Flapping Locked Rotation Locked Yaw Link Out (cps) Calculated	Flapping Locked Rotation Locked Yaw Link Out (cps) Measured
First wing beam		2.4	2.4	-	2.4	2.4	2.4	-	2.4
Mass rotation		-	-	-	3.2	4.0	3.3	-	3.3
First wing chord		4.4	4.5	-	4.5	4.4	4.3	-	4.0
Out of plane	*	-	-	-	-	9.9	10.0	-	-
Cyclic	*	-	-	-	-	15.7	-	-	6.0
In plane	*	7.2	-	-	-	7.1	-	-	-
Cyclic	*	7.2	7.8	-	7.3	7.5	7.8	-	8.0
Wing torsion		8.9	8.6	-	8.6	6.5	5.6	-	10.5
Out of plane collective		12.1	-	-	13.0	13.3	12.4	-	13.8
In plane collective		16.5	16.3	-	15.3	17.5	15.0	-	17.8
Pylon yaw		15.3	15.9	-	11.5	21.0	18.5	-	13.1
Second wing beam		38.0	26.0	-	26.0	-	26.0	-	26.0
In plane	*	27.3	-	-	-	27.4	-	-	-
Cyclic	*	27.7	30.2	-	28.0	28.1	30.1	-	-

*These modes occur in pairs

BELL HELICOPTER COMPANY

Use or disclosure of data on this page is subject to the restriction on the title page.

The basic structure of the rotor pod nacelle is a steel box beam weldment which is attached to the wingtip by means of a conversion spindle and links. The bending stiffness of the spindle is the same as the Model 300 conversion spindle. The conversion actuator is replaced by a link. A yaw link is also provided to simulate the pylon-to-wing attachment when the pylon is fully converted so that a downstop is engaged. Four aluminum bulkheads, attached to the weldment, support a fiberglass fairing over the structure. The fairing contour is made to the Model 300 nacelle lines with provisions for fold stowing the blades into the nacelle slots.

On the outboard side of the pod, an aerodynamic shaker is provided (Figure V-19). This shaker consists of a small airfoil mounted on a shaft, attached near the aft end of the nacelle. The shaker is oscillated by a SCAS hydraulic cylinder from a remote control which will vary both frequency and amplitude.

4. Fold Stow Lock

The fold mechanism contains an irreversible worm gear stage which will hold and lock the blade at any fold position. However, it is desirable to secure the blade spanwise to the pod to hold and cushion it without requiring any attachments through the blade trailing edge. Air inflatable boots of neoprene stretchable fabric lining the sides of the stowing slot in the pods were used for this purpose. The surface of the boots is impressed with a tread so it will grip and hold the blade. Contractor IR&D lab tests confirmed the lock capability and are reported in Reference 2, Section V, page 143.

Modifications of the tip pod to provide fold-stow sealing slots are as shown in Figure V-20. This design provides air pressure inflated diaphragms to secure the blade into the pod in the blade stow position. The design is based on using engine compressor bleed air as a pressure source regulated at 20 psig. Since the flow requirement and the boot volume are low, a pneumatic line size of 3/8-inch in the wing to 1/4-inch in the pod is used.

During the test, the normal wind-tunnel compressed air system, without any cleaning or drying provisions, was the source of pressure.

5. Rotor and Spinnder Fairing

The spinner of the Model 627 rotor is similar to the Model 300 spinner except that it is three inches longer for internal clearance. This provides a smooth aerodynamic cone to the pod contour.

The fairing of the blade grip intersection with the spinner was investigated during the predesign phase and also by a small-scale model. This is reported in Section IV.B.3.h of Reference 2.

A nonmovable fairing duplicating this concept was designed for the wind-tunnel program so that rotor folded drag data may be obtained. However, since only dynamic data are required by the contract work statement, this fairing was not fabricated and no testing of such a fairing was done. See Section VIII, paragraph B for recommended future work to evaluate lift and drag of the full-scale model with full fairings.

Use or disclosure of data on this page is subject to the restriction on the title page

E. INSTRUMENTATION

Conventional BHC flight-type instrumentation was used to measure loads, deflection, vibrations, and pressures during the test. Transducers included strain gages, potentiometers, accelerometers, and pressure transducers. Proprotor rotating system instrumentation channels utilized a 52-ring slip ring to provide 2 excitation channels and 18 data channels with one spare. In addition, 5 channels of fold and lock controls were routed through the instrumentation slip ring. Table V-VI is a summary of all the data channels for the dynamic folding proprotor test. There were 38 channels used during the dynamic test. System accuracy is estimated to be within ±3 percent (based on channel full scale with errors being the square root of the sum of the square of the individual errors). Data amplifiers were installed at the base of the model wing to provide gain, balance, calibrate inserts, and line driving ability to the control room.

Signals were distributed to various display devices in the control room such as peak reading meters, oscilloscopes, and direct write oscillographs. Three 13-channel oscillographs were used during the dynamic test to record permanent data.

TABLE V-VI. INSTRUMENTATION FOR MODEL 627 TEST PROGRAM

NO.	ITEM	LOCATION OR PART NUMBER	OPERATING LIMIT LOAD VALUE	100% DISPLAY VALUE	UPSCALE SIGN CONVENTION + = RIGHT = UPSCALE	READOUTS: OSCILLATORY	STEADY	OSCILLOGRAPH	METER-OSC	METER-STEADY	SLIP RING CHANNEL	OSC. SCOPE
	Red + White (Backup)	627-010-001-2										
1.	Blade Beam	Sta 33	± 27,000 In-Lb	± 70,000 In-Lb	Top Surface in Compression = +	X	X	X			X	
2.	Blade Beam	Sta 52.5	± 19,000 In-Lb	± 50,000 In-Lb	Top Surface in Compression = +	X	X	X	X		X	X
3.	Blade Chord	Sta 52.5	± 18,500 In-Lb	± 50,000 In-Lb	L.E. in Tension = +	X	X	X	X		X	X
4.	Blade Torsion	Sta 52.5	± 3,300 In-Lb	± 10,000 In-Lb	L.E. Up = +	X	X	X			X	
5.	Fold Arm Bending	627-010-105-2	5,800 In-Lb	7,000 In-Lb	Outboard Surface in Compression = +		X	X		X	X	
6.	Fold Arm Axial	627-010-105-2	± 3,500 Lb	± 5,000 Lb	Arm in Compression = +	X	X	X			X	
7.	Drag Link Axial	627-010-106-1	15,000 Lb	25,000 Lb	Link in Compression = +	X	X	▲		X	X	X
8.	Pitch Lock Bending	627-010-602-2	25,000 In-Lb	50,000 In-Lb	Right Side in Tension = +		X	X		X	X	
9.	Feather Position	627-010-100-2	92°	100°	High Pitch = +		X	X		X	X	
10.	Grip Lug Stress	627-010-102-2	1600 psi	5,000 psi	Tension Stress = +	X		X		X	X	
	Rotor											
11.	Pitch Link - Red	627-010-407-1	900 Lb ± 600 Lb	1,000 Lb ± 800 Lb	Link in Tension = +	X	X	X	X		X	
12.	Pitch Link - White	627-010-407-1	900 Lb ± 600 Lb	1,000 Lb ± 800 Lb	Link in Tension = +	X	X	X			X	
13.	Pitch Link - Green	627-010-407-1	900 Lb ± 600 Lb	1,000 Lb ± 800 Lb	Link in Tension = +	X	X	X			X	
14.	Mast Horizontal Bend	627-018-011-1	± 70,000 In-Lb	±100,000 In-Lb	Red Blade up Surface in Tension = +	X	X				X	
15.	Mast Vertical Bend	627-018-011-1	± 70,000 In-Lb	±100,000 In-Lb	Red Blade to Side Surface in Tension = +	X	X	X	X		X	
16.	Mast Torsion	627-018-011-1	30,000 In-Lb	50,000 In-Lb	Counter Clockwise Torque Looking Aft = +	X	X	X		X	X	
17.	Flapping - Red Blade	300-010-200-5 (Linear Pot)	± 8°	± 12°	Red Blade Aft = +	X		X			X	X
18.	Fore and Aft Hub Flapping	627-010-301-1 (Linear Pot)	± 8°	± 12°	Flap Aft = +		X	X		X		
19.	Lateral Hub Flapping	627-010-301-1 (Linear Pot)	± 8°	± 12°	Flap Aft = +		X	X				
20.	Collective Tube	627-010-013-1	5,400 Lb	10,000 Lb	Tension = +	X	X	X		X		
21.	Swashplate Drive Sideload	627-010-415-1	45 Lb	75 Lb	Tension Forward Surface = +		X	X		X		
22.	Blade Fold Position	627-010-102-2 (Rotary Pot to Blade)	90°	100°	Fold Aft = +		X	X		X	X	
23.	Rotor RPM - Generator	627-018-012 (Mast to Pylon Pulley)	460-540	600	Rotor RPM = +					X		
24.	Rotor RPM/Azimuth-Mag Pickup and Photo Cell	627-018-012 (Mast to Pylon Pulley)	460-540	600	Rotor RPM = + { Azimuth Mark: 1/REV from Mag Pickup; 6/REV from Photo Cell }		X	X		X		
25.	Hub Spring Temp	627-010-301-1	150°	300° F	Increase Temp = +					X		
	Pylon											
26.	Pod Conversion Link	300-018-028-13	± 1,200 Lb 8,000 Lb	± 2,000 Lb 12,000 Lb	Tension = +	X	X	X				
27.	Pod Yaw Link	300-018-038-3	± 2,000 Lb 15,000 Lb	± 5,000 Lb 25,000 Lb	Tension = +	X	X	X				
28.	Conversion Spindle Yaw	300-018-036-1	±100,000 In-Lb	±200,000 In-Lb	Top Surface of Spindle in Comp = +	X	X	X				
29.	Accelerometer - Vert. Fwd.	300-018-005-1	± 1.5 g	± 3 g	Up = +	X		X				X
30.	Accelerometer - Horiz. Fwd.	300-018-005-1	± 1.5 g	± 3 g	Outboard = +	X		X				
31.	Accelerometer - Vert. Aft	300-018-017	± 1.5 g	± 3 g	Up = +	X		X				X
32.	Accelerometer - Horiz. Aft	300-018-017	± 1.5 g	± 3 g	Outboard = +	X		X				X
33.	Accelerometer - Axial	300-018-005-1	± 1.5 g	± 3 g	Aft = +	X		X				X
	Wing											
34.	Wing Root Beam	300-018-015-1	±133,000 In-Lb 1,000K In-Lb	±250,000 In-Lb 1,300K In-Lb	Wind Bending Up = +	X	X	X		X		
35.	Wing Root Chord	300-018-015-1	±150,000 In-Lb	±250,000 In-Lb	L.E. in Tension = +	X	X	X				
36.	Wing Root Torsion	300-018-015-1	100K In-Lb	200K In-Lb	L.E. Up = +	X	X	X				
	Miscellaneous / Low Press											
37.	Hydraulic Press / Warning	627-018-010	3,000 psi	4,500 psi	Increase Press = + { Warning Light }					X		
38.	Air Press	627-018-010	20 psi	50 psi	Increase Press = + { Below 2000 psi }					X		

BELL HELICOPTER COMPANY

Use or disclosure of data on this page is subject to the restriction on the title page.

Use or disclosure of data on this page is subject to the restriction on the title page.

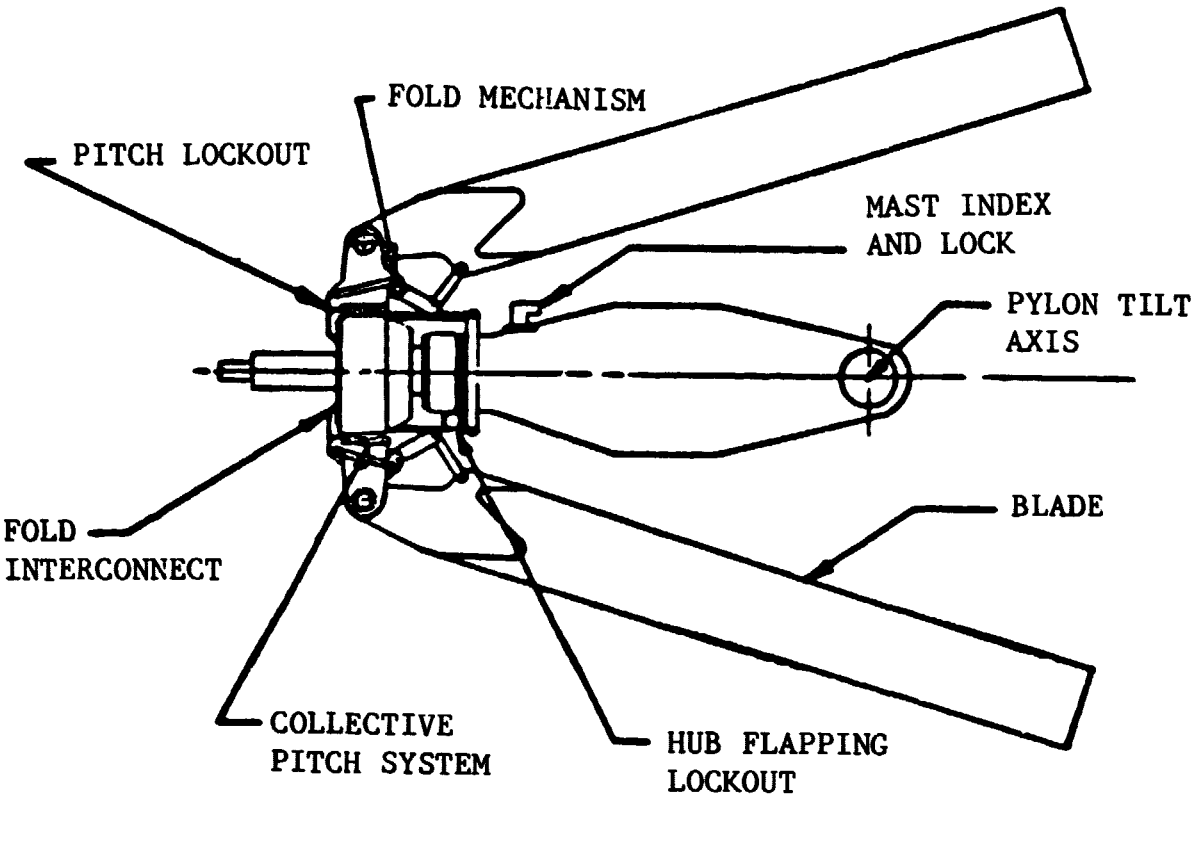


Figure V-1. Schematic of Model 627 Folding Proprotor.

Use or disclosure of data on this page is subject to the restriction on the title page.

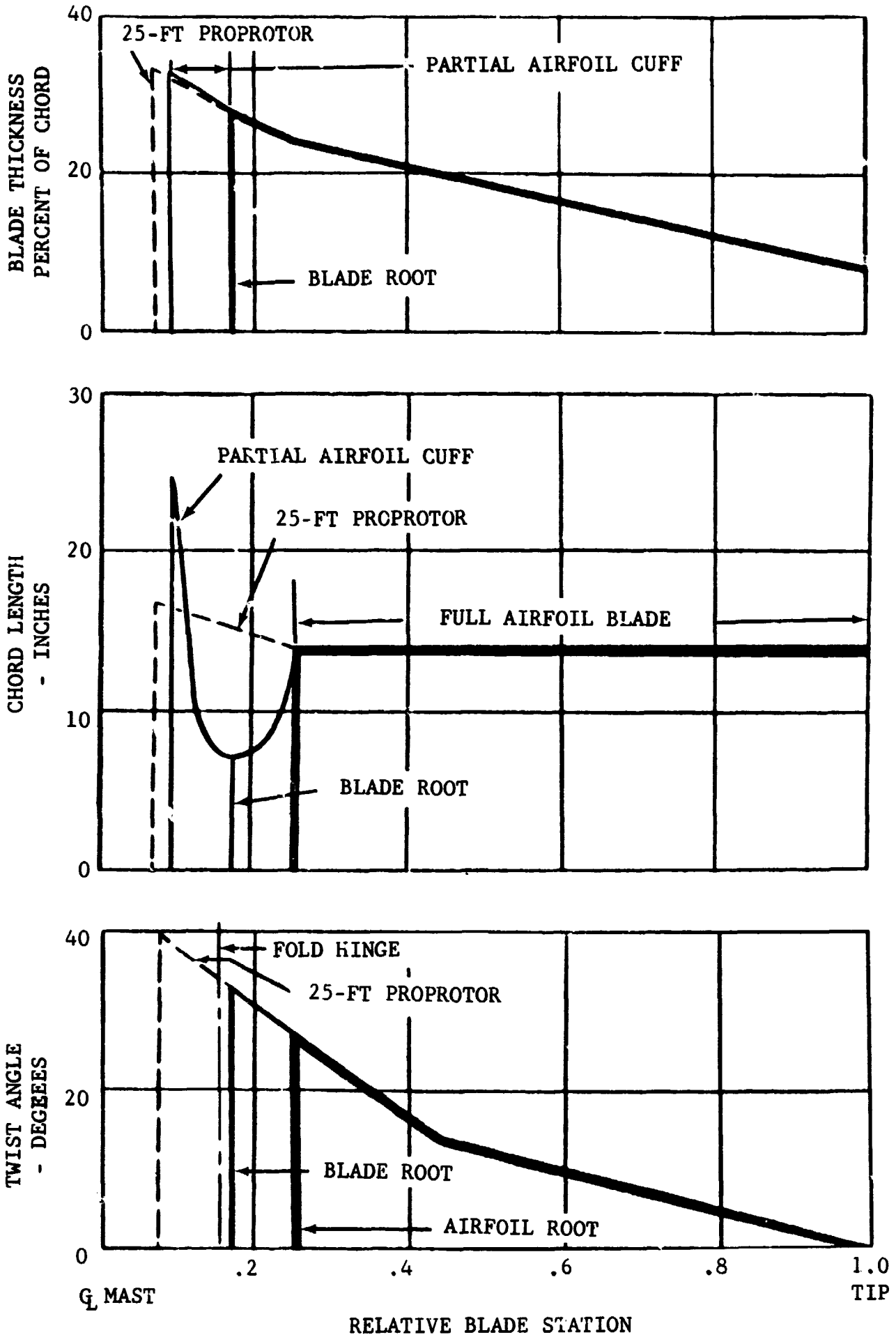


Figure V-2. 25-Foot Folding Proprotor Blade Geometry.

REPRODUCIBILITY OF THE ORIGINAL PAGE IS POOR.

Use or disclosure of data on this page is subject to the restriction on the title page.

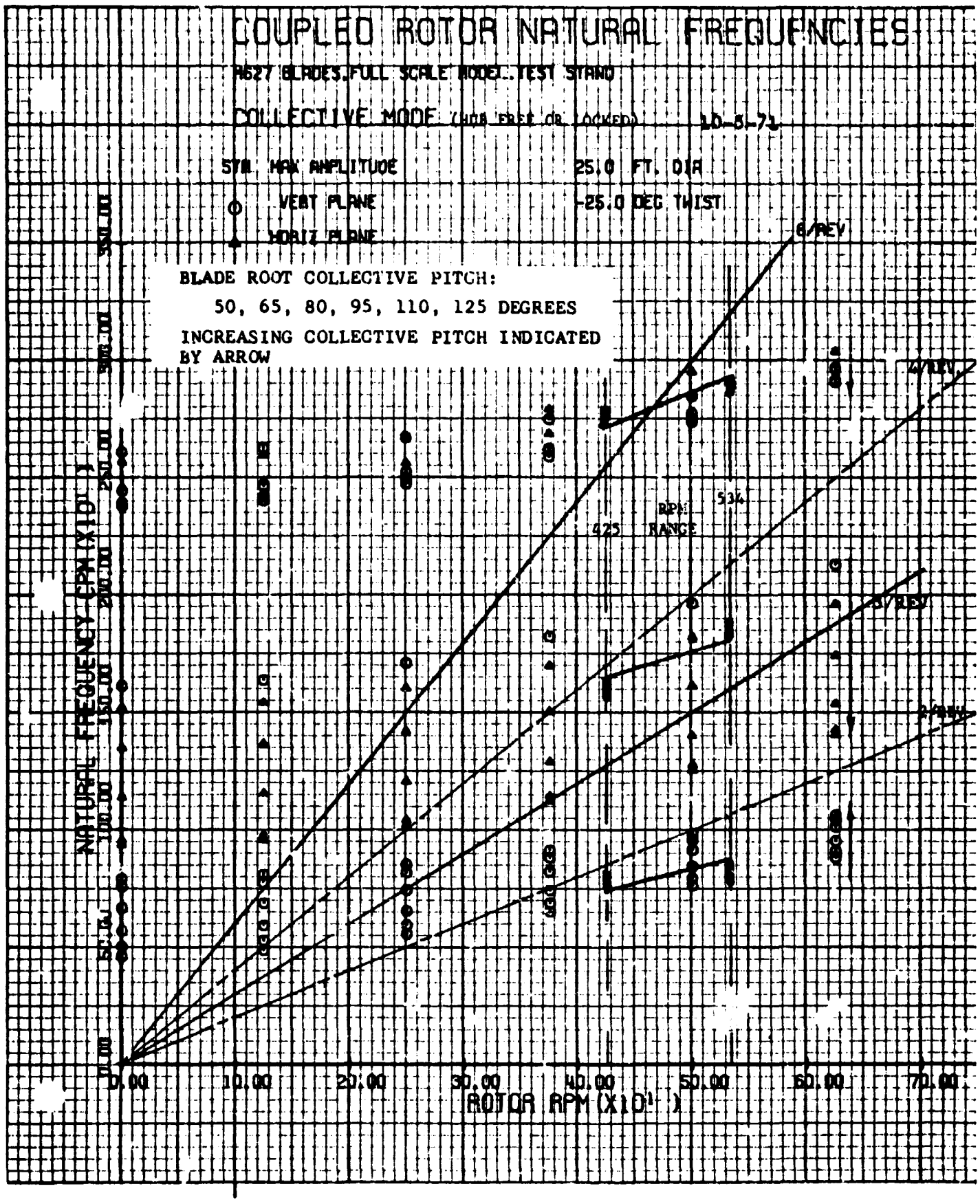


Figure V-3. Model 627 Folding Proprotor Collective Mode Natural Frequencies.

REPRODUCIBILITY OF THE ORIGINAL PAGE IS POOR

Use or disclosure of data on this page is subject to the restriction on the title page

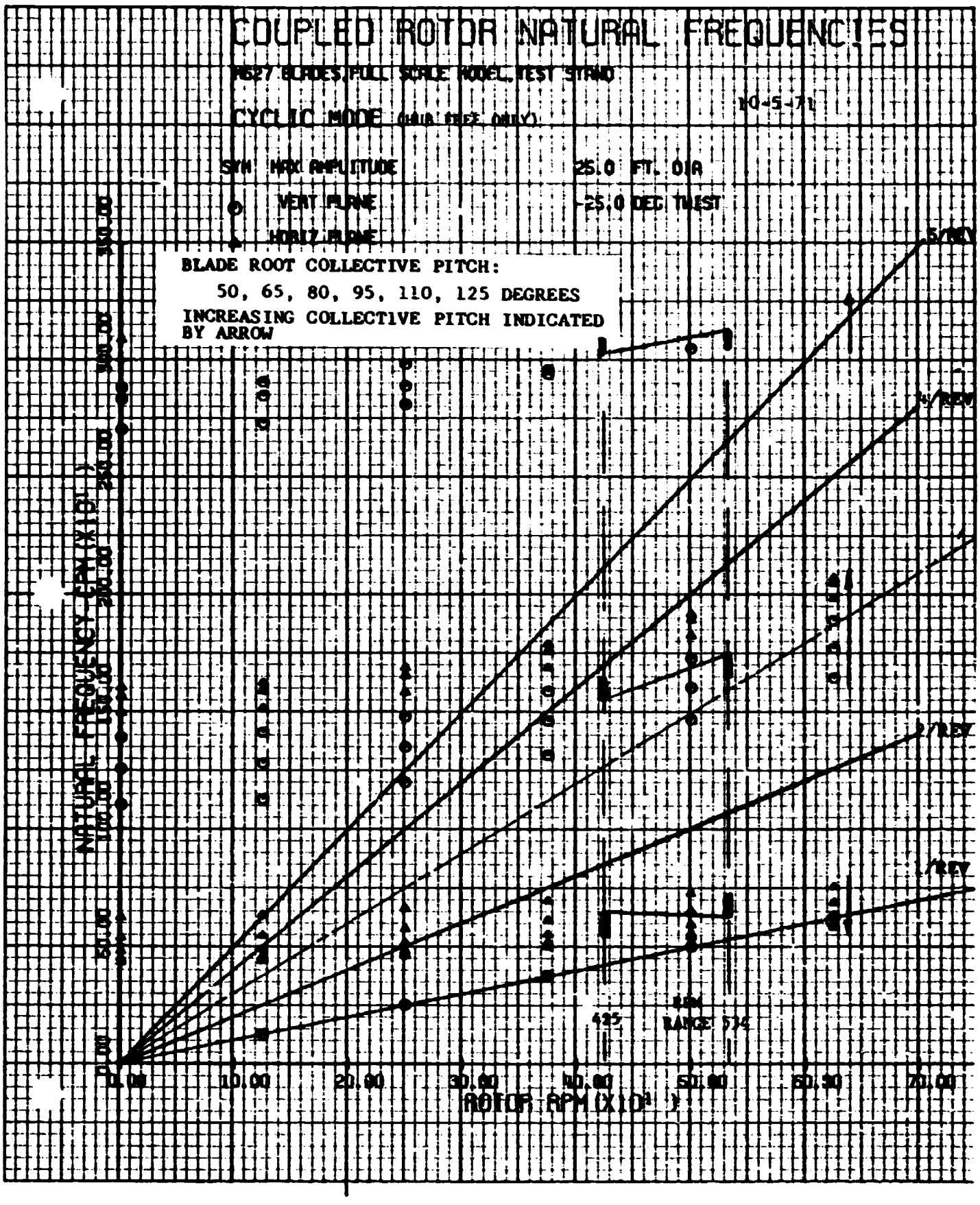


Figure V-4. Model 627 Folding Proprotor Cyclic Mode Natural Frequencies.

C-2

REPRODUCIBILITY OF THE ORIGINAL PAGE IS POOR

Use or disclosure of data on this page is subject to the restriction on the title page

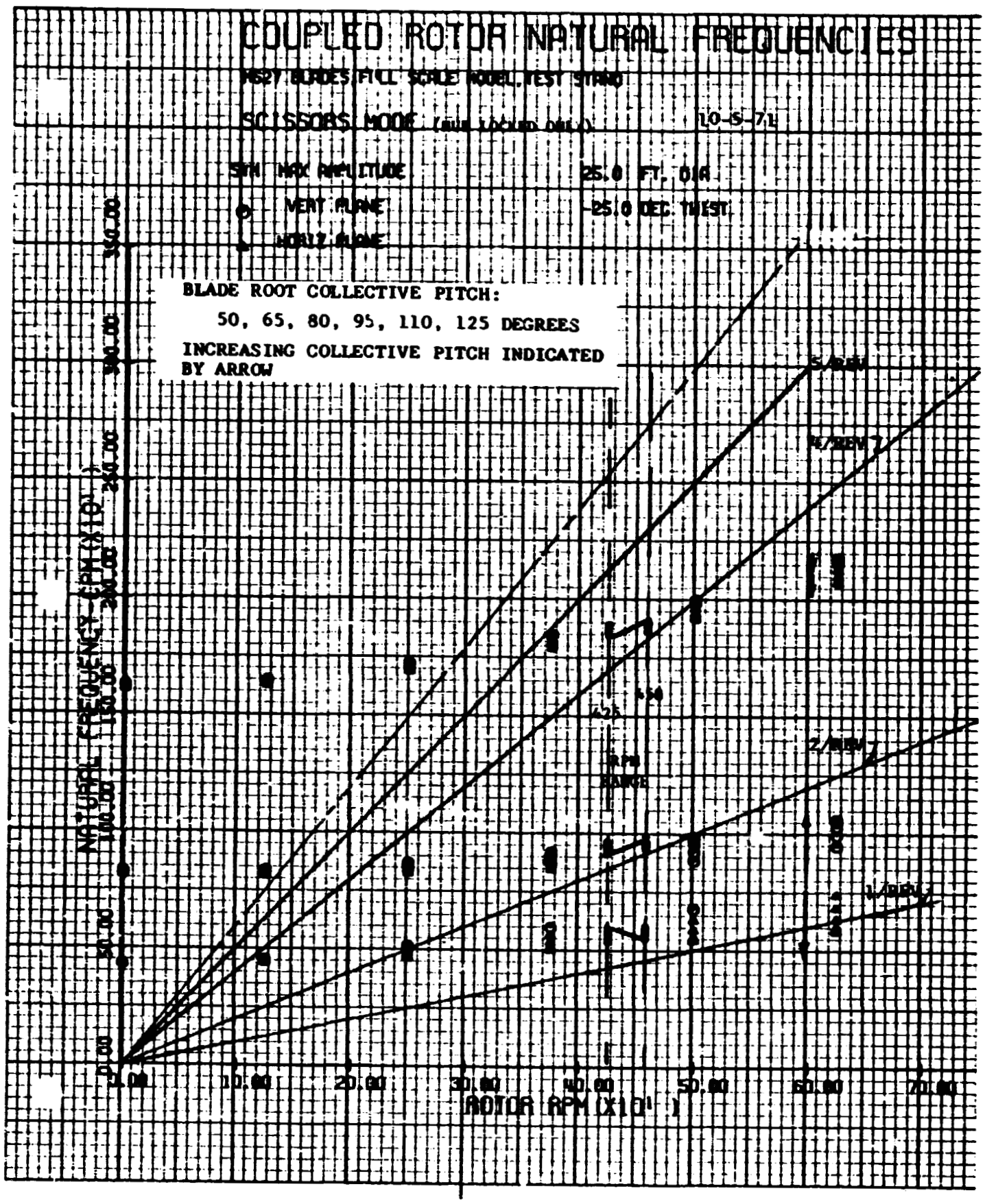


Figure V-5. Model 627 Folding Proprotor Scissors Mode Natural Frequencies.

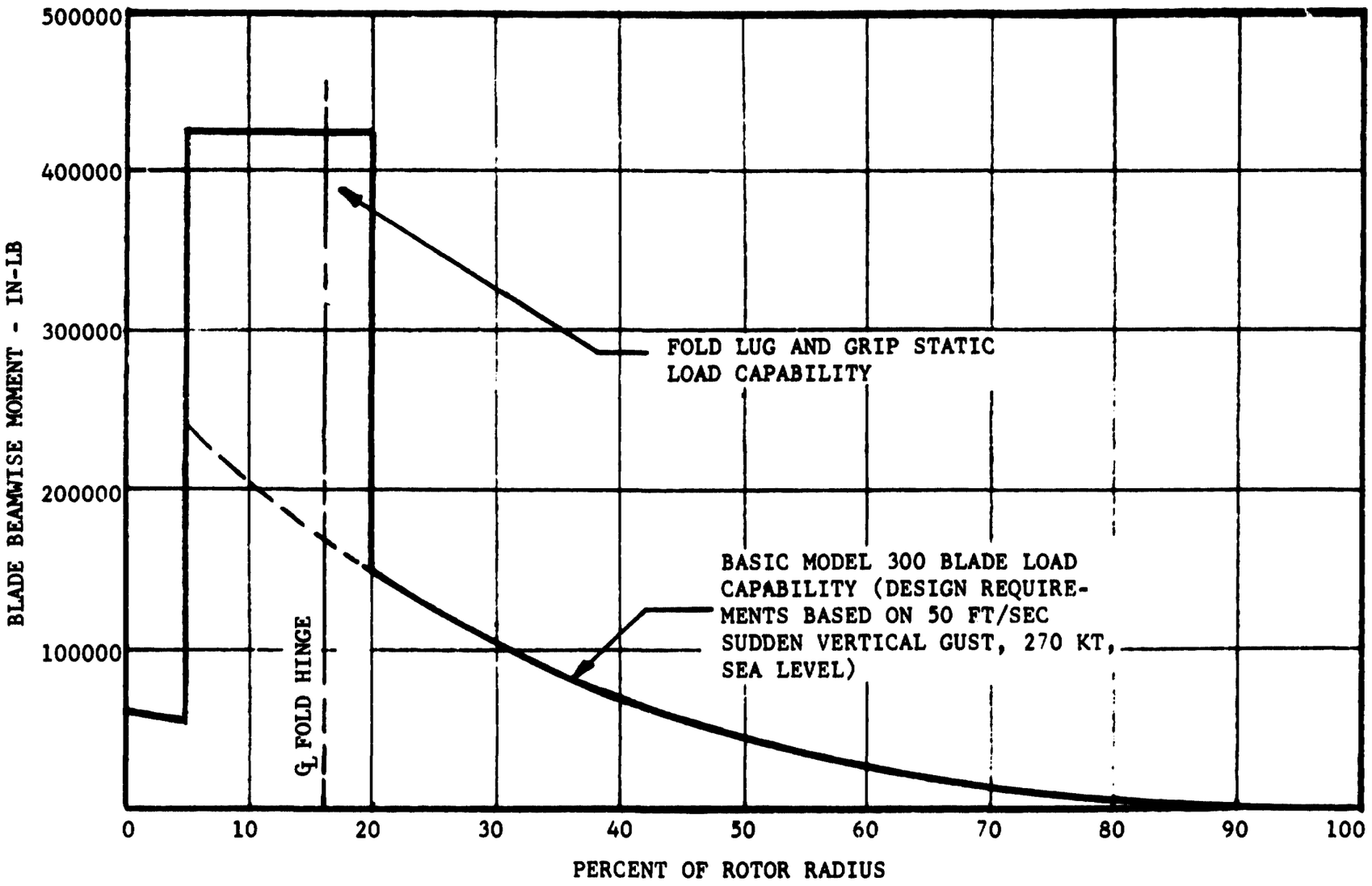


Figure V-6. Model 627 Blade Beamwise Limit Load Capability.

BELL HELICOPTER COMPANY

Use or disclosure of data on this page is subject to the restriction on the title page.

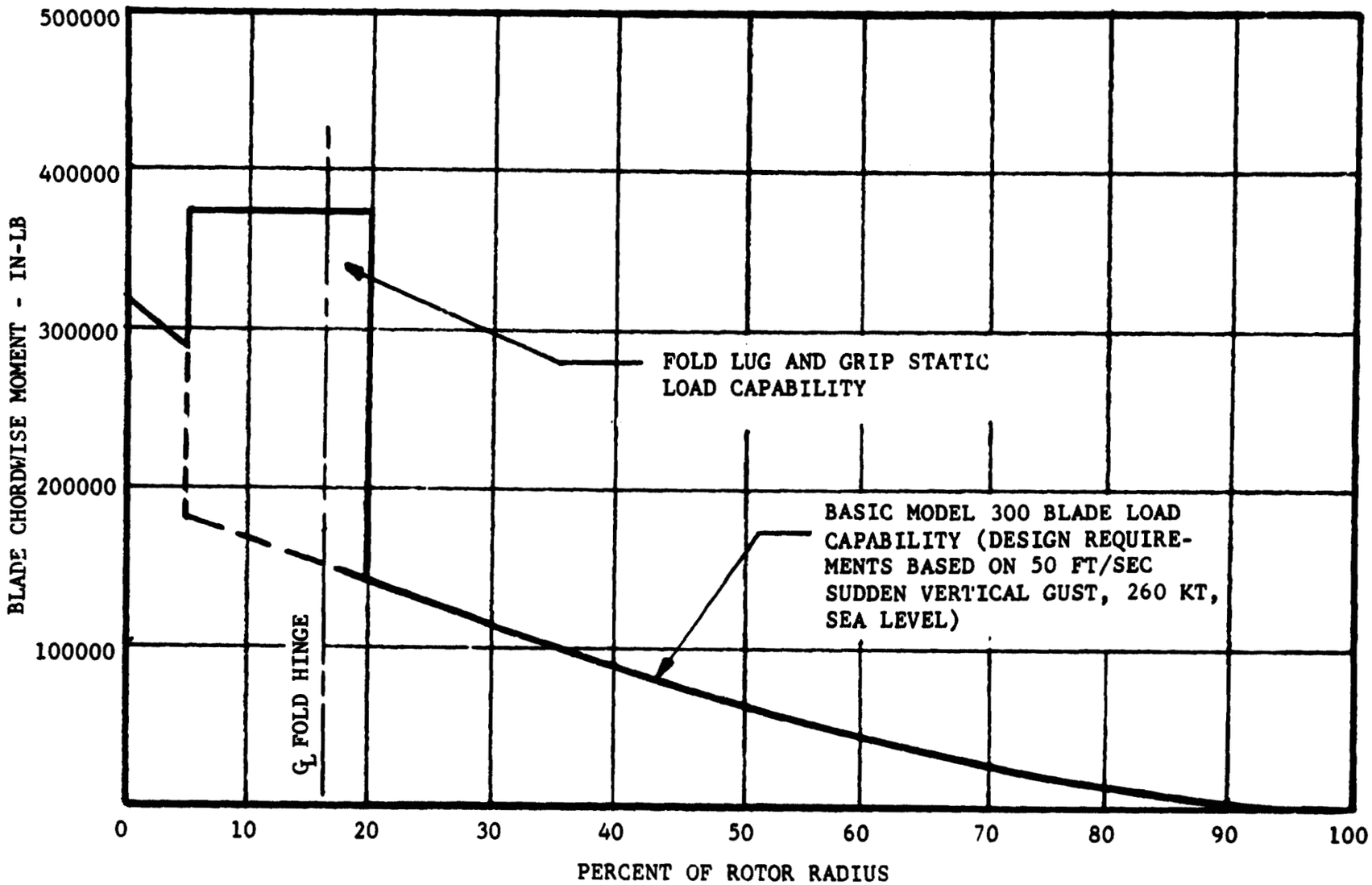


Figure V-7. Model 627 Blade Chordwise Limit Load Capability.

BELL HELICOPTER COMPANY

Use or disclosure of data on this page is subject to the restriction on the title page.

REPRODUCIBILITY OF THE ORIGINAL PAGE IS POOR.

Use or disclosure of data on this page is subject to the restrictions on the title page.

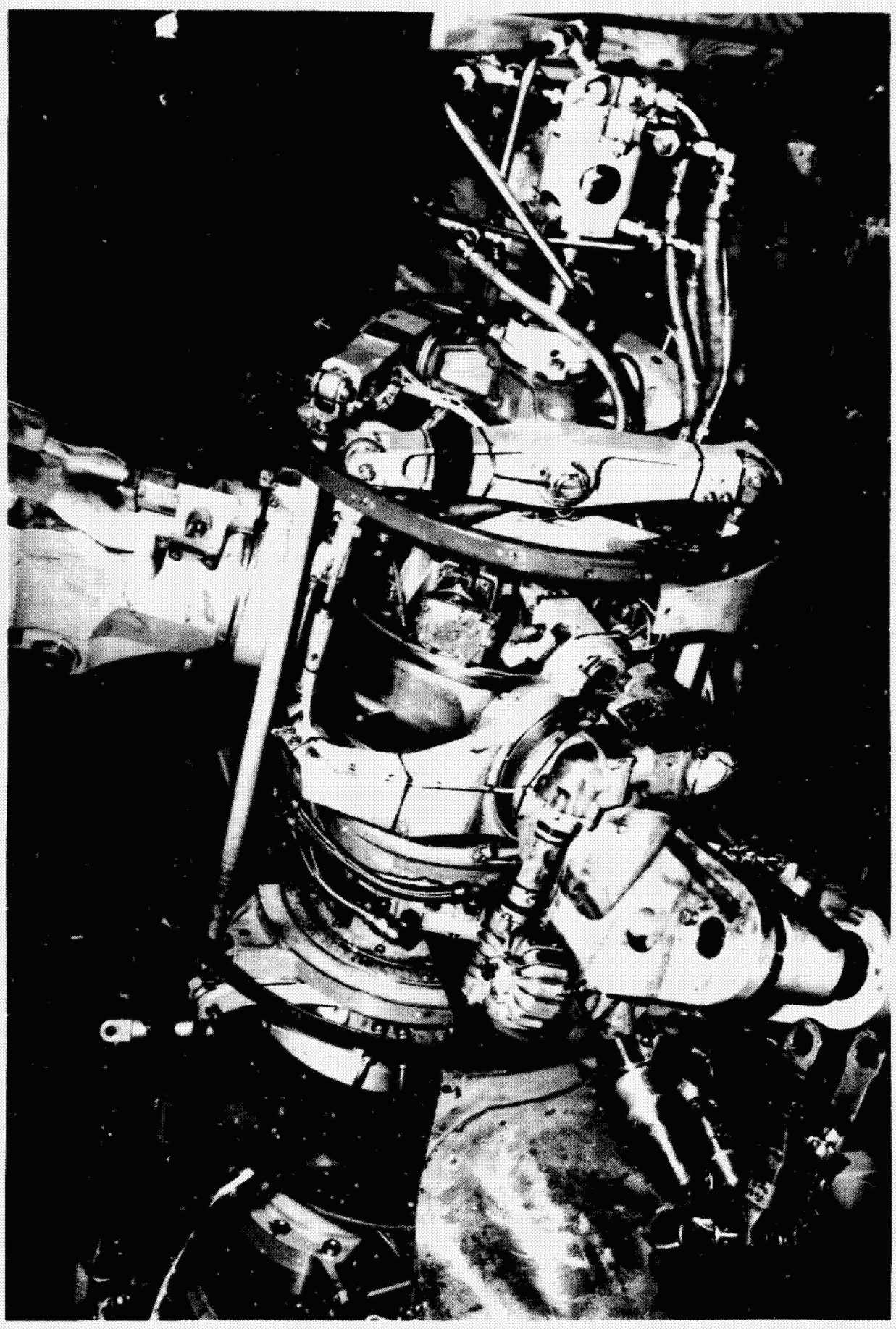
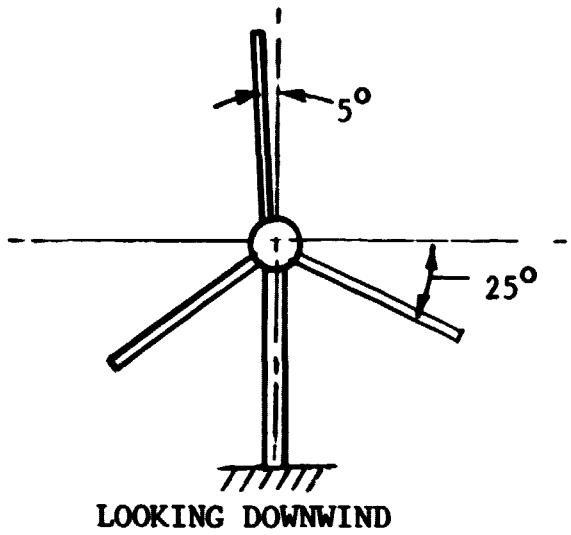


Figure V-8. Model 627 Folding Proprotor Hub, Controls, and Fold Mechanism.

Use or disclosure of data on this page is subject to the restriction on the title page.



LOOKING DOWNWIND

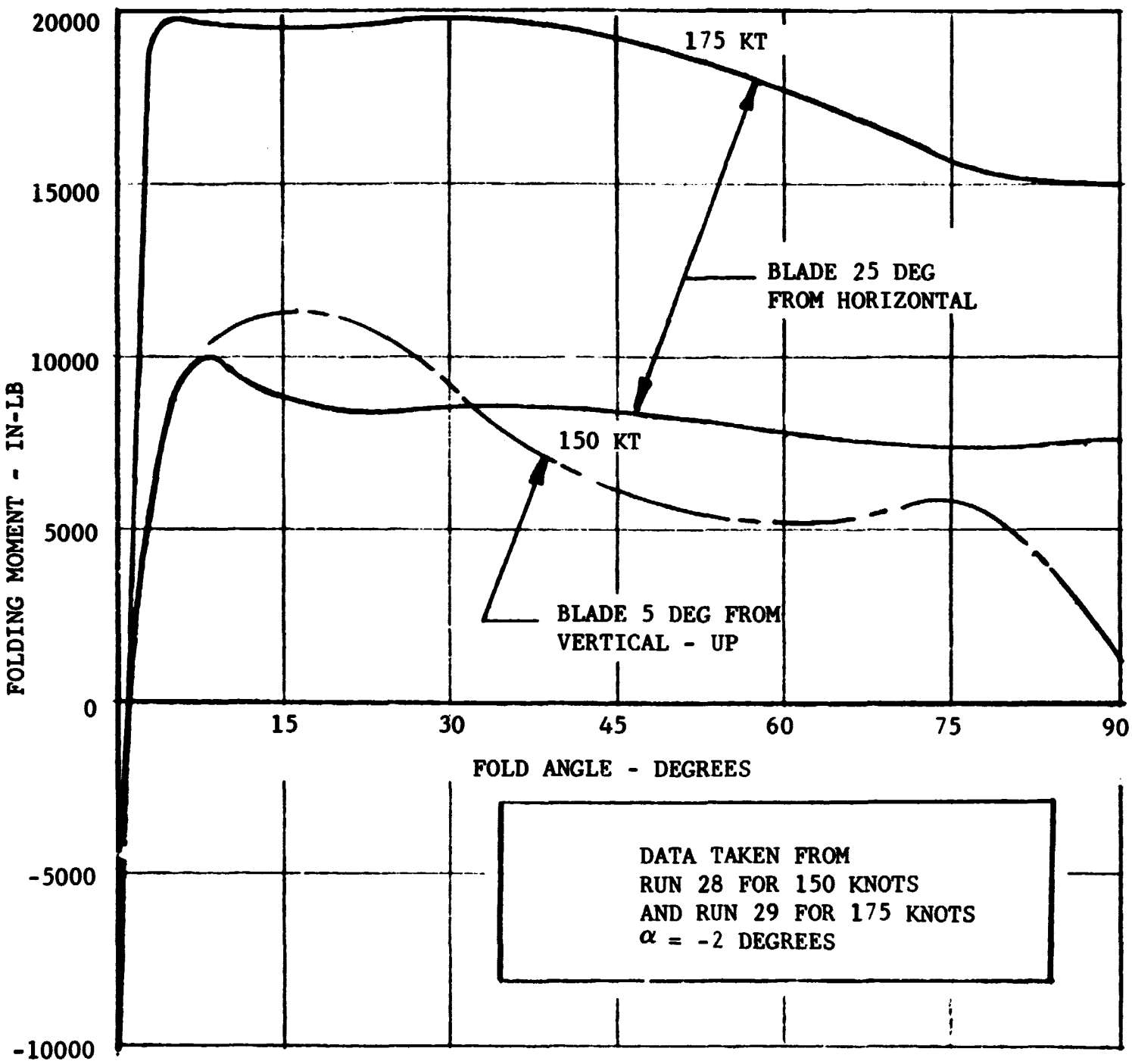


Figure V-9. Folding Moment at Hinge Centerline.

Use or disclosure of data on this page is subject to the restriction on the title page.

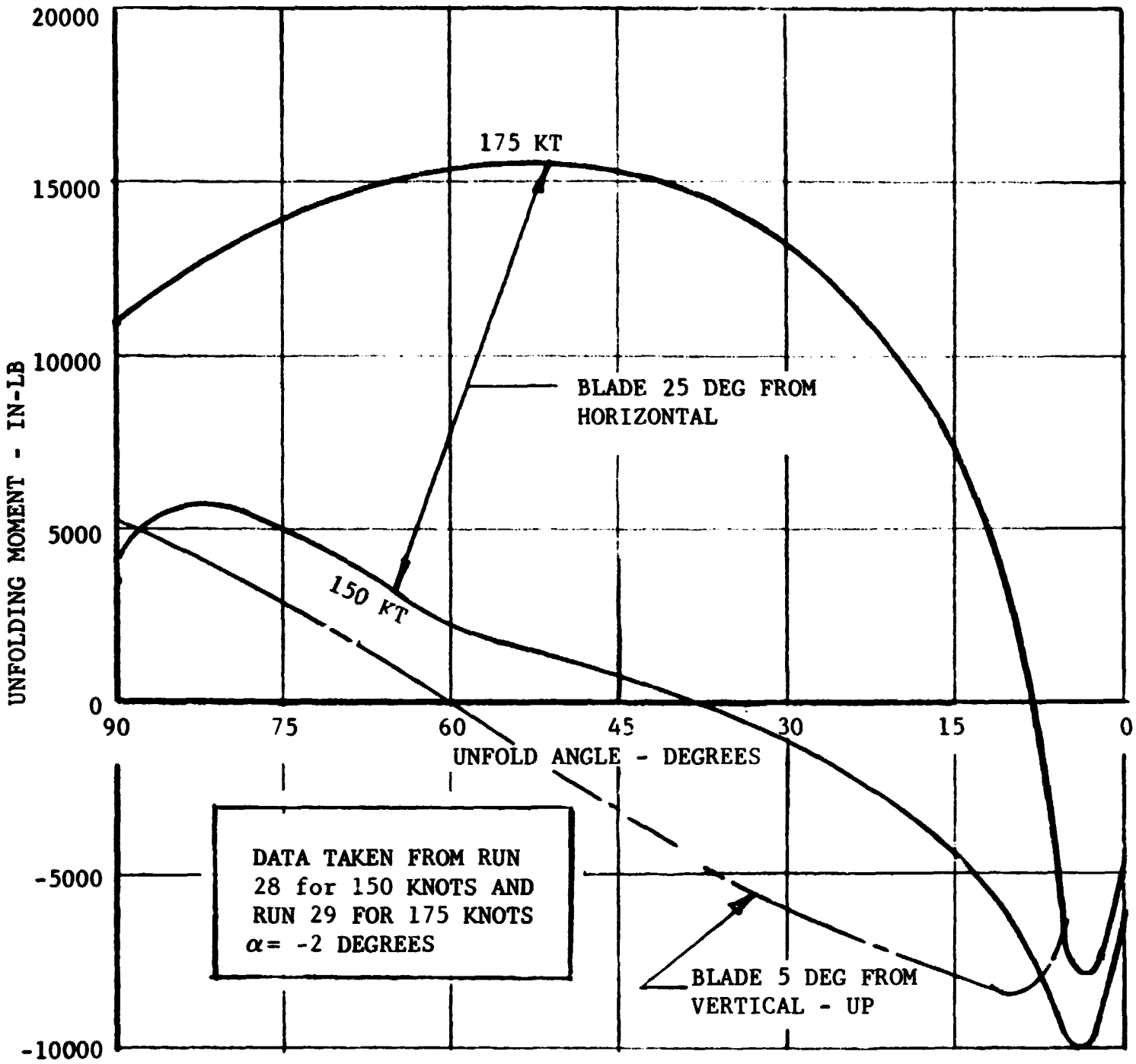


Figure V-10. Unfolding Moment at Hinge Centerline.

REPRODUCIBILITY OF THE ORIGINAL PAGE IS POOR.

Use or disclosure of data on this page is subject to the restriction on the title page.

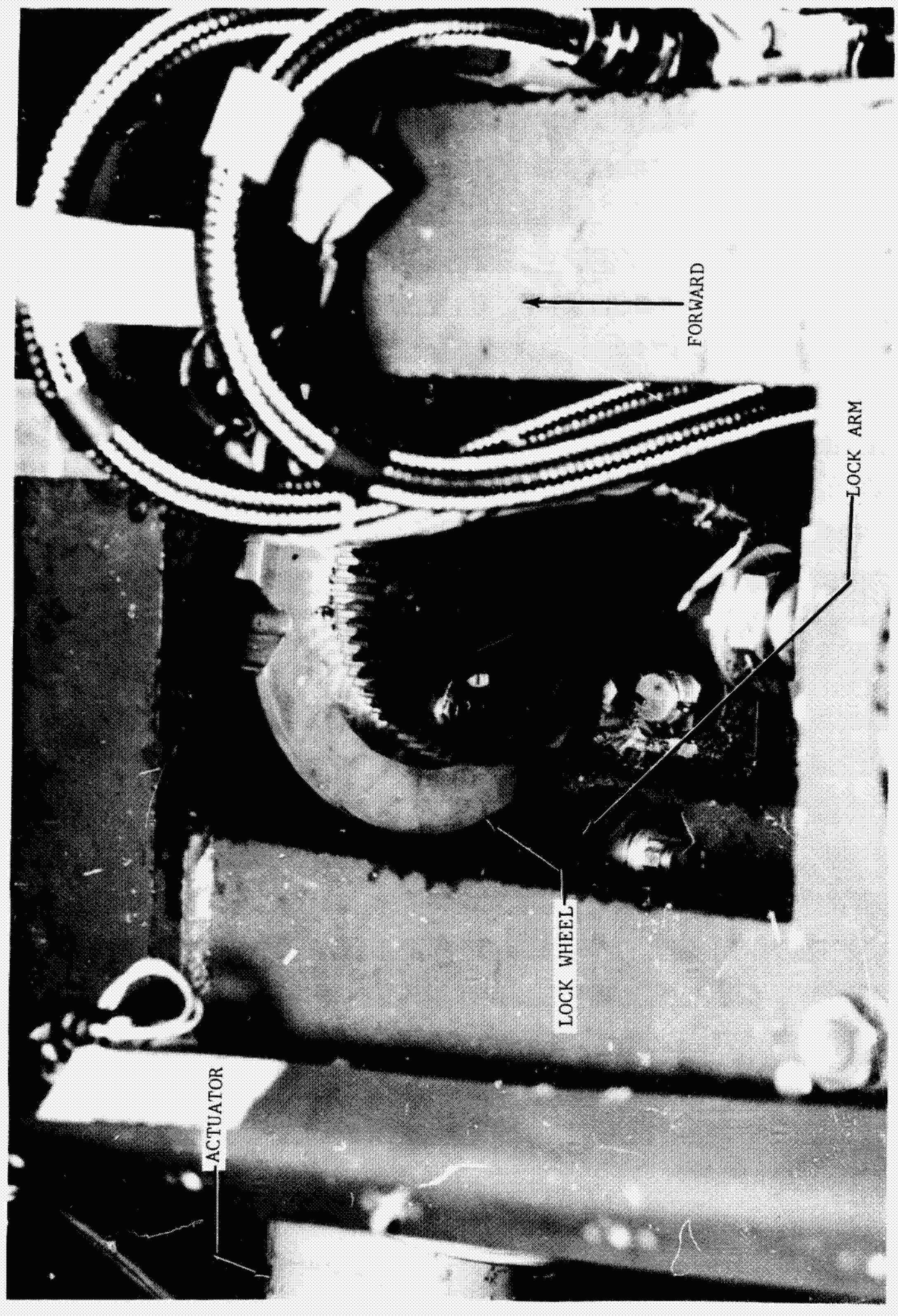


Figure V-11. Model 627 Folding Proprotor Mast Index Lock.

REPRODUCIBILITY OF THE ORIGINAL PAGE IS POOR.

Use or disclosure of data on this page is subject to the restriction on the title page.

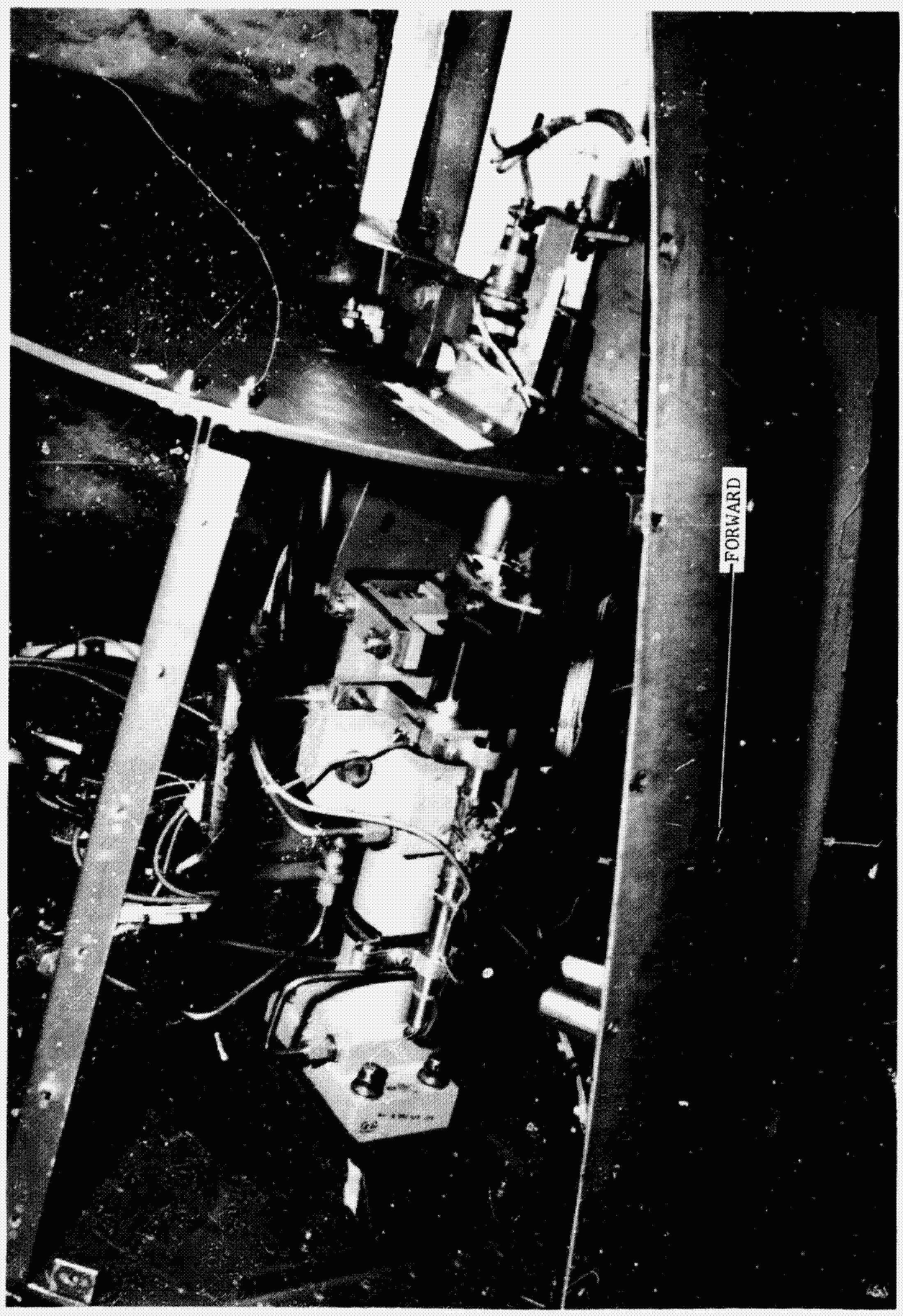


Figure V-12. Model 627 Folding Proprotor Collective Actuator and Boost Cylinder.

REPRODUCIBILITY OF THE ORIGINAL PAGE IS POOR.

Use or disclosure of data on this page is subject to the restriction on the title page.

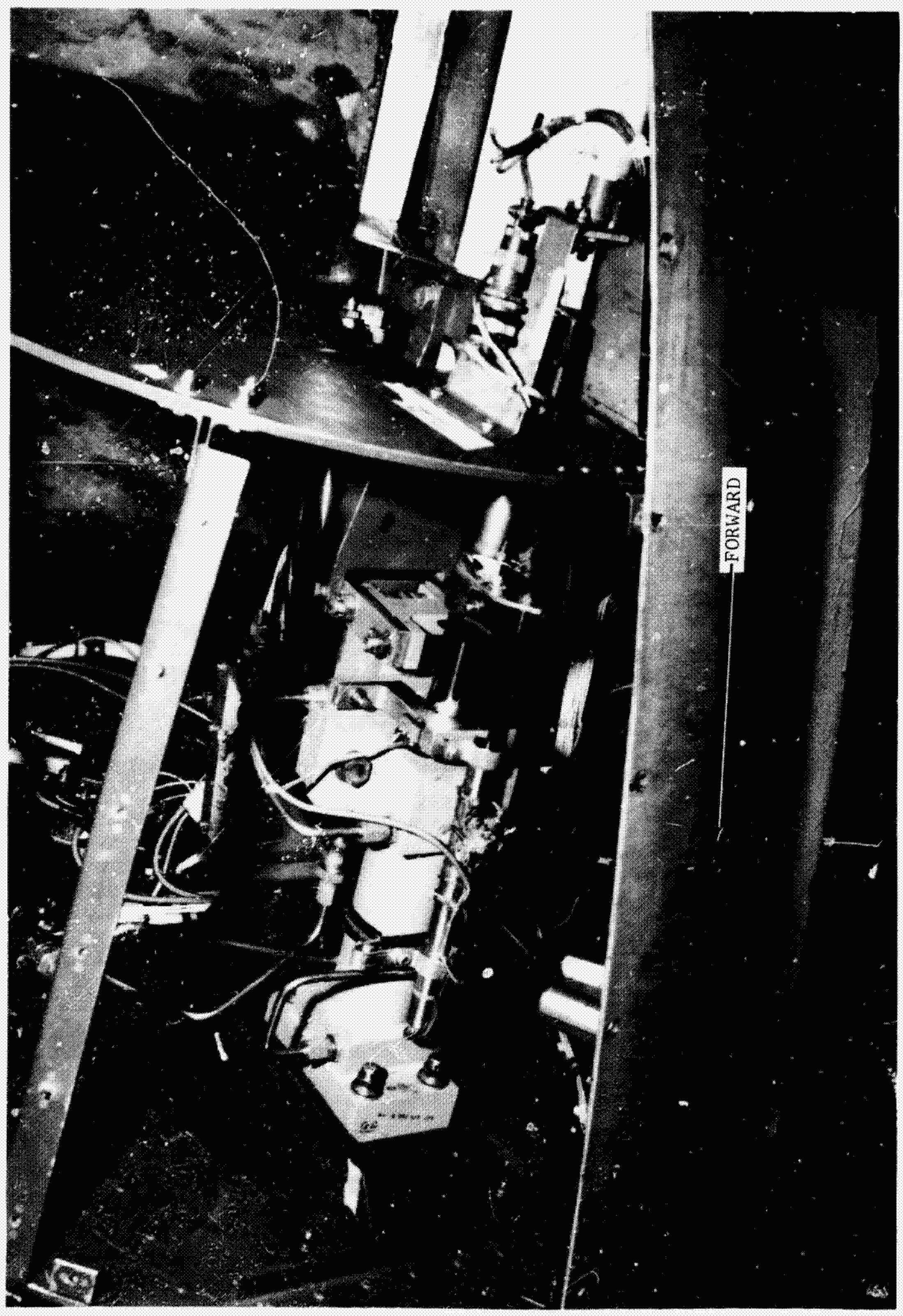


Figure V-12. Model 627 Folding Proprotor Collective Actuator and Boost Cylinder.

Use or disclosure of data on this page is subject to the restriction on the title page.

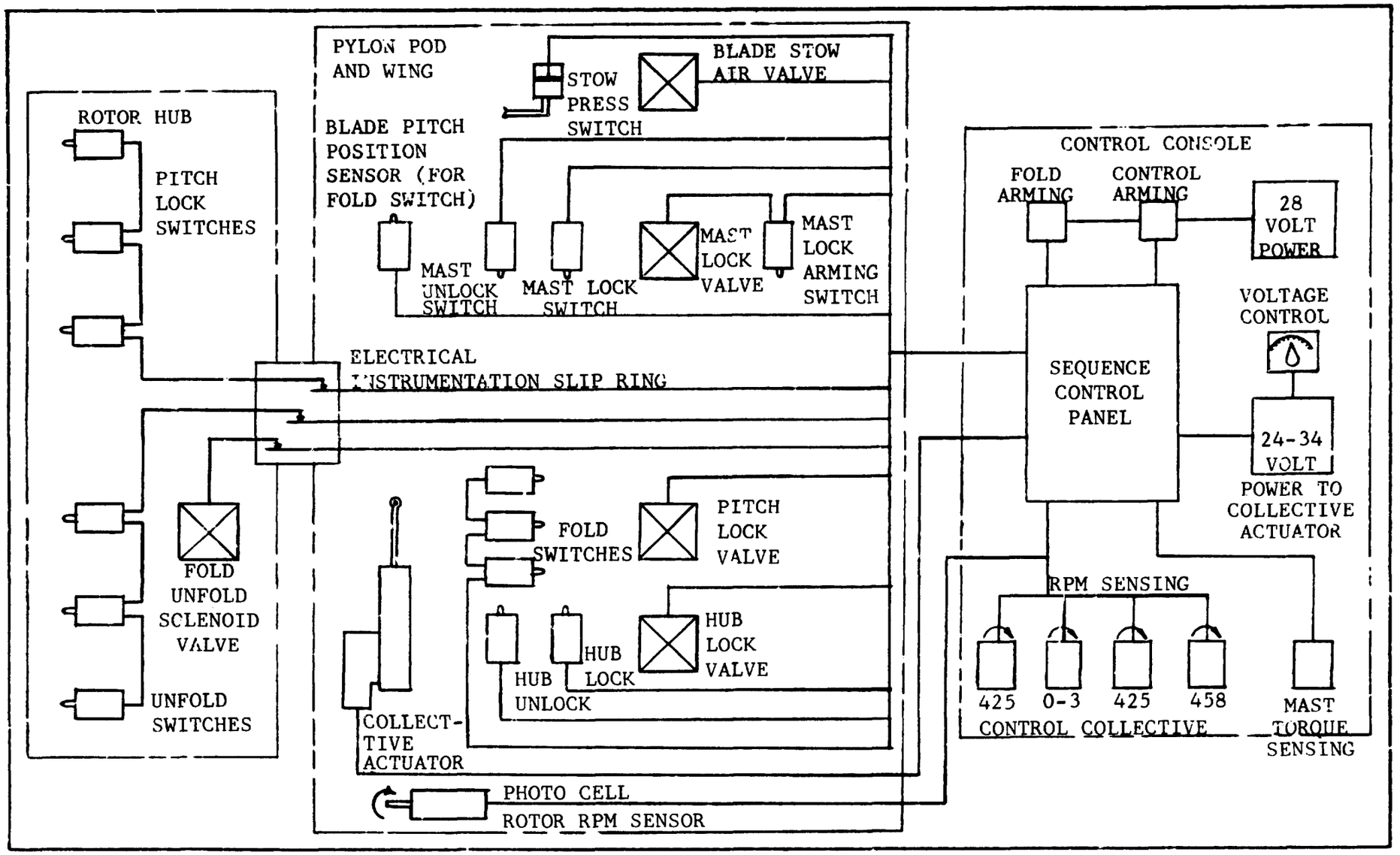


Figure V-13. Model 627 Folding Proprotor on Whirl Test Stand.

Use or disclosure of data on this page is subject to the restriction on the title page.



Figure V-13. Model 627 Folding Proprotor on Whirl Test Stand.



BELL HELICOPTER COMPANY

Use or disclosure of data on this page is subject to the restriction on the title page

Figure V-14. Model 627 Folding Proprotor Actuation Control Diagram.

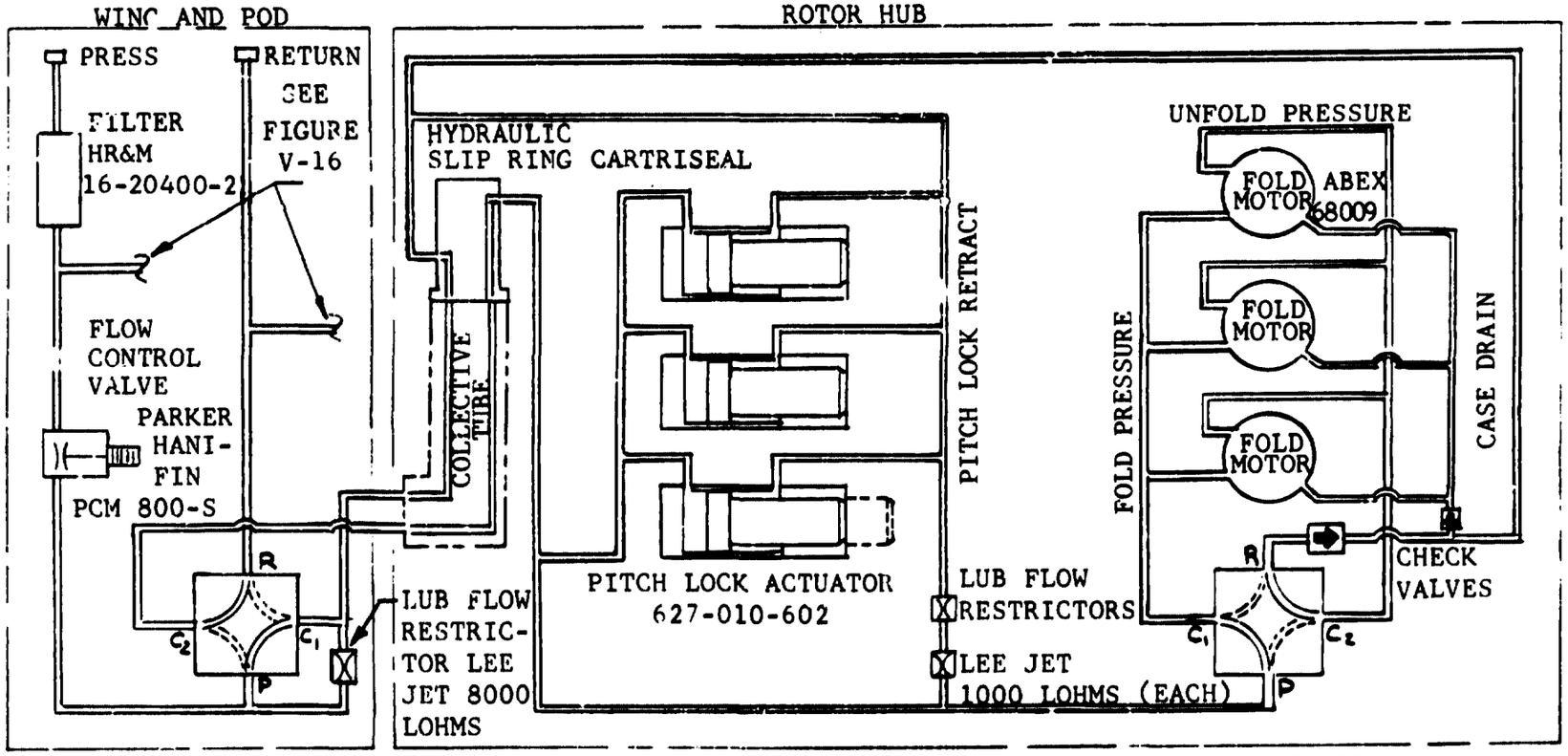


Figure V-15. Model 627 Test Hydraulic System, Blade Folding and Pitch Locking.

BELL HELICOPTER COMPANY

Use or disclosure of data on this page is subject to the restriction on the title page

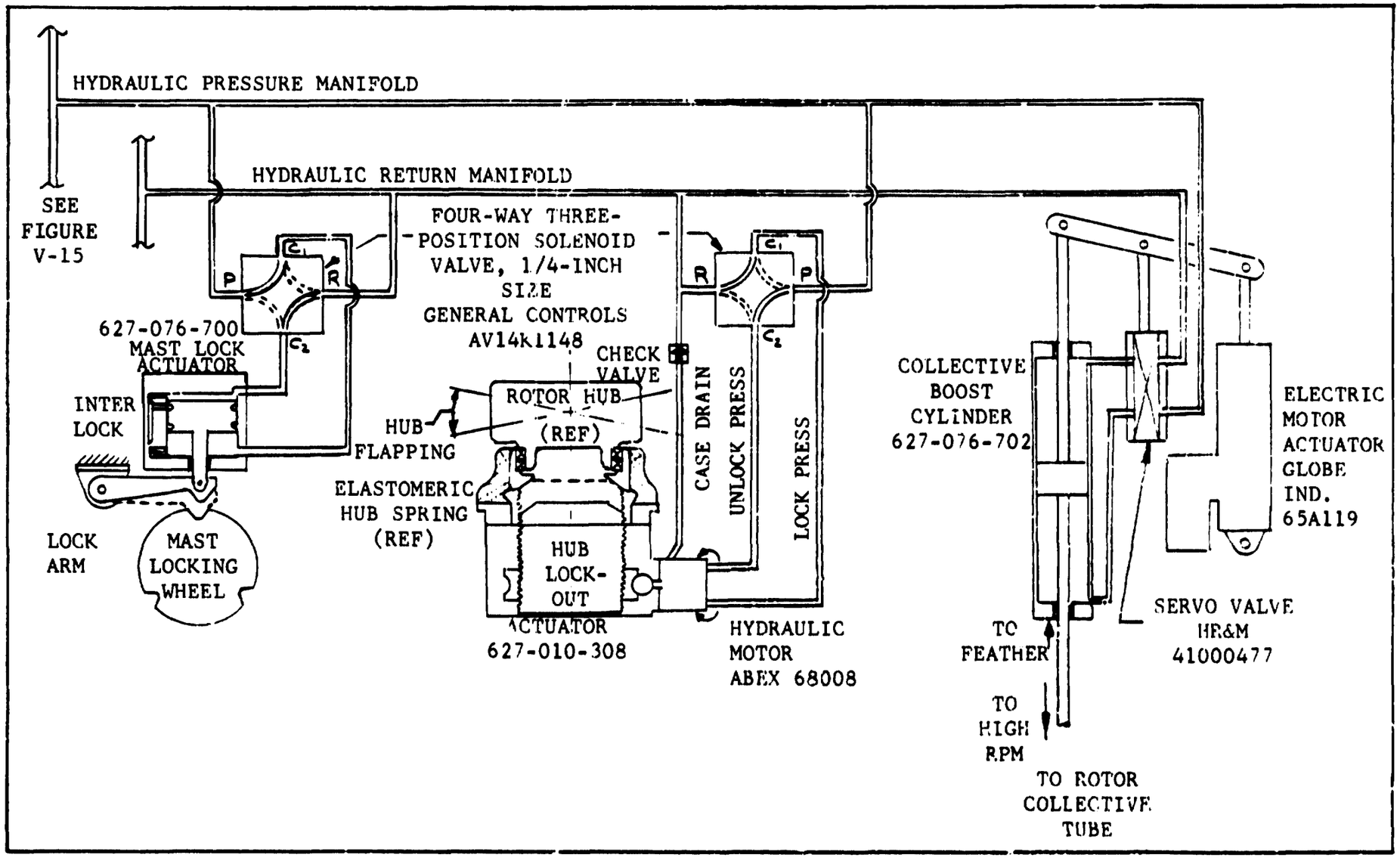


Figure V-16. Model 627 Test Hydraulic System, Hub Locking, Mast Locking, and Collective Actuator.

Use or disclosure of data on this page is subject to the restriction on the title page

Use or disclosure of data on this page is subject to the restriction on the title page.

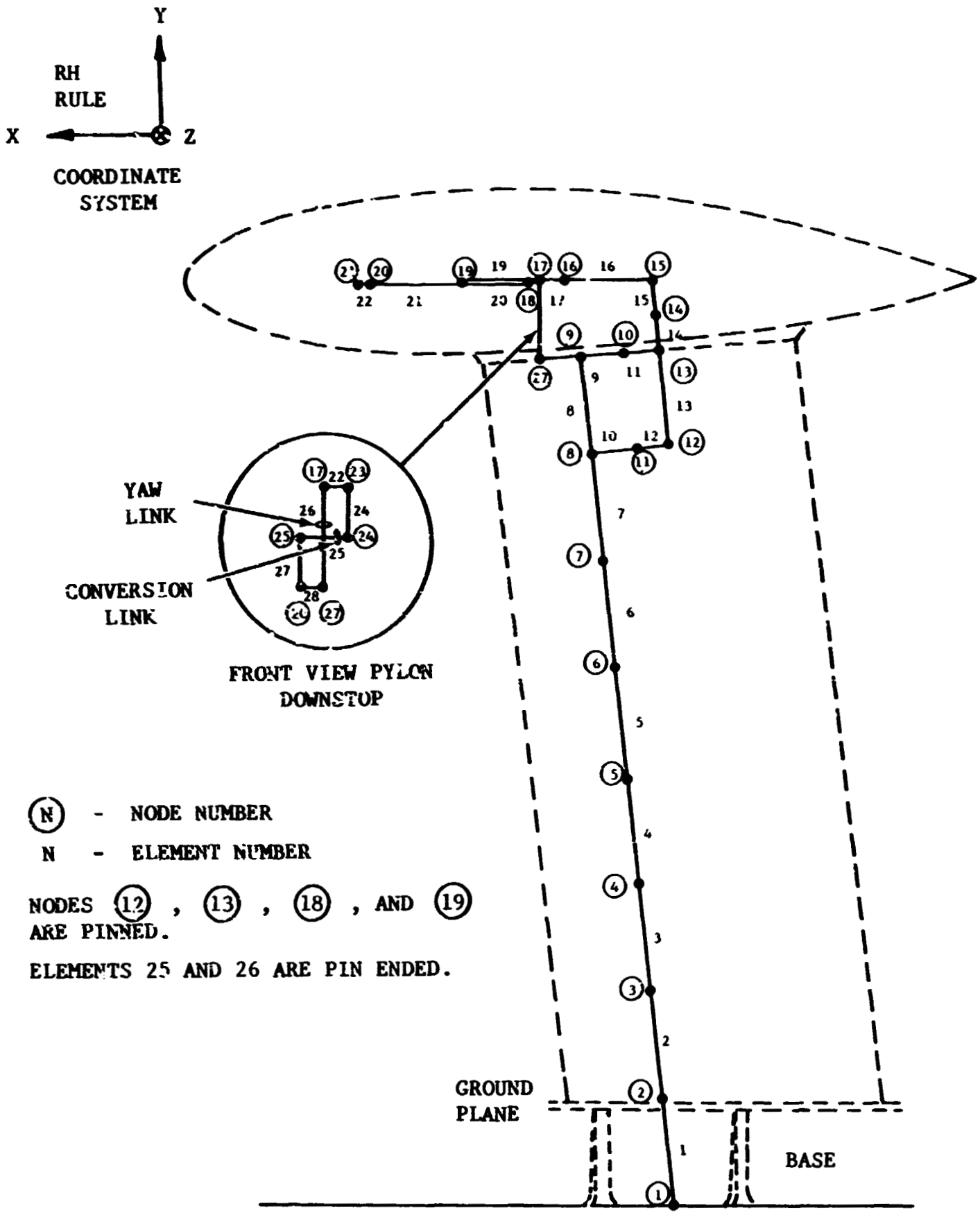


Figure V-17. NASTRAN Structural Model of Model 627 Rotor on Dynamic Test Stand.

Use or disclosure of data on this page is subject to the restriction on the title page.

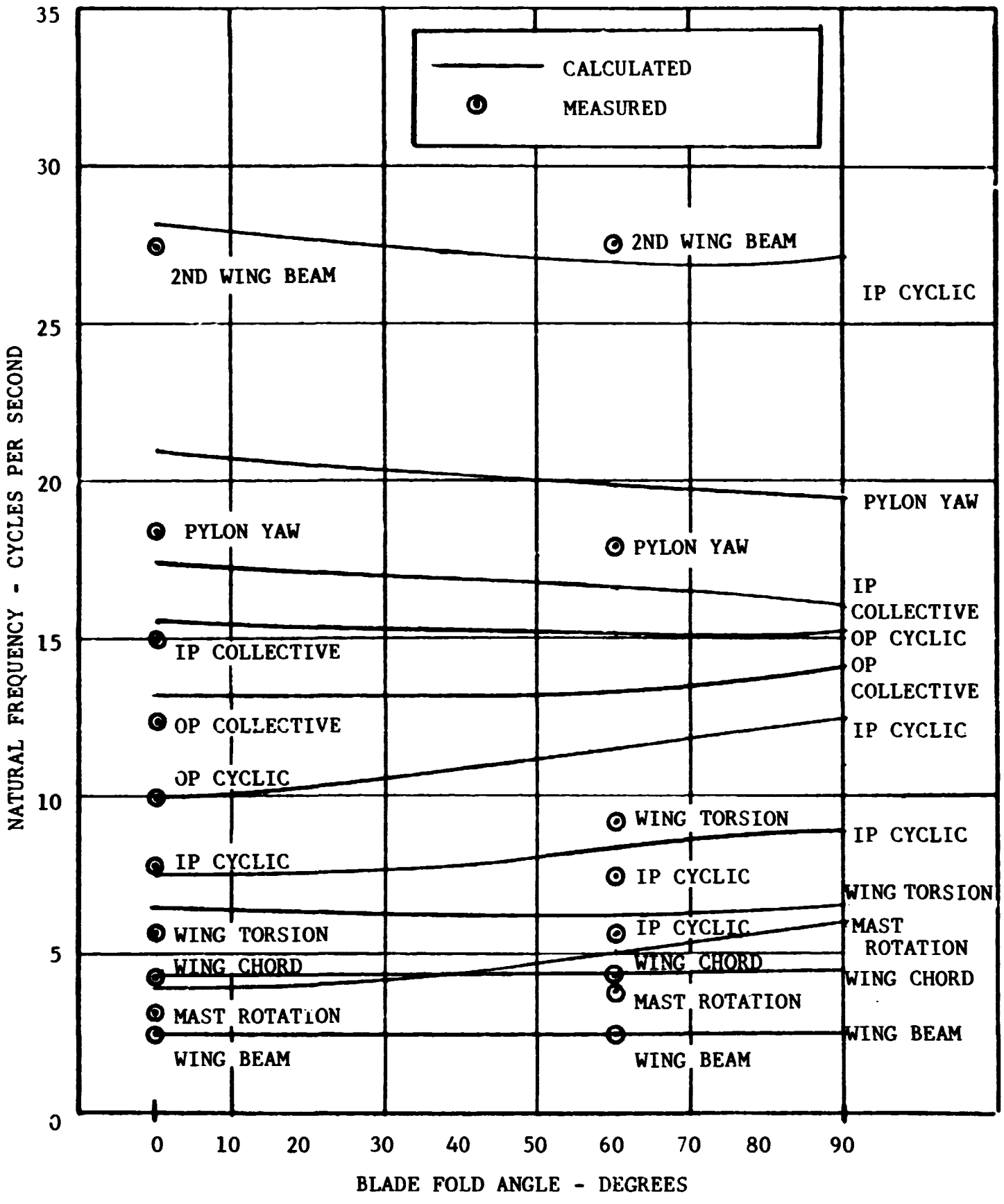


Figure V-18. Model 627 Folding Proprotor Dynamic Test Stand with Pylon Yaw, Hub Flapping, and Mast Rotation Locked, Blade Root Collective of 126 Degrees.

Use or disclosure of data on this page is subject to the restriction on the title page.

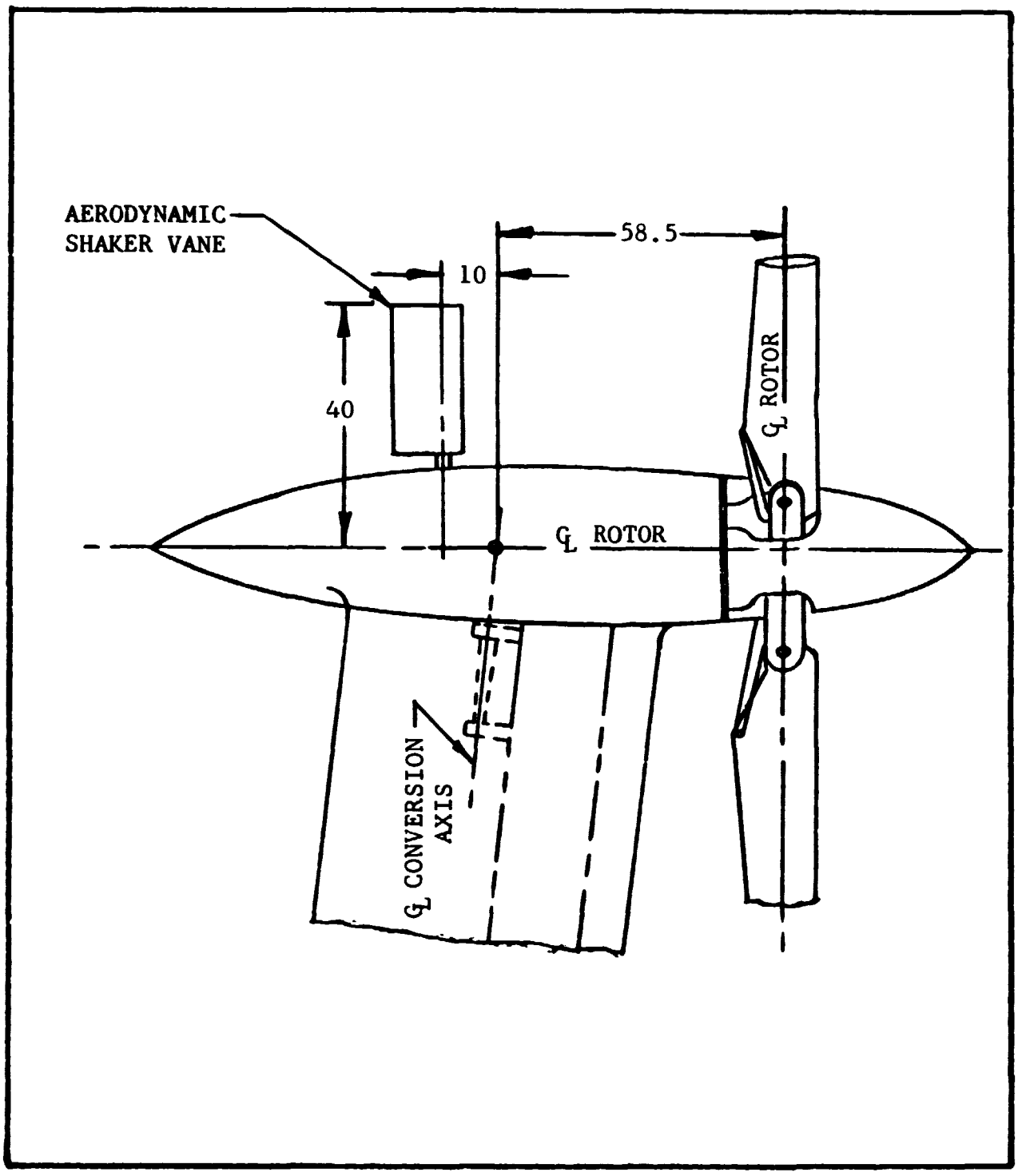


Figure V-19. Test Aerodynamic Shaker Vane Position.

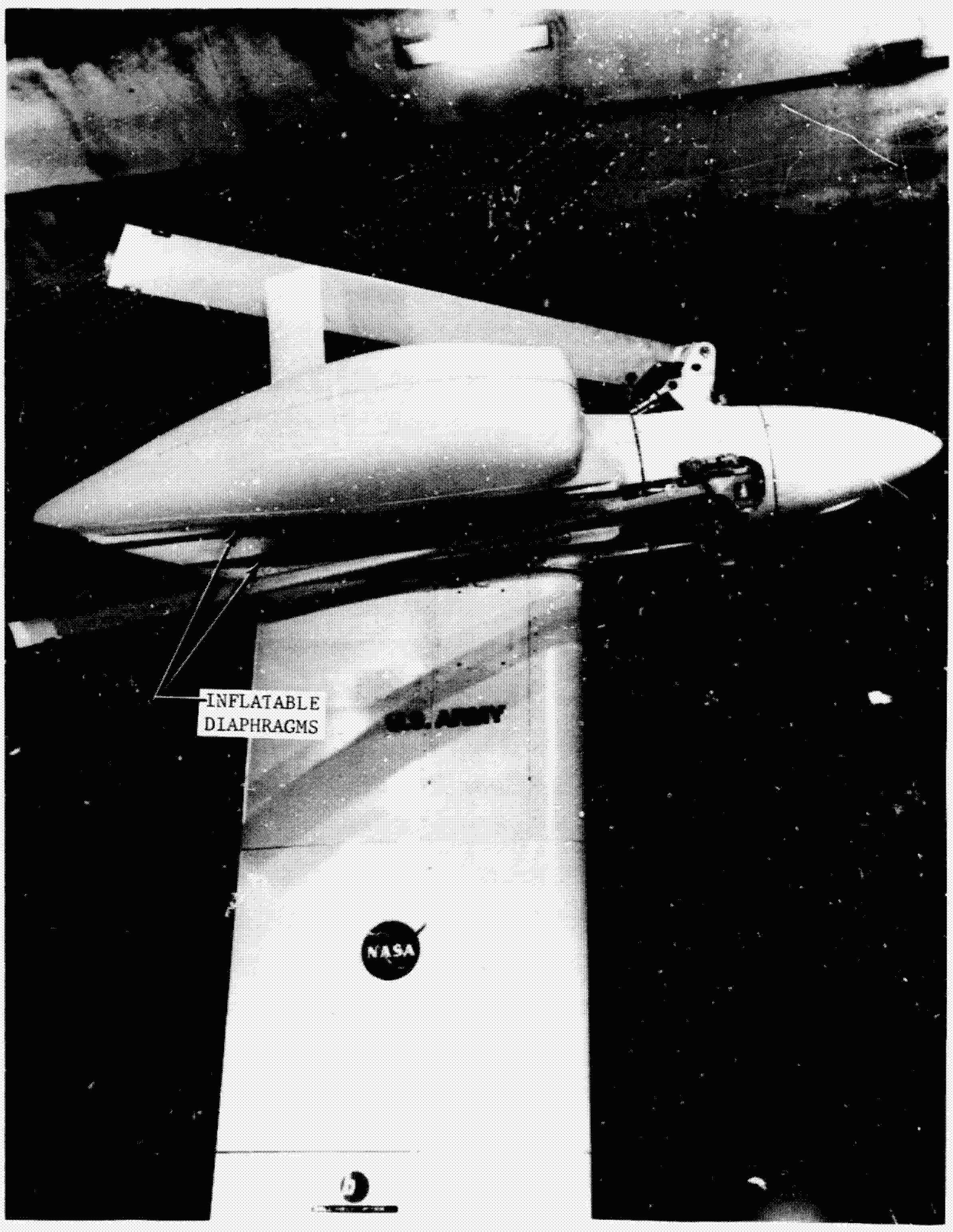


Figure V-20. Model 627 Folding Proprotor Pod with Fold Stow Slots.

Use or disclosure of data on this page is subject to the restriction on the title page.

VI. CONVERSION SEQUENCE DYNAMICS--TEST DATA AND CORRELATION WITH THEORY

A. TEST PROGRAM

Analytical studies of folding proprotor dynamics and small-scale model tests such as those described in References 7, 11, and 14 formed a basis for planning the Model 627 test program. A wind-tunnel test of a one-fifth-scale, semispan, aeroelastic model of the 627 folding proprotor conducted in February 1971 provided an excellent preview of the full-scale test.

These studies and model tests showed that the principal dynamic problems are associated with the stopping and starting events. These are: (1) an increase in blade oscillatory loads when flapping was locked out and a further increase during feathering, and (2) pylon vibrations at the wing natural frequencies during stopping or starting. No significant dynamic problems are associated with blade folding. Because of the relatively low airspeed at which conversion is accomplished, proprotor/pylon instability and flutter are not a problem.

The schedule of runs accomplished during the full-scale wind-tunnel test of February 1972 is shown in Table VI-I. Data on the stability and loads and vibration associated with stopping and starting the proprotor were obtained during the early runs, followed by similar data for blade folding. After mapping the dynamic characteristics of the stop, start and fold/unfold events, the complete conversion sequence was investigated. An investigation of the windmilling drag and the drag variation with blade fold angle was also made. The aerodynamic data from these are presented in the Appendix.

B. DESCRIPTION OF THEORY USED TO PREDICT DYNAMIC CHARACTERISTICS

Prediction of folding-proprotor dynamic stability, loads, and vibration during the conversion sequence was made using Bell Helicopter Company program DYN5. This digital computer program was developed under an Air Force contract (Reference 7) and is available to Government agencies and industry. A complete development of the theory, correlation with small-scale model data, and the program FORTRAN listing and input format is presented in AFFDL-TR-71-7 (Reference 11). A brief description of the program follows:

> Program DYN5 is a nonlinear, open-form aeroelastic analysis that may be used to calculate dynamic stability, loads, and vibrations in helicopter, conversion, and airplane modes, and during the feather-fold sequence.
>
> The dynamic equations of motion are derived using the Lagrangian method and include coupling between the proprotor and airframe dynamics. Provisions are made for large flapping and feathering motions. Small angle assumptions are made for the airframe and proprotor elastic degrees of freedom. Two-dimensional strip theory is used on the proprotor and blades; C_l, C_d, and C_m are input in tabular form for a 180-degree range of angle of attack and for Mach numbers up to 1.0. Aerodynamic interference between the wing and proprotor is represented in the program.

Use or disclosure of data on this page is subject to the restriction on the title page.

TABLE VI-I. RUN SCHEDULE OF MODEL 627 WIND-TUNNEL TEST

Run No.	Airspeed (kt)	Rotor RPM	Purpose	Remarks/Data
1-2	80	0-283	Track and balance	-
3	120	0-454	Track and balance	-
4	125	0-470	Track and balance	Frequency check rpm sweep
5	135	0-424	Track and balance	Aerovane rpm sweep
6	125	425	Sweep angle of attack (α)	Record flapping
7	125	425	Sweep angle of attack (α)	$\alpha = -2^{o}$ (minimum flapping)
8	125	0-150	Frequency response with stop/starts	Hub locked
9	125	0-475	Fast stop/starts	Response to angle of attack
10	140	475	Dynamic stability	Frequency and damping
11	150	450	Dynamic stability	Frequency and damping
12	150	0-435	Stop/starts versus α	Rotor response to angle of attack
13	165	450	Frequency response with flapping free and locked	Frequency and damping
14	175	450	Frequency response with flapping free and locked	Frequency and damping
15	150	0-420	Functional check and balance	-
16	175	0-435	Stop/starts versus α	Rotor response to angle of attack
17	185	435	Hub flapping free and locked, dynamic stability	Frequency and damping
18	190	435	Hub flapping free and locked, dynamic stability	Frequency and damping
19	100-175	435-0	Windmill drag with balance free	Drag versus α
20	125	0	Dynamic stability with blade folding	Frequency and damping
21	148	0	Dynamic stability with blade folding	Frequency and damping

Use or disclosure of data on this page is subject to the restriction on the title page.

TABLE VI-I. Concluded

Run No.	Airspeed (kt)	Rotor RPM	Purpose	Remarks/Data
22	175	0	Dynamic stability with blade folding	Frequency and damping
23	175-195	0	Dynamic stability with blade folding	Frequency and damping
24	148	0	0-30° blade folding loads with angle of attack	Load versus α
25	148	0	45-90° blade folding loads with angle of attack	Load versus α
26	125-175	0	30° blade fold loads with angle of attack	Loads versus α
27	150	0	Same as Run 26 except rotor azimuth changed 120°	Loads versus α
28	150	0	Stop/start, fold/ unfold sequence α = 0 -6°	Loads and response
29	175	0	Stop/start, fold/ unfold sequence	Loads and response
30	140	340	Windmill drag and high angle of attack with blade folding	Drag and loads
31	125	0	Mast torque oscillation	Response

DYN5 is programmed for solution by digital computer. A predictor-corrector integration technique is used for the solution of the simultaneous equations of motion. Input to the program consists of lumped parameters and the coupled normal modes of the wing, pylon, and proprotor. The output consists of a time history of the wing and pylon motions, and blade flapping and elastic deflections. Generally, initial conditions are input to minimize the time required for convergence to steady-state trim. For stability investigations, the transient response to external inputs or to initial conditions can be calculated. The program can simulate gust encounters and collective and cyclic control inputs.

Use or disclosure of data on this page is subject to the restriction on the title page.

C. DYNAMIC RESPONSE CHARACTERISTICS DURING THE FEATHER-FOLD SEQUENCE

In order to provide a background for the loads and vibration data presented in this section, the dynamic response characteristics during the feather-fold sequence (and unfold-unfeather sequence) are reviewed.

Figures VI-1 and VI-2, respectively, are time histories obtained during the full-scale tunnel tests of continuous feather-fold and unfold-unfeather sequences. These time histories are at 150 knots and four degrees angle of attack, simulating a 1.5 g condition. The significant events such as gimbal lockout, feather, and index, for example, have been identified below and on Figures VI-1 and VI-2 to facilitate a discussion of the dynamic response characteristics associated with each event.

80-Percent Hover RPM, Gimbal Free (Event 1)

The feather-fold sequence is initiated with the proprotor windmilling at 70 to 80 percent of hover rpm, with the gimbal free to flap. This condition is characterized by low blade loads and moderate pylon vibration levels. The vibration is at the blade passage frequency.

80-Percent Hover RPM, Gimbal Locked Out (Event 2)

Before feathering the blades, the gimbal flapping freedom is locked out. This causes an increase in oscillatory blade loads and in the proprotor normal force (H-force), since flapping no longer attenuates the blade one-per-rev angle-of-attack variation resulting from the mast angle of attack. The increase in the proprotor normal force is reflected in the wing beam bending moment and torsion. During engagement of the gimbal lockout, there is an overshoot in blade loads of about 10 percent of the steady state oscillatory load. The pylon vibration levels are not significantly changed from the gimbal-free loads.

Blade Feathering (Event 3)

During blade feathering, there is a build-up in oscillatory loads and vibration. The blades are feathered rapidly to minimize the time that the proprotor and airframe are exposed to the increased loads and vibrations. The proprotor rotational kinetic energy is dissipated by a perturbation thrust force which is reflected in the wing chordwise bending moment. The increase in inflow angle as the blades are feathered causes the one-per-rev airloads and the proprotor normal force to increase. This is reflected in an increase in blade oscillatory bending moment and torsion. As the proprotor rpm decreases, pylon vibration and wing loads at the frequencies of the wing fundamental beam, chord bending, and torsion modes build up and decay as each mode is transited by the blade passage frequency. The pitch link steady load decreases as rpm decreases until the blade is fully feathered; then there is a sudden increase in pitch link load when the blade pitch stop is engaged. The feather pitch stop is set such that the proprotor is windmilling at 6-10 rpm after the blades are feathered.

Use or disclosure of data on this page is subject to the restriction on the title page.

Index and Lockout Mast Rotation (Event 4)

The proprotor is self-indexing since it is windmilling at 6 to 10 rpm. When the mast rotation lockout is actuated, the lockout becomes engaged when the rotor azimuth coincides with any of the three blade fold positions (see Figure V-9). Rotation is arrested instantaneously since lockout is accomplished by a tapered detent engaging a slot in the mast. The sudden stopping creates an impact loading that produces a large mast torque and excites the wing beamwise bending mode. This is the only significant dynamic response.

After the mast rotation is locked out, the blade pitch is locked out. No significant dynamic response was observed when this event occurred.

Blade Folding (Event 5)

The blades are folded in approximately nine seconds. The system response during blade folding is confined to changes in the steady loads on the proprotor and wing. The most significant of these are the pitch lockout bending and mast torque at angle of attack. There was negligible dynamic response associated with starting and stopping blade folding. The only significant dynamic response observed was associated with folding and was caused by a slight free-play clearance in the mast rotational lockout. When operating at conditions where mast torque was near zero, the rotor would oscillate through the free play at a very low frequency. This oscillation was apparently driven by fluctuations in the aerodynamic forces on the proprotor blades.

The dynamic response during unfolding-unfeathering was essentially a mirror image of the feather-fold response. However, the magnitude of the oscillatory loads and vibration during unfeathering was considerably lower than during feathering.

D. DYNAMIC STABILITY CHARACTERISTICS

1. Test Procedure

The test stand dynamic stability boundaries are well above the maximum speed of the 40- by 80-foot wind tunnel. However, the frequency and damping of the principal modes of the test stand/proprotor system were measured to provide an indication of the stability characteristics.

The frequency and damping were determined by means of a two-square-foot aerodynamic vane located on the outboard side of the nacelle fairing as shown in Figure V-19 (page V-35). The vane was oscillated in pitch so as to aerodynamically force the selected structural mode at resonance. A Lissajous figure was generated on a dual-axis oscilloscope to facilitate identification of resonant frequencies. When the response at resonance was sufficiently high, the vane excitation was turned off and the resulting decay of the test-stand motion was analyzed to determine the mode frequency and damping. Figure VI-3 shows a typical decay history and illustrates the method used to calculate frequency and damping.

This method was used both with the rotor turning, and stopped and folded. For each configuration, a slow frequency sweep from 20 to 30 cps was made to identify the dominant structural modes. With the rotor turning, the only modes showing significant response were the test stand fundamental beamwise bending and torsion modes. Since the vane excitation in the test stand chordwise direction was low, the frequency and damping of the stand fundamental chord bending mode could not be determined with the vane. However, collective pitch pulses proved to be an acceptable means of exciting the chord mode. With the proprotor stopped, the blade bending modes were also excited with the vane.

The majority of the dynamic stability data was taken with the wind-tunnel balance frame locked out. A previous test (Reference 3) showed that coupling with the balance frame modes significantly influenced the frequency and damping of the test stand modes, particularly the wing chordwise bending mode.

During the Model 627 folding-proprotor test, the damping of the wing chord mode was noticeably lower when running with the balance frame free. And, even with the balance locked out, coupling with the balance modes affects frequency and damping of the chord mode, as is discussed later in this section.

2. Measured Stability Characteristics

Proprotor-pylon stability was investigated during Task II of the Advancement of Tilt-Proprotor Technology effort and reported in Reference 3. With the gimbal free, the Model 627 folding-proprotor stability characteristics were found to be essentially the same as those of the Model 300 proprotor (see Figure V-6 and V-7 of Reference 3). This was expected since the configurations are similar.

With the gimbal locked out, the frequency and damping were determined as a function of airspeed and proprotor rpm, down to zero rpm. These data are shown in Figures VI-4 and VI-5, respectively. The damping of the wing modes is slightly higher than the gimbal-free damping. Rotor speed was found to have only a small effect on the damping. No damping data for wing chord are available at low airspeeds since the wing chord mode could not be excited sufficiently to measure damping.

With the proprotor stopped, the frequency and damping of the wing and blade modes were measured as a function of blade fold angle, angle of attack, and airspeed. Figures VI-6 and VI-7 show the frequency and damping variation with blade fold angle. The decrease in damping as the blades are folded is due to the reduction in blade effective area. No damping data for blade beam bending mode are available since the mode could not be excited sufficiently to measure damping.

Figure VI-8 shows the variation of frequency and damping with airspeed at a typical partial fold angle of 30 degrees. At partial fold positions such as 30 degrees, damping increases in proportion to airspeed. There was no variation in frequency and damping for angles of attack below stall. At and above stall, the buffet amplitude was very low.

Use or disclosure of data on this page is subject to the restriction on the title page.

The effect of aerodynamic vane excitation amplitude on frequency and damping of the wing modes was investigated and found to be significant for the chord bending mode. The variation with amplitude is shown in Table VI-II. This variation is believed to be caused by coupling with the balance frame modes.

TABLE VI-II. VARIATION OF WING CHORD MODE FREQUENCY AND DAMPING WITH EXCITATION AMPLITUDE

Amplitude	Frequency	Damping Percent Critical
31400 in-lb	4.2 cps	0.65
42000 in-lb	4.1 cps	1.1
62500 in-lb	4.0 cps	1.56

3. Correlation of Theory with Measured Characteristics

Calculated frequency and damping characteristics are shown in Figure VI-4 through VI-8. In general, the correlation is good, with the analysis being somewhat conservative. The greatest discrepancy occurs in the prediction of damping with the rotor stopped and the blades near fully open, where the wing beam bending damping is under predicted as shown in Figures VI-6 and VI-8. This has also been indicated in correlating with the results of small-scale model tests (References 11 and 14). The reason for this discrepancy is believed to be due to the two-dimensional strip theory used for the rotor blade aerodynamic over-predicting the extent of the blade that is stalled.

E. PROPROTOR AND CONTROL LOAD CHARACTERISTICS

1. Test Procedure

Loads during the rotor turning and stopping and starting conditions were obtained by going through a gimbal lockout, feather, unfeather, unlock-gimbal sequence. This sequence was first accomplished at zero angle of attack and then repeated at progressivley higher angles of attack until established limits were reached. Throughout this report angle of attack refers to the yaw table angle; positive angle of attack corresponding to negative yaw. At zero angle of attack the wing chordline and mast are parallel to the wind-tunnel centerline. Loads with the rotor stopped were obtained from angle-of-attack sweeps at constant fold angle.

As noted earlier, the fold hinge lug oscillatory loads were determined prior to the test to be the critical load during proprotor stopping and starting. For test purposes, the calculated load for 100,000 cycles was used as a limit for the lug. During the test, the number of cycles which exceeded the endurance limit (10^8 cycles) were counted, and a damage fraction calculated. The overall damage fraction resulting from the test was only 0.00276. The lug load was not measured directly, but, based on a calculated bending moment distribution, the bending moment at blade Station 33.0 was extrapolated to the

Use or disclosure of data on this page is subject to the restriction on the title page.

lug for monitoring purposes The bending moments at the blade Station 52.5, mast bending, and the pitch link axial loads were also monitored.

During blade folding, the critical loads were (1) the blade pitch lockout bending moment, and (2) the mast rotation lockout torque. The pitch lockout reacts blade bending moments when the blades are folded and when at angle of attack, these moments become large. The pitch lockout load limit was 50,000 inch-pounds. The mast rotation lockout reacts proprotor torques; while the mast torque is low at zero angle of attack, it increases as angle of attack increases. The mast lockout load limit was set conservatively at 70,000 inch-pounds. During the test, these component load limits were approached at high angles of attack.

2. Measured Blade and Control Loads

Blade and control system oscillatory loads with the gimbal free are shown versus angle of attack in Figure VI-9. The frequency of the oscillatory load is one per rev. The load does not vary significantly with angle of attack since the rotor is free to flap and relieve the aerodynamic moments. Loads measured during tests of the Model 300 25-foot proprotor (Reference 3) are also shown.

Locking out the gimbal freedom increases blade load sensitivity to angle of attack since blade rigid body flapping no longer relieves the one-per-rev aerodynamic moment. However, there was some flapping due to the elasticity of the lockout mechanisms. Figure VI-10 compares flapping versus angle of attack for gimbal free and gimbal locked out. Minimum flapping occurred at approximately -1 degree to -2 degrees rather than 0 degree angle of attack because there was approximately 1 degree of aft cyclic pitch which could not be zeroed out. This 1 degree of aft cyclic pitch also caused the angle of attack for minimum blade loads to occur at -1 degree. Representation of the lockout elasticity (K_H) also proved to be essential in order to achieve correlation with the measured loads.

The blade beamwise bending moment variation with angle of attack with hub locked out is shown in Figure VI-11. The oscillatory chord bending moment and pitch link loads were small and, therefore, not presented. The influence of airspeed on the beamwise moment is shown in Figure VI-12.

The blade beamwise oscillatory bending moments during feathering are the highest loads encountered in the feather-fold sequence. Only four or five cycles occur when stopping the proprotor, but these are sufficiently high to do fatigue damage. The loads during starting are somewhat lower but still incur fatigue damage. Figures VI-13 and VI-14, respectively, show the peak amplitude of the blade oscillatory bending moments during feathering and unfeathering versus mast angle of attack. The influence of airspeed on the peak oscillatory load during stopping and starting is shown in Figure VI-15.

The effect of rate of feathering on the magnitude of the oscillatory blade loads is negligible. By feathering the blades rapidly, the number of high cycles is minimized.

Use or disclosure of data on this page is subject to the restriction on the title page.

Figures VI-16 and VI-17 show the influence of folding the blades on proprotor loads. As noted earlier, oscillatory loads during blade folding were negligible. Note that while the blade bending moments and mast torque fall off as the blades are folded, the pitch link axial loads and the pitch lockout moment have a maximum at about 60 to 70 degrees fold angle. This characteristic arises from the blade root beamwise bending moments being reacted by the pitch link and pitch lockout when the blade is folded back from the fully open position (i.e., resolving the bending moments about the pitch change axis produces a moment about that axis equal to $M_\beta \sin \gamma$).

The variation in steady blade beamwise bending moment, pitch link axial load, pitch lockout bending moment, and mast torque with angle of attack at two fold angles is shown in Figures VI-18, VI-19, and VI-20, respectively. The loads increase with angle of attack up to wing stall. Wing stall occurred at about 16 degrees angle of attack as indicated by a drop in wing bending moment and a slight buffet. The blade beamwise bending moment began to level off at an angle of attack several degrees below the wing stall angle, but blade buffet was not evident.

The loads shown in Figures VI-18, VI-19, and VI-20 are for the blade lying in the plane of the wing (i.e., vertical in the tunnel). The other blades experienced lower loads as shown in Figure VI-21. These data were obtained by indexing the instrumented blade to the 120 degree and 240 degree azimuth positions. The influence of airspeed on the proprotor loads during folding is shown in Figure VI-22. The increase is essentially linear with dynamic pressure reflecting high stiffness of the wing and proprotor.

3. Correlation of Theory with Measured Loads

Calculated loads are compared with the measured loads in Figures VI-9 through VI-22. The correlation is considered acceptable for design purposes. However, there are several areas where there is a significant variation between the calculated and measured loads.

The measured blade bending moments with the gimbal locked out, were found to be about 30 percent less sensitive to angle of attack than the pretest calculations indicated. When the pretest calculations were made, the gimbal lockout was assumed to be inelastic. Following the test, this discrepancy was investigated. By using a hub flapping lockout spring rate as discussed in paragraph 2, much better correlation was achieved. The spring rate (4500 foot-pound/degree of flapping) was used to generate the calculated loads shown in Figures VI-11 through VI-15.

A second discrepancy is in blade beamwise bending moments calculated for zero fold angle ($\gamma = 0^o$). These are considerably lower than the measured moments. The cause of this is probably over predicting the portion of the blade that is stalled the same as that which caused the theory to predict the wing beam bending mode damping too low at $\gamma = 0^o$. The calculated blade loads at large fold angles are also significantly lower than the measured loads. This is believed to be caused by lack of wingtip vortex representation in the theory. Neither of these conditions is critical from a design loads standpoint since maximum measured loads at $\gamma = 0^o$ through 90° are within allowables.

Use or disclosure of data on this page is subject to the restriction on the title page.

F. WING LOAD AND PYLON VIBRATION CHARACTERISTICS

1. Test Procedures

Data on pylon vibration and wing loads were obtained concurrently with the acquisition of proprotor loads data. The most significant wing/pylon response during blade feathering or unfeathering is the vibration buildup which occurs at the wing fundamental beam, chord, and torsion natural frequencies. As the blades are feathered to stop, peaks in the vibration level occur when the rpm is such that the blade passage frequency is in resonance with a given wing mode. (The forces at the blade passage frequency arise from aerodynamic interference between the wing and proprotor.)

There are also significant transient responses resulting from the sudden changes in proprotor aerodynamic forces during stopping or starting. The most significant of these is the wing chordwise bending resulting from the thrust perturbation during stopping or starting. The pylon dynamic response is especially significant because it can be used to predict crew station and cabin vibration levels during feathering or unfeathering. During blade folding, the vibration is negligible, and the wing steady loads are the principal interest.

2. Measured Wing Loads and Pylon Vibration

Pylon blade passage frequency vibrations and wing oscillatory loads did not change significantly when the gimbal was locked out (80 percent hover rpm). Wing oscillatory loads were negligible at 80 percent hover rpm.

The peaks in pylon vibration during feathering or unfeathering are strongly influenced by the rates of feathering or unfeathering. Figures VI-23 and VI-24 show the effect of feathering and unfeathering rate on the magnitude of the vibration peaks at the wing natural frequencies. The zero rate points were obtained by slowly increasing rpm from zero to 80 percent of hover rpm to determine each rpm at which blade passage excitation was in resonance with wing modes. At each resonance rpm, the system was allowed to reach the steady state amplitude. The Model 627 feather/unfeather rate of about 25 to 30 degrees per second was selected on the basis of the optimum feathering rate discussed in Reference 11. As indicated by the trend of the data points in Figures VI-23 and VI-24, this rate resulted in a significant reduction in the amplitude of pylon vibration during feathering and unfeathering over a slower rate.

The effect of angle of attack on the pylon response at the wing-pylon natural frequencies is shown in Figures VI-25 and VI-26. The effect on the wing torsional mode is significant, but is negligible for the beam and chord bending modes. The variation with airspeed in vibration at the wing natural frequencies is shown in Figure VI-27.

Figures VI-28 and VI-29 show the effect of rate of feathering and unfeathering on the peak oscillatory bending moments at the wing natural frequencies and the transient chord bending moment. The effect of angle of attack on these loads is shown in Figures VI-30 and VI-31, respectively. The peak oscillatory loads on the wing were below the endurance limit.

Use or disclosure of data on this page is subject to the restriction on the title page.

The wing root steady bending moment and torque variation with blade fold angle, angle of attack, and airspeed are shown in Figures VI-32, VI-33, and VI-34, respectively. It should be noted that the wing loads for the cantilever condition in the wind tunnel may be slightly higher than those in free flight.

3. Correlation of Theory with Measured Characteristics

Calculated vibration levels and loads are compared to the measured characteristics in Figures VI-23 through VI-34. The correlation is fairly good, both in magnitude and in the trend with fold angle, angle of attack, and airspeed. In general, the theory under predicts vibration for the stopping cases and over-predicts the starting cases.

G. COMPARISON WITH RESULTS OF SMALL-SCALE MODEL TESTS

Data from the test of the one-fifth-scale model of the 627 folding proprotor include dynamic stability characteristics, dynamic response during stopping and starting as a function of angle of attack and feathering rate, and proprotor and wing loads during blade folding. The airspeed and angle-of-attack ranges were similar to those of the full-scale test.

The agreement between the small-scale and full-scale dynamic data is reasonably good. Figures VI-35 and VI-37 compare the peak oscillatory blade loads and peak pylon vibration during feathering measured with the small-scale model and with those measured during the full-scale test. The results are nearly identical except that full-scale loads and vibration are less than one-fifth scale and there is no correlation of the wing torsion loads. A time history of a one-fifth scale continuous feather-fold sequence at 150 knots and 3 degrees mast angle of attack is shown in Figure VI-37. When compared to the full-scale time history (Figure VI-1), it is evident that the model has dynamic response characteristics very similar to the full-scale characteristics.

H. CALCULATED TIME HISTORY OF FEATHER-FOLD SEQUENCE

Figures VI-38 and VI-39 are computed time histories of continuous feather-fold and unfold-unfeather sequences at 150 knots. These computed time histories were assembled from three separate runs for each of the major events in the conversion sequence: gimbal lockout, feather-stop, mast rotation lockout, and with the blade folded.

Comparison of the computed history of the system dynamic response with the measured response (Figure VI-1) indicates that the computer program effectively predicts the significant dynamic responses of the conversion sequence.

I. ACTUAL FEATHER-FOLD SEQUENCE TIME HISTORY AT 175 KNOTS

Figures VI-40 through VI-50 are actual reproductions of oscillograph data taken at 175 knots for the full sequence. The identification of channels and the scale factors are given on the figures. Figures VI-40 and VI-41 show the effect of hub flapping lockout at an angle of attack of one degree and four degrees, respectively. The most noticeable effect of hub lockout is the increase in blade bending and mast bending loads as the angle of attack is

Use or disclosure of data on this page is subject to the restriction on the title page.

increased. Figure VI-42 shows the strong transient influence of the mast torque and wing bending. Blade folding and unfolding, as shown in Figures VI-44 through VI-47, are again easily accomplished at 175 knots as shown in Figure VI-1 for 150 knots.

J. CONCLUSIONS FROM THE DYNAMIC TEST PROGRAM

1. Stability

There was no evidence of dynamic instability or flutter since there was no condition of approaching neutral stability at any time during the test up to the maximum wind-tunnel speed of 195 knots and a rotor speed from zero to 458 rpm. The predicted stability characteristics are shown in Figure VI-51.

2. Loads

The fold hinge lug oscillatory bending moment during the feather-stop and unfeather-start events was the critical load during the conversion sequence and established a limit on mast angle of attack. During the test, a number of stop/start sequences were made, incurring a lug damage fraction of 0.00276. It should be noted that at and near zero mast angle of attack no damaging cycles are incurred.

The lug allowables used during the test are believed to be conservatively estimated. In order to firmly establish mast angle of attack limits for flight, a fatigue test of the lug is required. However, even if the wind-tunnel test allowable is used, the Model 627 proprotor has sufficient strength for a research flight-test program (assuming that the wind-tunnel and flight-test mast angle-of-attack spectrums are similar). Figure VI-52 shows the load factor envelope as a function of airspeed, within which no fatigue damage would be incurred during a stop/start sequence, and the load factor above which significant fatigue damage would be incurred.

During blade folding the oscillatory loads are negligible. Extrapolation of the steady loads during folding indicates that limit loads are not exceeded at the conversion sequence design load factors of -0.0g to +2.0g at the limit airspeed of 200 knots. The load level of the test envelope in terms of angle of attack is shown in Figure I-4.

3. Dynamic Response

The pylon vibratory response during stopping and starting was within acceptable vibration limits even at high angles of attack. The maximum accelerations on the pylon were less than ±2g. Wing and pylon oscillatory loads were always below the endurance limit.

Crew station and cabin vibration levels during proprotor stopping and starting were estimated by using calculated mode shapes for the free-free aircraft and the measured pylon accelerations. For a 150-knot, zero degree mast angle-of-attack sequence, the following vibration levels were calculated:

	Crew Station (g)	Cabin (cg) (g)
Vertical at wing beam natural frequency	±0.060	±0.050
Axial at wing chord natural frequency	±0.080	±0.080
Peak transient longitudinal acceleration		
- Stopping	±0.176	±0.176
- Starting	±0.146	±0.146

The vibration occurring at the wing beam and chord natural frequencies has a very significant influence on subjective comfort because at the low frequencies of these modes the subjective discomfort threshold is quite low. As noted in Reference 11, a criterion for an acceptable level of crew station and cabin response is needed. Presently available discomfort criteria (Reference 18) are based on continuous, sinusoidal vibration whereas the response during feathering is a damped transient of a few seconds duration.

4. Optimum Feather/Unfeather Time

Hardware limitations prevented evaluation of a range of feathering rates. The rate tested was near the optimum suggested in Reference 11, 2.2 seconds. By using a fast feathering rate, the product of the magnitude times the duration of the oscillatory loads and vibratory response is kept to a minimum. A slower rate of feathering would allow loads and vibration to build-up and persist at the higher amplitudes.

The principal disadvantage of the fast rate is the longitudinal acceleration of the aircraft which would be experienced in flight due to thrust perturbations. For the cases shown in Figures VI-1 and VI-2, the average acceleration/deceleration of an aircraft during the two-second rotor stopping/starting would be approximately 0.1g with a momentary peak of approximately 0.35g.

5. Computer Program Correlation

Correlation between the computer program and the measured dynamic response is sufficiently accurate to use the program for folding proprotor guidance. The program will handle rotor parameters of two through four blades, any airfoil, and any fold-hinge location.

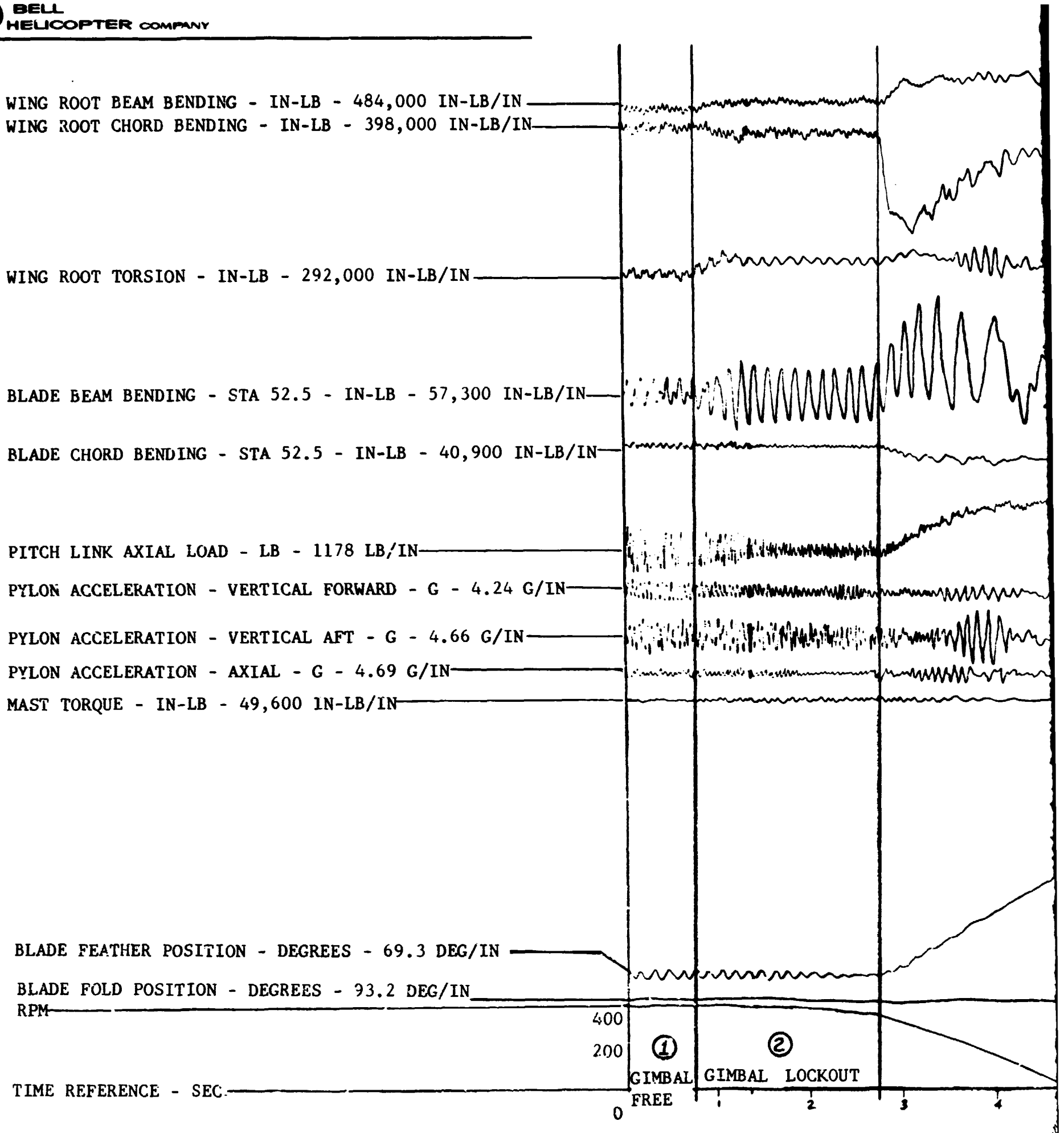
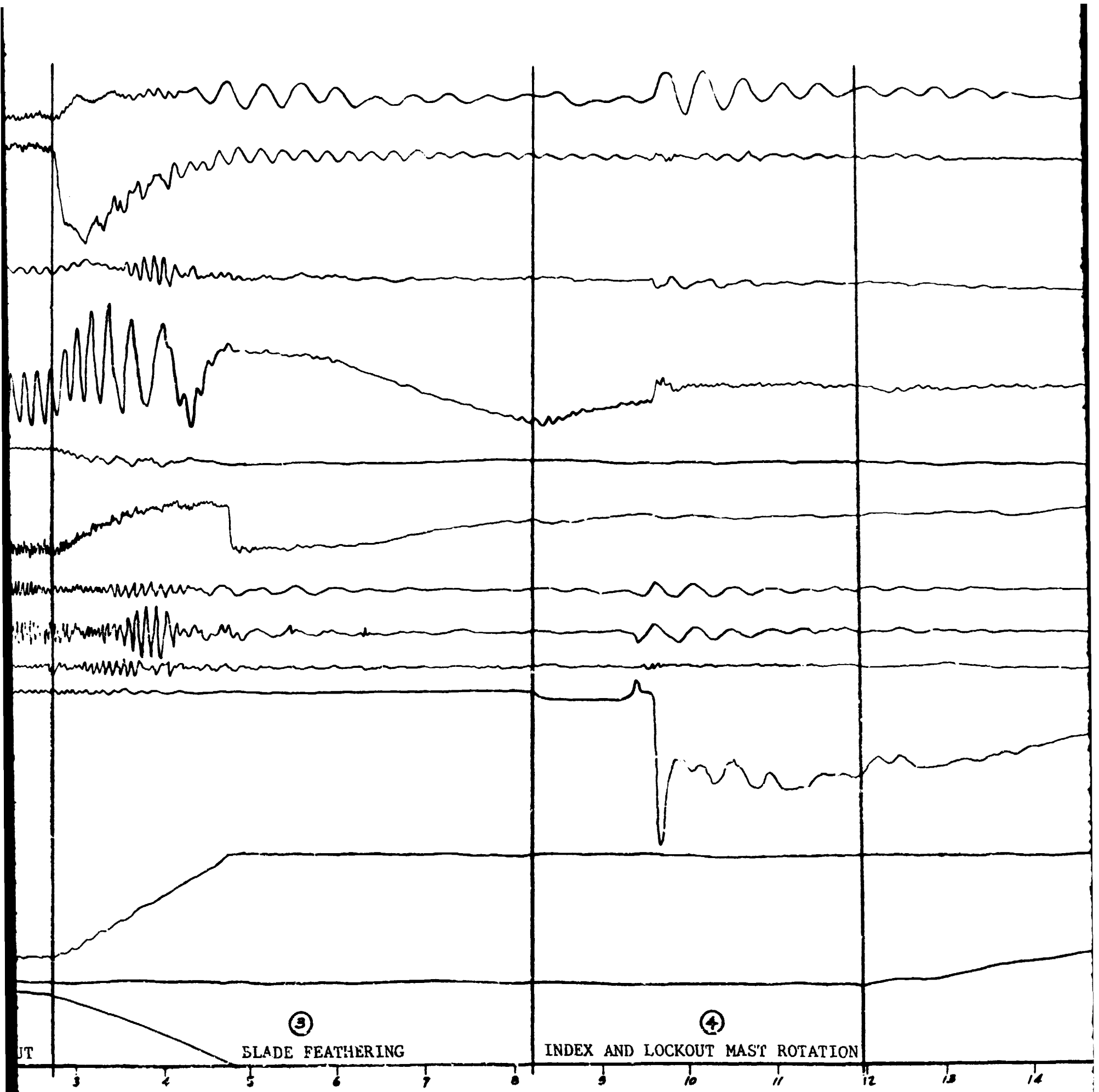


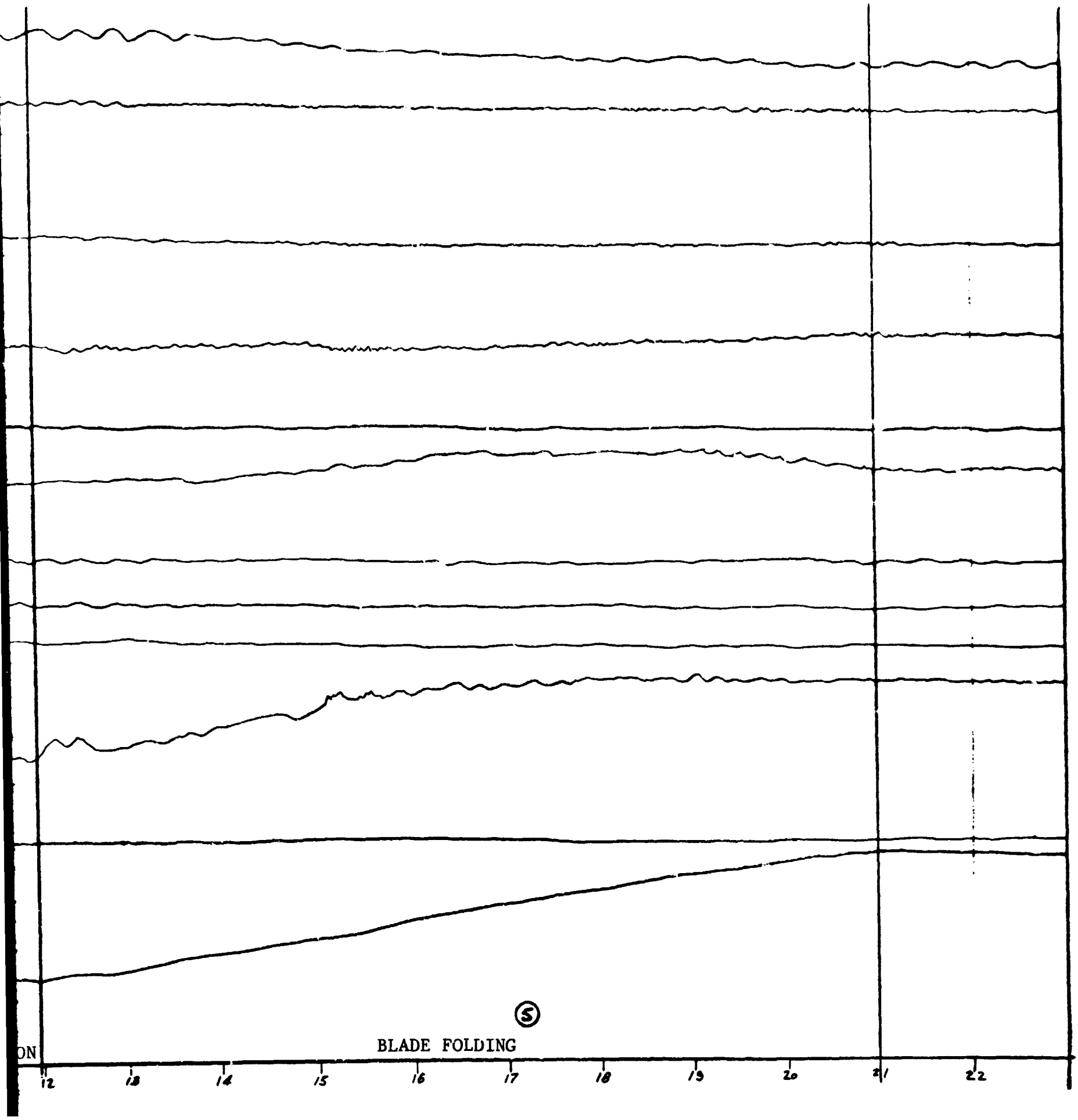
Figure VI-1. Time Histor
150 Knots,

FOLDOUT FRAME 1



e VI-1. Time History of Full-Scale Test Feather-Fold Sequence Dynamics, 150 Knots, $\alpha_{MAST} = 4^{o}$.

FOLDOUT FRAME 2



FOLDOUT FRAME 3

BELL HELICOPTER COMPANY

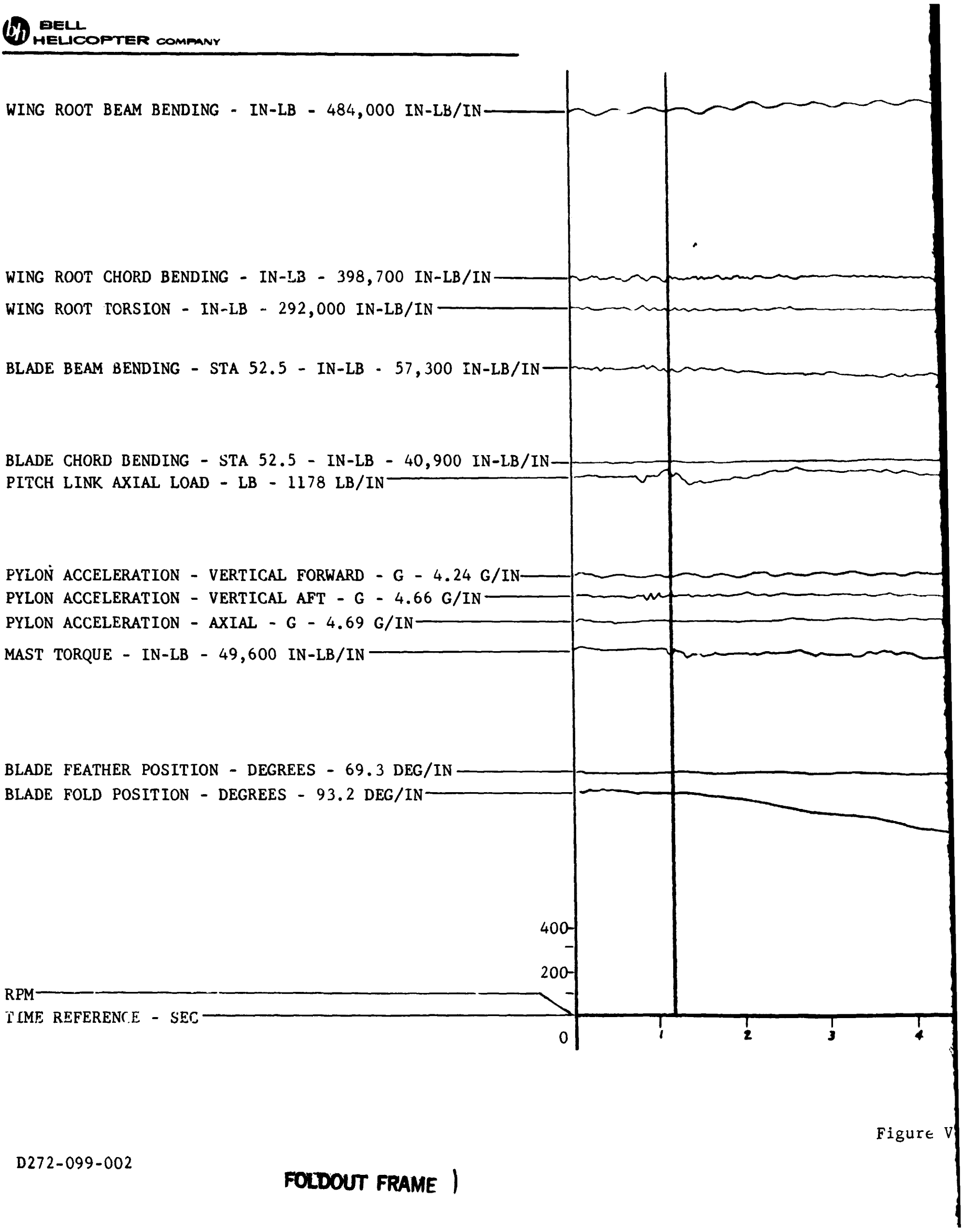


Figure V

D272-099-002

FOLDOUT FRAME 1

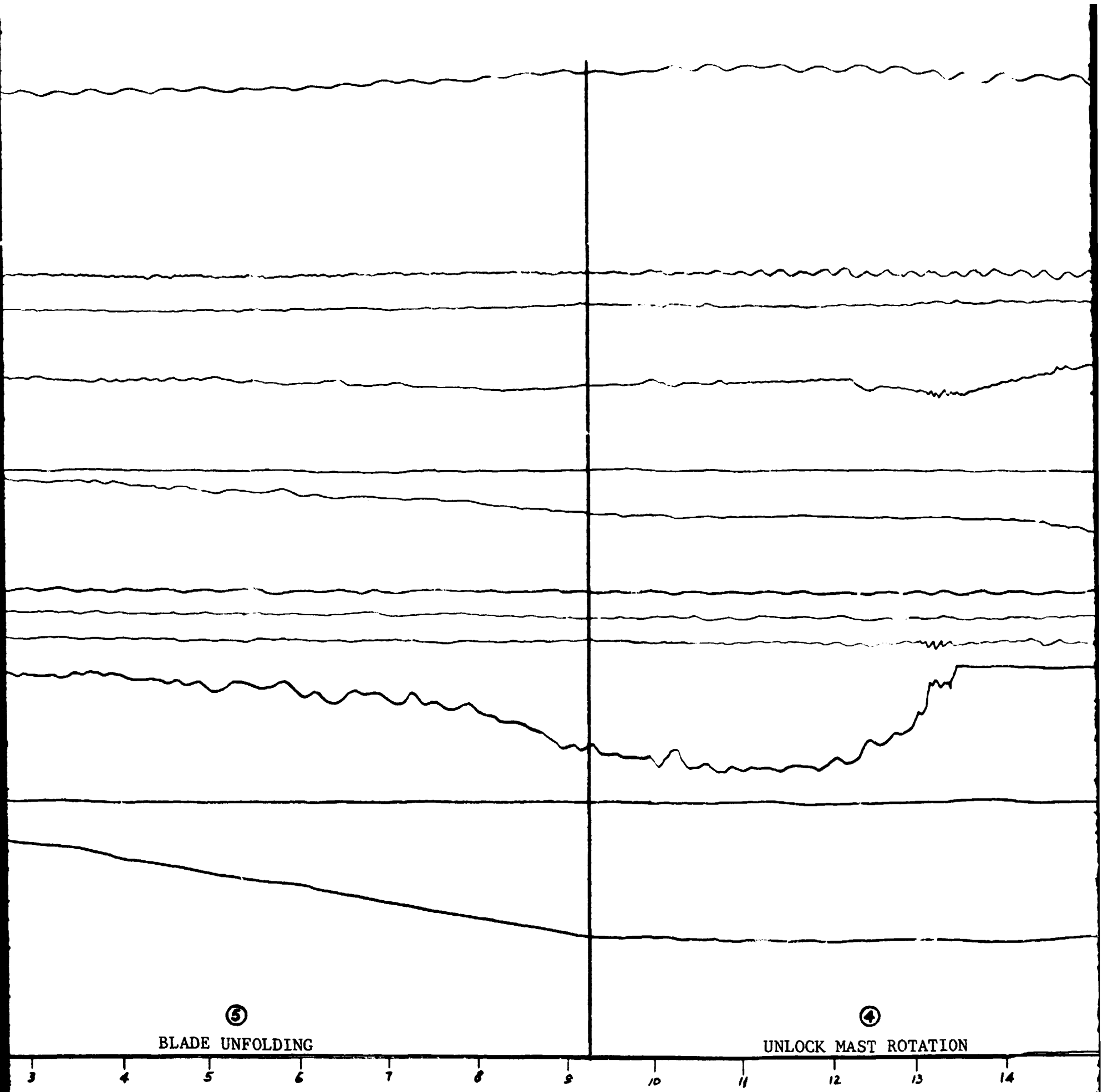
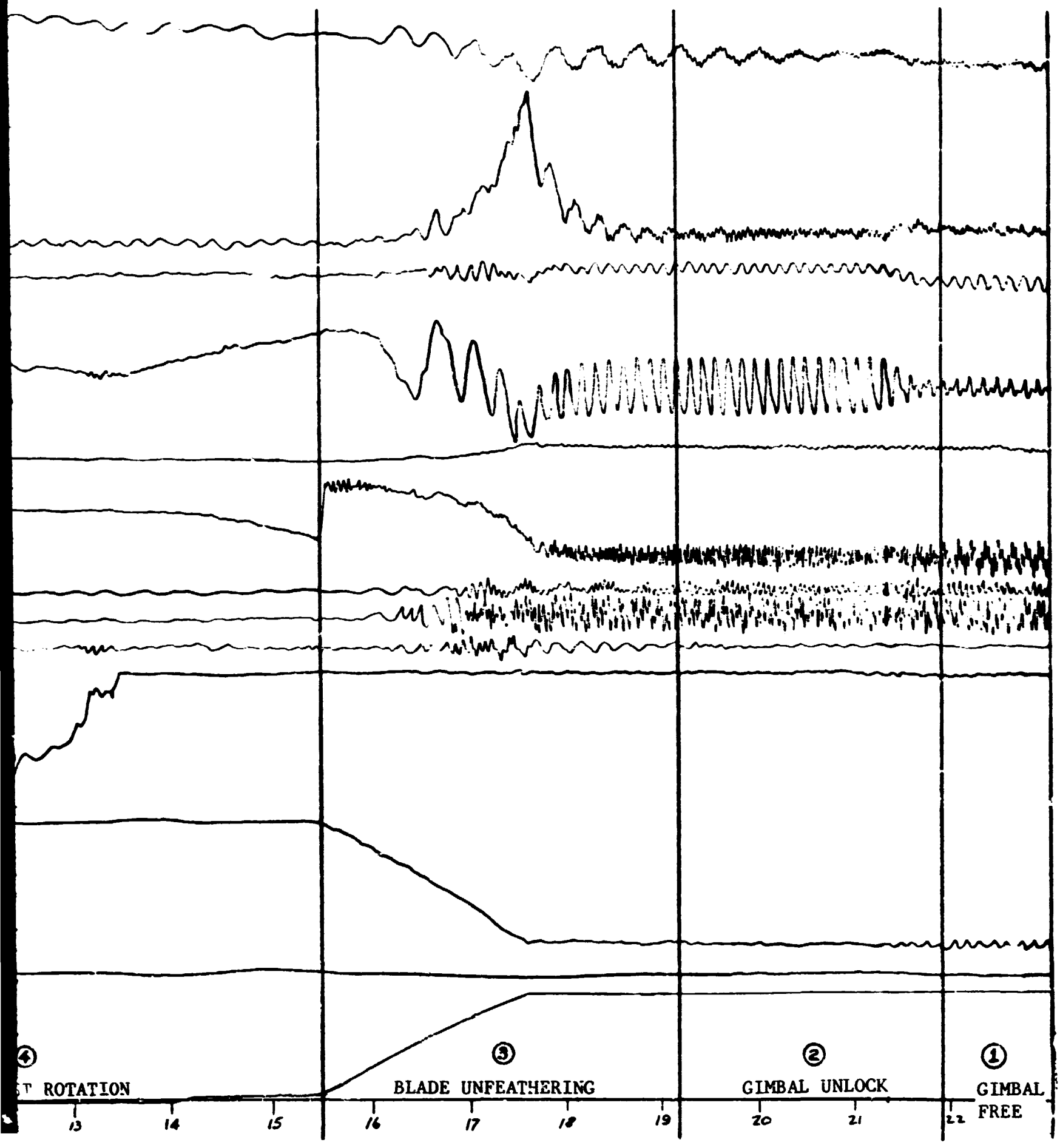


Figure VI-2. Time History of Full-Scale Test Unfold-Unfeather Sequence Dynamics, 150 Knots, $\alpha_{MAST} = 4^{\circ}$.

FOLDOUT FRAME 2



FOLDOUT FRAME 3

Use or disclosure of data on this page is subject to the restriction on the title page.

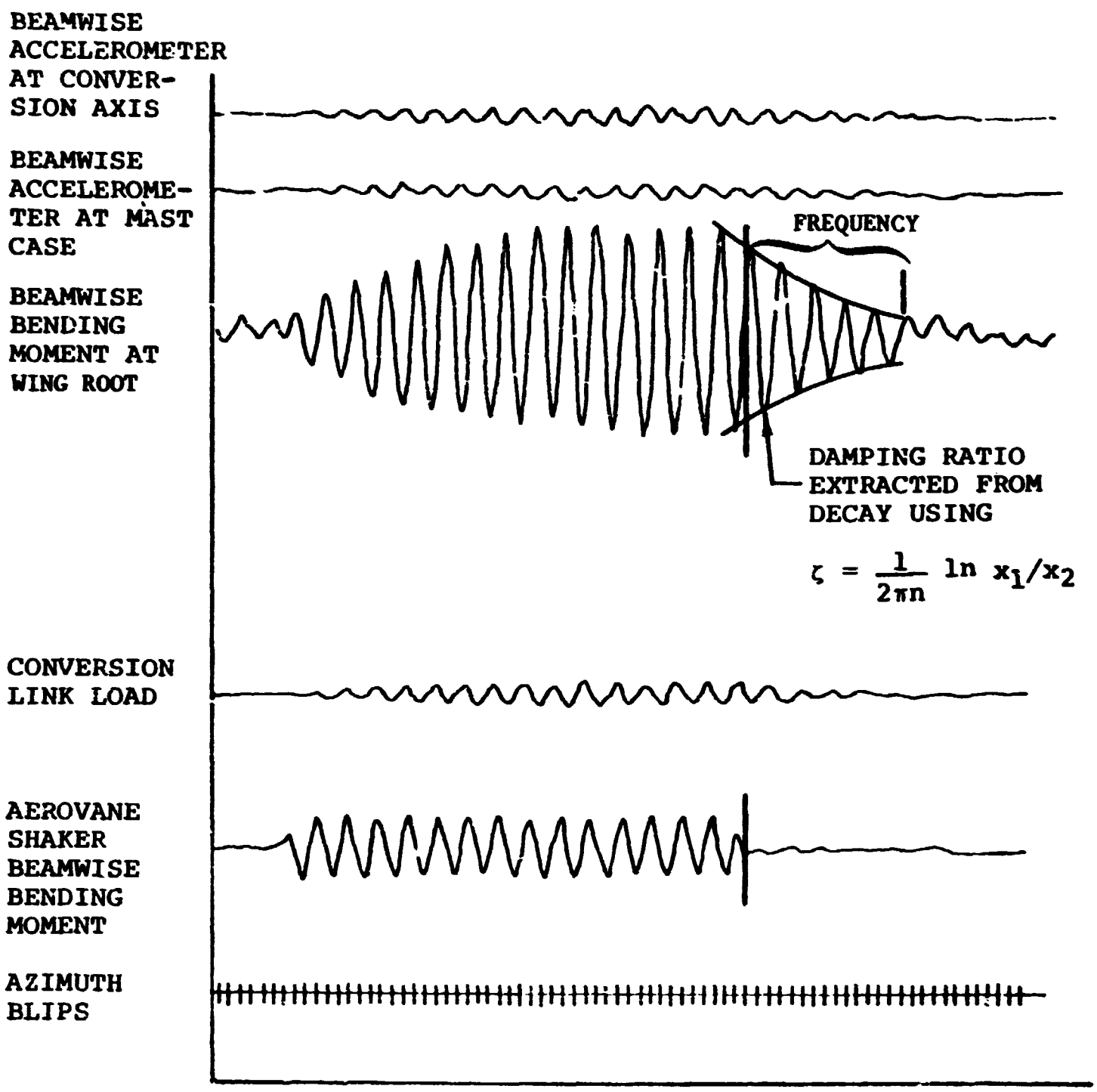
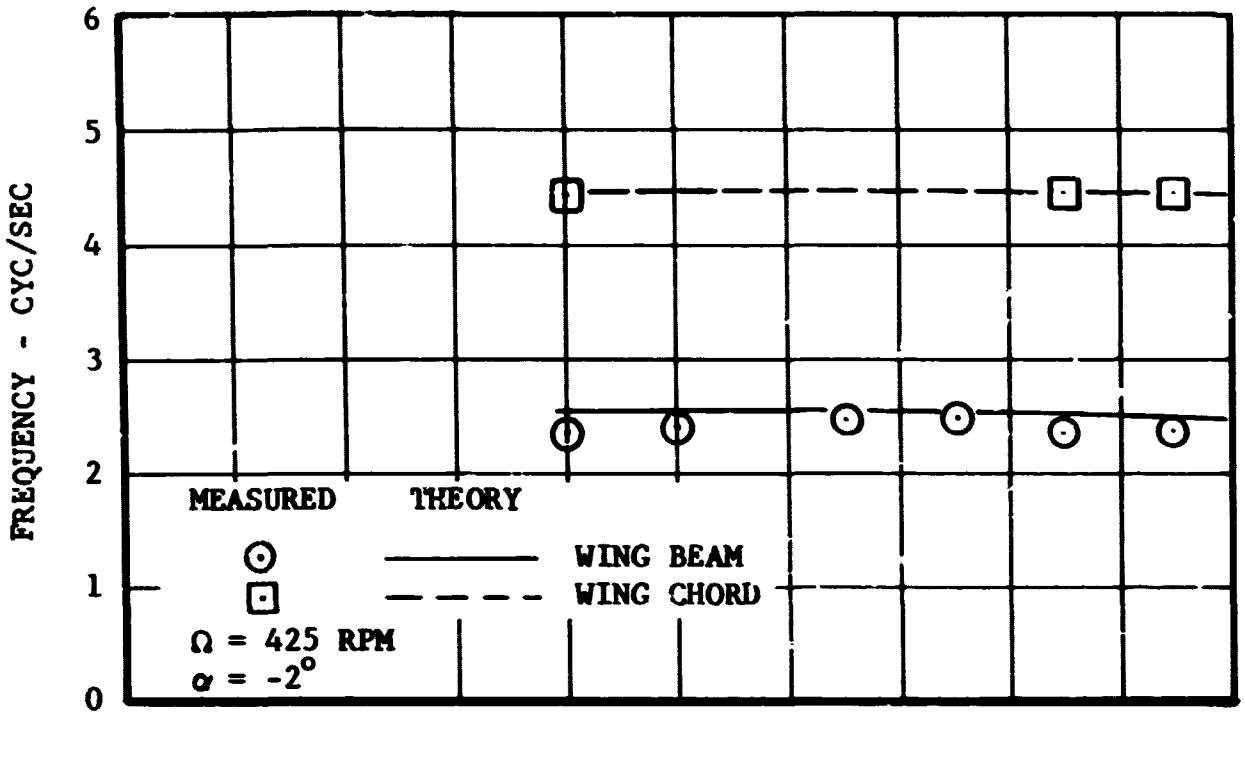


Figure VI-3. Method of Extracting Dynamic Stability Characteristics.

Use or disclosure of data on this page is subject to the restriction on the title page.



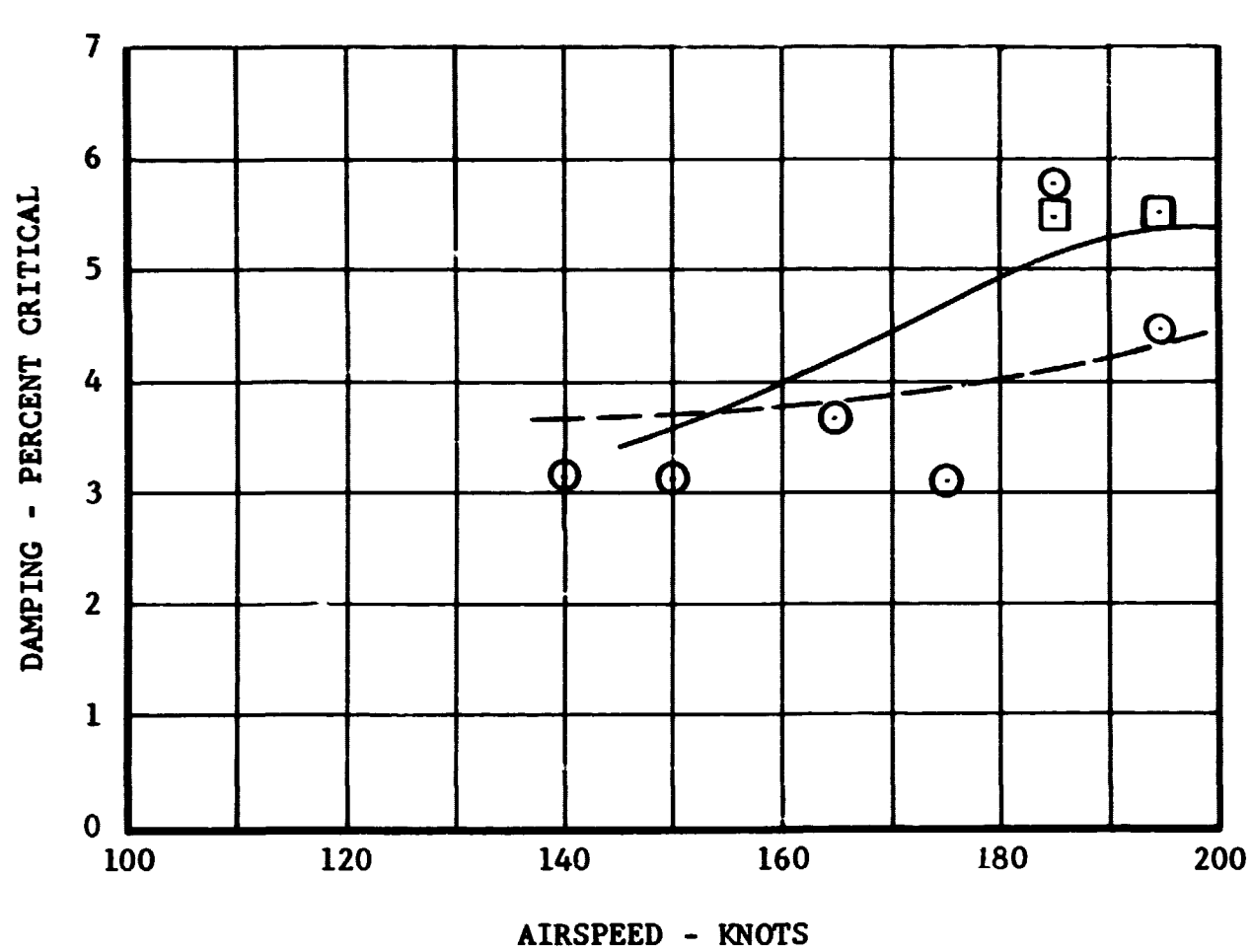


Figure VI-4. Wing Beam and Chord Bending Modes Frequency and Damping Versus Airspeed Gimbal Locked Out.

Use or disclosure of data on this page is subject to the restriction on the title page.

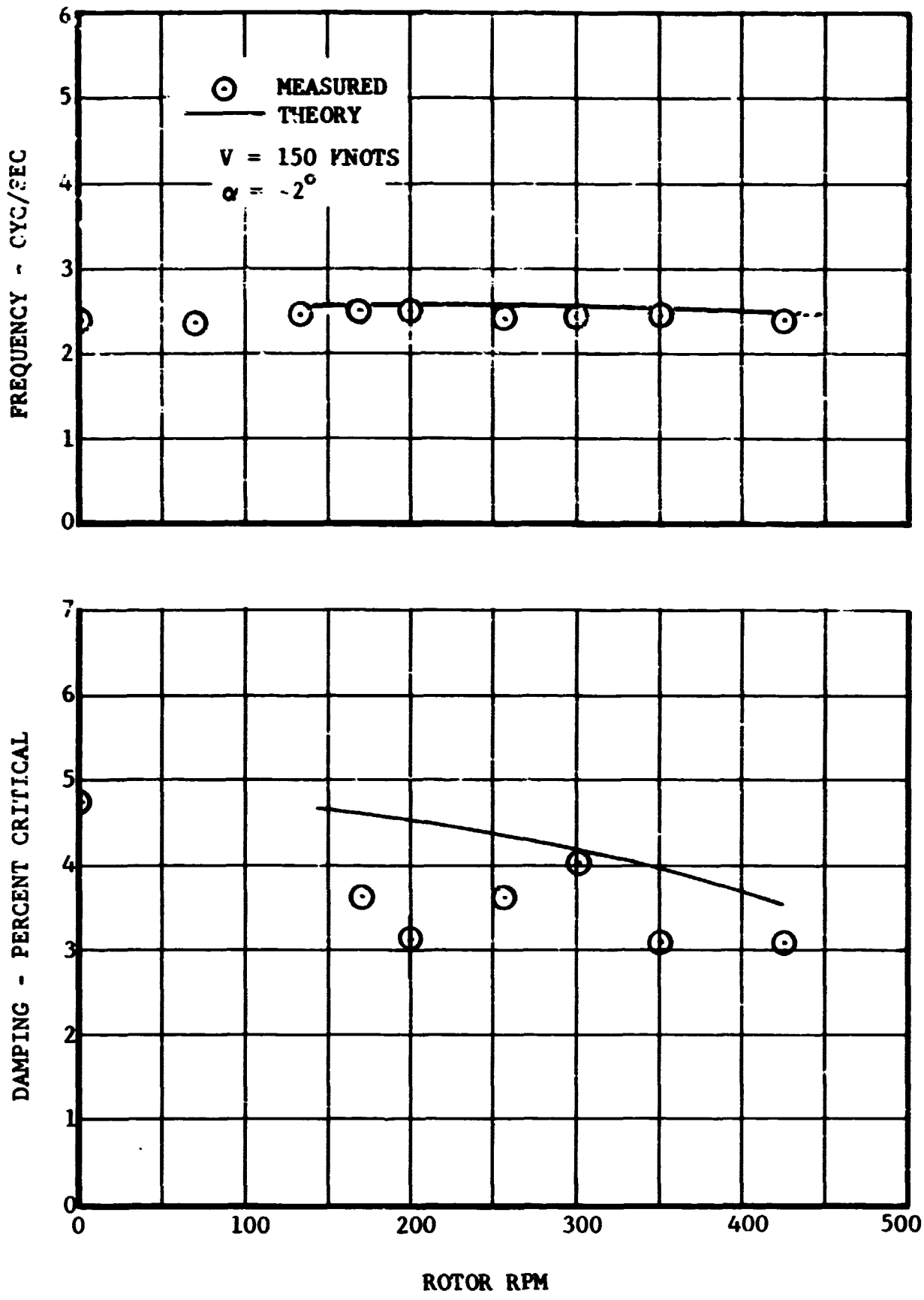


Figure VI-5. Wing Beam Bending Mode Frequency and Damping Versus RPM, Gimbal Locked Out.

Use or disclosure of data on this page is subject to the restriction on the title page.

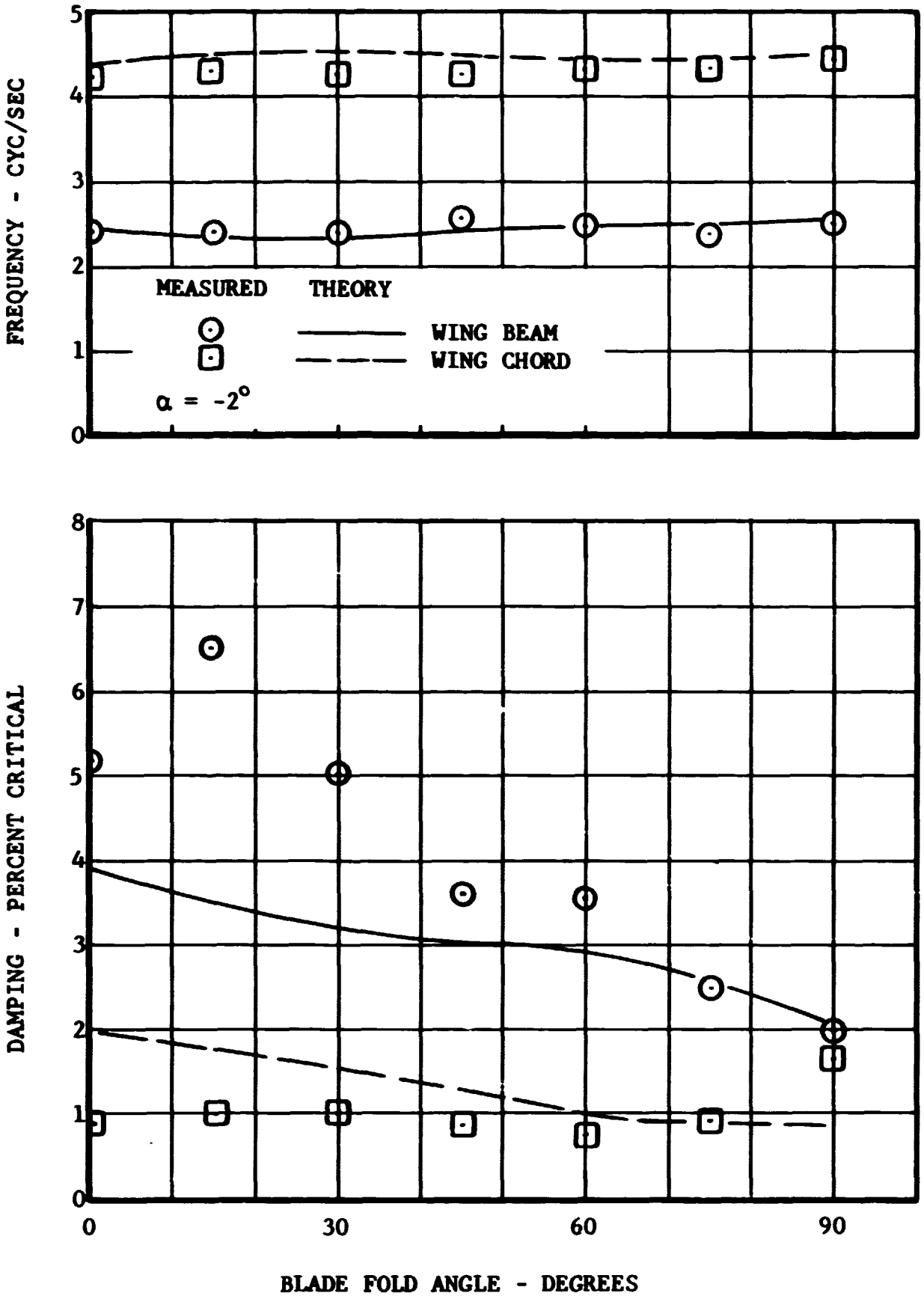
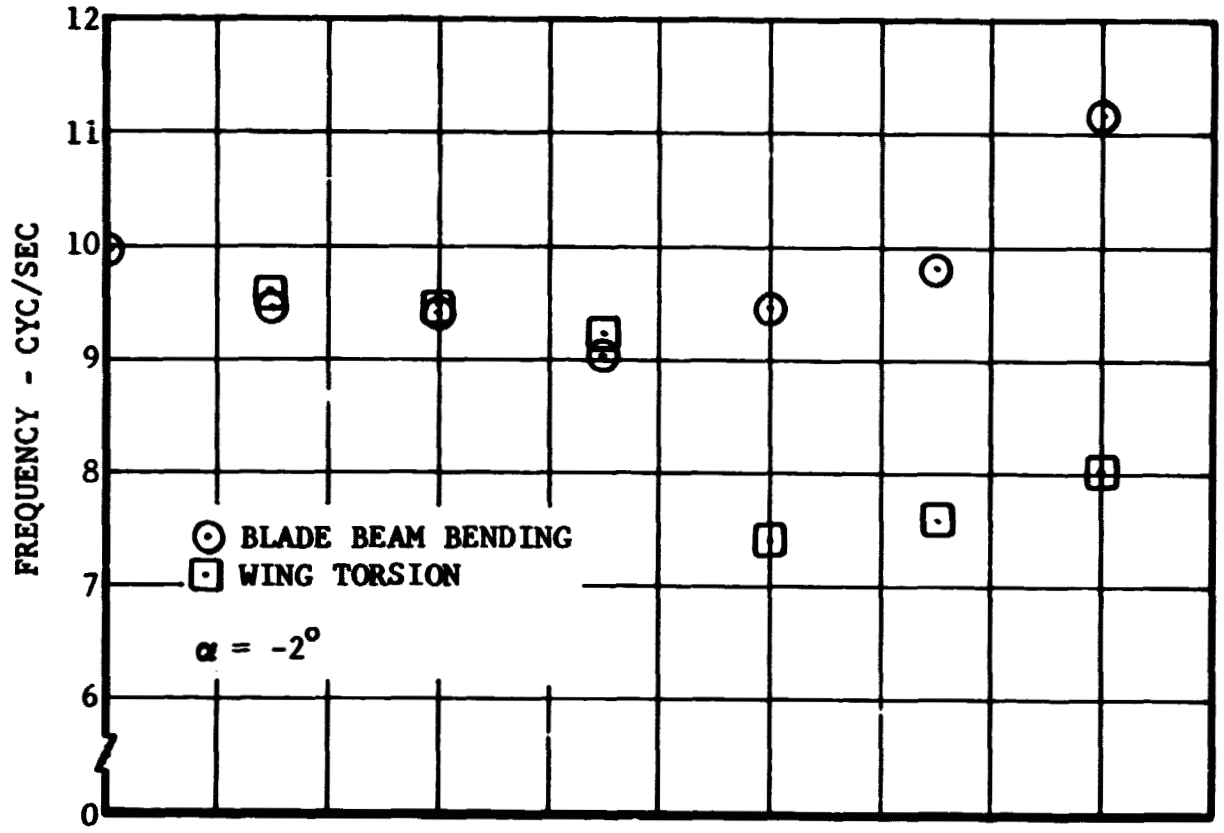


Figure VI-6. Wing Beam and Chord Mode Frequency and Damping Versus Blade Fold Angle, 150 Knots Airspeed.

Use or disclosure of data on this page is subject to the restriction on the title page.



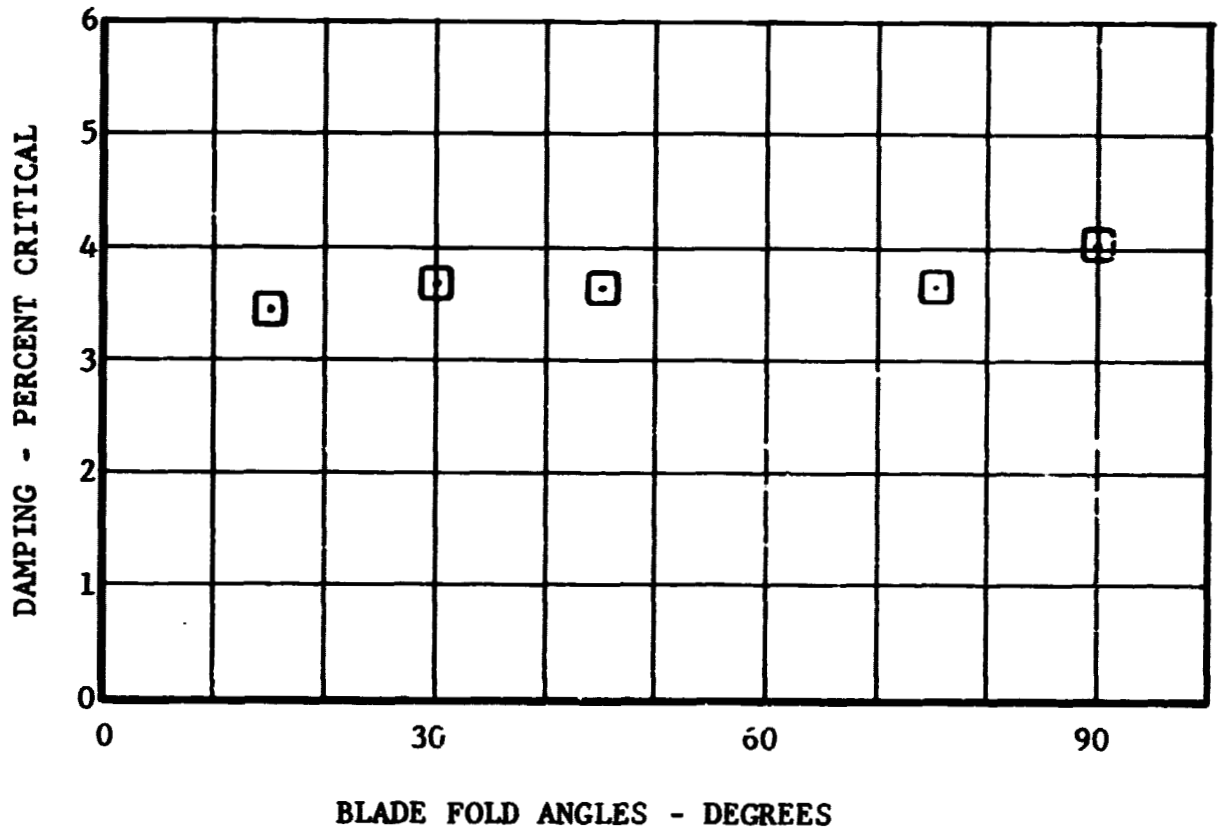
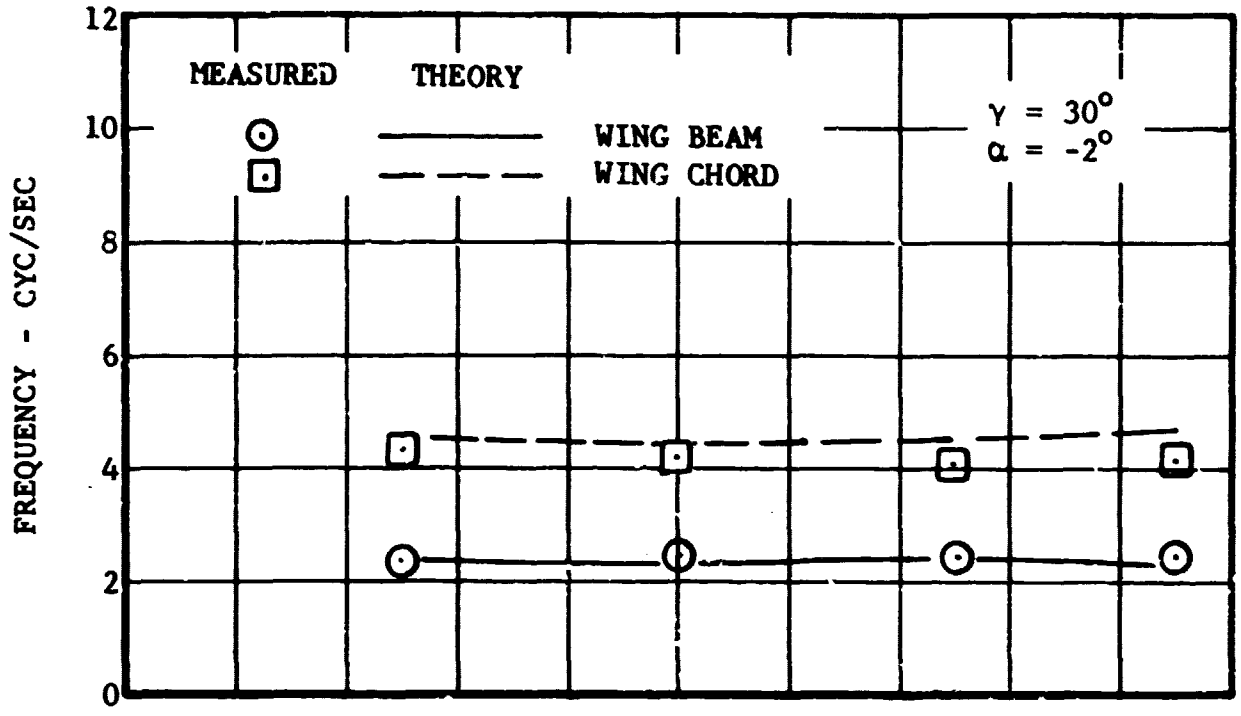


Figure VI-7. Measured Wing Torsion Frequency and Damping, and Measured Blade Beam Bending Frequency Versus Blade Fold Angle, 150 Knots Airspeed.

Use or disclosure of data on this page is subject to the restriction on the title page.



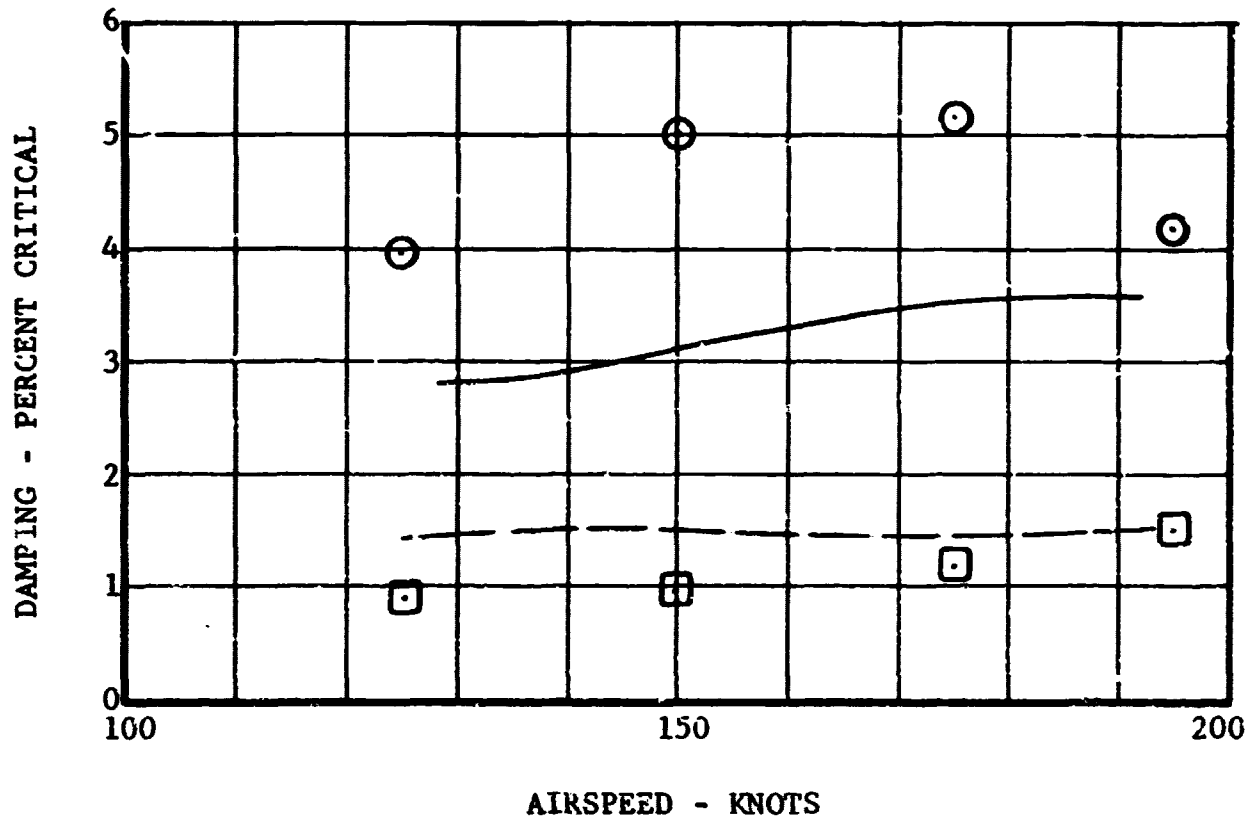


Figure VI-8. Wing Beam and Chord Frequency and Damping Versus Airspeed for 30-Degree Blade Fold Angle.

Use or disclosure of data on this page is subject to the restriction on the title page.

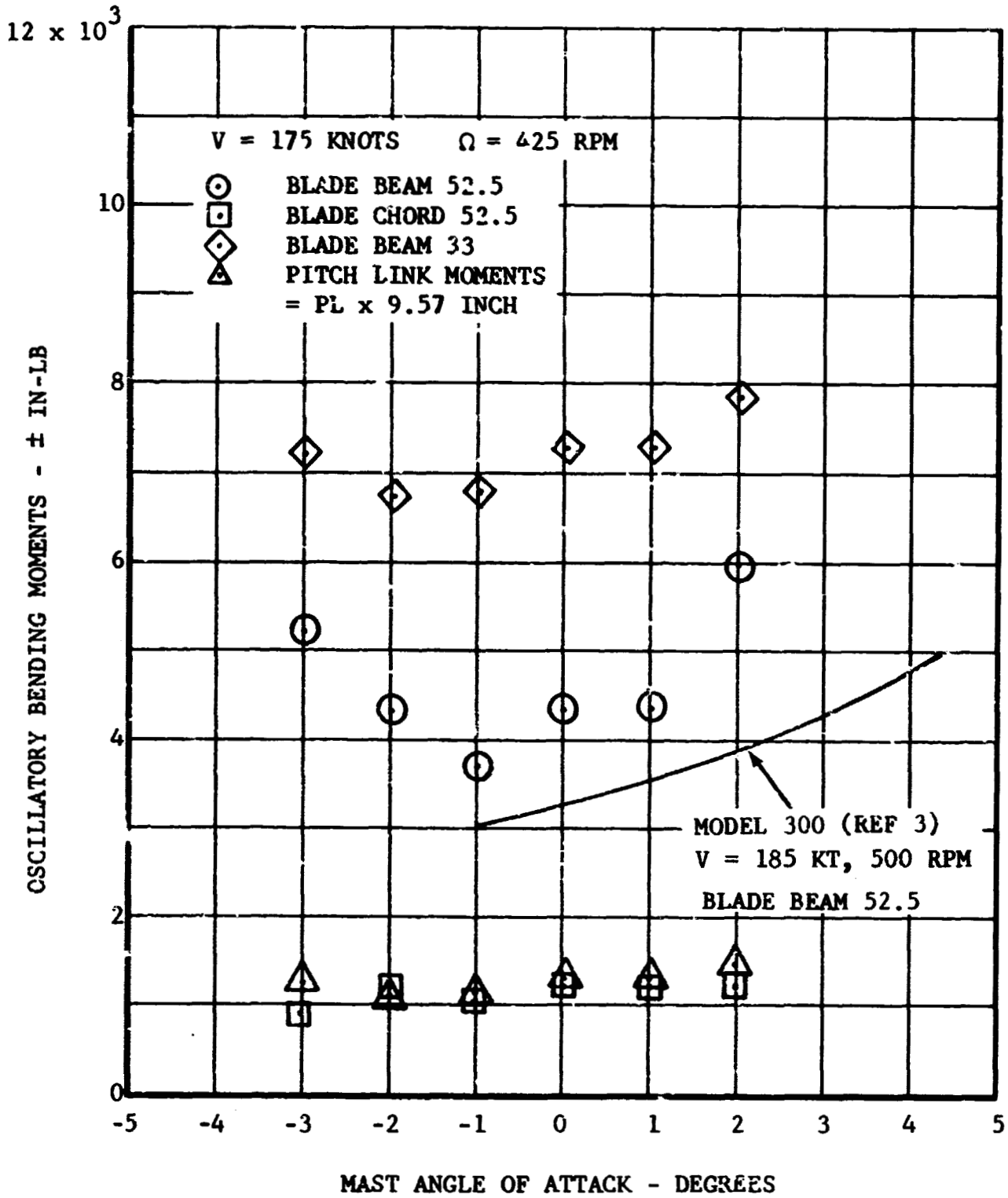


Figure VI-9. Blade and Control System Oscillatory Loads Versus Angle of Attack, Gimbal Free.

Use or disclosure of data on this page is subject to the restriction on the title page.

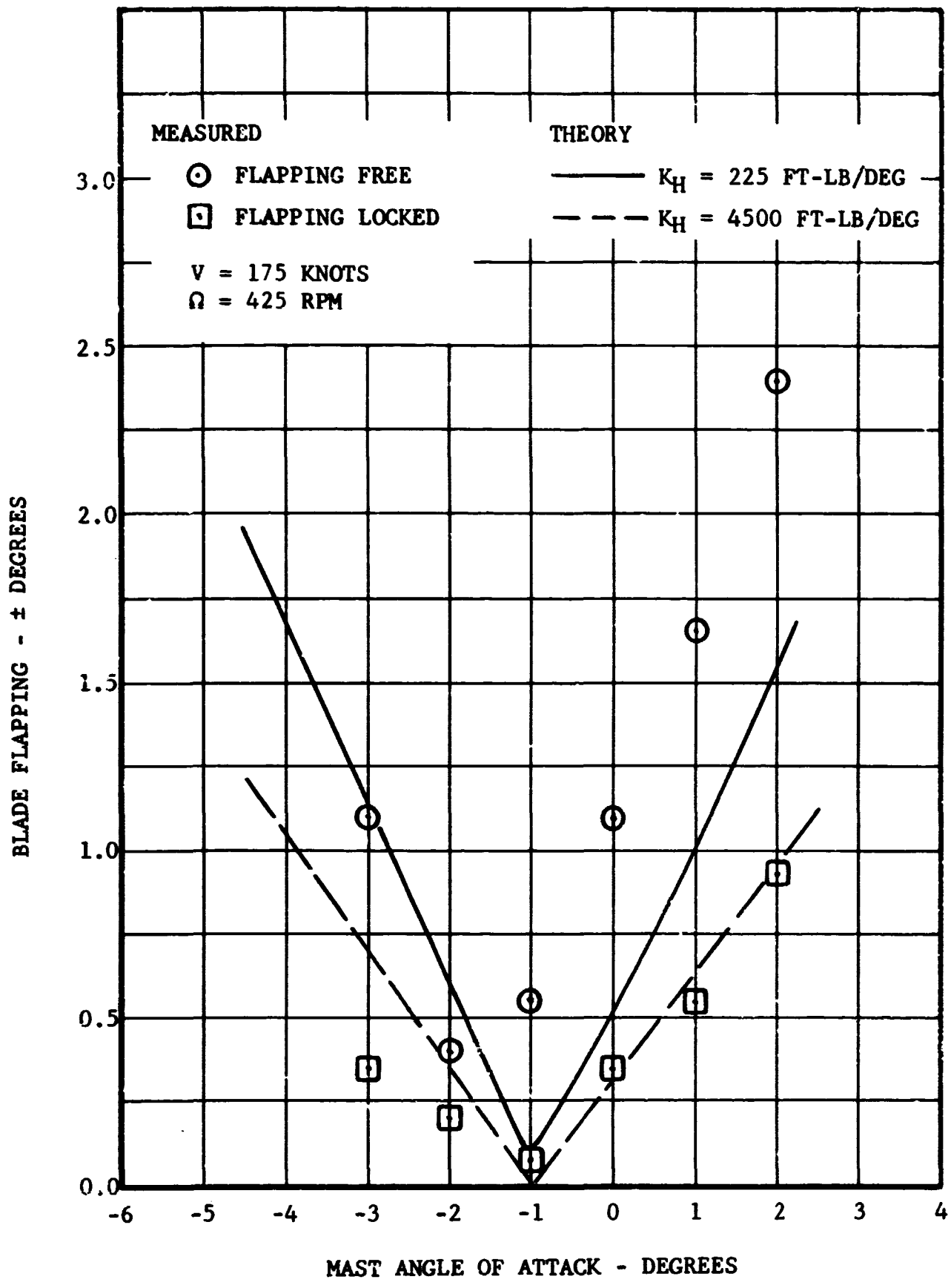


Figure VI-10. Blade Flapping Versus Angle of Attack, Gimbal Free and Gimbal Locked Out.

Use or disclosure of data on this page is subject to the restriction on the title page.

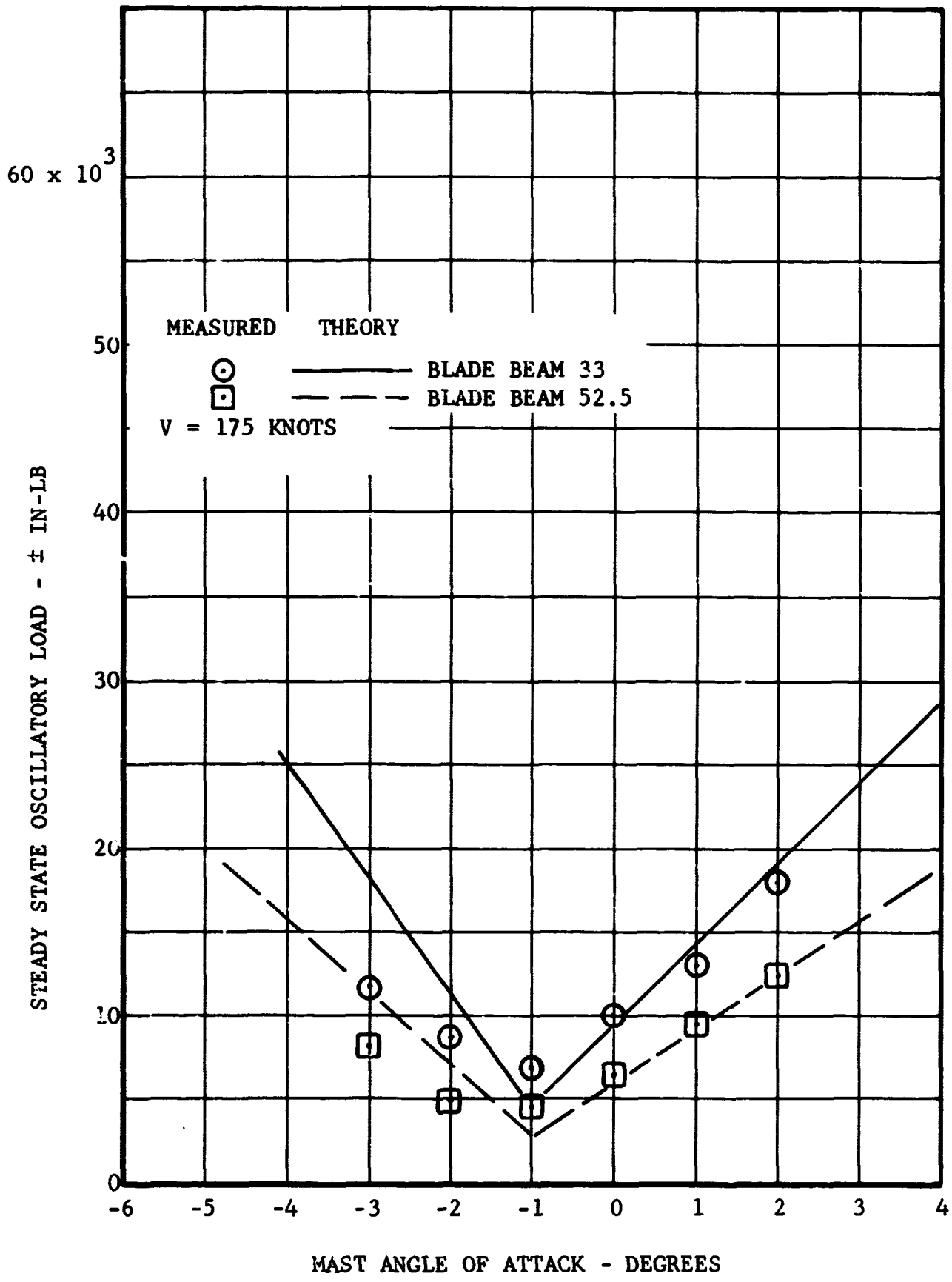


Figure VI-11. Blade Steady-State Oscillatory Loads Versus Angle of Attack, 425 RPM, Gimbal Locked Out.

Use or disclosure of data on this page is subject to the restriction on the title page.

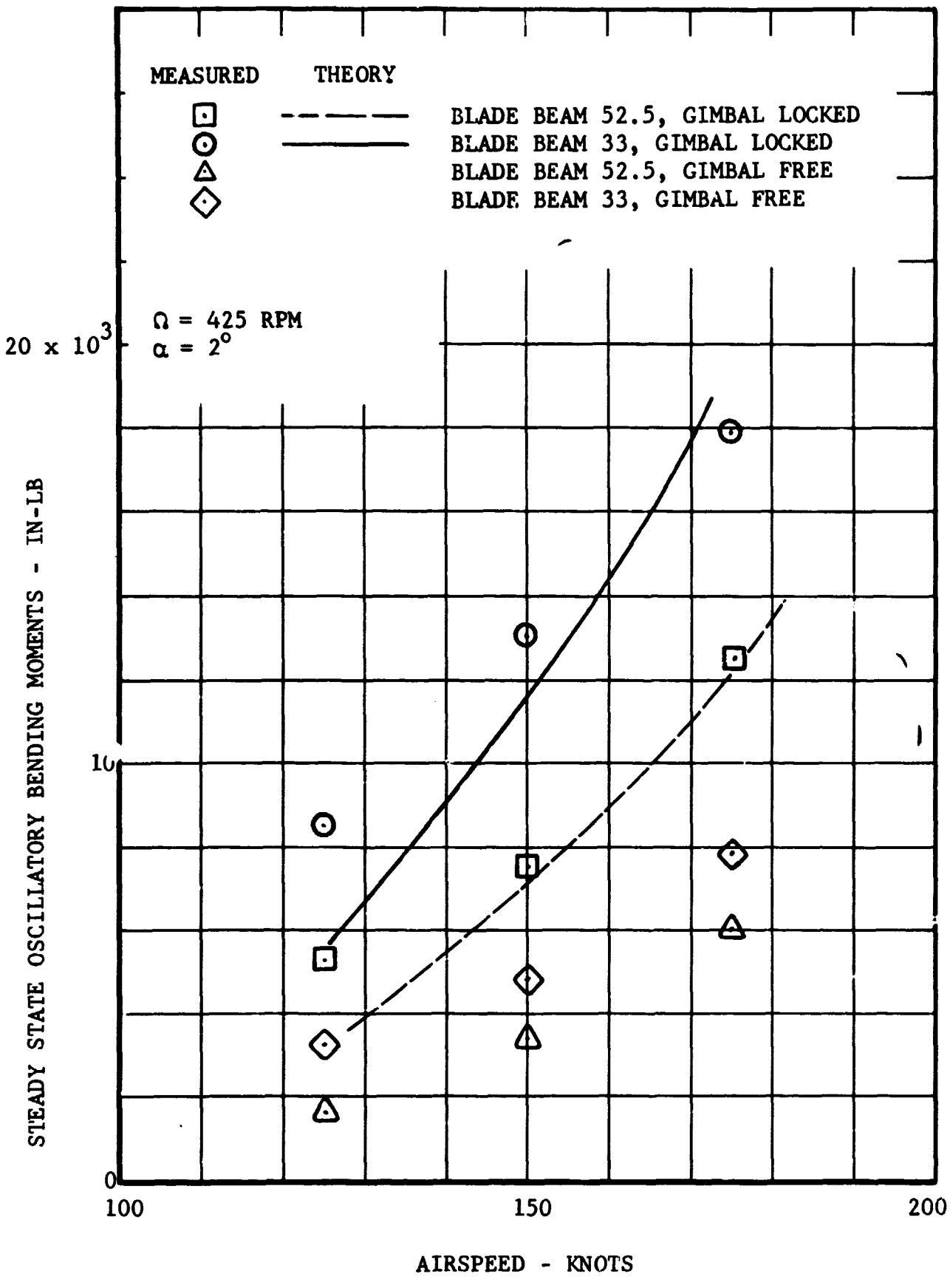


Figure VI-12. Blade Steady-State Oscillatory Loads Versus Airspeed, 425 RPM, Gimbal Locked Out and Gimbal Free.

Use or disclosure of data on this page is subject to the restriction on the title page.

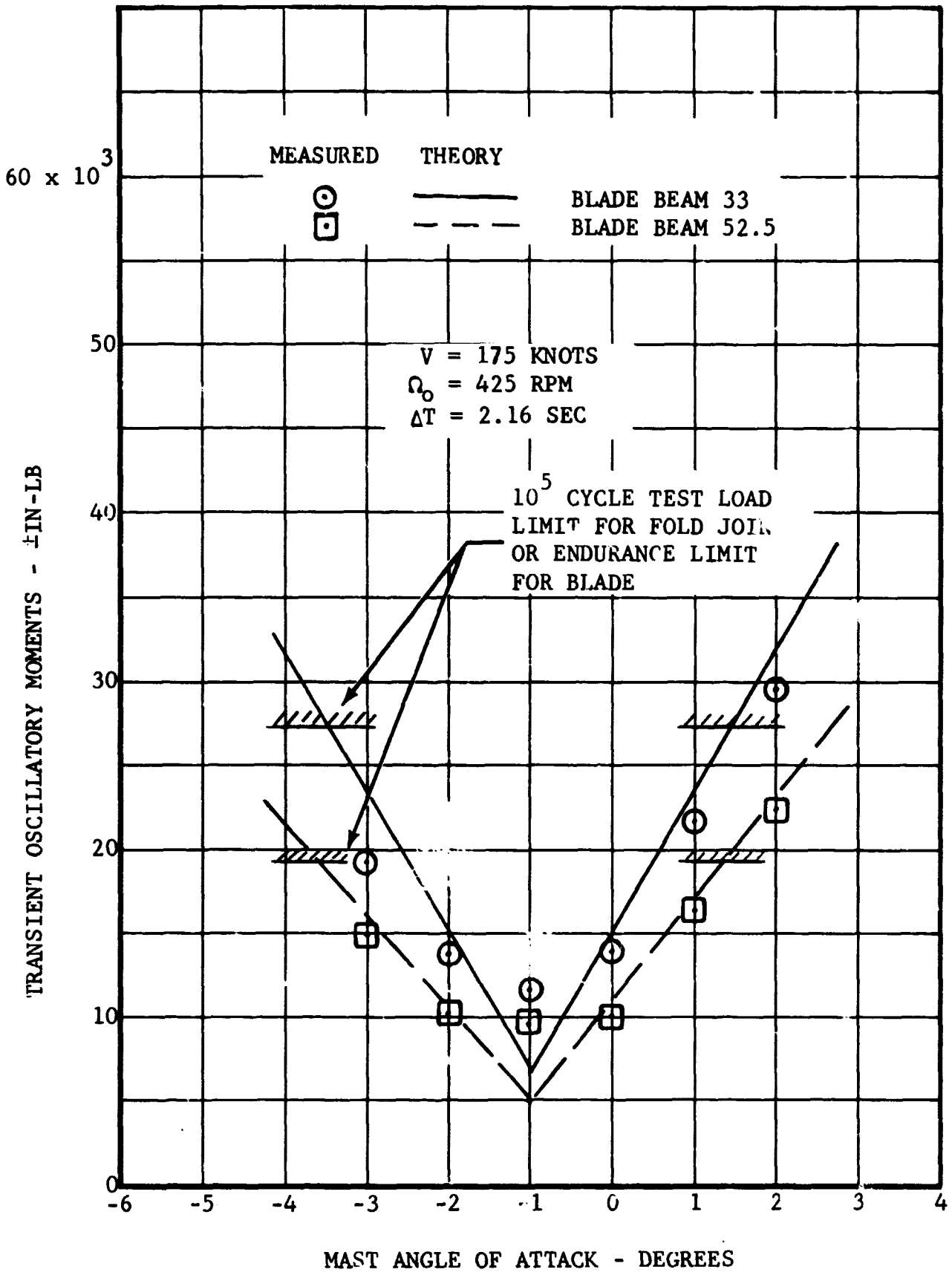


Figure VI-13. Peak Blade Oscillatory Loads During Proprotor Stop Sequence Versus Angle of Attack, 175 Knots Airspeed, Gimbal Locked Out.

Use or disclosure of data on this page is subject to the restriction on the title page.

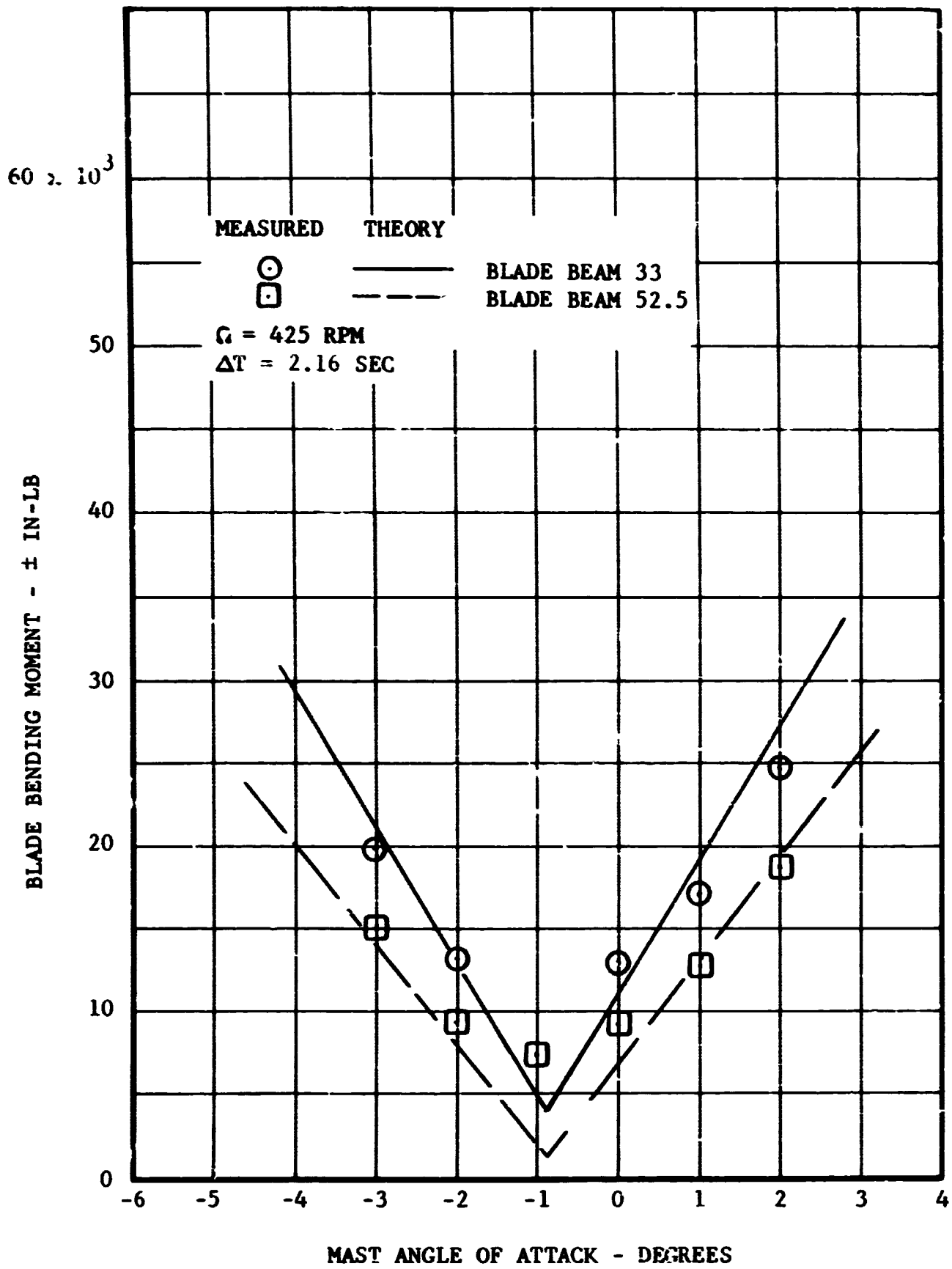


Figure VI-14. Peak Blade Oscillatory Loads During Proprotor Start Sequence Versus Angle of Attack, 175 Knots Airspeed.

Use or disclosure of data on this page is subject to the restriction on the title page.

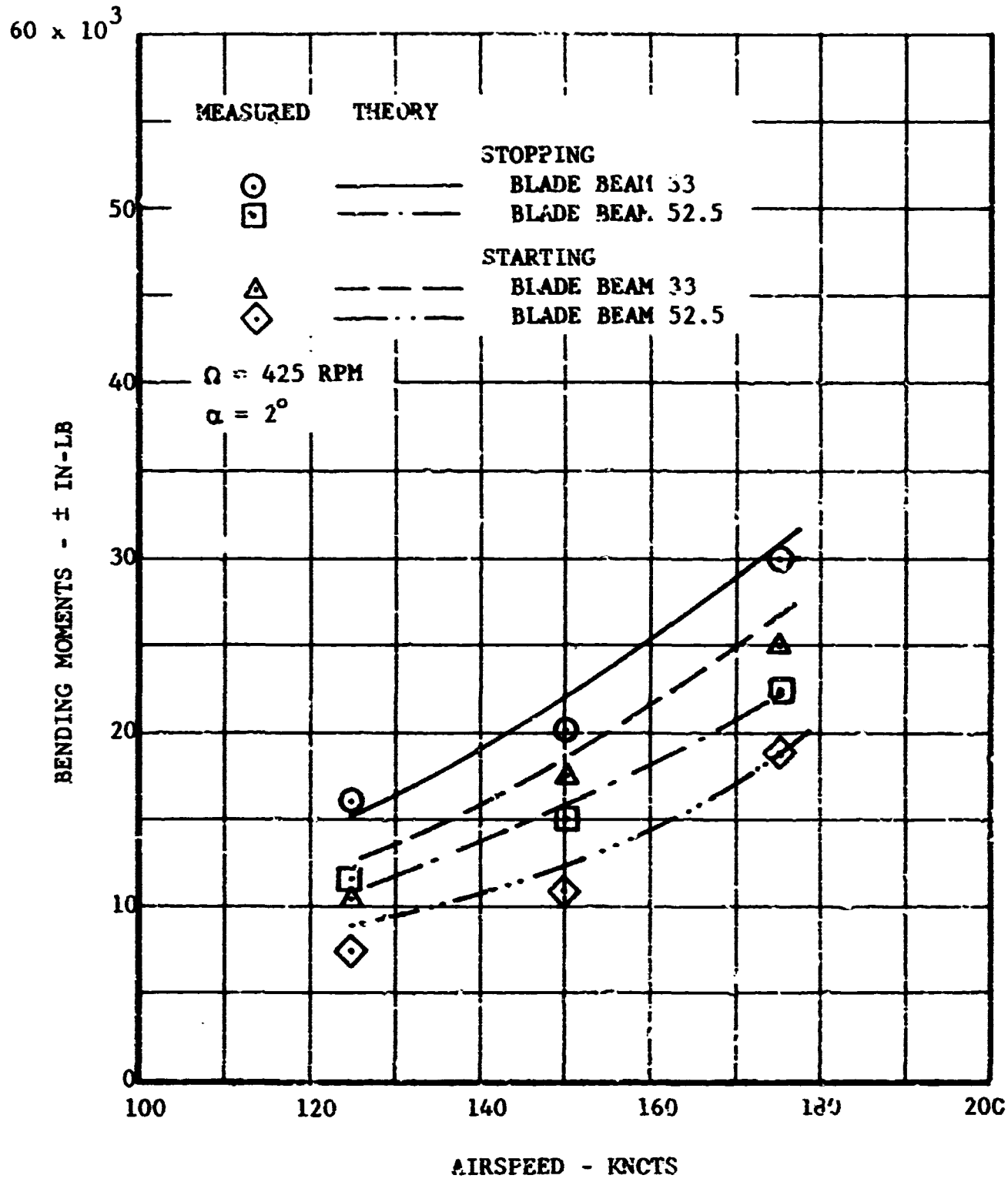


Figure VI-15. Peak Blade Oscillatory Loads During Stop/Start Sequence Versus Airspeed, Gimbal Locked Out.

Use or disclosure of data on this page is subject to the restriction on the title page

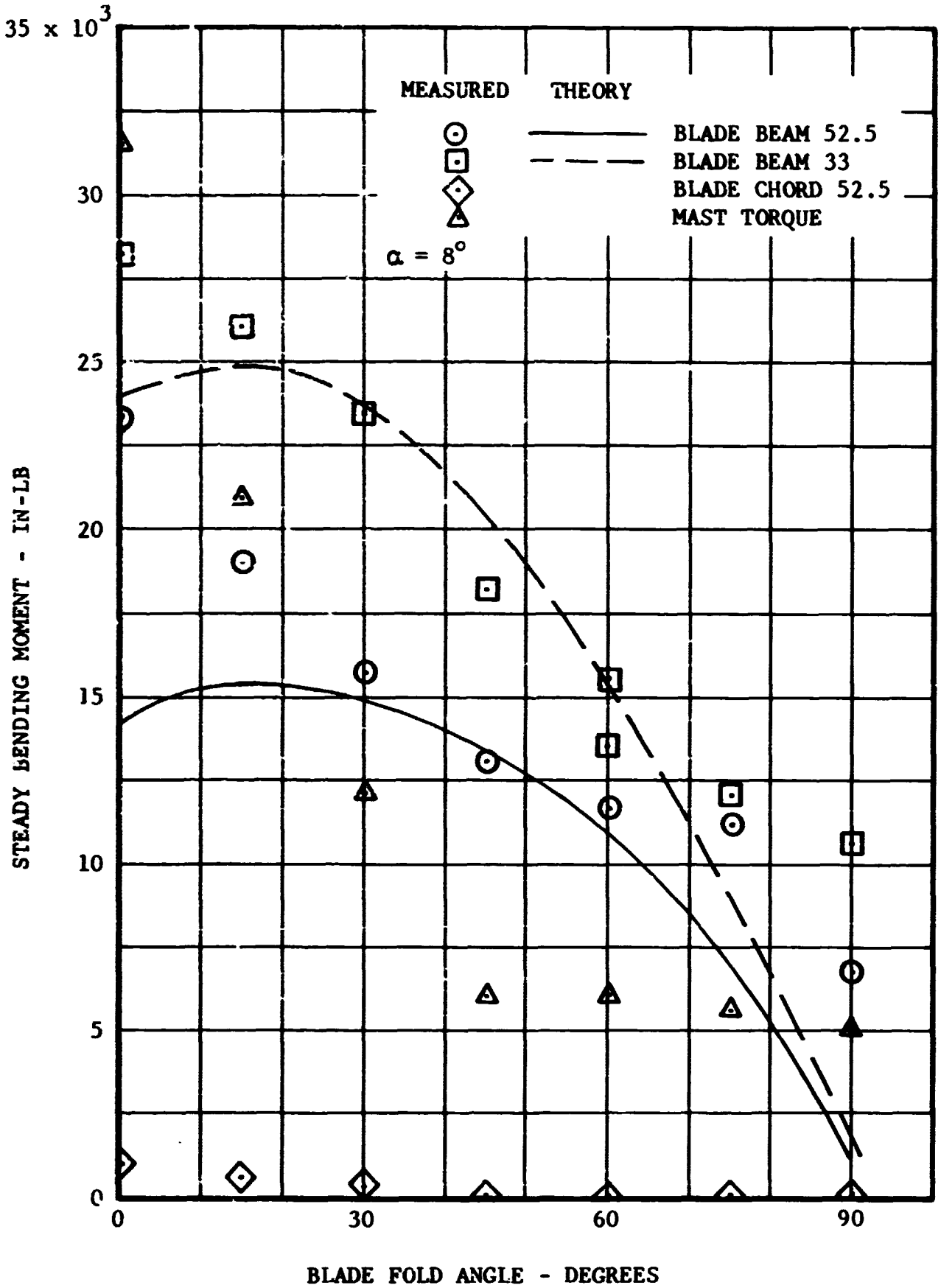


Figure VI-16. Steady Blade Bending Moments and Mast Torque Versus Blade Fold Angle, 150 Knots Airspeed.

Use or disclosure of data on this page is subject to the restriction on the title page

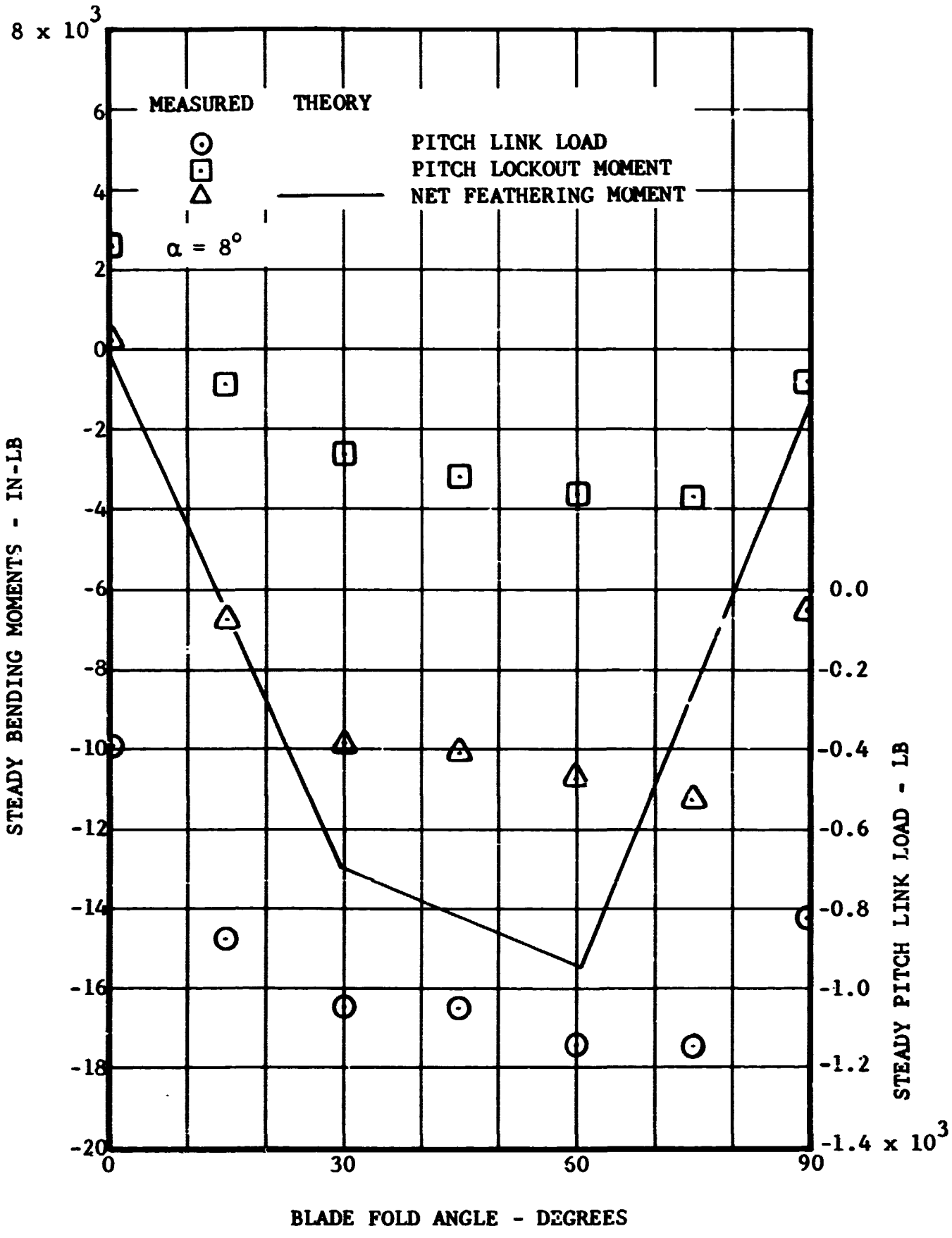


Figure VI-17. Pitch Link Axial Load and Pitch Lockout Moment Versus Blade Fold Angle, 150 Knots Airspeed.

Use or disclosure of data on this page is subject to the restriction on the title page

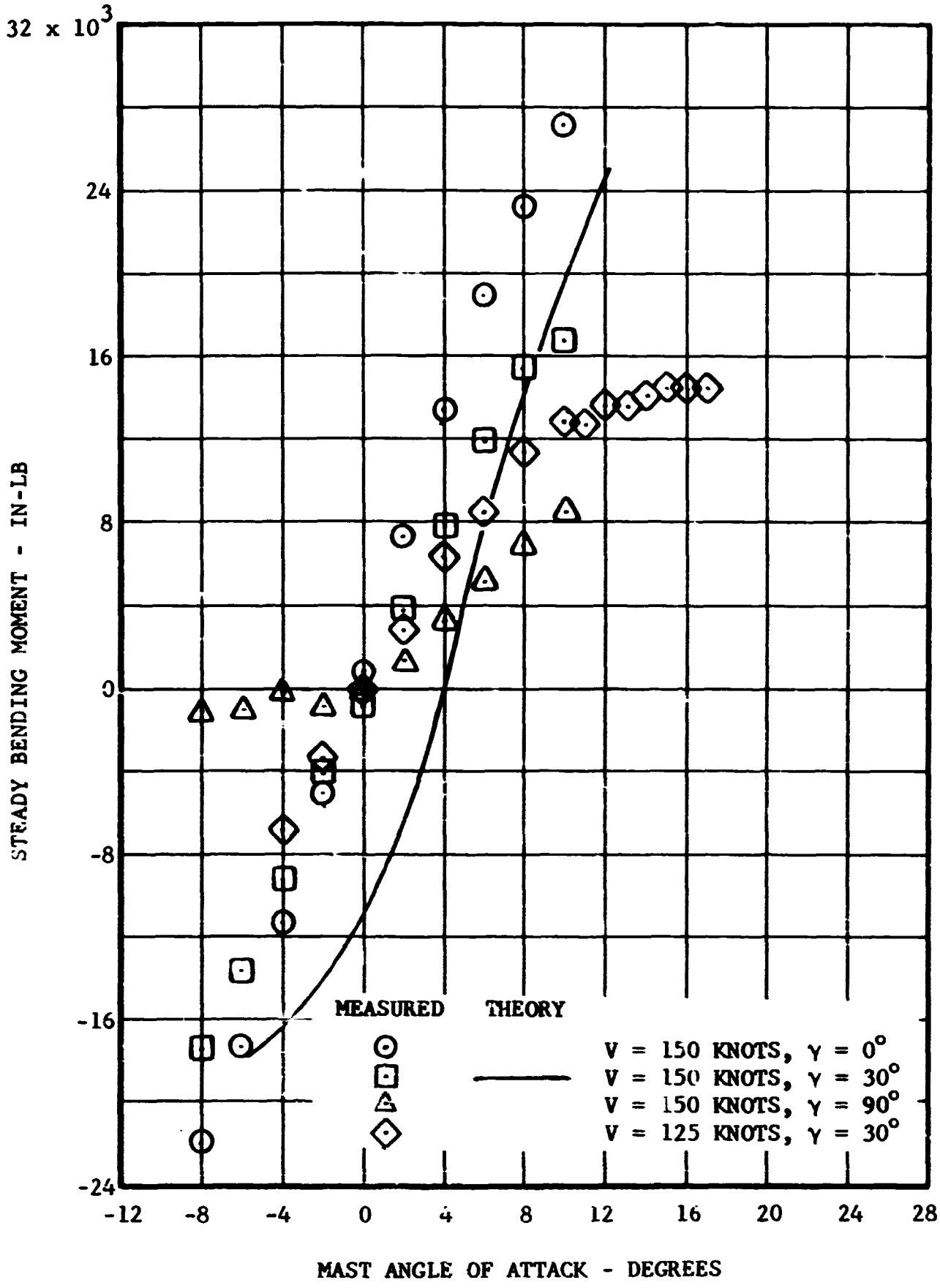


Figure VI-18. Blade Station 52.5 Steady Beam Bending Moment Versus Angle of Attack for Several Blade Fold Angles.

Use or disclosure of data on this page is subject to the restriction on the title page

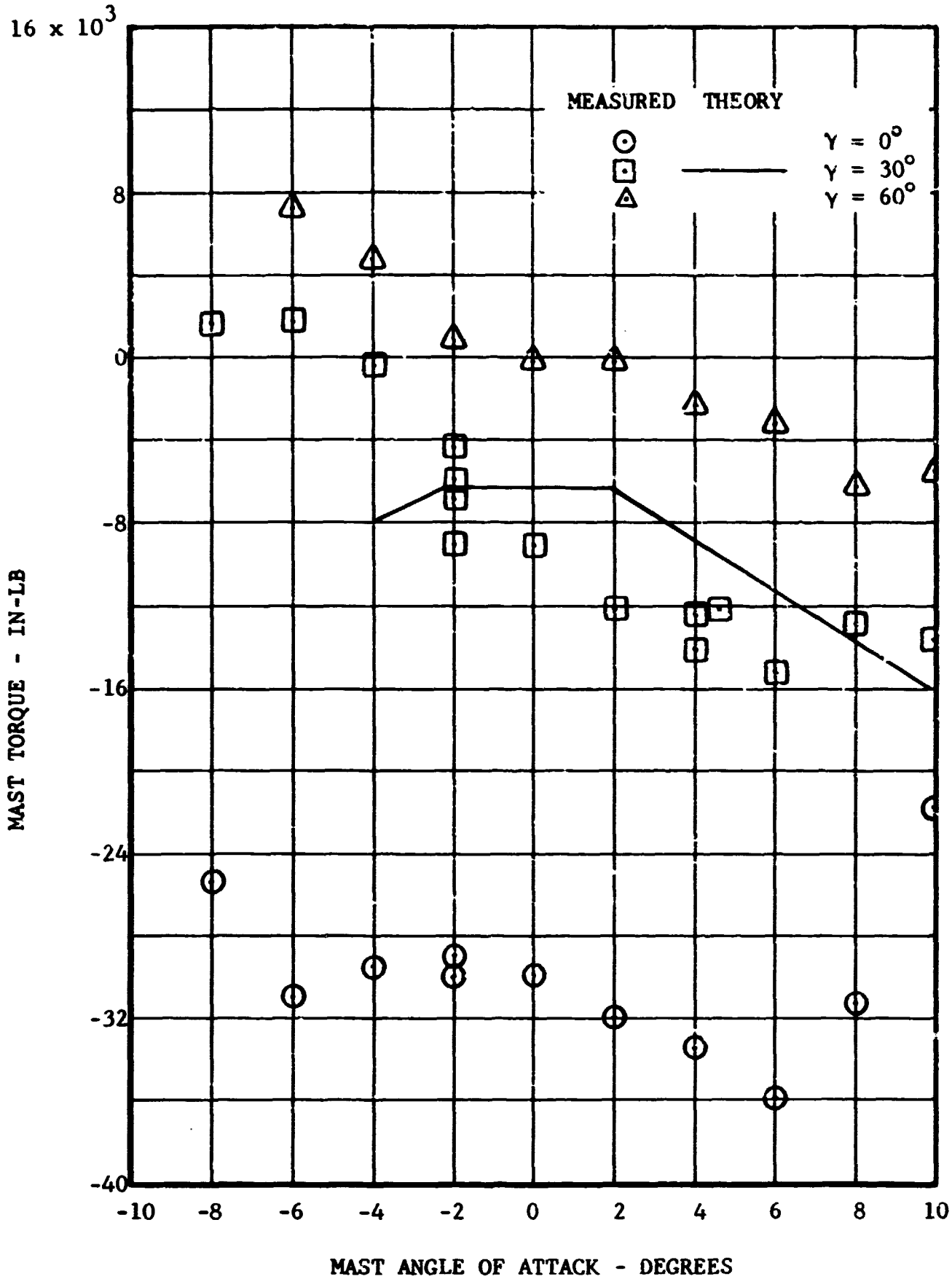


Figure VI-19. Mast Torque Variation With Mast Angle of Attack for Several Blade Fold Angles, 150 Knots Airspeed.

Use or disclosure of data on this page is subject to the restriction on the title page.

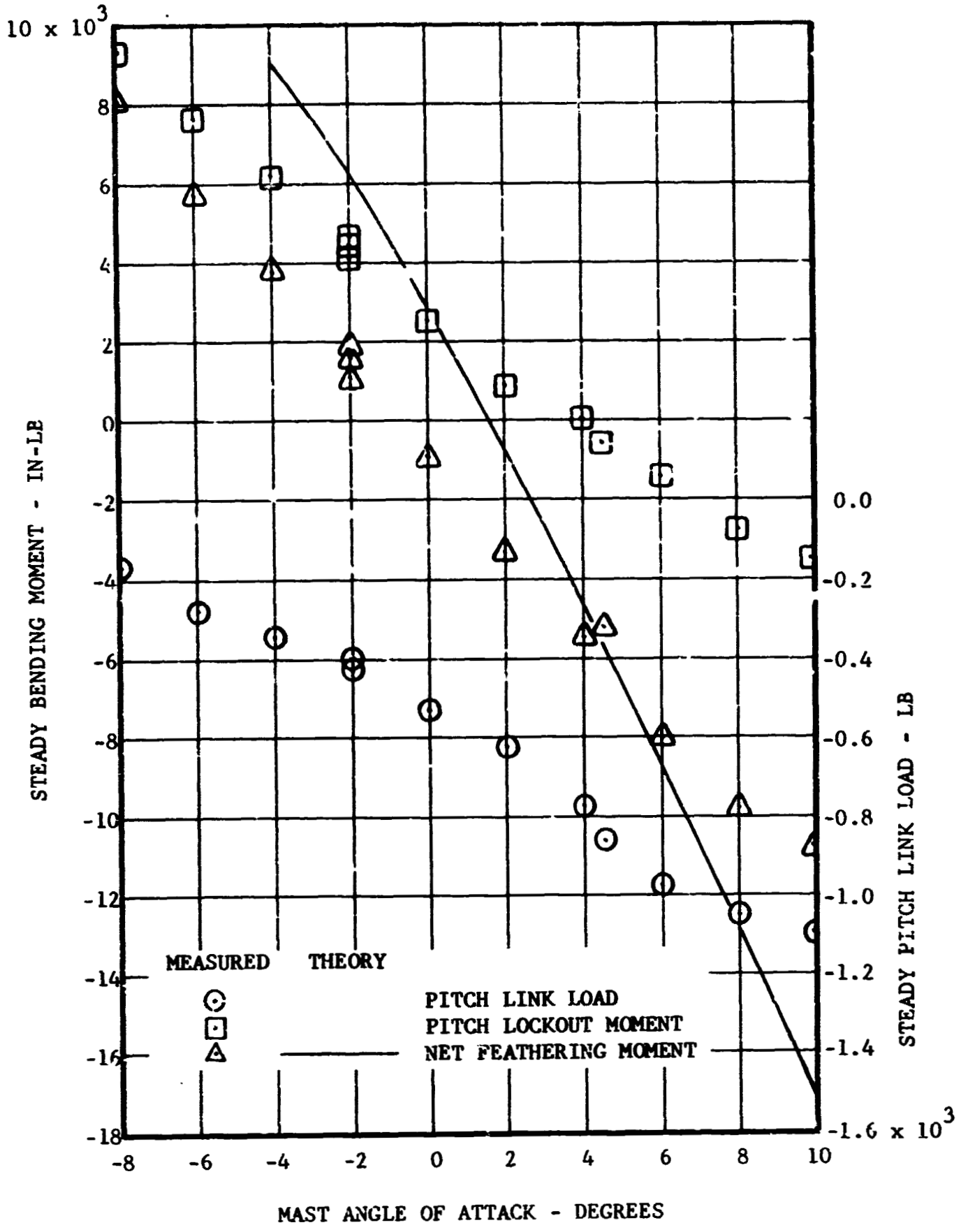


Figure VI-20. Pitch Link Axial Load and Pitch Lockout Moment Versus Angle of Attack for 30-Degree Blade Fold Angle 150 Knots Airspeed.

Use or disclosure of data on this page is subject to the restriction on the title page.

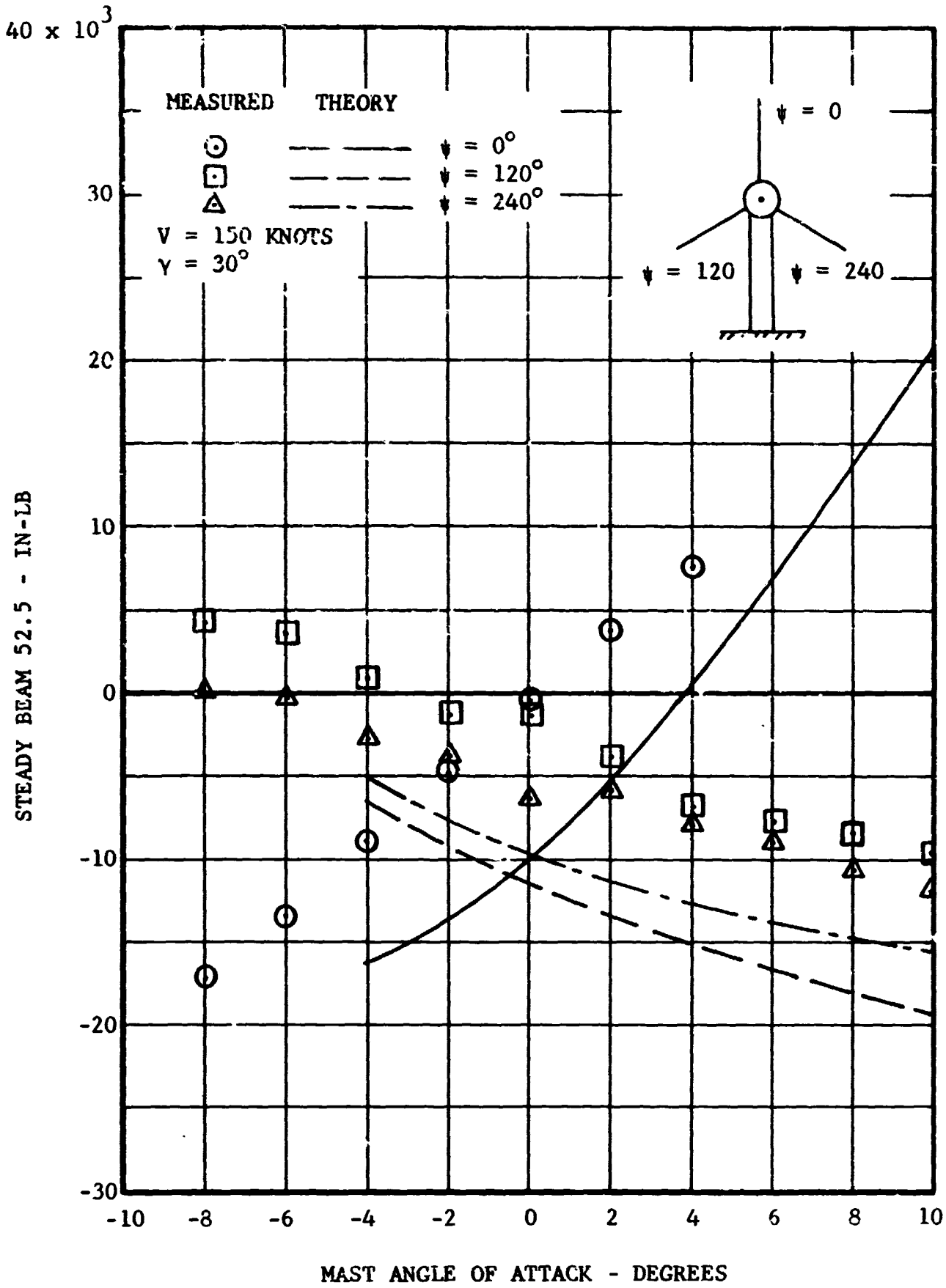


Figure VI-21. Comparison of Blade Steady Loads Versus Angle of Attack For Three Azimuth Positions.

Use or disclosure of data on this page is subject to the restriction on the title page.

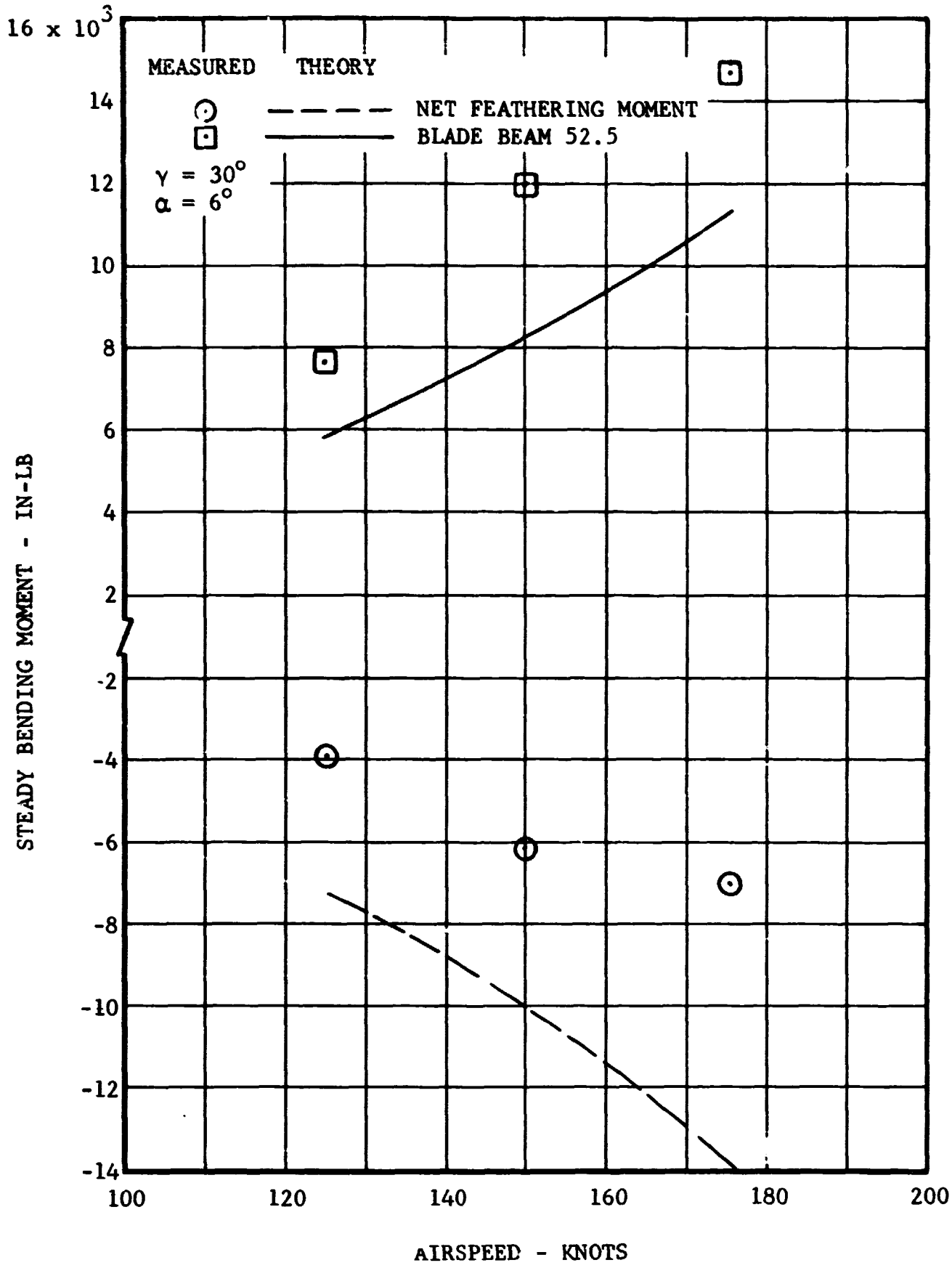


Figure VI-22. Steady Blade and Control Loads Versus Airspeed.

Use or disclosure of data on this page is subject to the restriction on the title page.

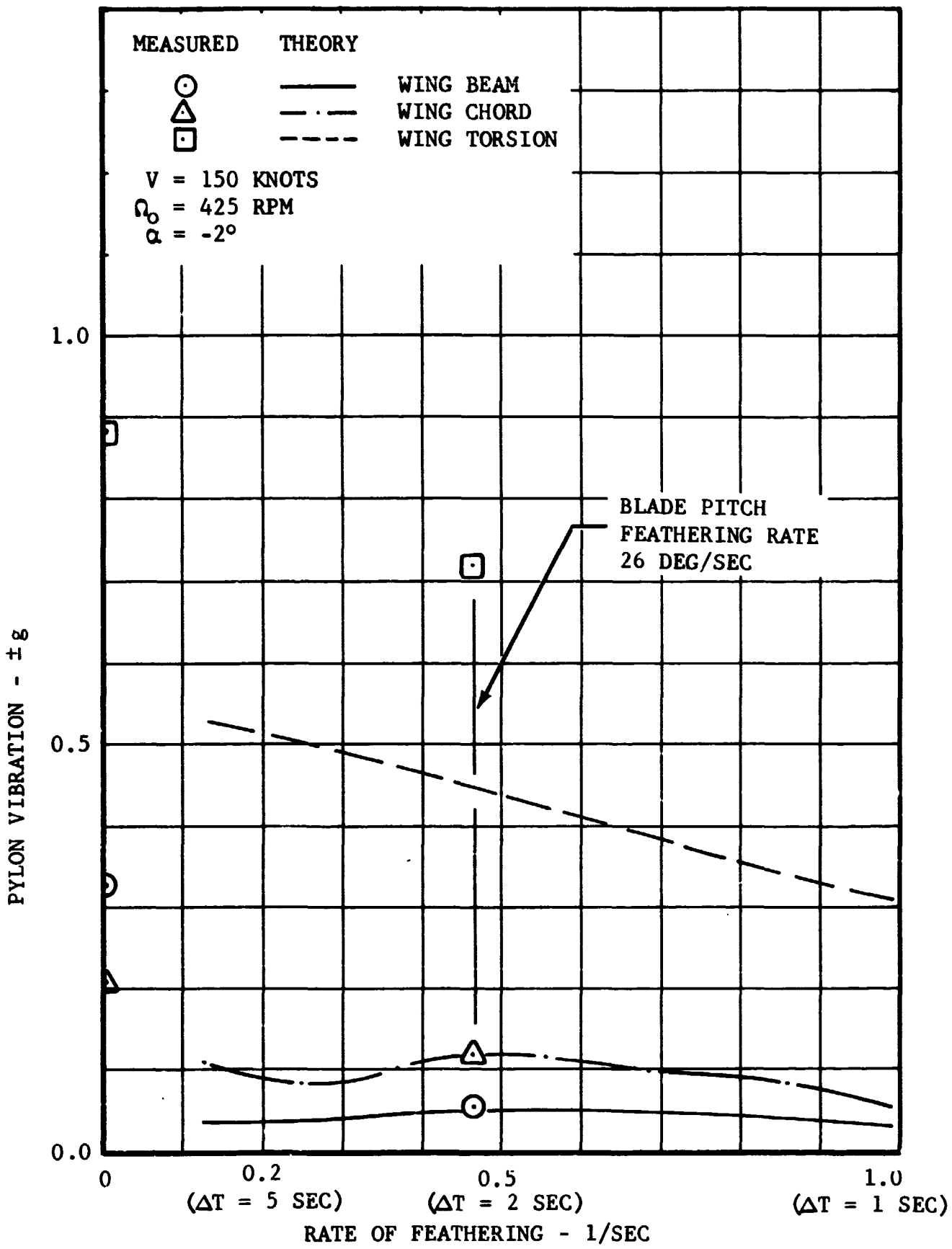


Figure VI-23. Pylon Vibration at Blade Passage Frequency Versus Rate of Feathering.

Use or disclosure of data on this page is subject to the restriction on the title page.

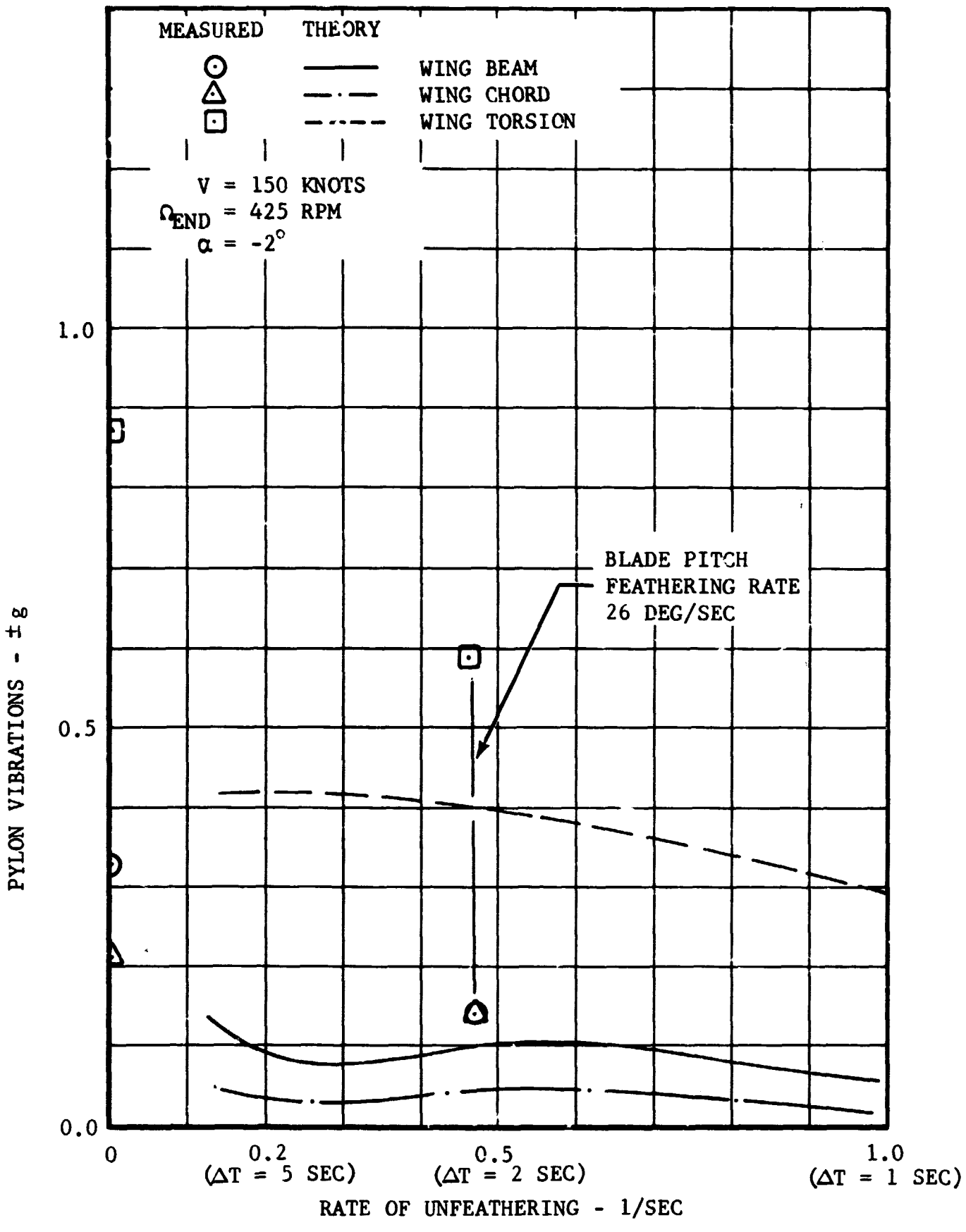


Figure VI-24. Pylon Vibration at Blade Passage Frequency Versus Rate of Unfeathering.

Use or disclosure of data on this page is subject to the restriction on the title page

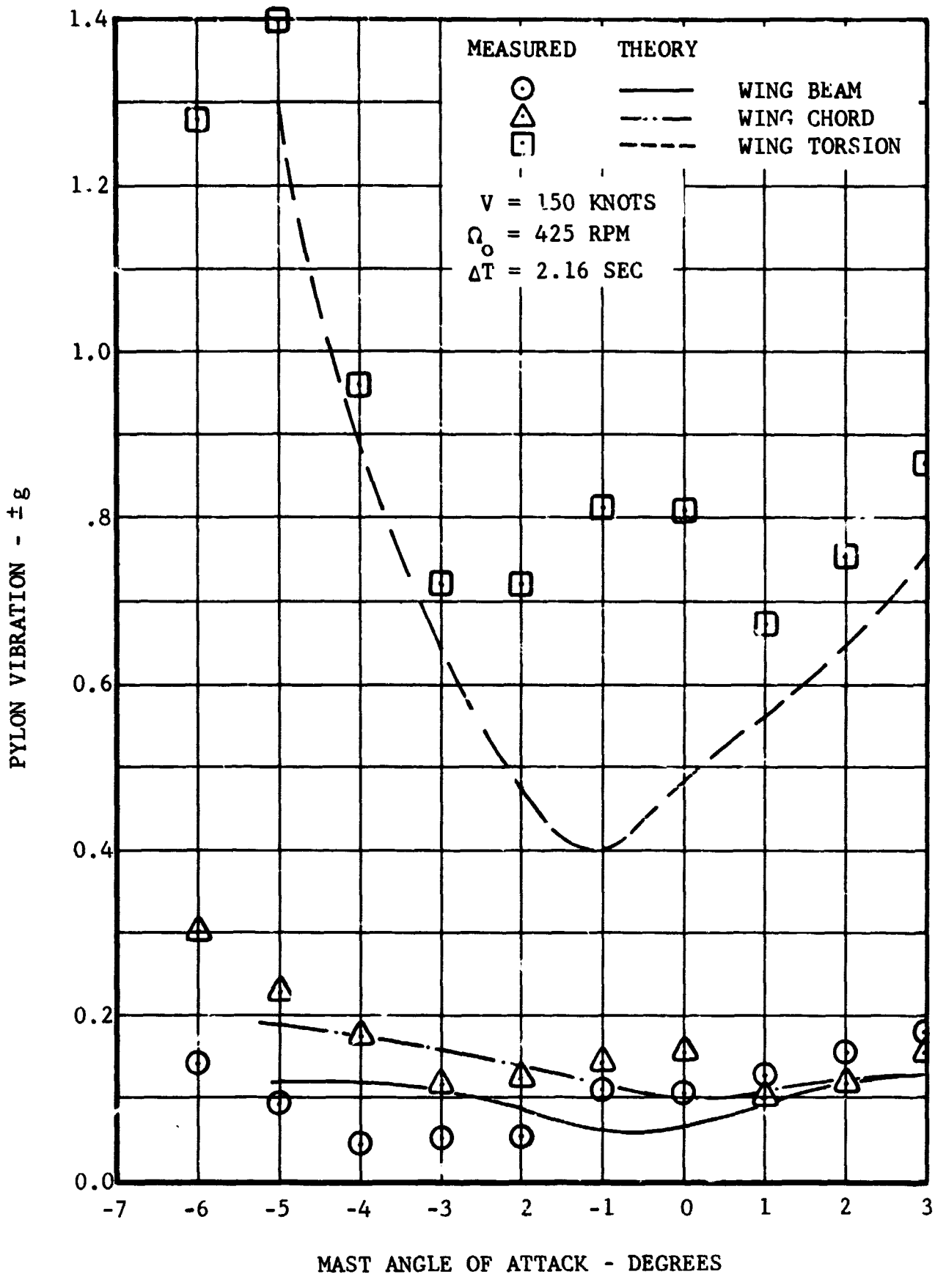


Figure VI-25. Pylon Vibration at Blade Passage Frequency Versus Mast Angle of Attack During Feathering.

Use or disclosure of data on this page is subject to the restriction on the title page.

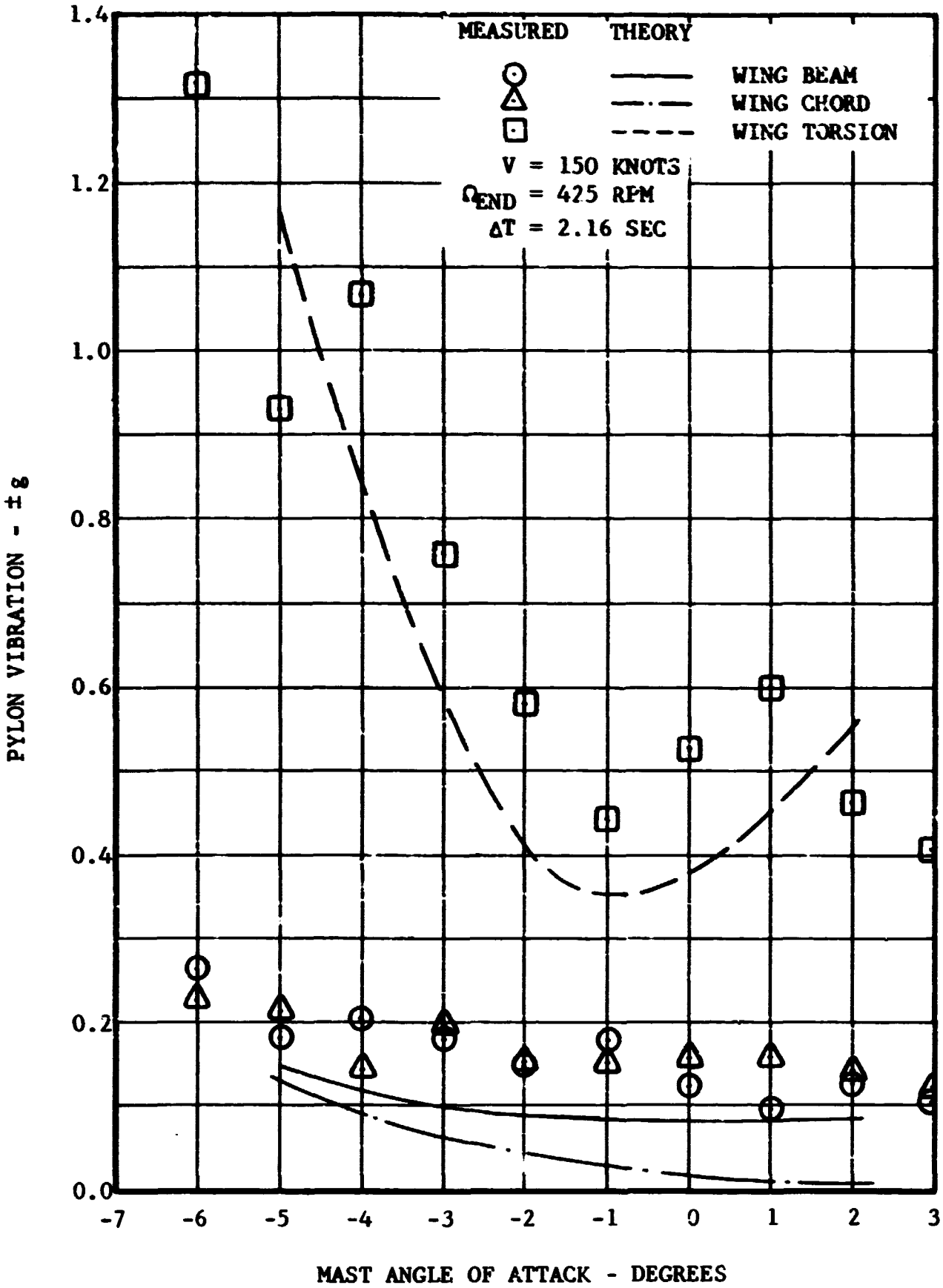
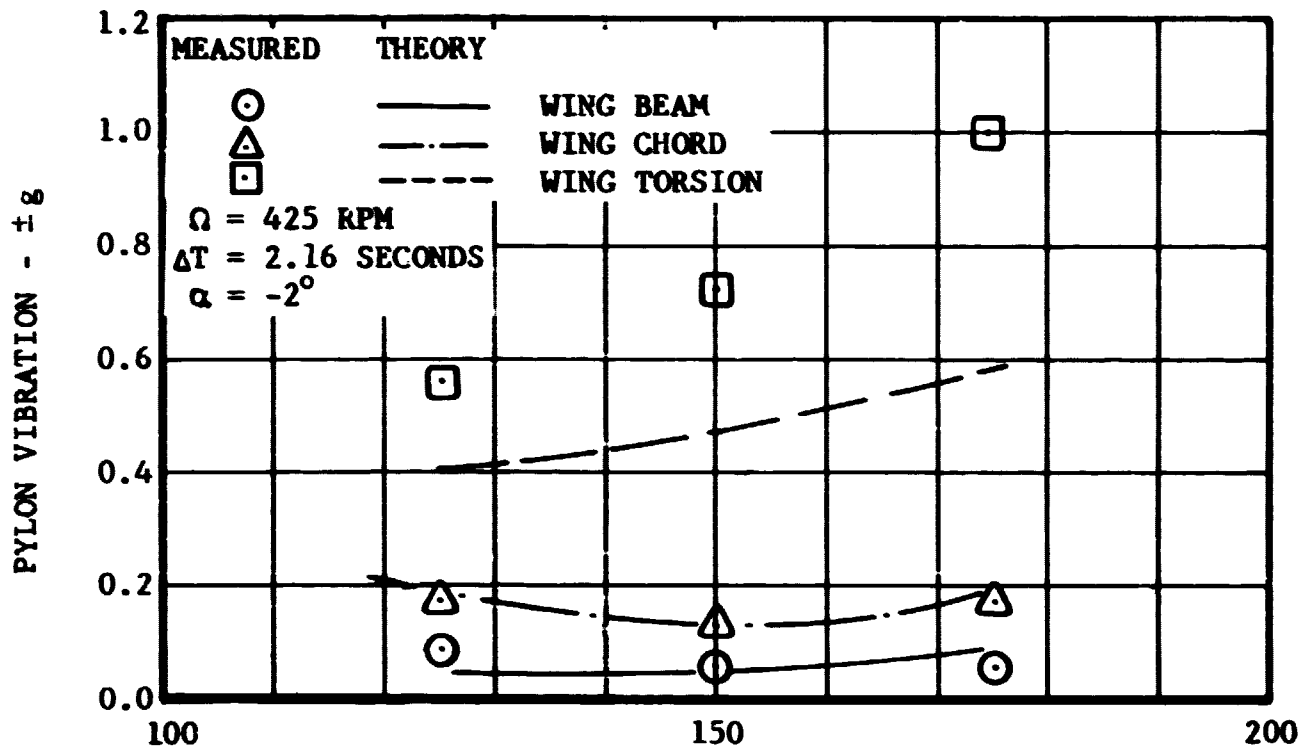


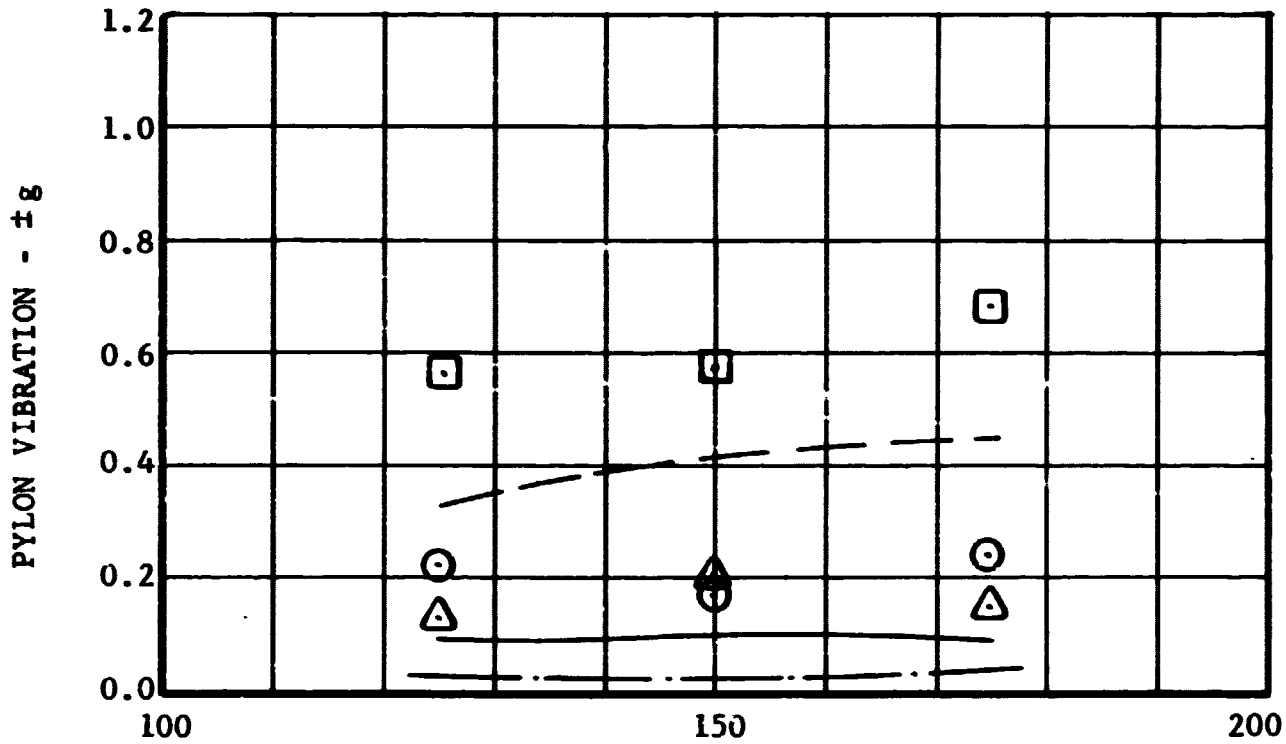
Figure VI-26. Pylon Vibration at Blade Passage Frequency Versus Mast Angle of Attack During Unfeathering.

C-3

Use or disclosure of data on this page is subject to the restriction on the title page.



(a) FEATHERING



(b) UNFEATHERING

Figure VI-27. Pylon Vibration at Blade Passage Frequency Versus Airspeed During Feathering/Unfeathering.

Use or disclosure of data on this page is subject to the restriction on the title page.

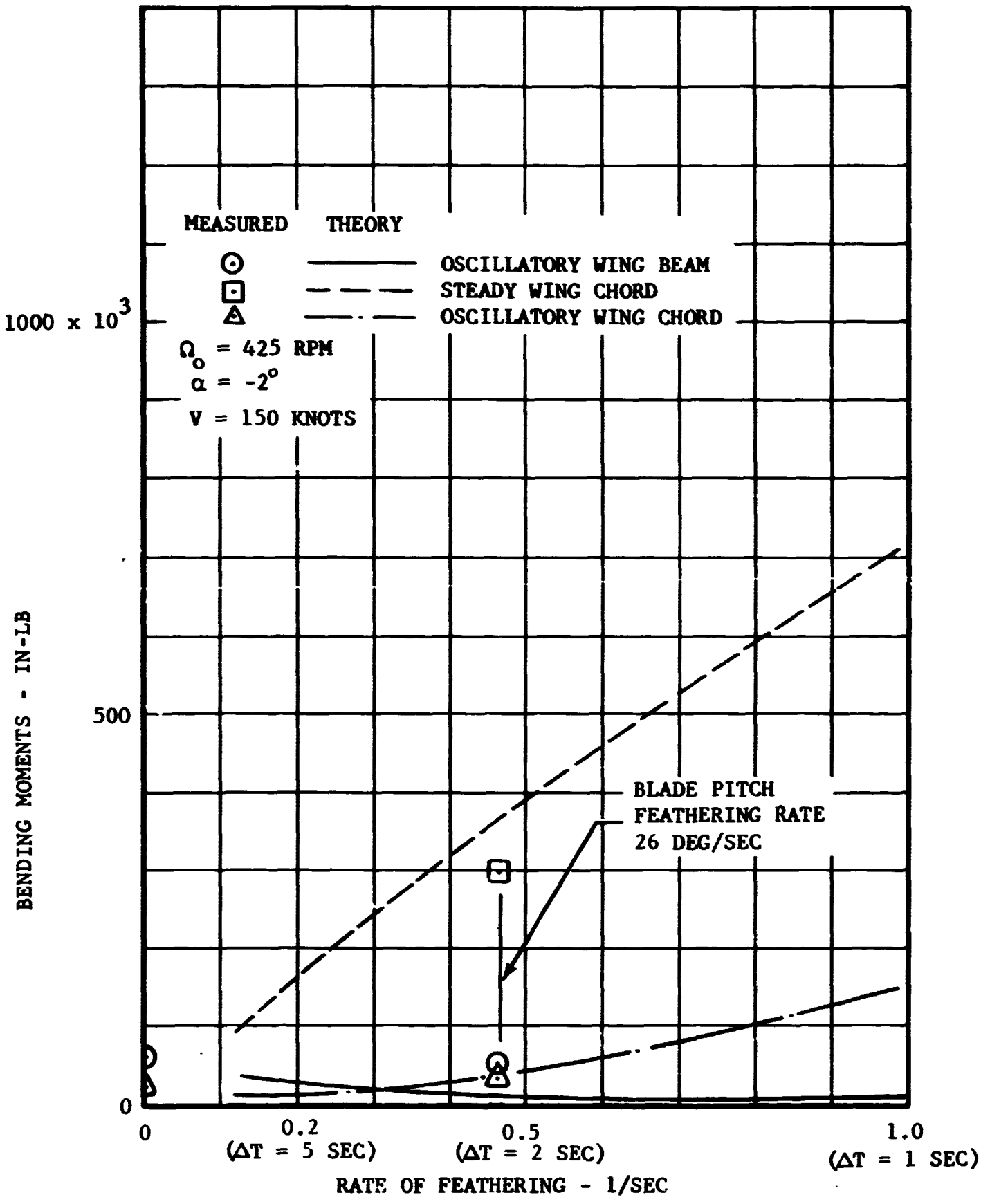


Figure VI-28. Wing Root Loads Versus Rate of Feathering.

Use or disclosure of data on this page is subject to the restriction on the title page.

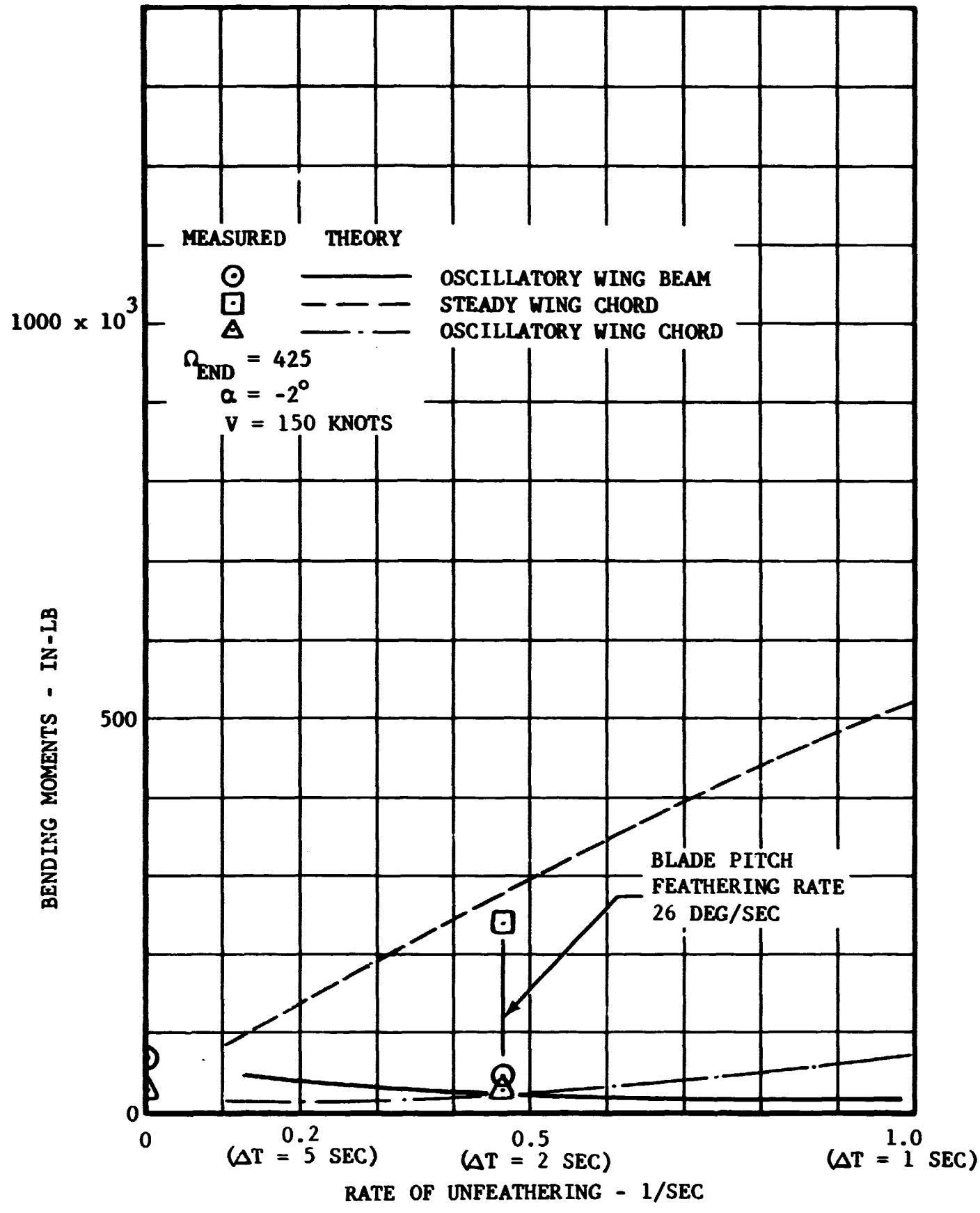


Figure VI-29. Wing Root Loads Versus Rate of Unfeathering.

Use or disclosure of data on this page is subject to the restriction on the title page.

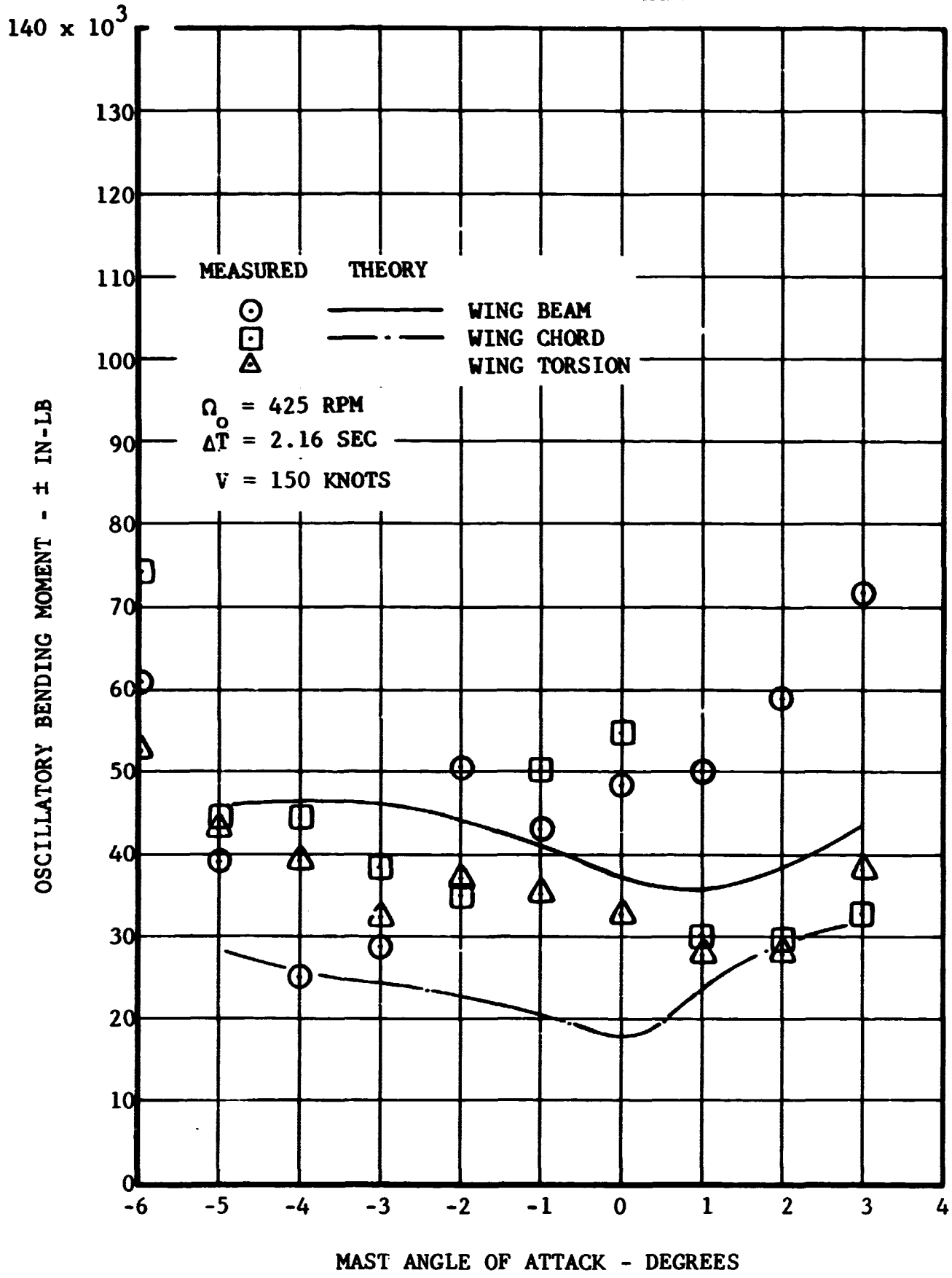


Figure VI-30. Wing Root Loads Versus Mast Angle of Attack During Feathering.

Use or disclosure of data on this page is subject to the restriction on the title page.

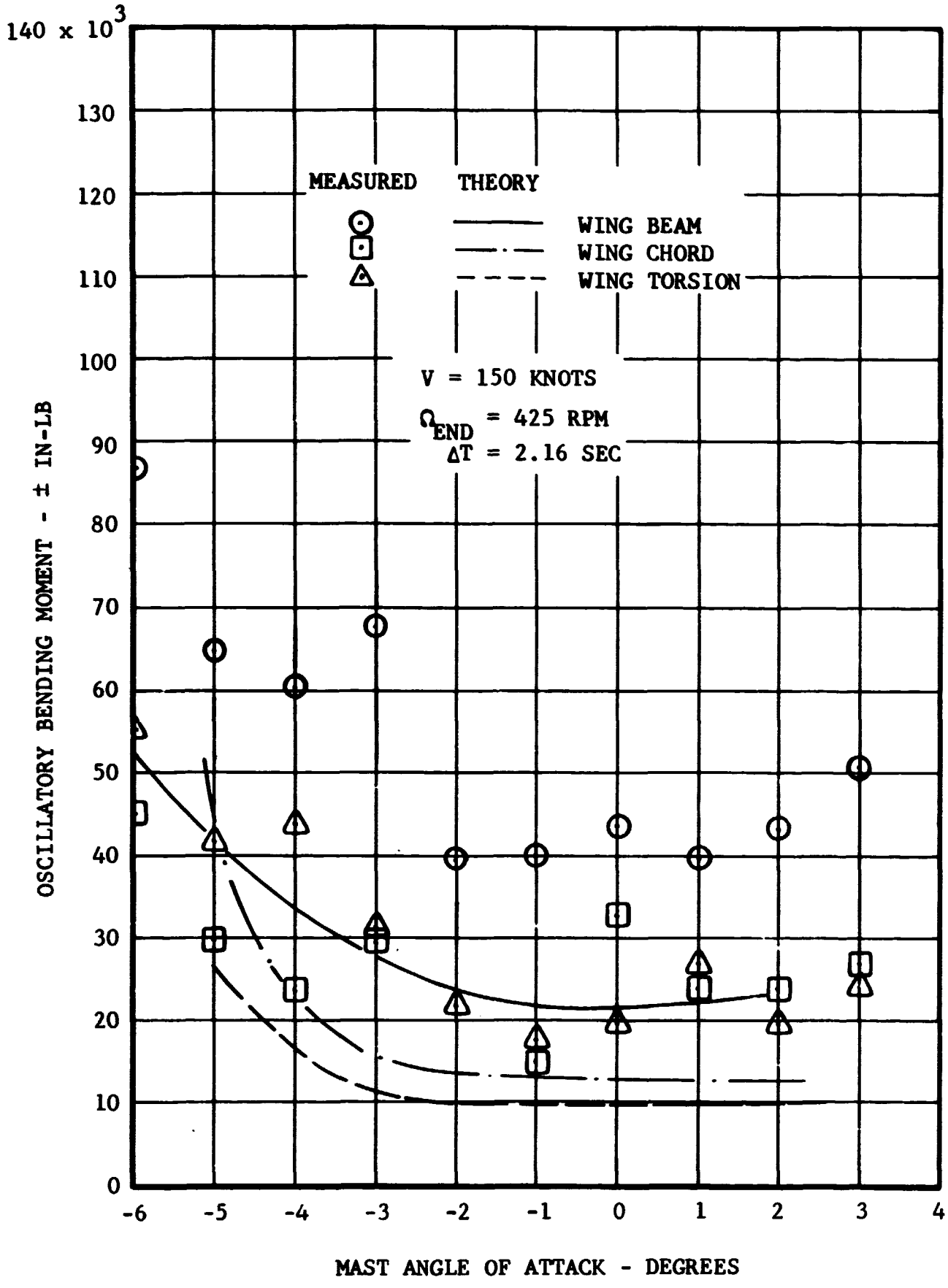


Figure VI-31. Wing Root Loads Versus Mast Angle of Attack During Unfeathering.

Use or disclosure of data on this page is subject to the restriction on the title page.

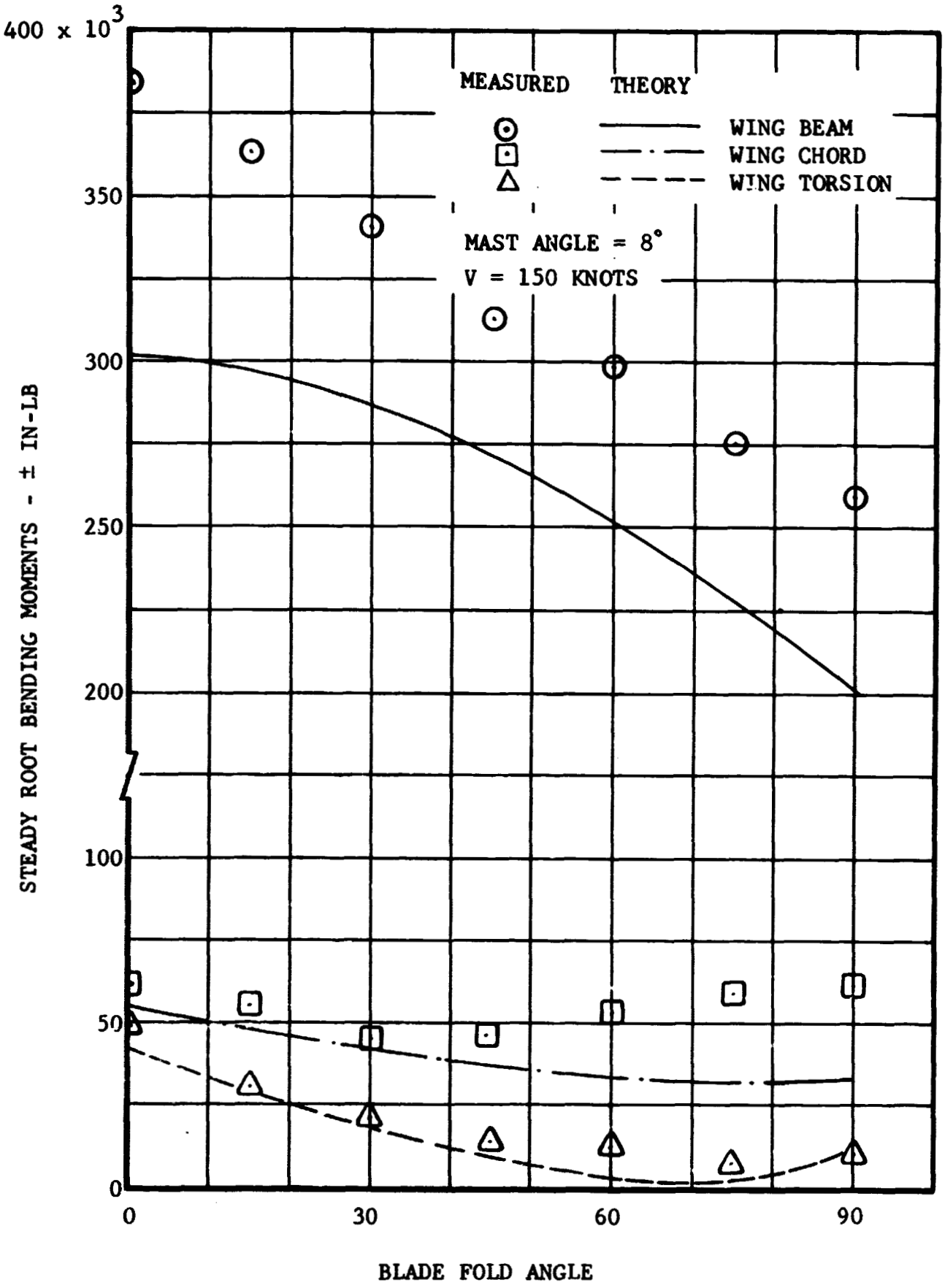


Figure VI-32. Wing Root Steady Bending Moment Versus Blade Fold Angle.

Use or disclosure of data on this page is subject to the restriction on the title page.

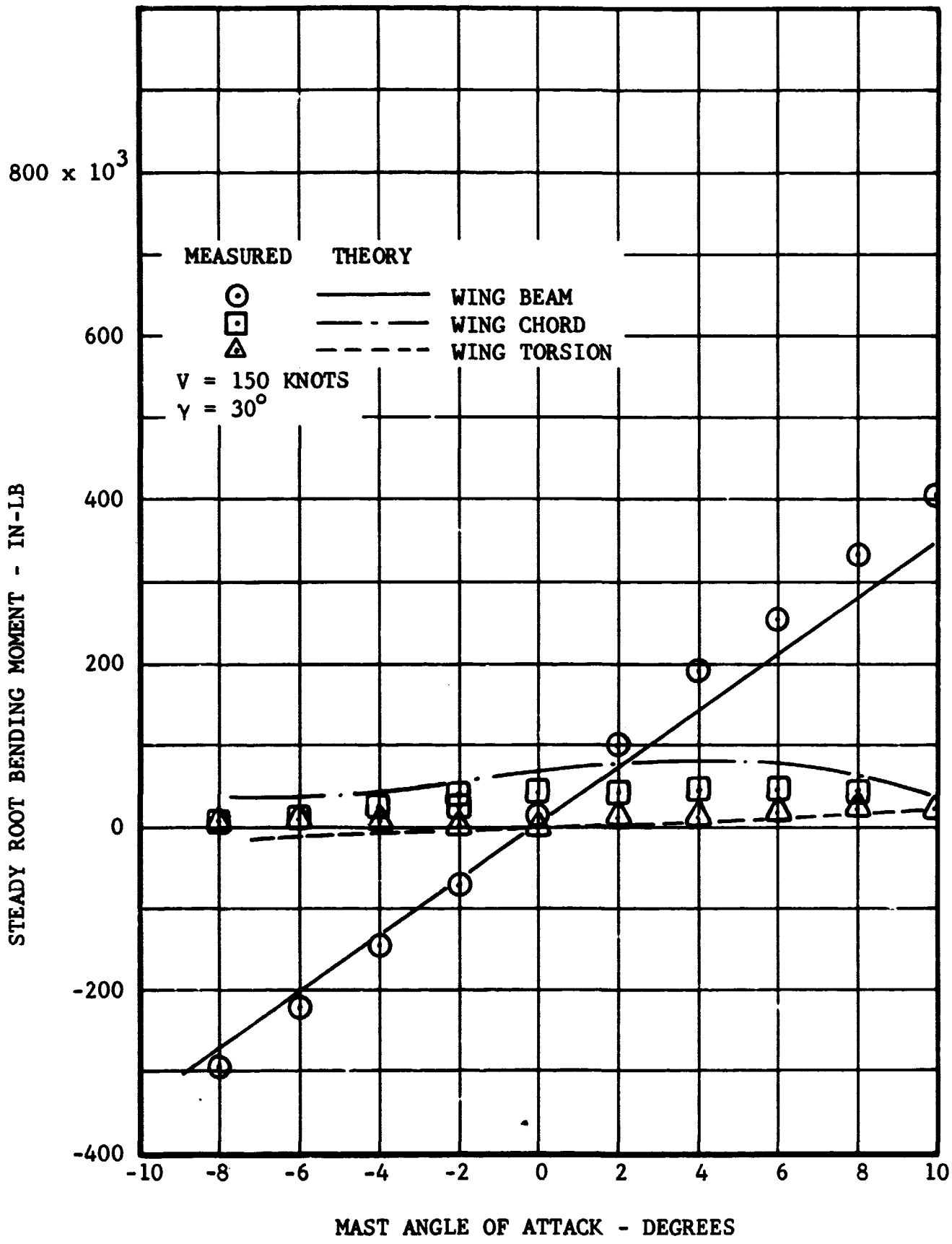


Figure VI-33. Wing Root Steady Bending Moment Versus Mast Angle of Attack.

Use or disclosure of data on this page is subject to the restriction on the title page.

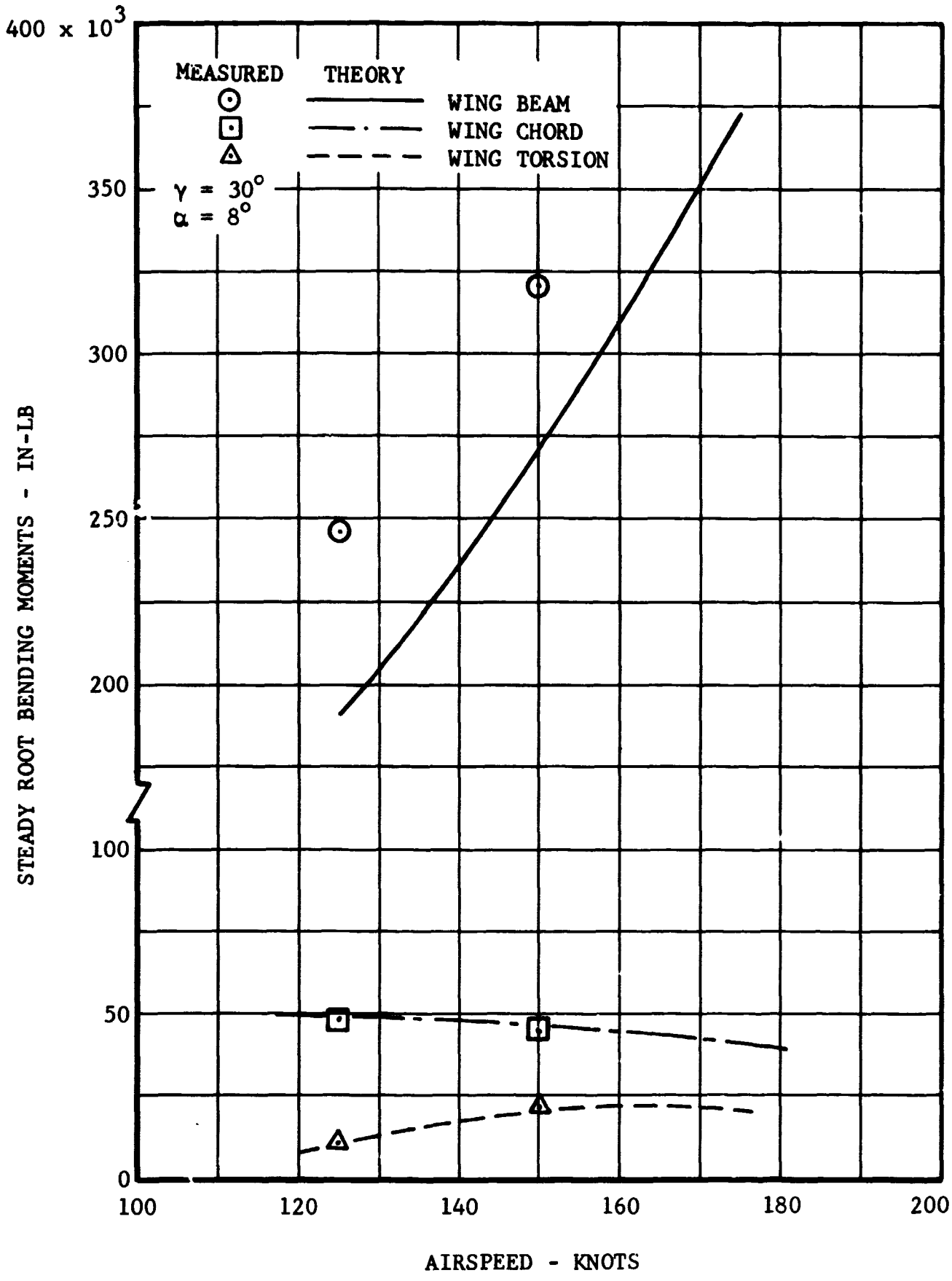


Figure VI-34. Wing Root Steady Bending Moment Versus Airspeed.

Use or disclosure of data on this page is subject to the restriction on the title page.

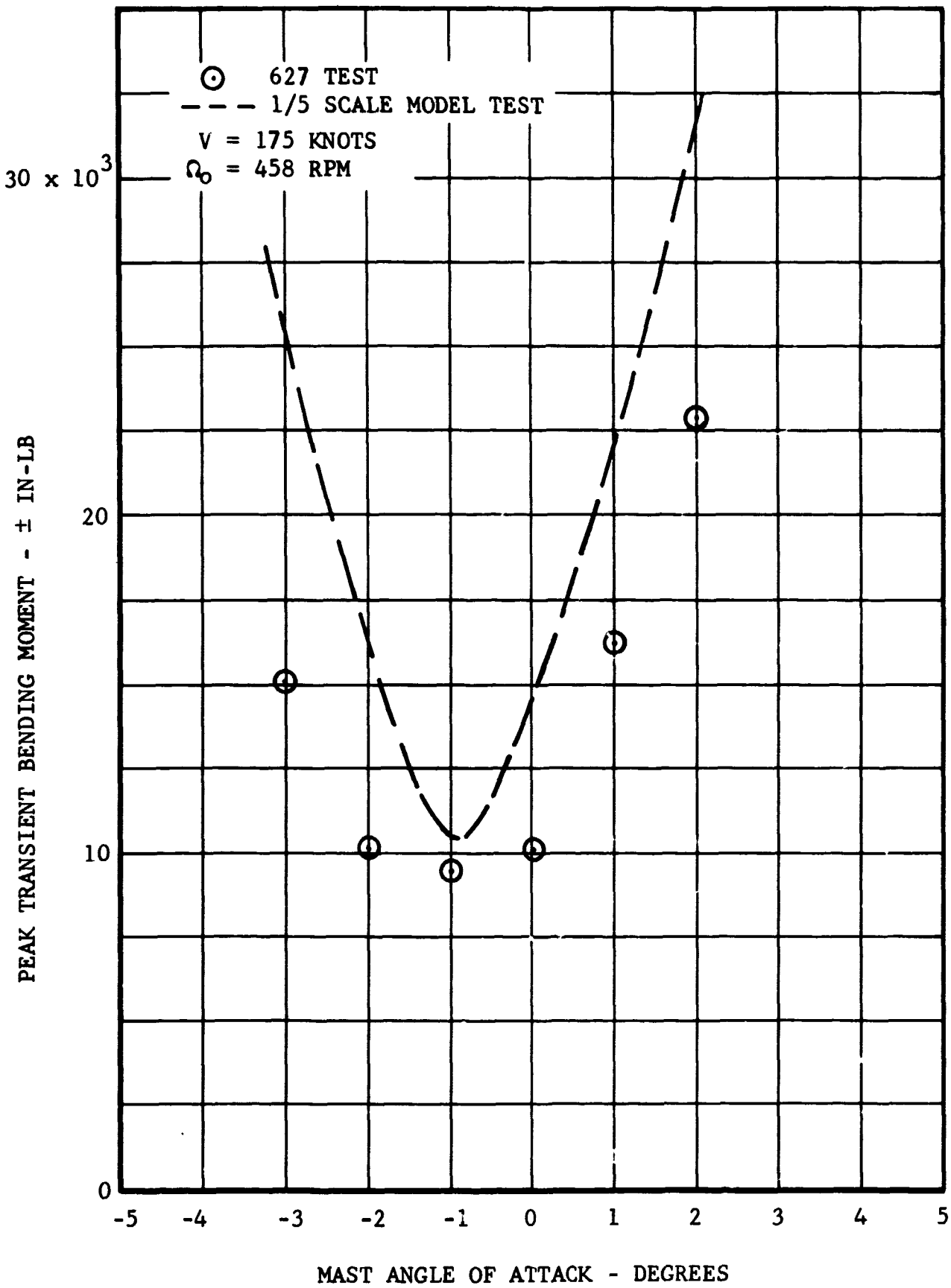


Figure VI-35. Comparison of Small-Scale and Full-Scale Measured Peak Blade Station 52.5 Oscillatory Loads During Feathering.

Use or disclosure of data on this page is subject to the restriction on the title page.

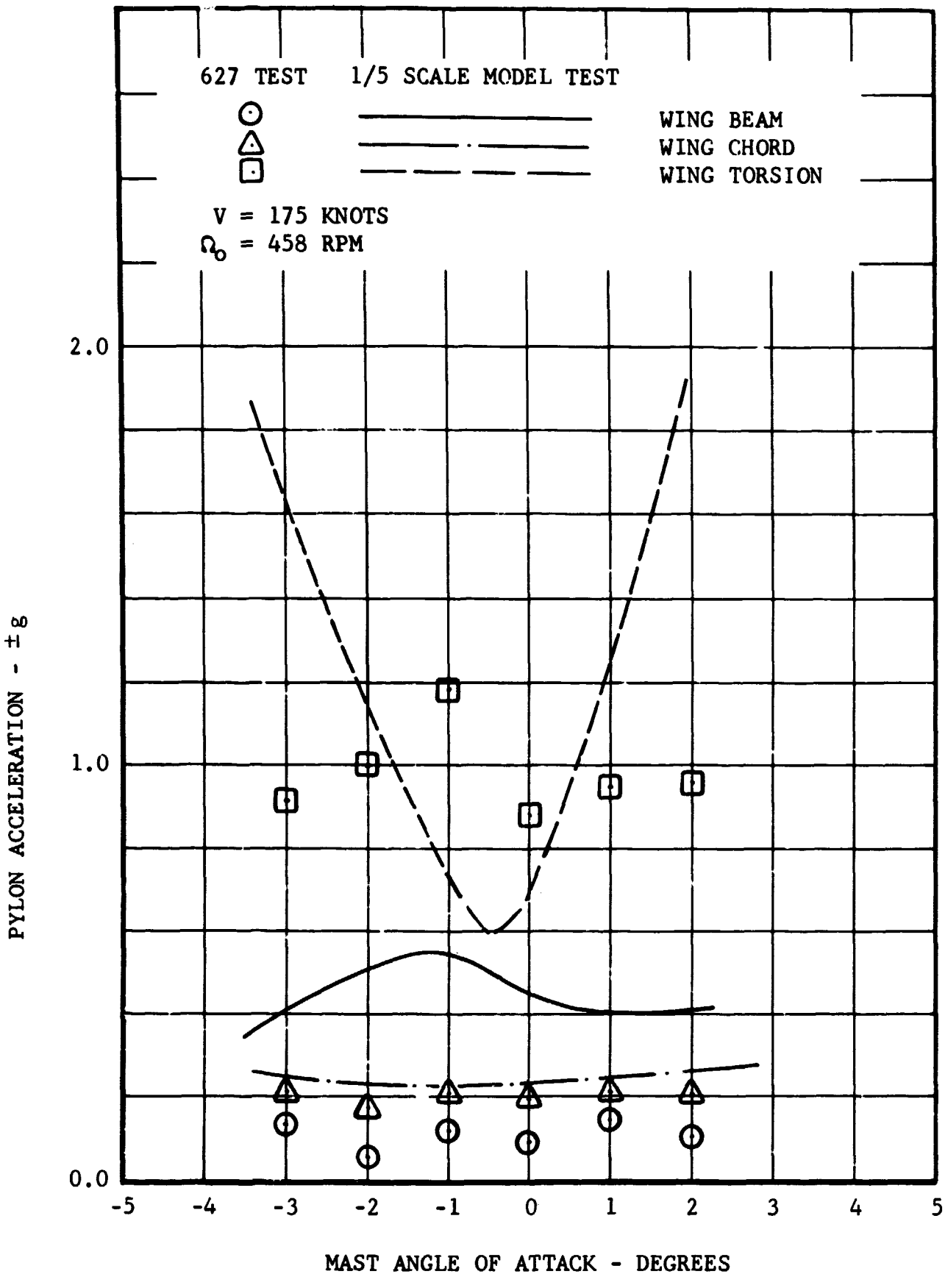


Figure VI-36. Comparison of Small-Scale and Full-Scale Measured Pylon Acceleration During Blade Feathering.

REPRODUCIBILITY OF THE ORIGINAL PAGE IS POOR

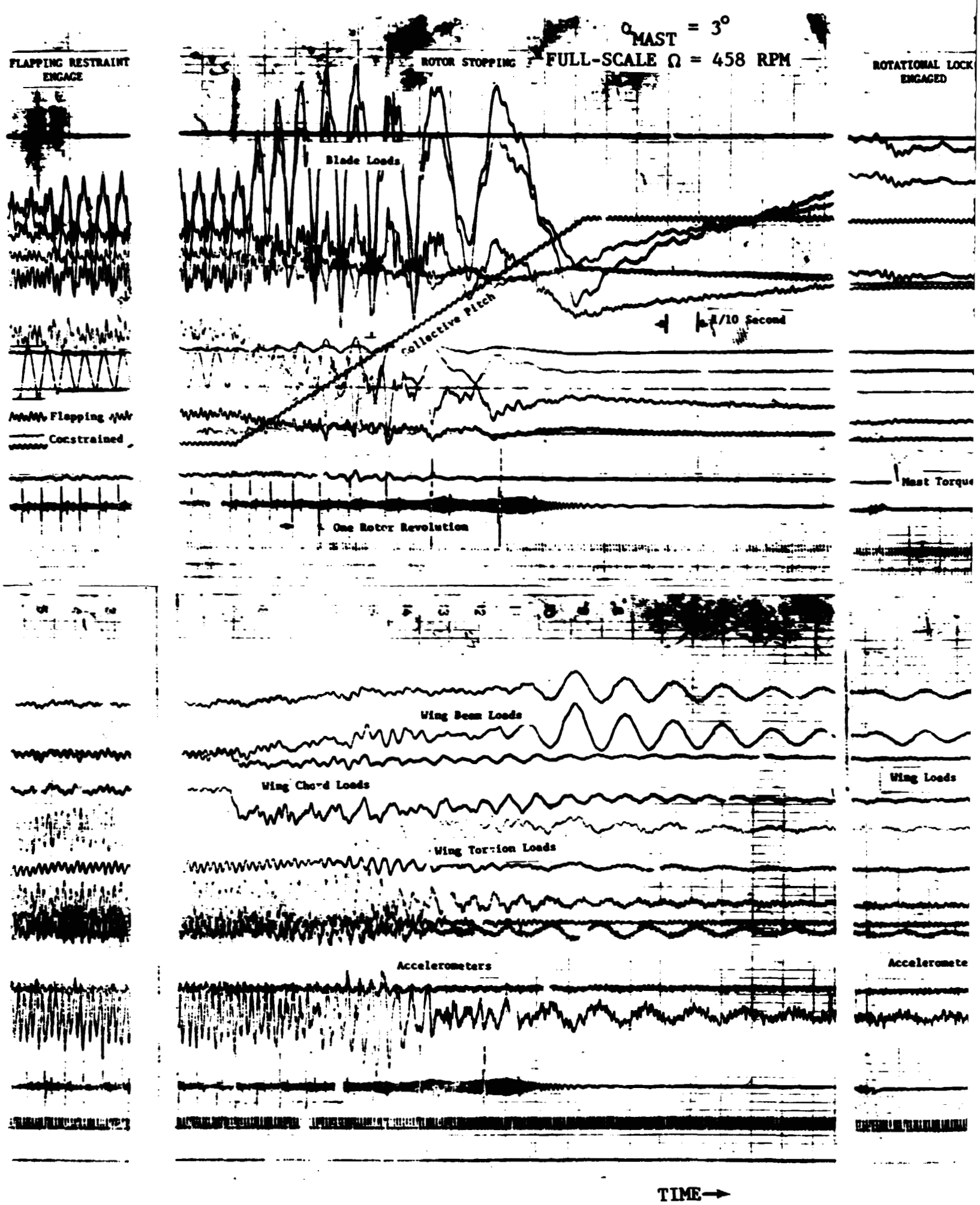
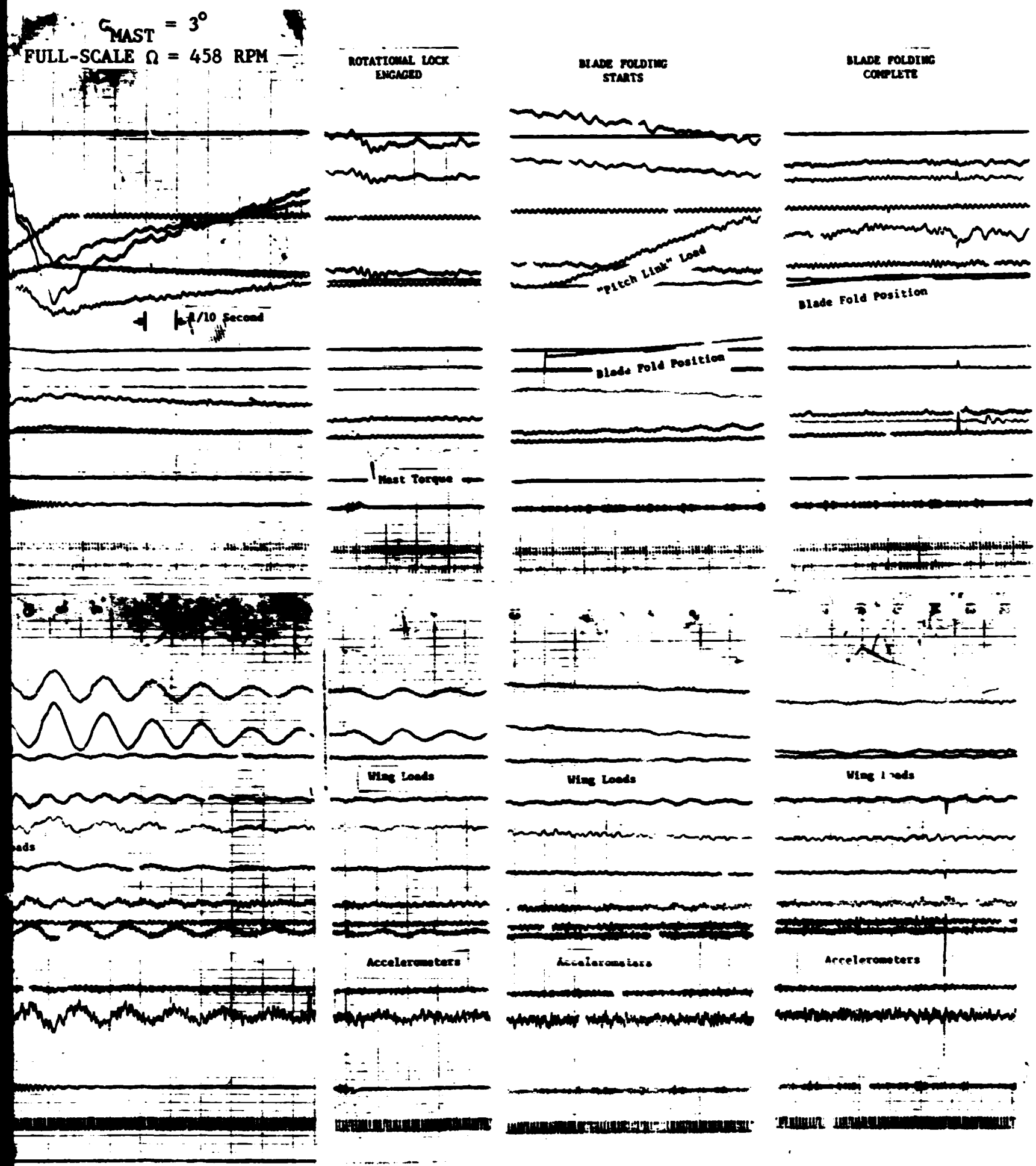


Figure VI-37. Time History of Dynamic Response During Feather-Fo
Full-Scale and Six Degrees Wing Angle of Attack, 0

FOLDOUT FRAME 1

REPRODUCIBILITY OF THE ORIGINAL PAGE IS POOR

Use or disclosure of data on this page is subject to the restriction on the title page.



y of Dynamic Response During Feather-Fold Sequence at 175 Knots and Six Degrees Wing Angle of Attack, One-Fifth Scale Model.

FOLDOUT FRAME 2

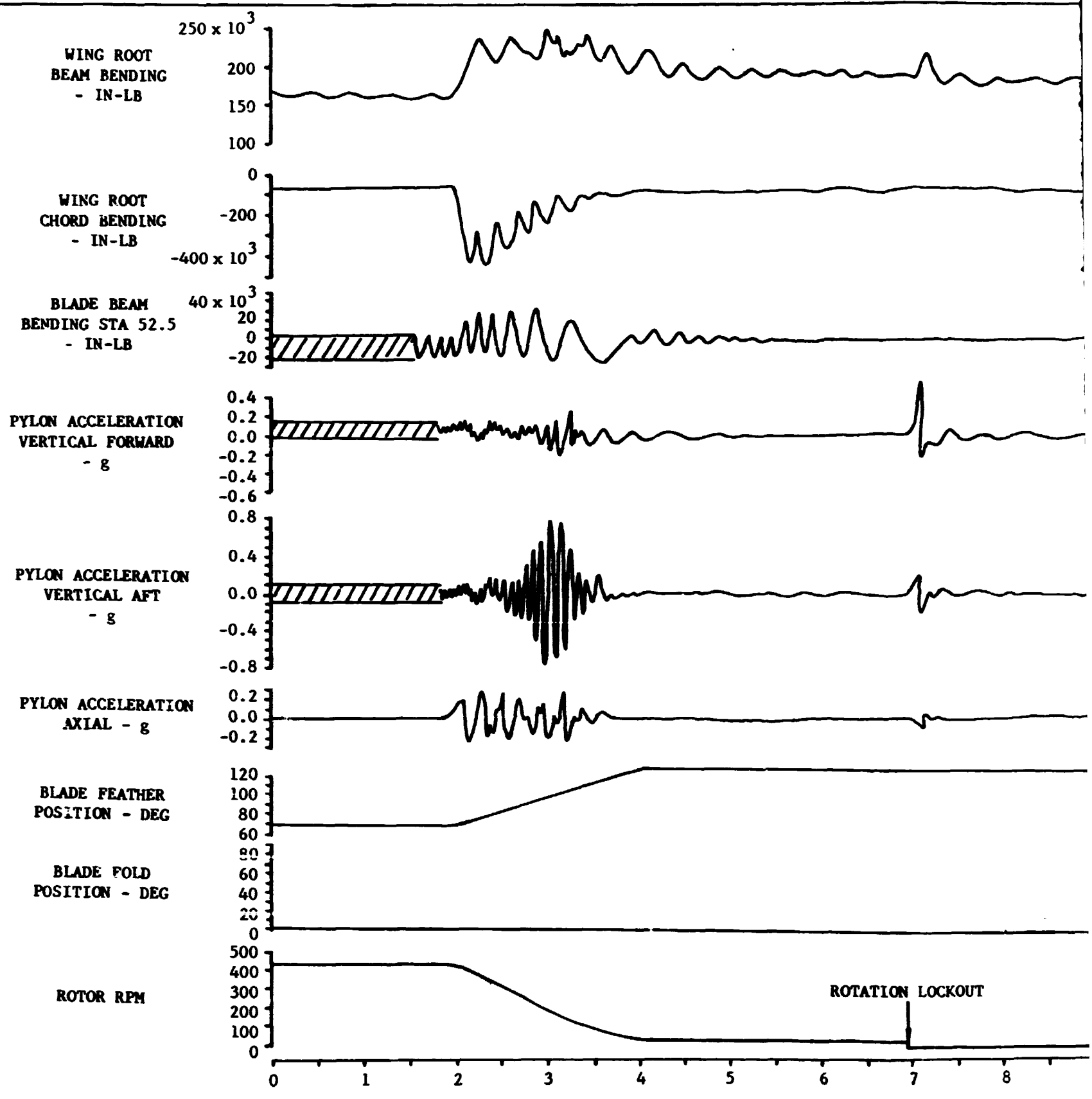
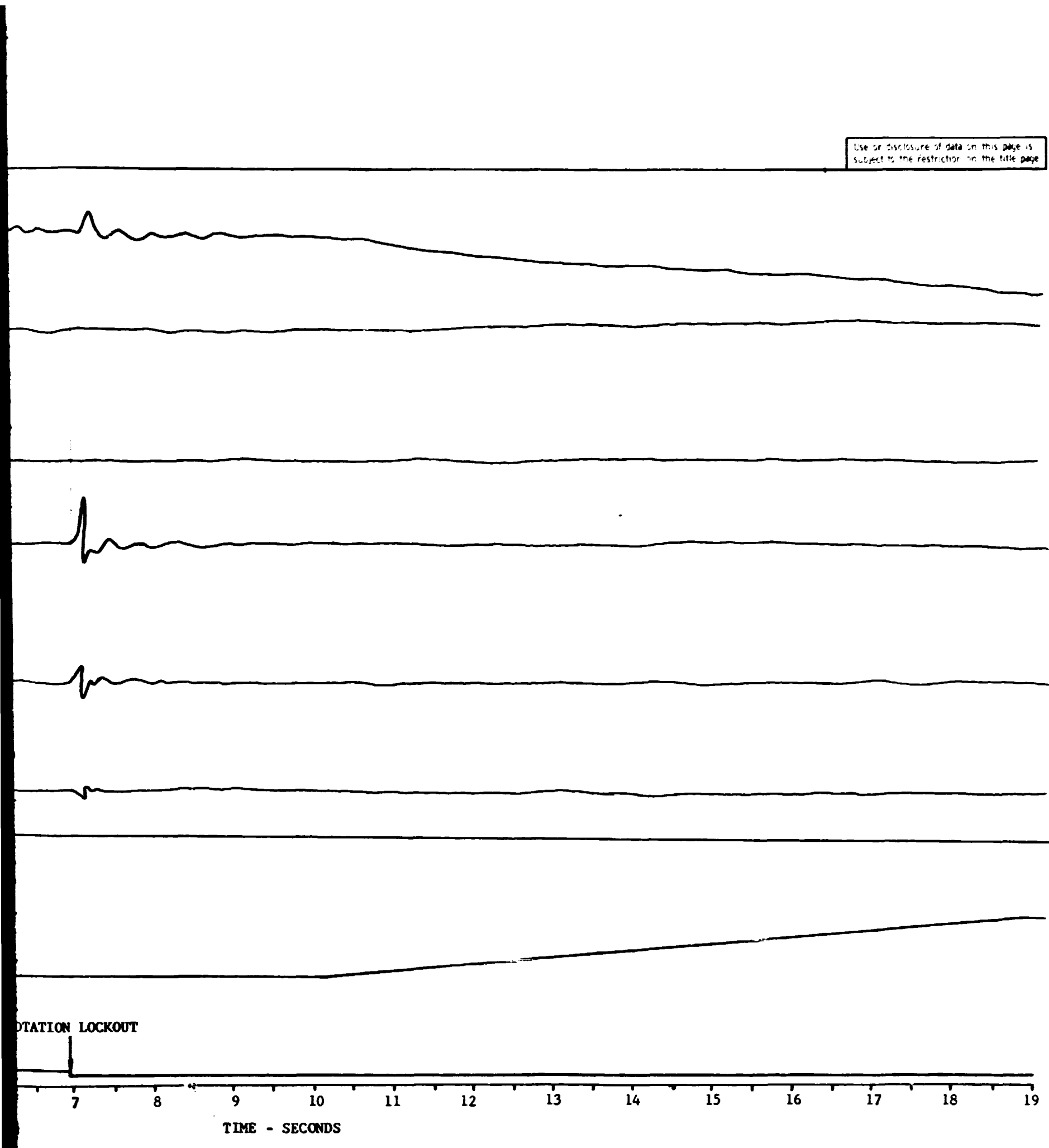


Figure VI-38. Calculated Time History of F
Four Degrees Mast Angle of A

FOLDOUT FRAME

Use or disclosure of data on this page is subject to the restriction on the title page



lculated Time History of Feather-Fold Sequence, 150 Knots Airspeed,
ur Degrees Mast Angle of Attack.

FOLDOUT FRAME 2

Use or disclosure of data on this page is subject to the restriction on the title page.

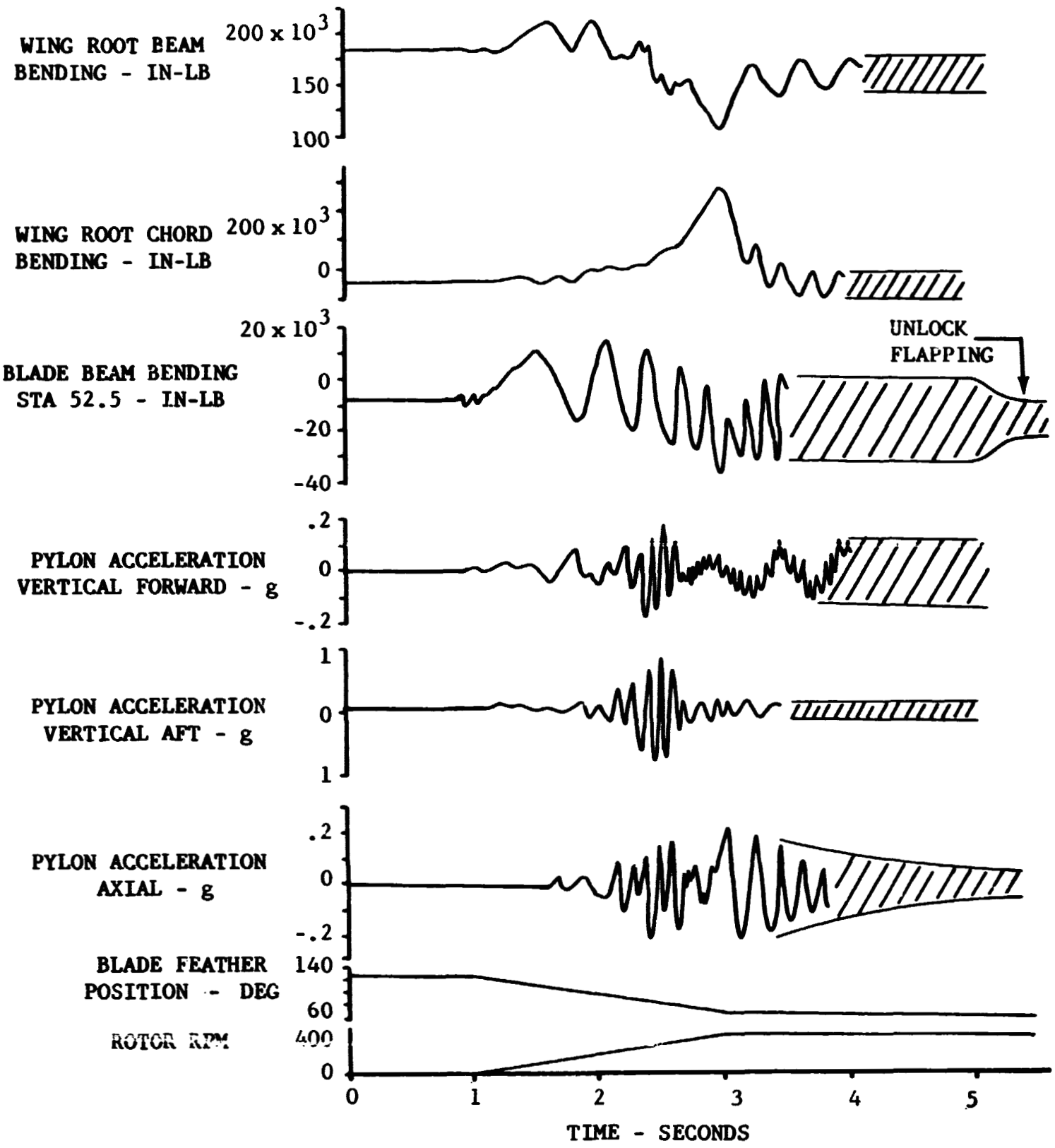


Figure VI-39. Calculated Time History of Unfeather Sequence, 150 Knots Airspeed, Four Degrees Mast Angle of Attack.

Parameter Oscillograph No. 1		Oscillograph Trace Scale Factor
1. Wing Root Beam	in-lb/in	367469 ±183700
2. Wing Root Chord	in-lb/in	296000 ±148000
3. Wing Root Torsion	in-lb/in	219103 ±109550
4. Red Blade Sta. 52.5	in-lb/in	43200 ± 21600
5. Red Blade Chord Sta. 52.5	in-lb/in	30700 ± 15350
6. Red Blade Pitch Link	lb/in	879
7. Fore and Aft Hub Flapping	-	-
8. Lateral Hub Flapping	-	-
9. Mast Torque	in-lb/in	74400
10. Red Blade Pitch Lock Bending	in-lb/in	35700
11. Red Blade Feathering Position	deg/in	52
12. Red Blade Fold Position	deg/in	70.1
13. Collective Actuator Position	deg/in	46.2
16. RPM/Azimuth		

OSCILLOGRAPH NO. 1

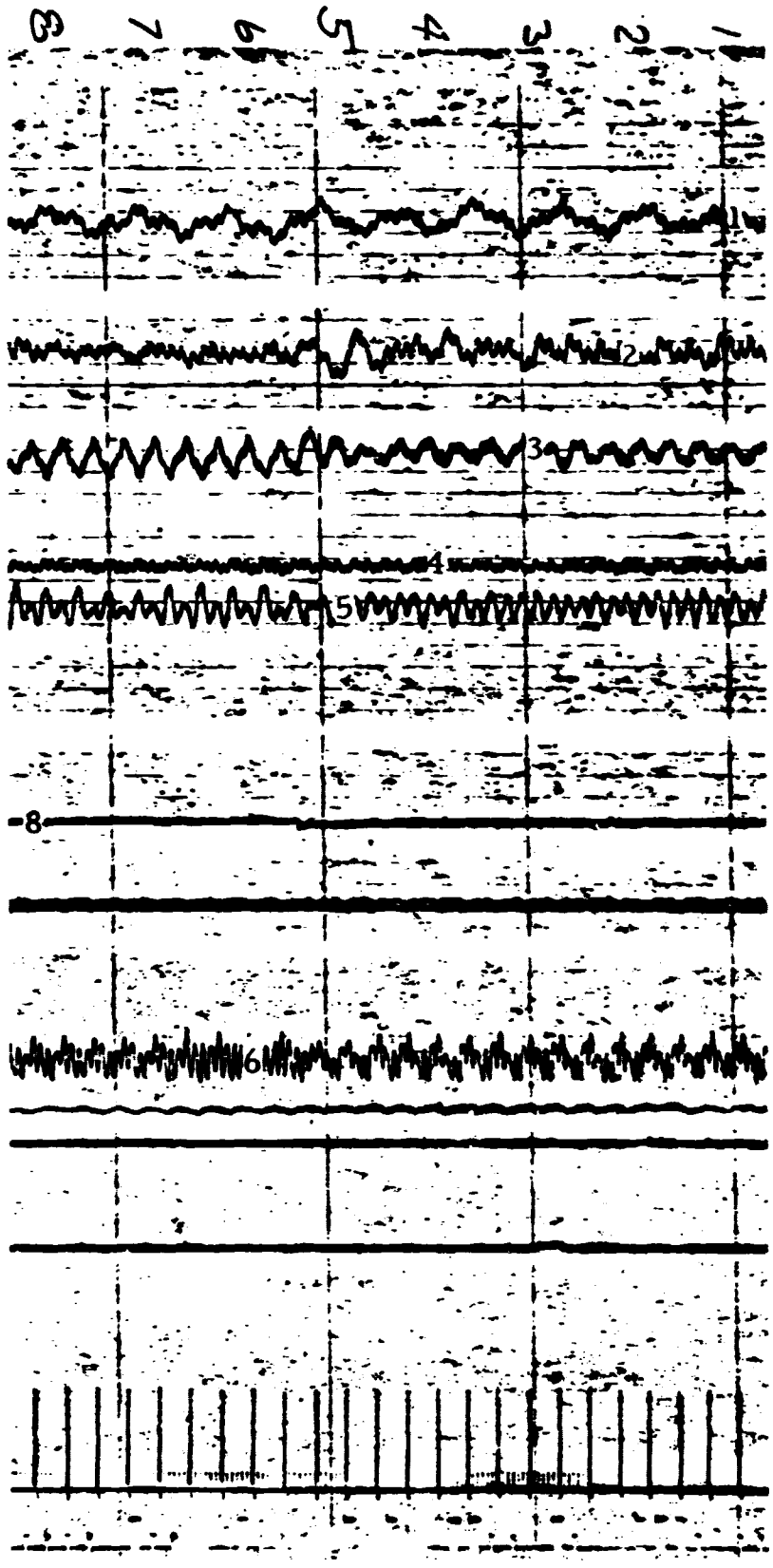


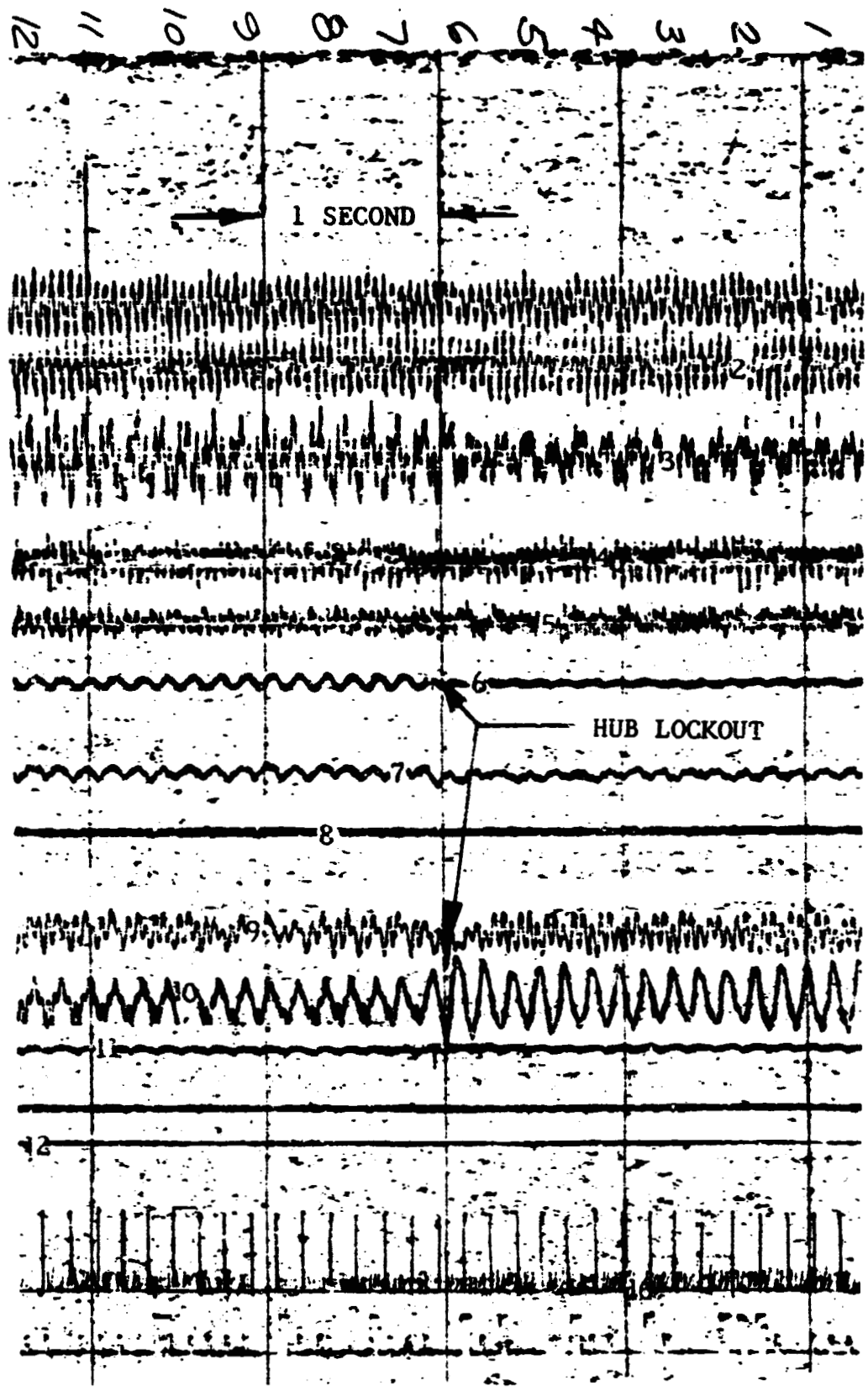
Figure VI-40. Hub Flapping Lockout Time of Attack Minus One Degree

FOLDOUT FRAME 1

Use or disclosure of data on this page is subject to the restriction on the title page.

Parameter Oscillograph No. 2	Oscillograph Trace Scale Factor	
1. Acceleration Vertical Fwd	g/in	3.14 ±1.57
2. Acceleration Horizontal Fwd	g/in	3.19 ±1.59
3. Acceleration Vertical Aft	g/in	3.5 ±1.75
4. Acceleration Horizontal Aft	g/in	3.11 ±1.56
5. Acceleration Axial	g/in	3.52 ±1.76
6. Flapping - Red Blade	deg/in	18.45 ±9.22
7. Pod Conversion Link	lb/in	17000
8. Pod Yaw Link	-	-
9. Conversion Spindle Yaw	-	-
10. Mast Vertical Bending	in-lb/in	94300
11. Red Blade Feathering Position	deg/in	50.5
12. Red Blade Fold Position	deg/in	67.3
13. Collective Actuator Position	deg/in	50.2
16. RPM/Azimuth		

OSCILLOGRAPH NO. 2



Lockout Time History, 175 Knots, Mast Angle nus One Degree (Run 16.7).

FOLDOUT FRAME 2

REPRODUCIBILITY OF THE ORIGINAL PAGE IS POOR.

Parameter Oscillograph No. 1	Oscillograph Trace Scale Factor	
1. Wing Root Beam	in-lb/in	367469 ±183700
2. Wing Root Chord	in-lb/in	296000 ±148000
3. Wing Root Torsion	in-lb/in	219103 ±109550
4. Red Blade Sta. 52.5	in-lb/in	43200 ± 21600
5. Red Blade Chord Sta. 52.5	in-lb/in	30700 ± 15350
6. Red Blade Pitch Link	lb/in	879
7. Fore and Aft Hub Flapping	-	-
8. Lateral Hub Flapping	-	-
9. Mast Torque	in-lb/in	74400
10. Red Blade Pitch Lock Bending	in-lb/in	35700
11. Red Blade Feathering Position	deg/in	52
12. Red Blade Fold Position	deg/in	70.1
13. Collective Actuator Position	deg/in	46.2
16. RPM/Azimuth		

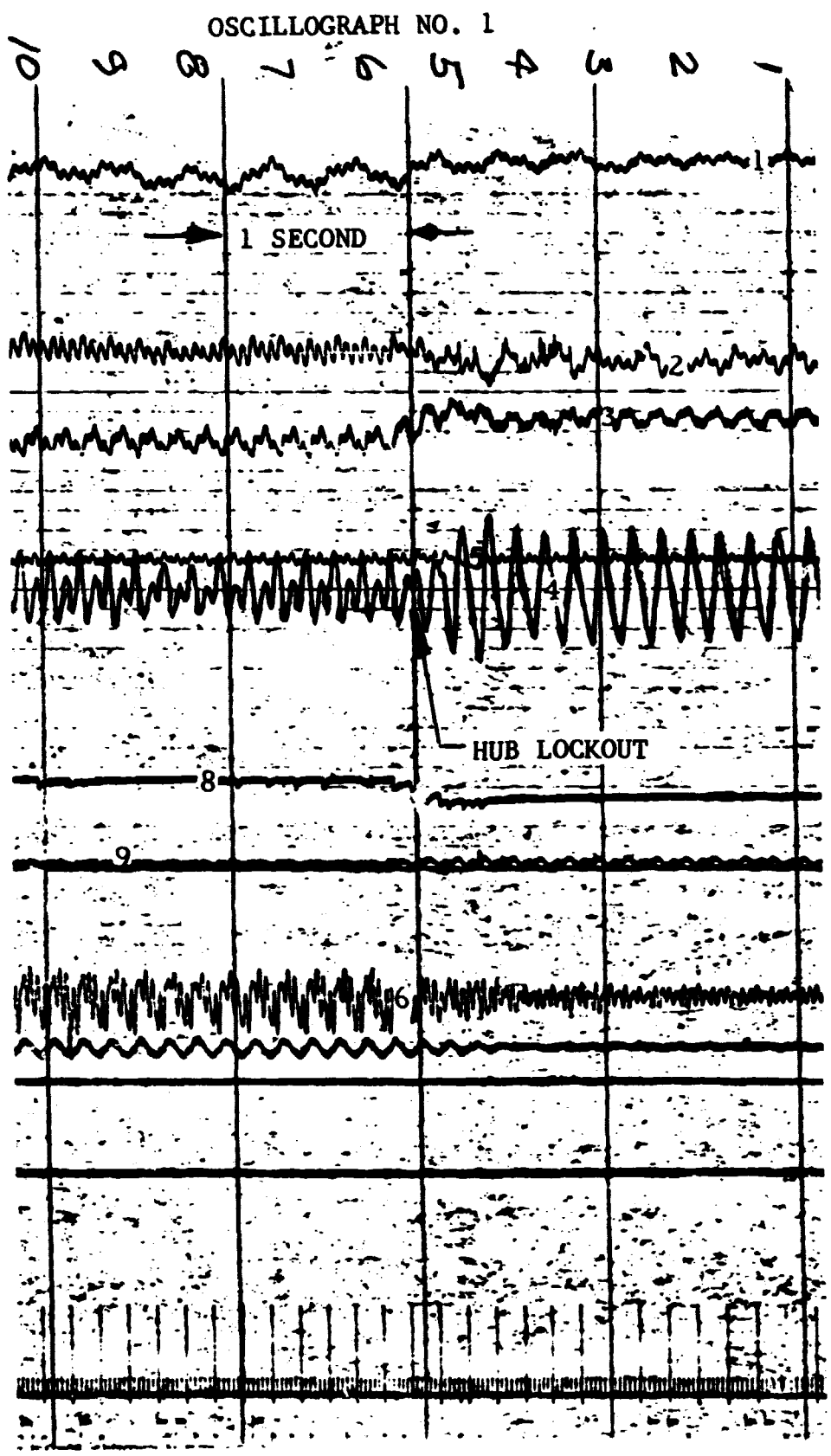


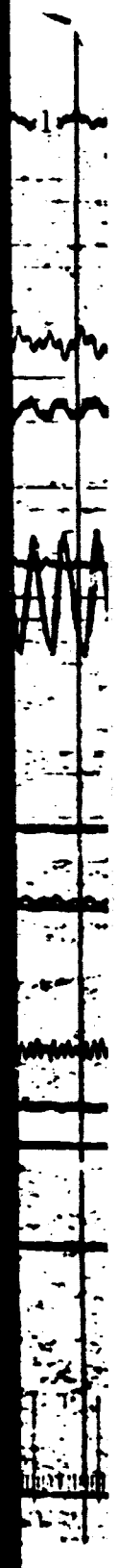
Figure VI-41. Hub Flapping Lockout Time His
of Attack Two Degrees (Run 16

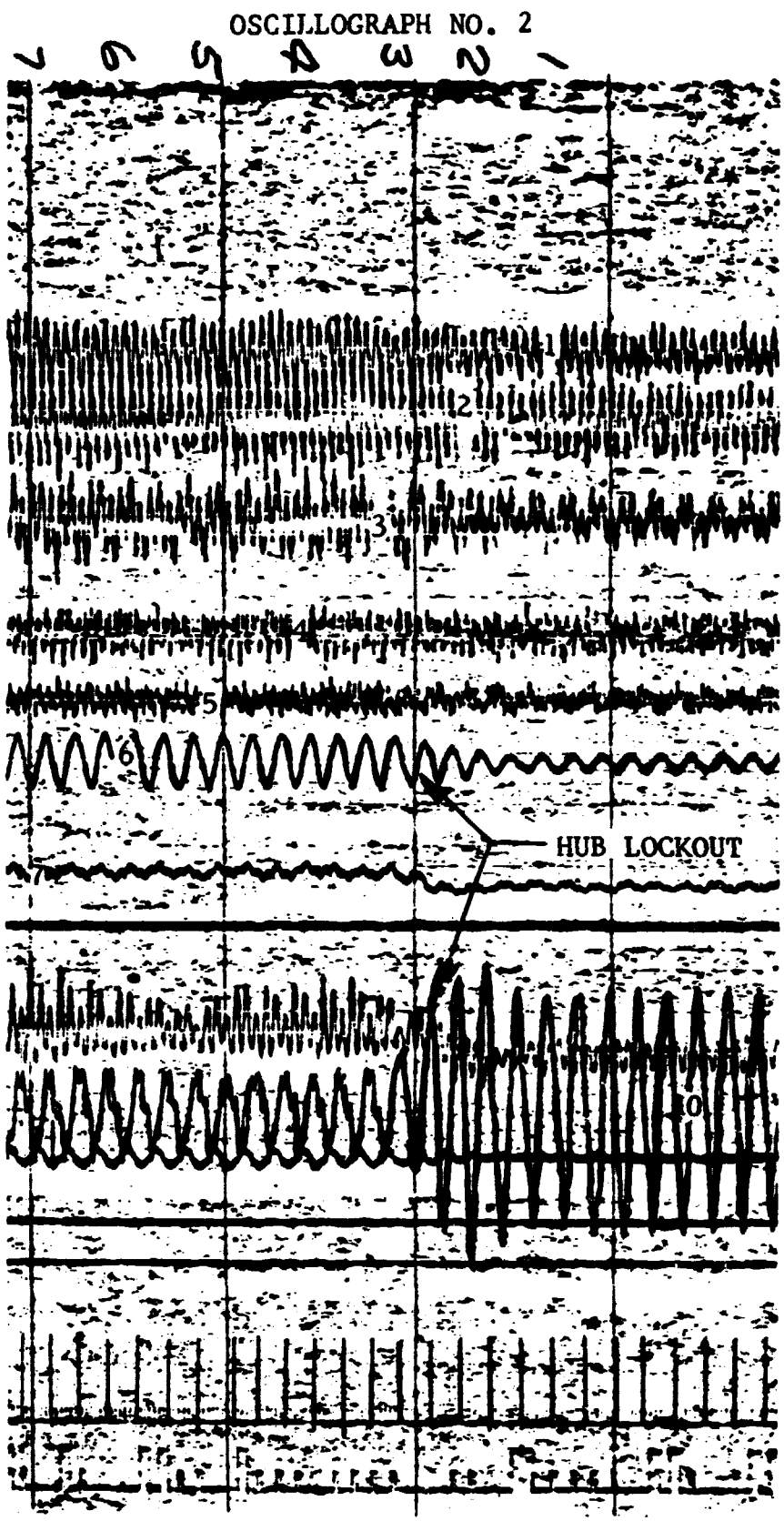
FOLDOUT FRAME |

REPRODUCIBILITY OF THE ORIGINAL PAGE IS POOR.

Use or disclosure of data on this page is subject to the restriction on the title page.

Parameter Oscillograph No. 2	Oscillograph Trace Scale Factor	
1. Acceleration Vertical Fwd	g/in	3.14 ±1.57
2. Acceleration Horizontal Fwd	g/in	3.19 ±1.59
3. Acceleration Vertical Aft	g/in	3.5 ±1.75
4. Acceleration Horizontal Aft	g/in	3.11 ±1.56
5. Acceleration Axial	g/in	3.52 ±1.76
6. Flapping - Red Blade	deg/in	18.45 ±9.22
7. Pod Conversion Link	lb/in	17000
8. Pod Yaw Link	-	-
9. Conversion Spindle Yaw	-	-
10. Mast Vertical Bending	in-lb/in	94300
11. Red Blade Feathering Position	deg/in	50.5
12. Red Blade Fold Position	deg/in	67.3
13. Collective Actuator Position	deg/in	50.2
16. RPM/Azimuth		





ockout Time History, 175 Knots, Mast Angle Degrees (Run 16.13).

REPRODUCIBILITY OF THE ORIGINAL PAGE IS POOR.

Parameter Oscillograph No. 1	Oscillograph Trace Scale Factor	
1. Wing Root Beam	in-lb/in	363000
2. Wing Root Chord	in-lb/in	299000
3. Wing Root Torsion	in-lb/in	219103
4. Red Blade	in-lb/in	43000
5. Red Blade Chord Sta. 52.5	in-lb/in	40700
6. Red Blade Pitch Link	lb/in	884.5
7. Fore and Aft Flapping	-	-
8. Lateral Hub Flapping	-	-
9. Mast Torque	in-lb/in	37200
10. Red Blade Pitch Lock Bending	in-lb/in	10150
11. Red Blade Feathering Position	deg/in	52.0
12. Red Blade Fold Position	deg/in	69.9
13. Collective Actuator Position	deg/in	45.7
16. RPM/Azimuth		

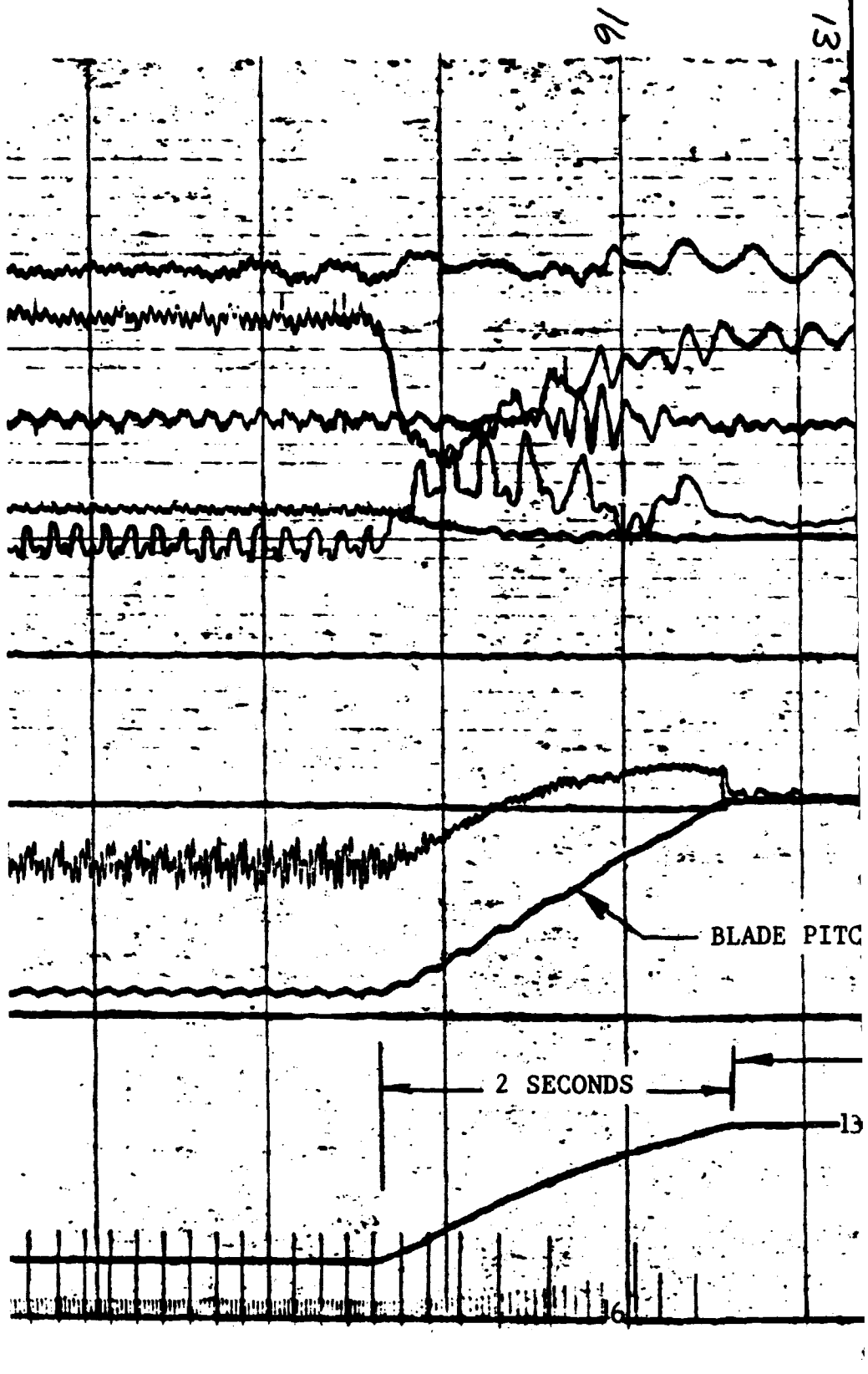


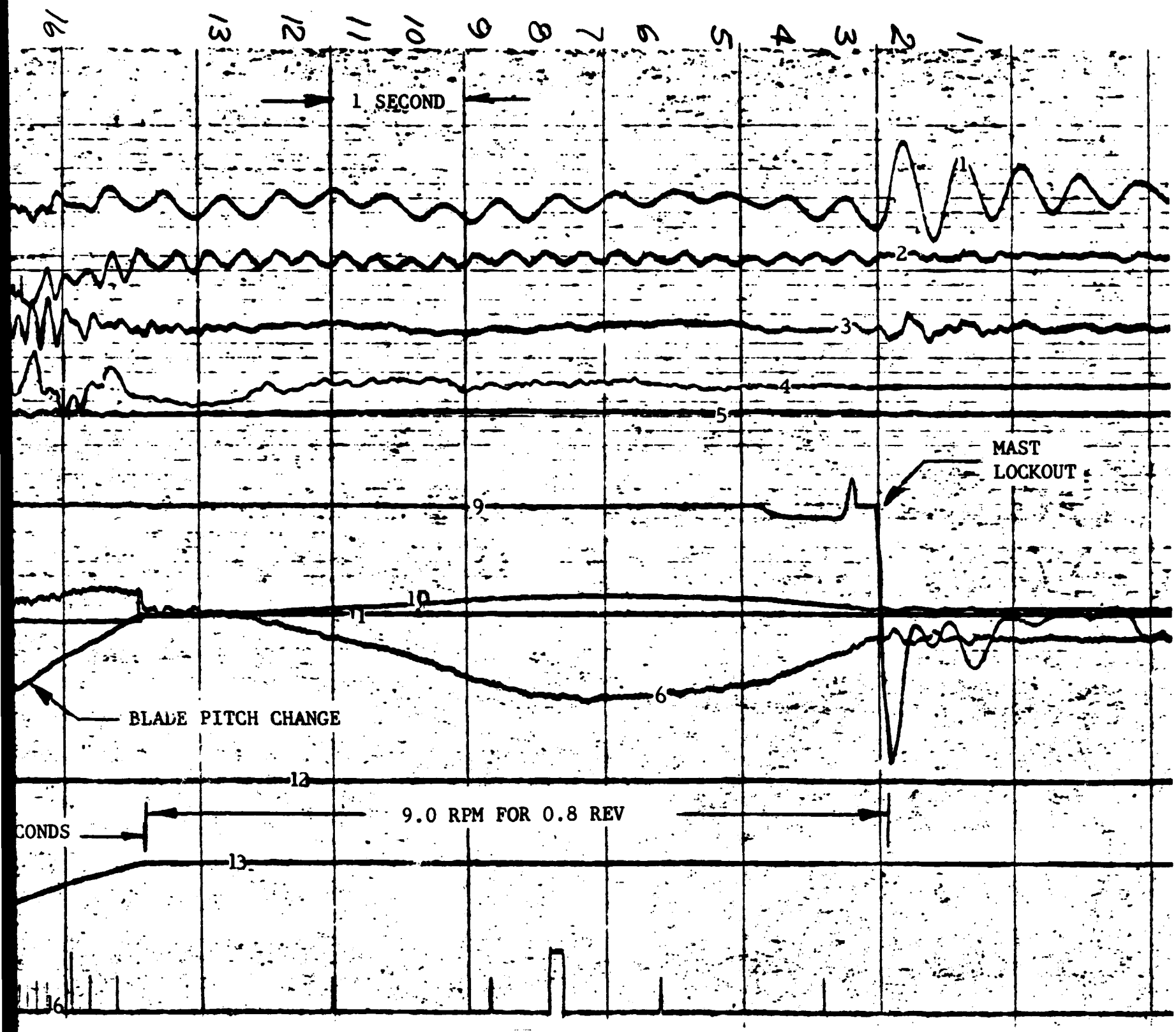
Figure VI-42. Rotor Stopping and Mast Lockout Angle of Attack Minus Two Degre

FOLDOUT FRAME

REPRODUCIBILITY OF THE ORIGINAL PAGE IS POOR.

Use or disclosure of data on this page is subject to the restriction on the title page.

OSCILLOGRAPH NO. 1



ing and Mast Lockout Time History, 175 Knots, Mast
tack Minus Two Degrees (Run 29.2).

FOLDOUT FRAME 2

REPRODUCIBILITY OF THE ORIGINAL PAGE IS POOR.

Parameter Oscillograph No. 2		Oscillograph Trace Scale Factor
1. Acceleration Vertical Fwd	g/in	3.18
2. Acceleration Horizontal Fwd	g/in	3.17
3. Acceleration Vertical Aft	g/in	3.50
4. Acceleration Horizontal Aft	g/in	3.11
5. Acceleration Axial	g/in	3.52
6. Flapping - Red Blade	deg/in	10.9
7. Pod Conversion Link	lb/in	17.3
8. Pod Yaw Link	-	-
9. Conversion Spindle Yaw	-	-
10. Mast Vertical Bending	in-lb/in	92500
11. Red Blade Feathering Position	deg/in	50
12. Red Blade Fold Position	deg/in	68
13. Collective Actuator Position	deg/in	50.2
16. RPM/Azimuth		

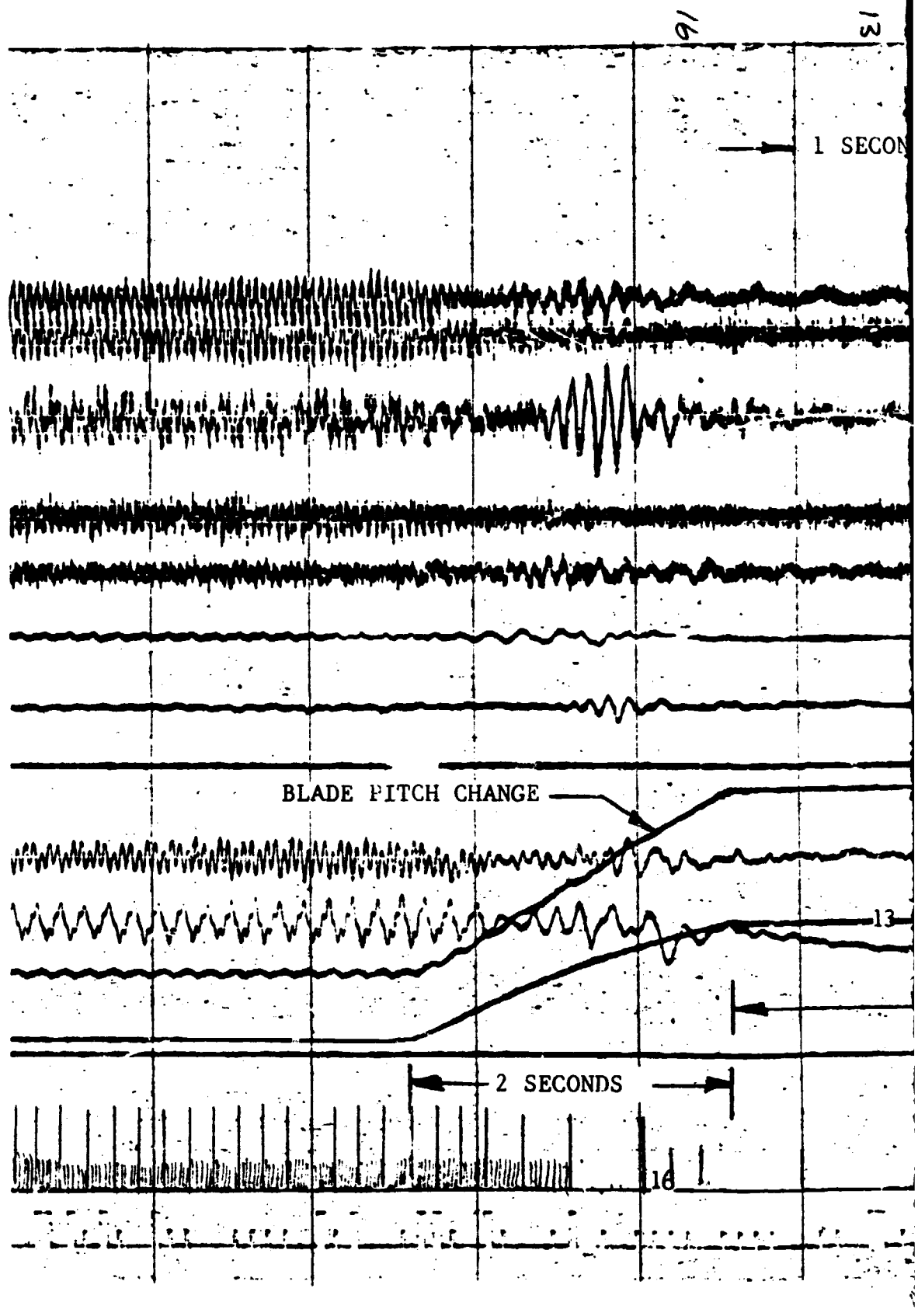
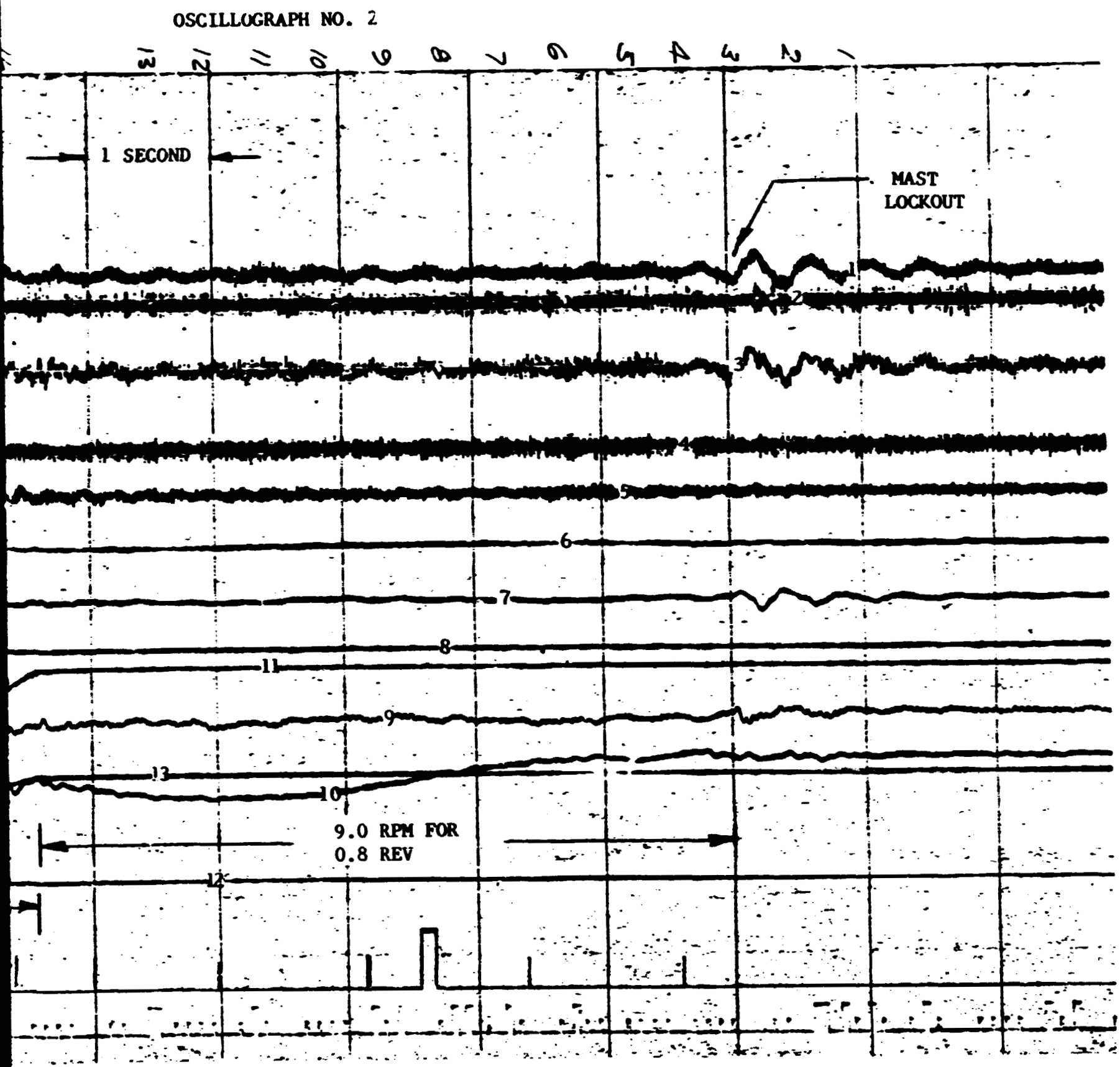


Figure VI-43. Rotor Stopping and Mast Lockout Mast Angle of Attack Minus Two

FOLDOUT FRAME

REPRODUCIBILITY OF THE ORIGINAL PAGE IS POOR

Use or disclosure of data on this page is subject to the restriction on the title page.



nd Mast Lockout Time History, 175 Knots,
tack Minus Two Degrees (Run 29.2).

FOLDOUT FRAME 2

REPRODUCIBILITY OF THE ORIGINAL PAGE IS POOR

Parameter Oscillograph No. 1	Oscillograph Trace Scale Factor	
1. Wing Root Beam	in-lb/in	363000
2. Wing Root Chord	in-lb/in	299000
3. Wing Root Torsion	in-lb/in	219103
4. Red Blade	in-lb/in	43000
5. Red Blade Chord Sta. 52.5	in-lb/in	40700
6. Red Blade Pitch Link	lb/in	884.5
7. Fore and Aft Flapping	-	-
8. Lateral Hub Flapping	-	-
9. Mast Torque	in-lb/in	37200
10. Red Blade Pitch Lock Bending	in-lb/in	10150
11. Red Blade Feathering Position	deg/in	52.0
12. Red Blade Fold Position	deg/in	69.9
13. Collective Actuator Position	deg/in	45.7
16. RPM/Azimuth		

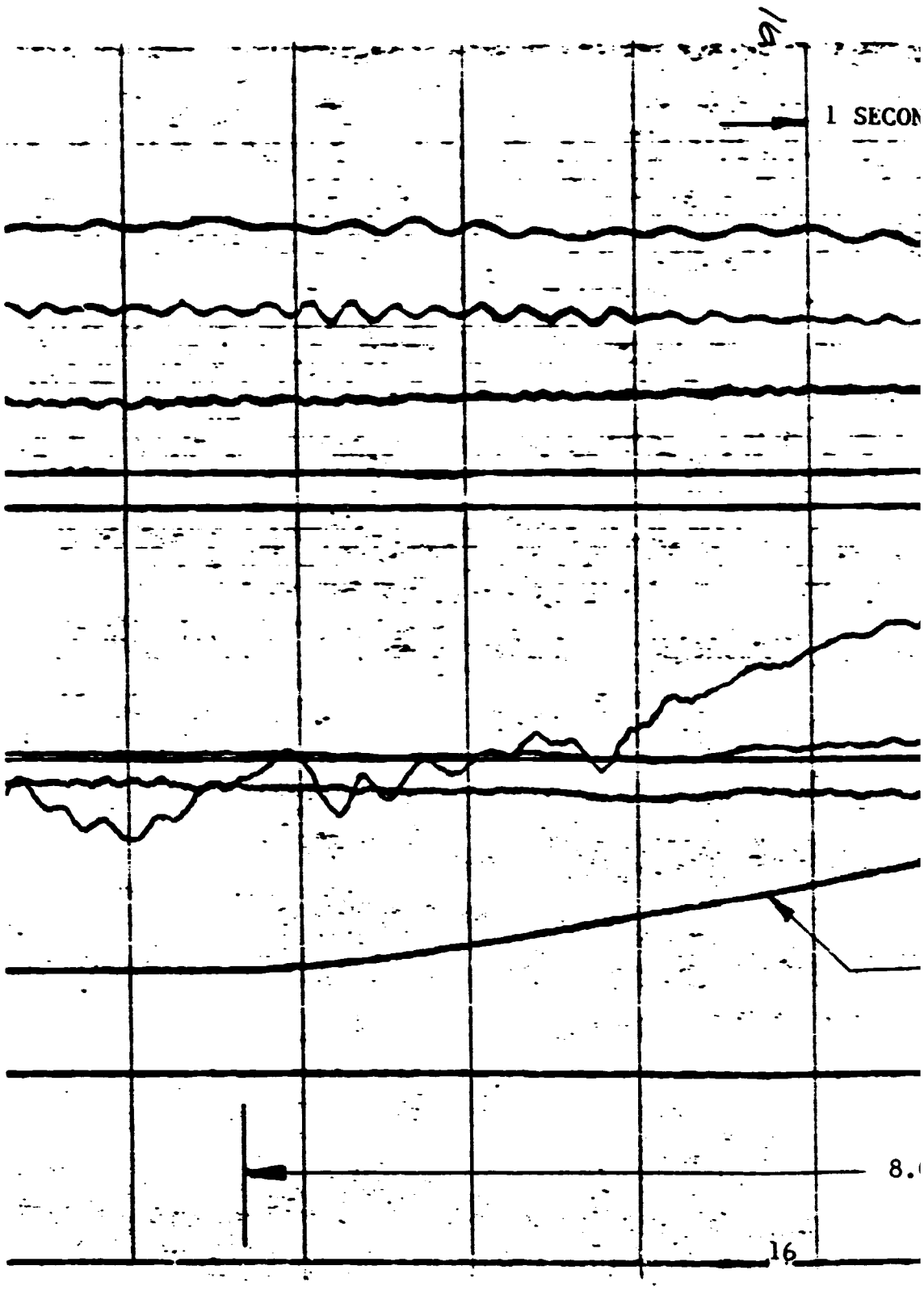


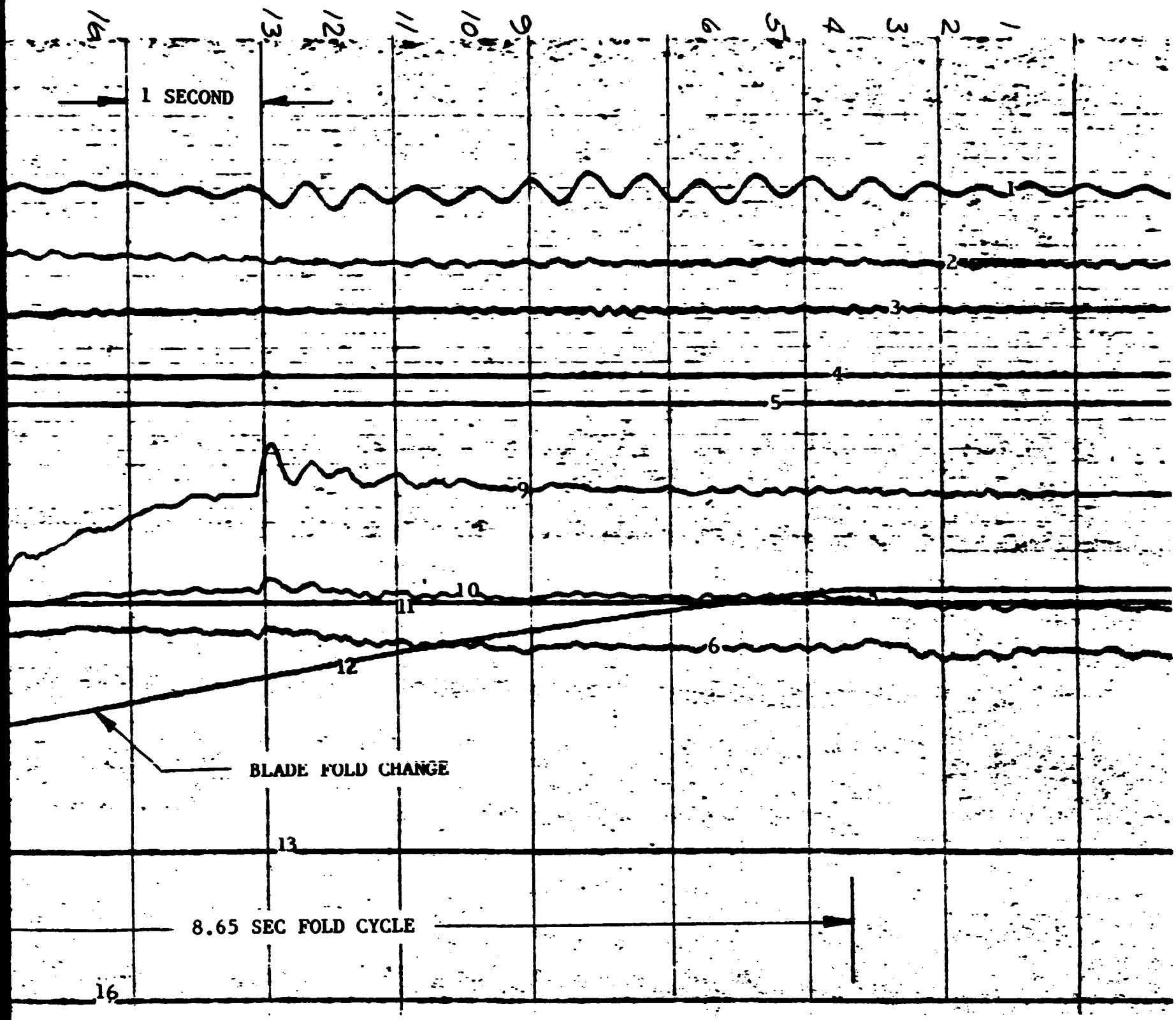
Figure VI-44. Blade Folding Time History, 175 K
Minus Two Degrees (Run 29.2).

FOLDOUT FRAME

REPRODUCIBILITY OF THE ORIGINAL PAGE IS POOR.

Use or disclosure of data on this page is subject to the restriction on the title page.

OSCILLOGRAPH NO. 1



ime History, 175 Knots, Mast Angle of Attack
es (Run 29.2).

FOLDOUT FRAME 2

REPRODUCIBILITY OF THE ORIGINAL PAGE IS POOR

Parameter Oscillograph No. 2		Oscillograph Trace Scale Factor
1. Acceleration Vertical Fwd	g/in	3.18
2. Acceleration Horizontal Fwd	g/in	3.17
3. Acceleration Vertical Aft	g/in	3.50
4. Acceleration Horizontal Aft	g/in	3.11
5. Acceleration Axial	g/in	3.52
6. Flapping - Red Blade	deg/in	10.9
7. Pod Conversion Link	lb/in	17.3
8. Pod Yaw Link	-	-
9. Conversion Spindle Yaw	-	-
10. Mast Vertical Bending	in-lb/in	92500
11. Red Blade Feathering Position	deg/in	50
12. Red Blade Fold Position	deg/in	68
13. Collective Actuator Position	deg/in	50.2
16. RPM/Azimuth		

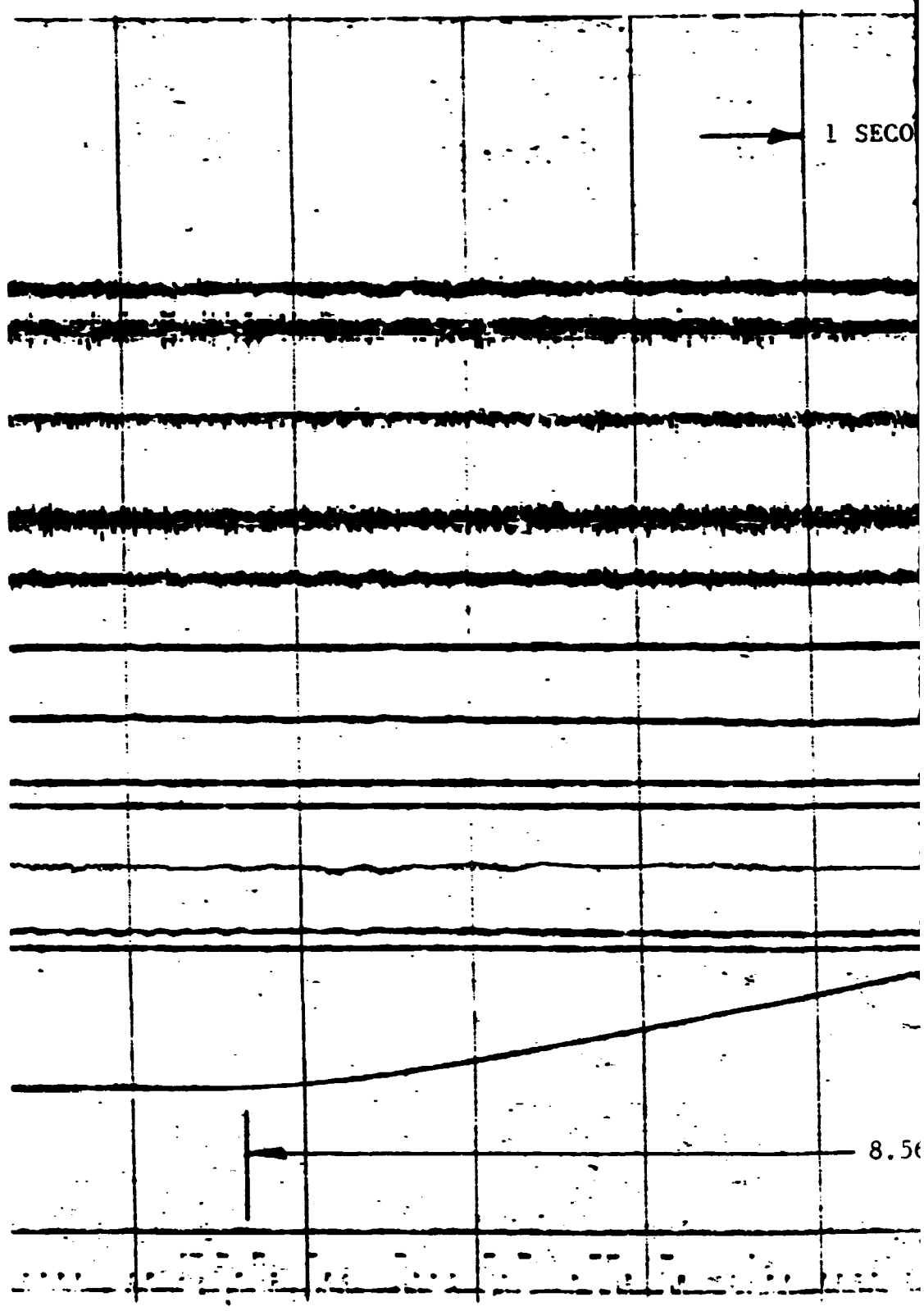
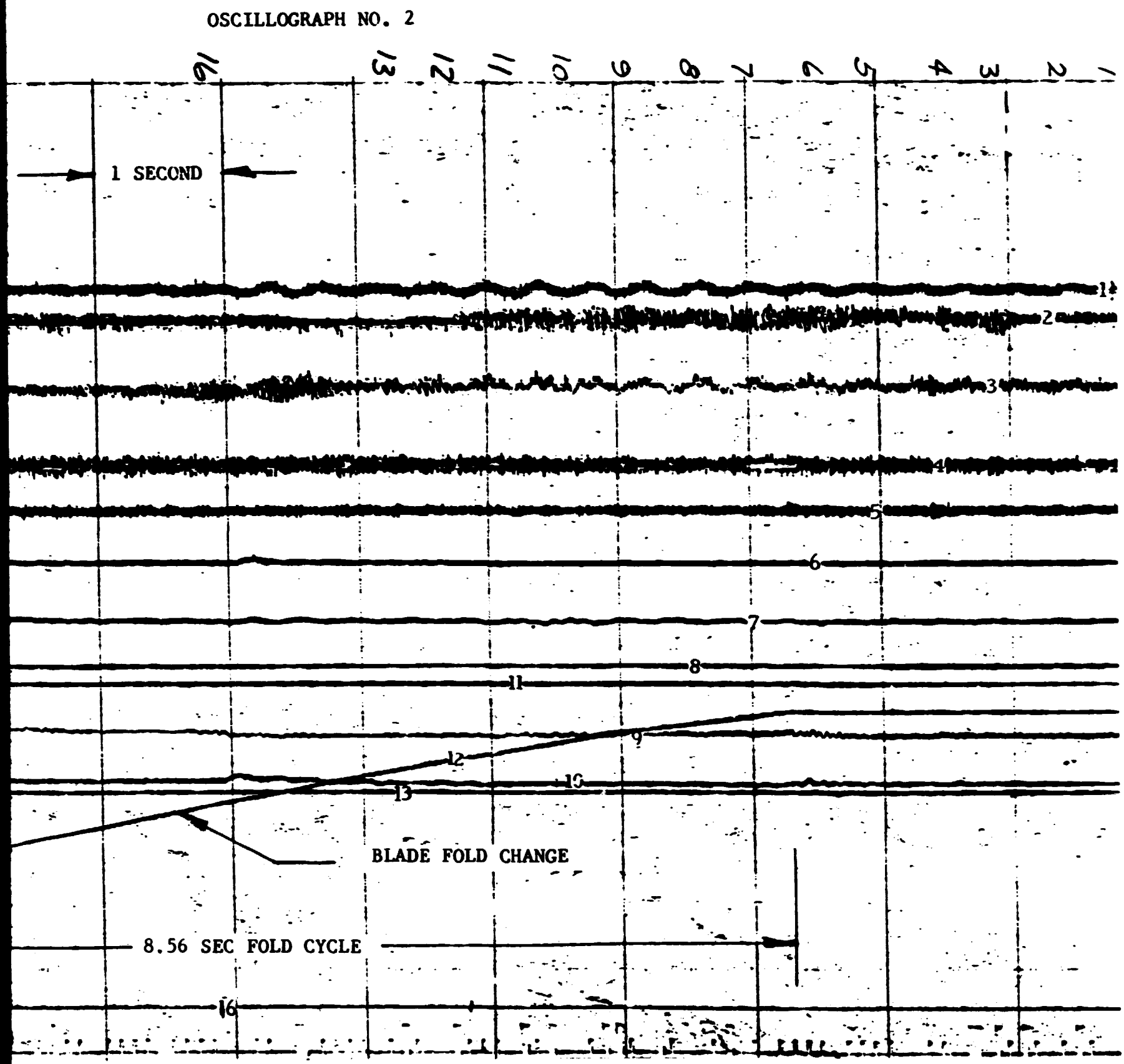


Figure VI-45. Blade Folding Time History, 17 Minus Two Degrees (Run 29.2).

FOLDOUT FRAME

REPRODUCIBILITY OF THE ORIGINAL PAGE IS POOR

Use or disclosure of data on this page is subject to the restriction on the title page.



ime History, 175 Knots, Mast Angle of Attack
es (Run 29.2).

FOLDOUT FRAME 2

REPRODUCIBILITY OF THE ORIGINAL PAGE IS POOR

Parameter Oscillograph No. 1	Oscillograph Trace Scale Factor	
1. Wing Root Beam	in-lb/in	363000
2. Wing Root Chord	in-lb/in	299000
3. Wing Root Torsion	in-lb/in	219103
4. Red Blade	in-lb/in	43000
5. Red Blade Chord Sta. 52.5	in-lb/in	40700
6. Red Blade Pitch Link	lb/in	884.5
7. Fore and Aft Flapping	-	-
8. Lateral Hub Flapping	-	-
9. Mast Torque	in-lb/in	37200
10. Red Blade Pitch Lock Bending	in-lb/in	10150
11. Red Blade Feathering Position	deg/in	52.0
12. Red Blade Fold Position	deg/in	69.9
13. Collective Actuator Position	deg/in	45.7
16. RPM/Azimuth		

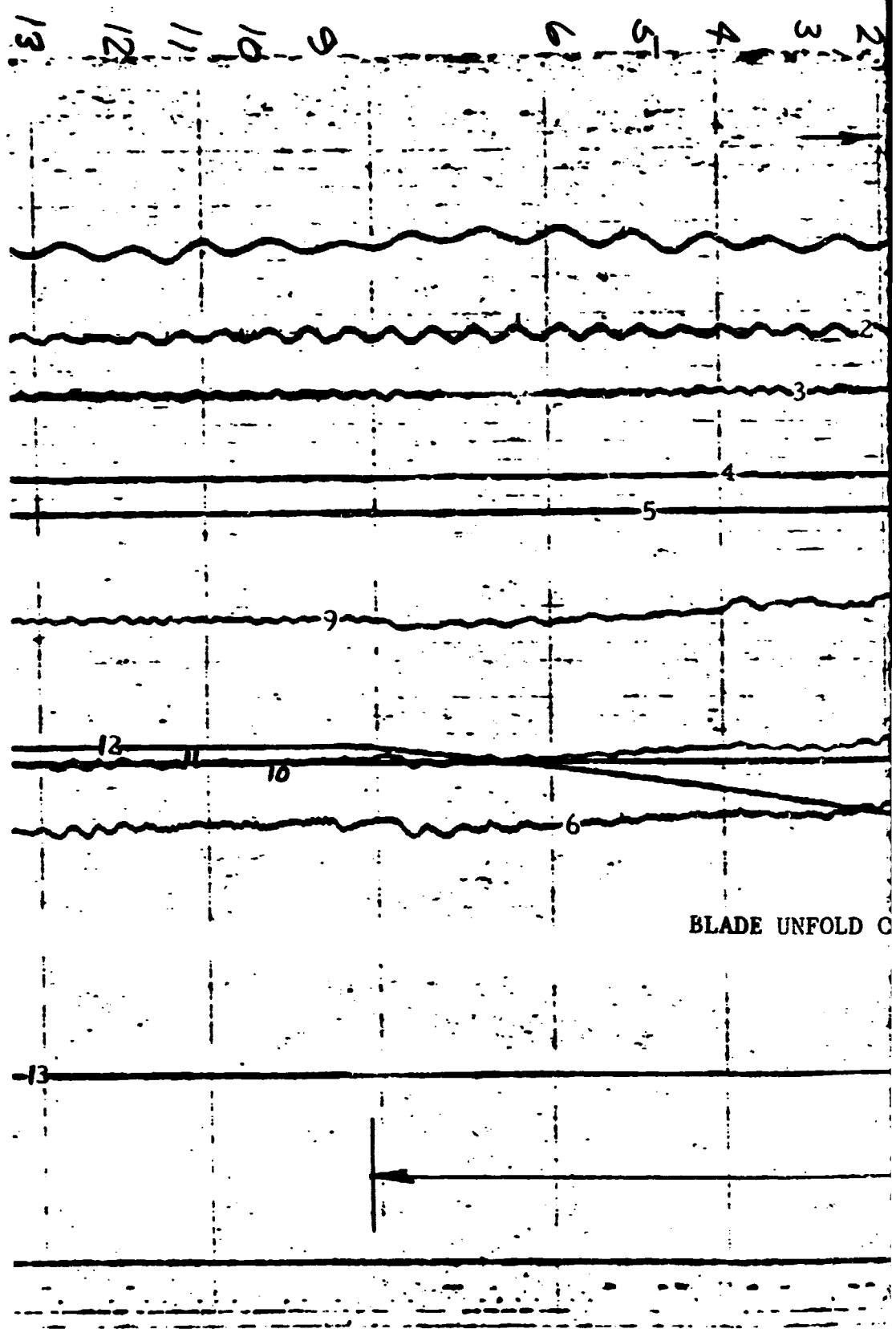


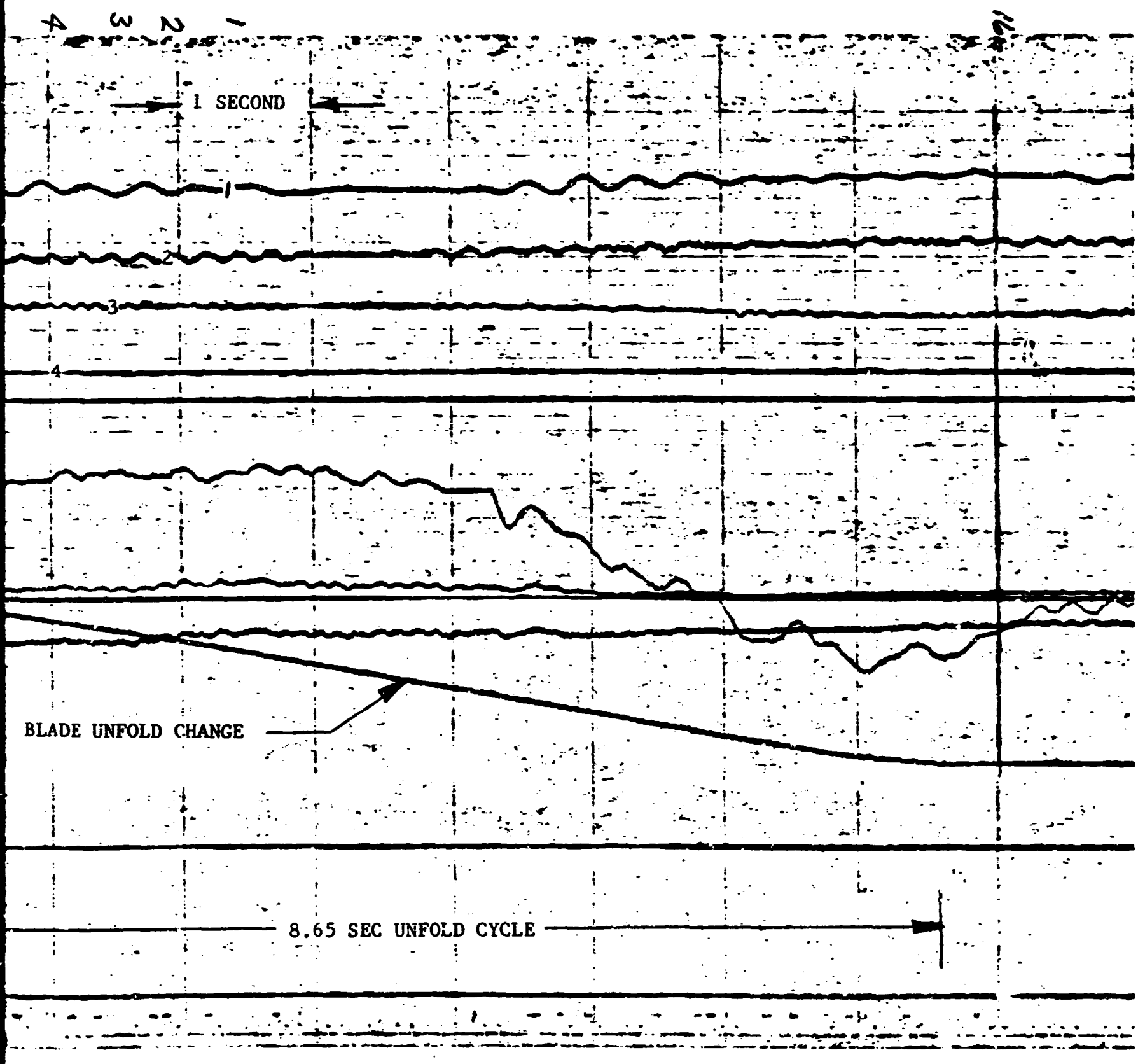
Figure VI-46. Blade Unfolding Time History, 1 Minus Two Degrees (Run 29.3).

FOLDOUT FRAME

REPRODUCIBILITY OF THE ORIGINAL PAGE IS POOR

Use or disclosure of data on this page is subject to the restriction on the title page

OSCILLOGRAPH NO. 1



Time History, 175 Knots, Mast Angle of Attack
es (Run 29.3).

FOLDOUT FRAME 2

REPRODUCIBILITY OF THE ORIGINAL PAGE IS POOR.

Parameter Oscillograph No. 2	Oscillograph Trace Scale Factor	
1. Acceleration Vertical Fwd	g/in	3.18
2. Acceleration Horizontal Fwd	g/in	3.17
3. Acceleration Vertical Aft	g/in	3.50
4. Acceleration Horizontal Aft	g/in	3.11
5. Acceleration Axial	g/in	3.52
6. Flapping - Red Blade	deg/in	10.9
7. Pod Conversion Link	lb/in	17.3
8. Pod Yaw Link	-	-
9. Conversion Spindle Yaw	-	-
10. Mast Vertical Bending	in-lb/in	92500
11. Red Blade Feathering Position	deg/in	50
12. Red Blade Fold Position	deg/in	68
13. Collective Actuator Position	deg/in	50.2
16. RPM/Azimuth		

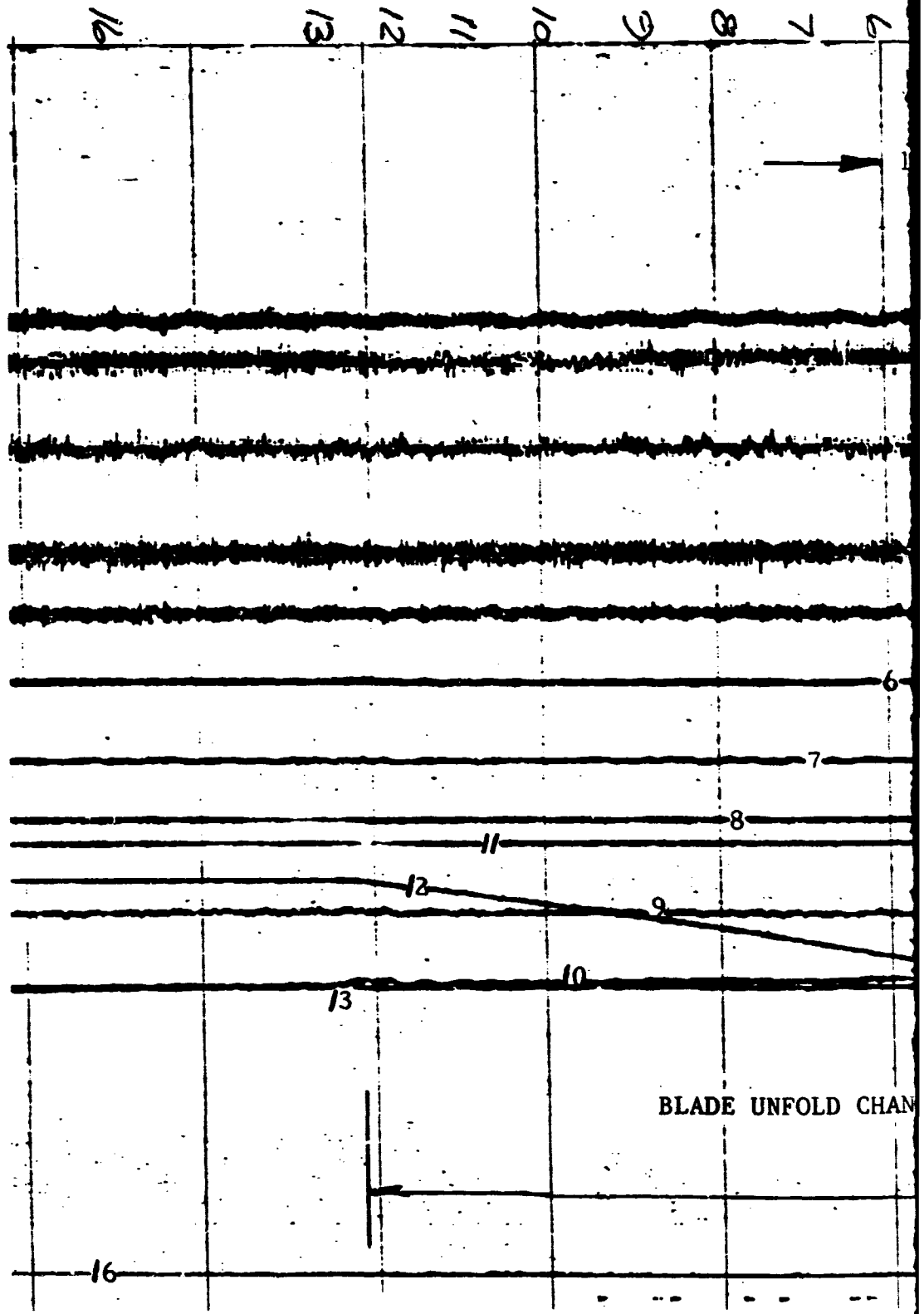


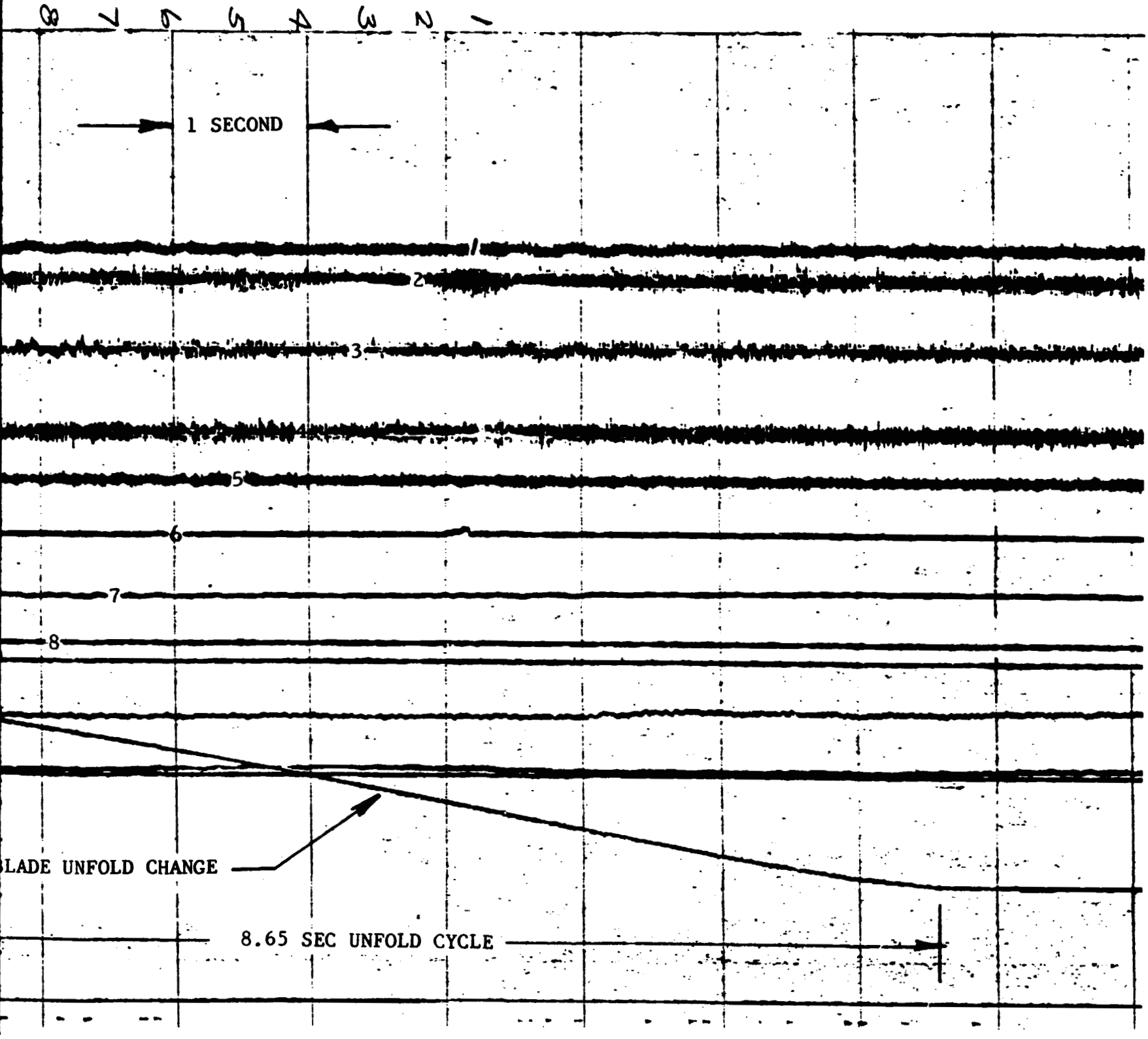
Figure VI-47. Blade Unfolding Time History, 1
Minus Two Degrees (Run 29.3).

FOLDOUT FRAME

REPRODUCIBILITY OF THE ORIGINAL PAGE IS POOR.

Use or disclosure of data on this page is subject to the restriction on the title page.

OSCILLOGRAPH NO. 2



; Time History, 175 Knots, Mast Angle of Attack
es (Run 29.3).

FOLDOUT FRAME 2

REPRODUCIBILITY OF THE ORIGINAL PAGE IS POOR.

Parameter Oscillograph No. 1	Oscillograph Trace Scale Factor	
1. Wing Root Beam	in-lb/in	363000
2. Wing Root Chord	in-lb/in	299000
3. Wing Root Torsion	in-lb/in	219103
4. Red Blade	in-lb/in	43000
5. Red Blade Chord Sta. 52.5	in-lb/in	40700
6. Red Blade Pitch Link	lb/in	884.5
7. Fore and Aft Flapping	-	-
8. Lateral Hub Flapping	-	-
9. Mast Torque	in-lb/in	37200
10. Red Blade Pitch Lock Bending	in-lb/in	10150
11. Red Blade Feathering Position	deg/in	52.0
12. Red Blade Fold Position	deg/in	69.9
13. Collective Actuator Position	deg/in	45.7
16. RPM/Azimuth		

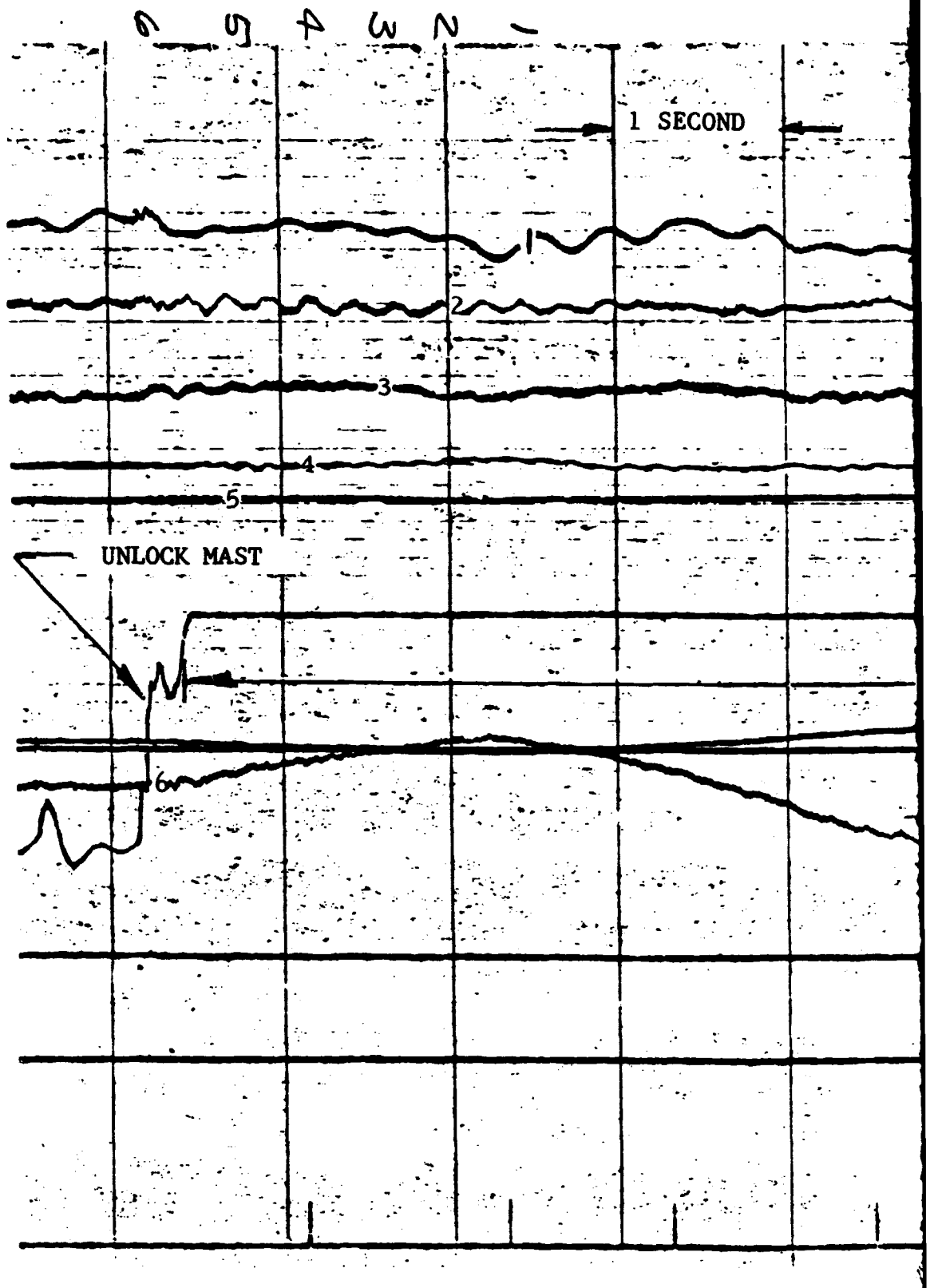


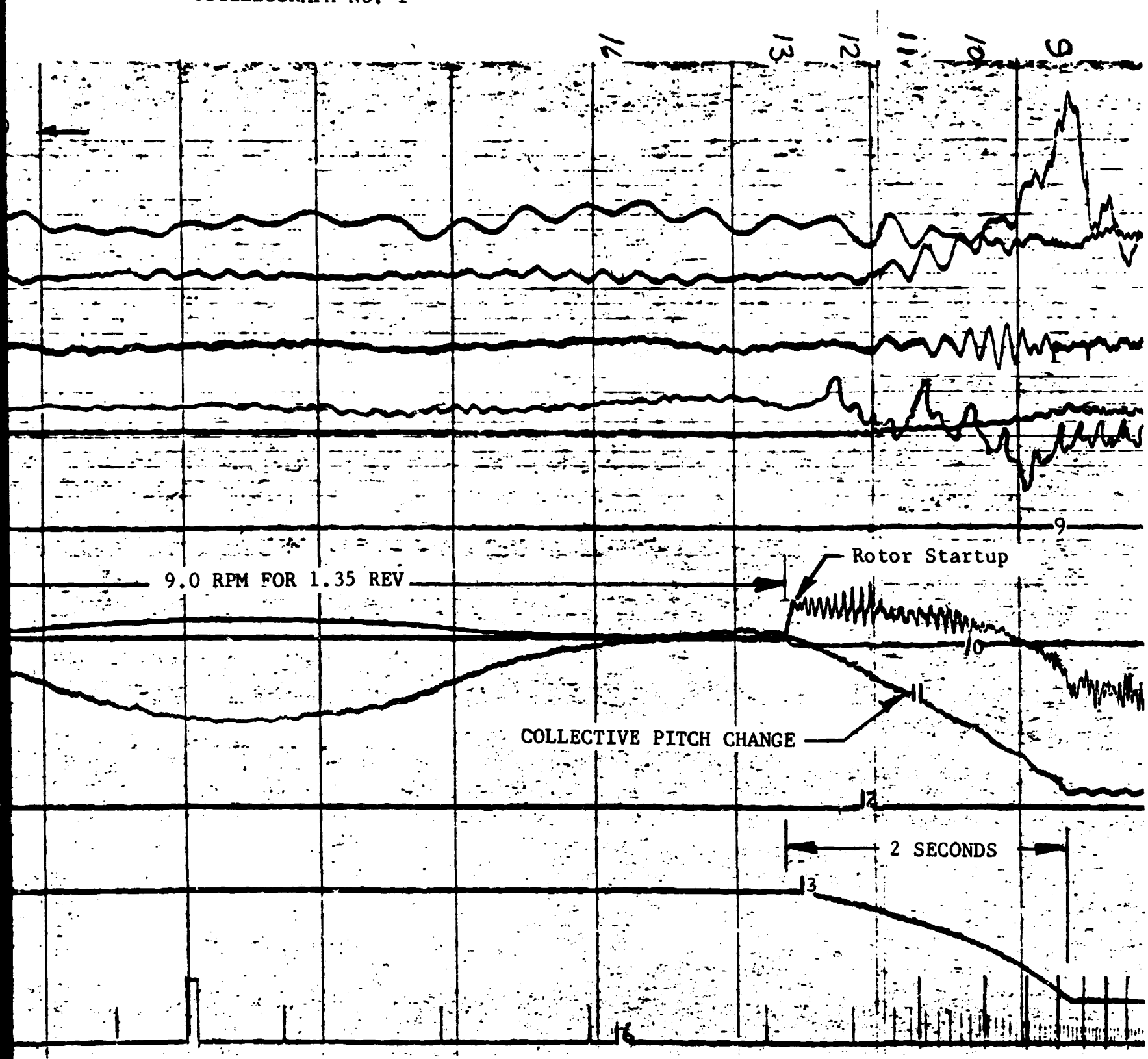
Figure VI-48. Mast Unlock and Rotor Start Time of Attack Minus Two Degrees (Run

FOLDOUT FRAME 1

REPRODUCIBILITY OF THE ORIGINAL PAGE IS POOR.

Use or disclosure of data on this page is subject to the restriction on the title page.

OSCILLOGRAPH NO. 1



r Start Time History, 175 Knots, Mast Angle
Degrees (Run 29.3).

FOLDOUT FRAME 2

REPRODUCIBILITY OF THE ORIGINAL PAGE IS POOR.

Parameter Oscillograph No. 2		Oscillograph Trace Scale Factor
1. Acceleration Vertical Fwd	g/in	3.18
2. Acceleration Horizontal Fwd	g/in	3.17
3. Acceleration Vertical Aft	g/in	3.50
4. Acceleration Horizontal Aft	g/in	3.11
5. Acceleration Axial	g/in	3.52
6. Flapping - Red Blade	deg/in	10.9
7. Pod Conversion Link	lb/in	17.3
8. Pod Yaw Link	-	-
9. Conversion Spindle Yaw	-	-
10. Mast Vertical Bending	in-lb/in	92500
11. Red Blade Feathering Position	deg/in	[illegible]
12. Red Blade Fold Position	deg/in	68
13. Collective Actuator Position	deg/in	50.2
16. RPM/Azimuth		

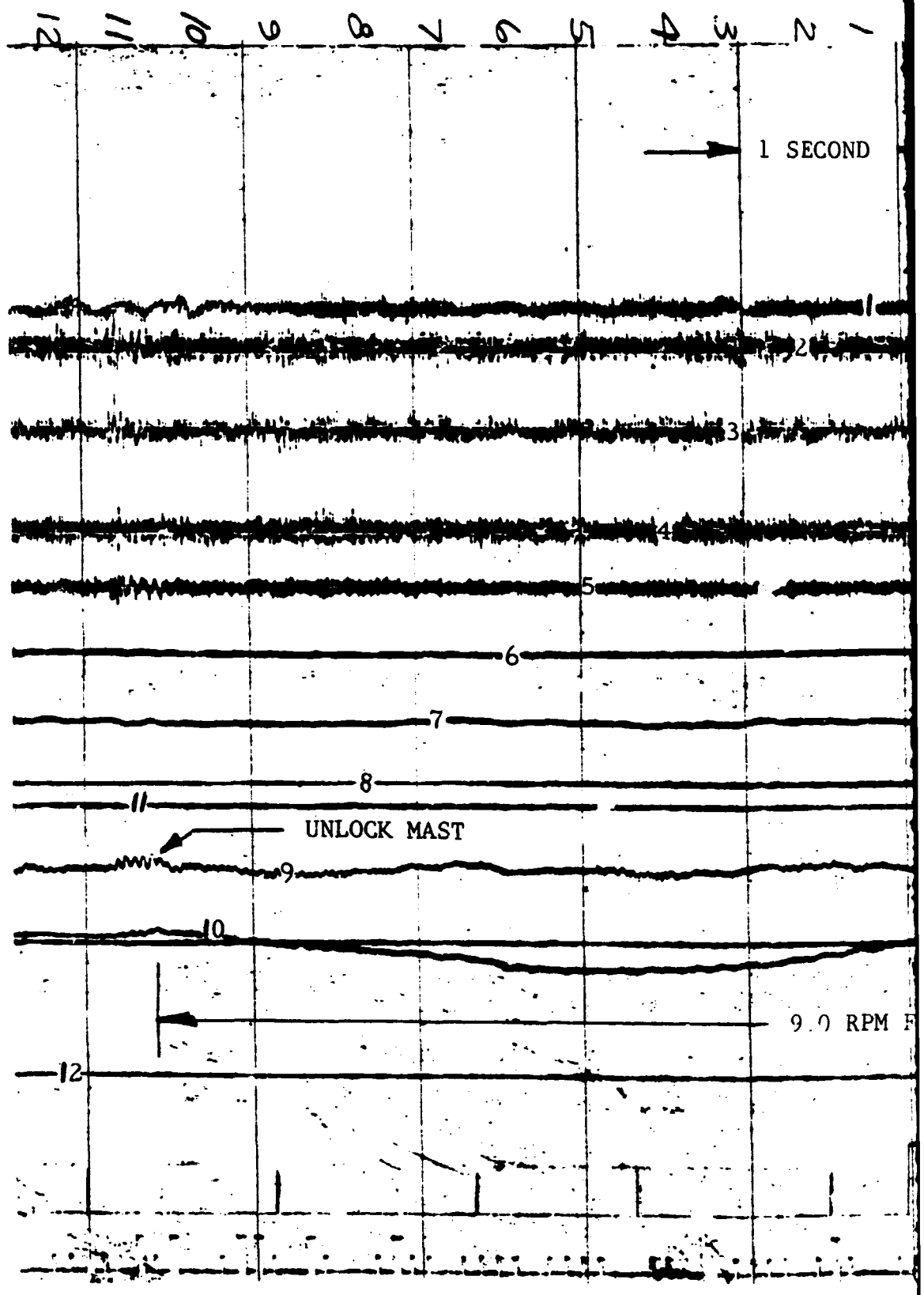


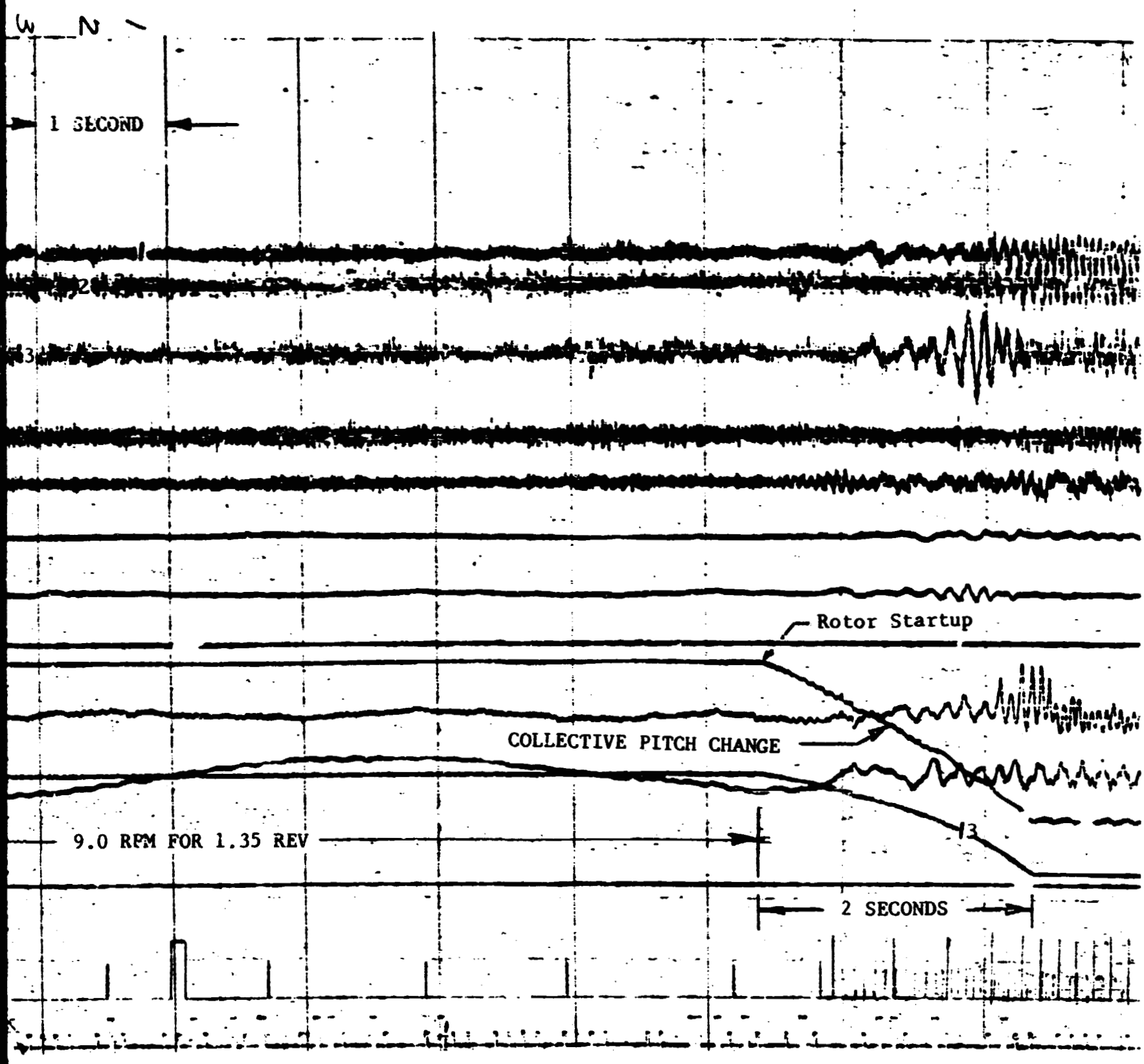
Figure VI-49. Mast Unlock and Rotor Start Time Hi
of Attack Minus Two Degrees (Run 29

FOLDOUT FRAME

REPRODUCIBILITY OF THE ORIGINAL PAGE IS POOR.

Use or disclosure of data on this page is subject to the restriction on the title page

OSCILLOGRAPH NO. 2



r Start Time History, 175 Knots, Ma t Angle
Degrees (Run 29.3).

FOLDOUT FRAME 2

REPRODUCIBILITY OF THE ORIGINAL PAGE IS POOR

Parameter Oscillograph No. 1	Oscillograph Trace Scale Factor	
1. Wing Root Beam	in-lb/in	367469 ±183700
2. Wing Root Chord	in-lb/in	296000 ±148000
3. Wing Root Torsion	in-lb/in	219103 ±109550
4. Red Blade Sta. 52.5	in-lb/in	43200 ± 21600
5. Red Blade Chord Sta. 32.5	in-lb/in	30700 ±15350
6. Red Blade Pitch Link	lb/in	879
7. Fore and Aft Hub Flapping	-	-
8. Lateral Hub Flapping	-	-
9. Mast Torque	in-lb/in	74400
10. Red Blade Pitch Lock Bending	in-lb/in	35700
11. Red Blade Feathering Position	deg/in	52
12. Red Blade Fold Position	deg/in	70.1
13. Collective Actuator Position	deg/in	46.2
16. RPM/Azimuth		

OSCILLOGRAPH NO. 1

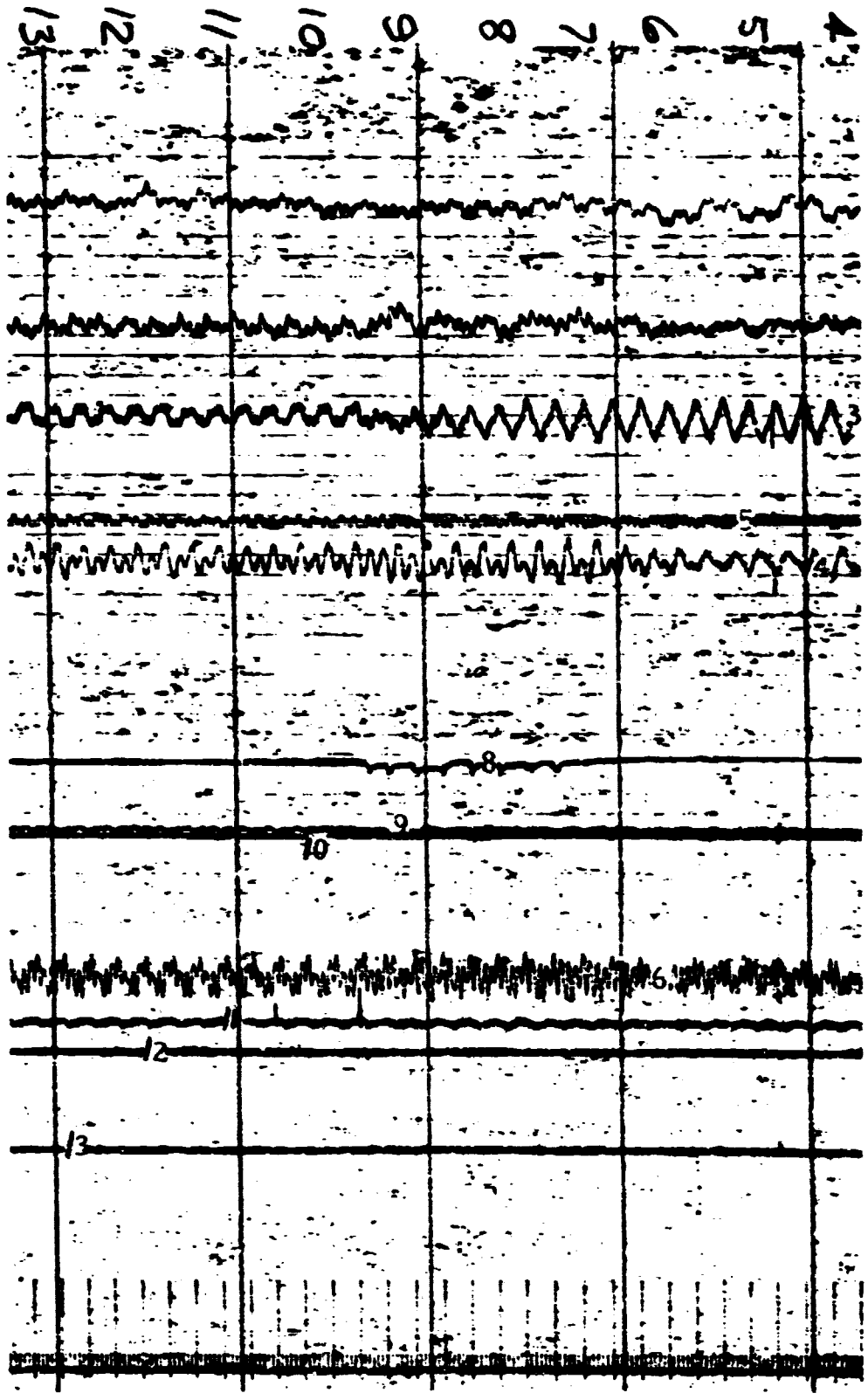


Figure VI-50. Hub Flapping Unlock Time History, Minus One Degree (Run 16.8).

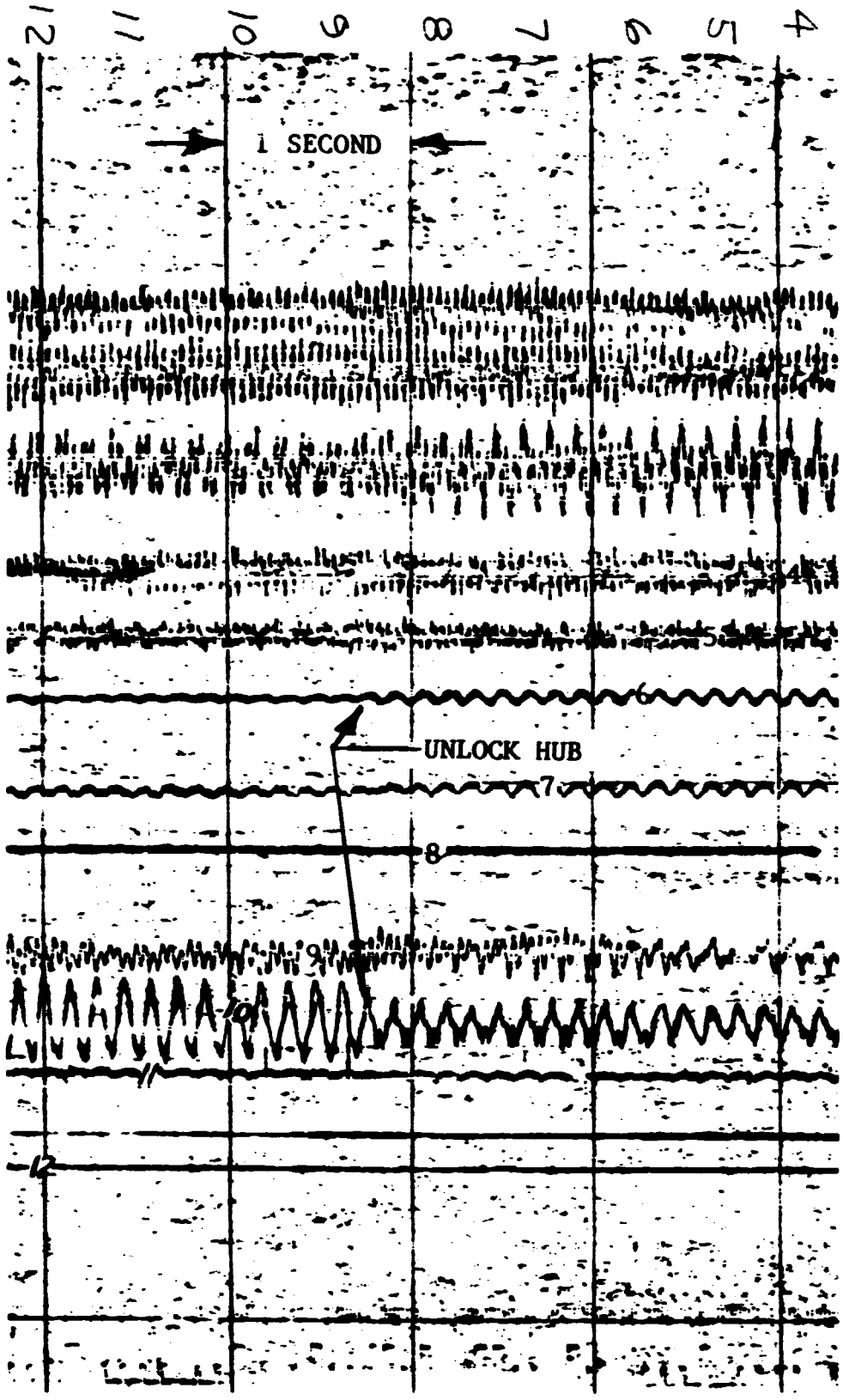
FOLDOUT FRAME

REPRODUCIBILITY OF THE ORIGINAL PAGE IS POOR

Use or disclosure of data on this page is subject to the restriction on the title page

Parameter Oscillograph No. 2	Oscillograph Trace Scale Factor	
1. Acceleration Vertical Fwd	g/in	3.14 ±1.57
2. Acceleration Horizontal Fwd	g/in	3.19 ±1.59
3. Acceleration Vertical Aft	g/in	3.5 ±1.75
4. Acceleration Horizontal Aft	g/in	3.11 ±1.56
5. Acceleration Axial	g/in	3.52 ±1.76
6. Flapping - Red Blade	deg/in	18.45 ±9.22
7. Pod Conversion Link	lb/in	17000
8. Pod Yaw Link	-	-
9. Conversion Spindle Yaw	-	-
10. Mast Vertical Bending	in-lb/in	94300
11. Red Blade Feathering Position	deg/in	50.5
12. Red Blade Fold Position	deg/in	67.3
13. Collective Actuator Position	deg/in	50.2
16. RPM/Azimuth		

OSCILLOGRAPH NO. 2



k Time History, 175 Knots, Mast Angle of Attack
Run 16.8).

FOLDOUT FRAME 2

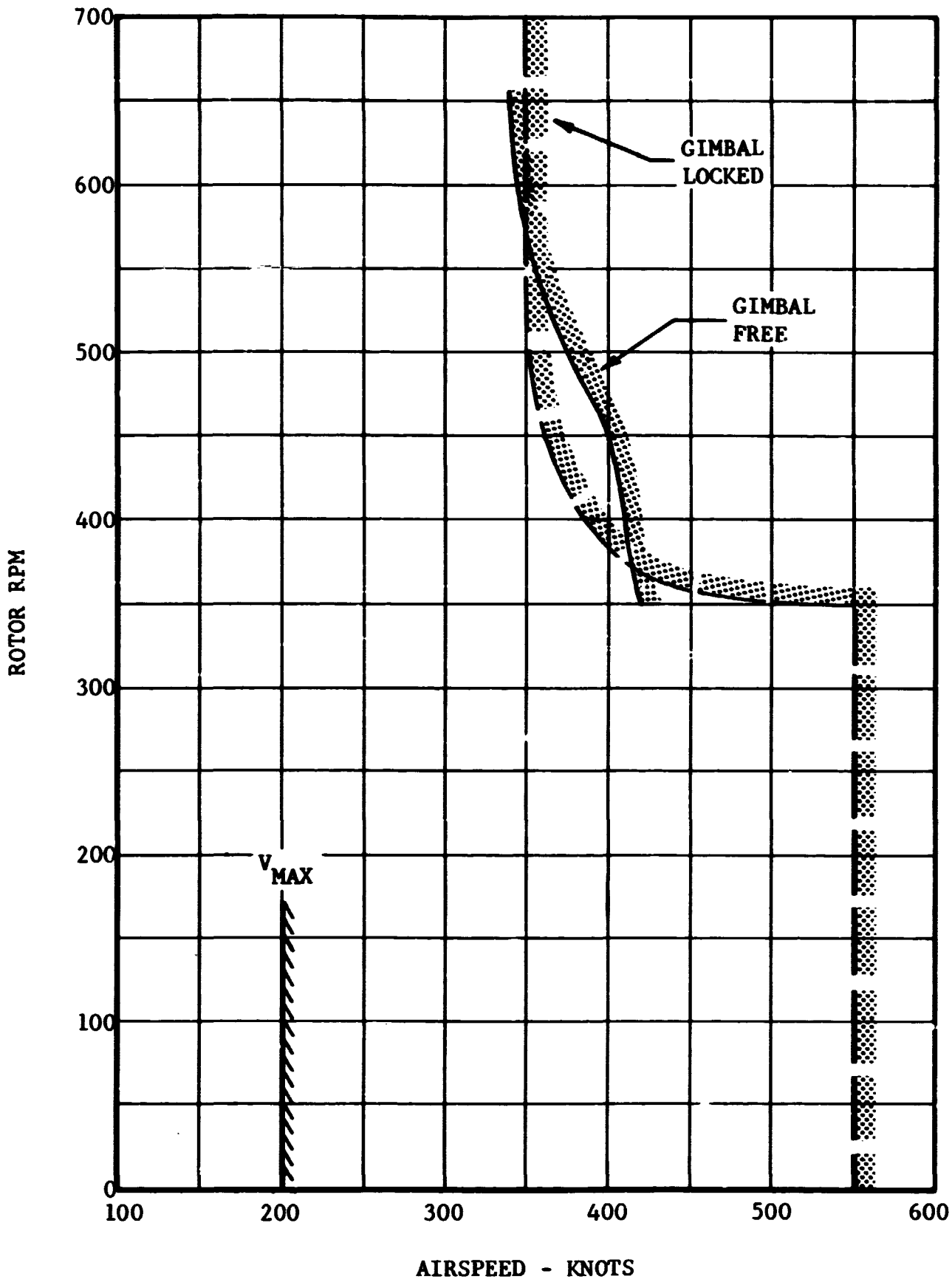


Figure VI-51. Model 627 Predicted Proprotor Stability Boundaries with Gimbal Free/Gimbal Locked, Cantilevered Wing.

Use or disclosure of data on this page is subject to the restriction on the title page.

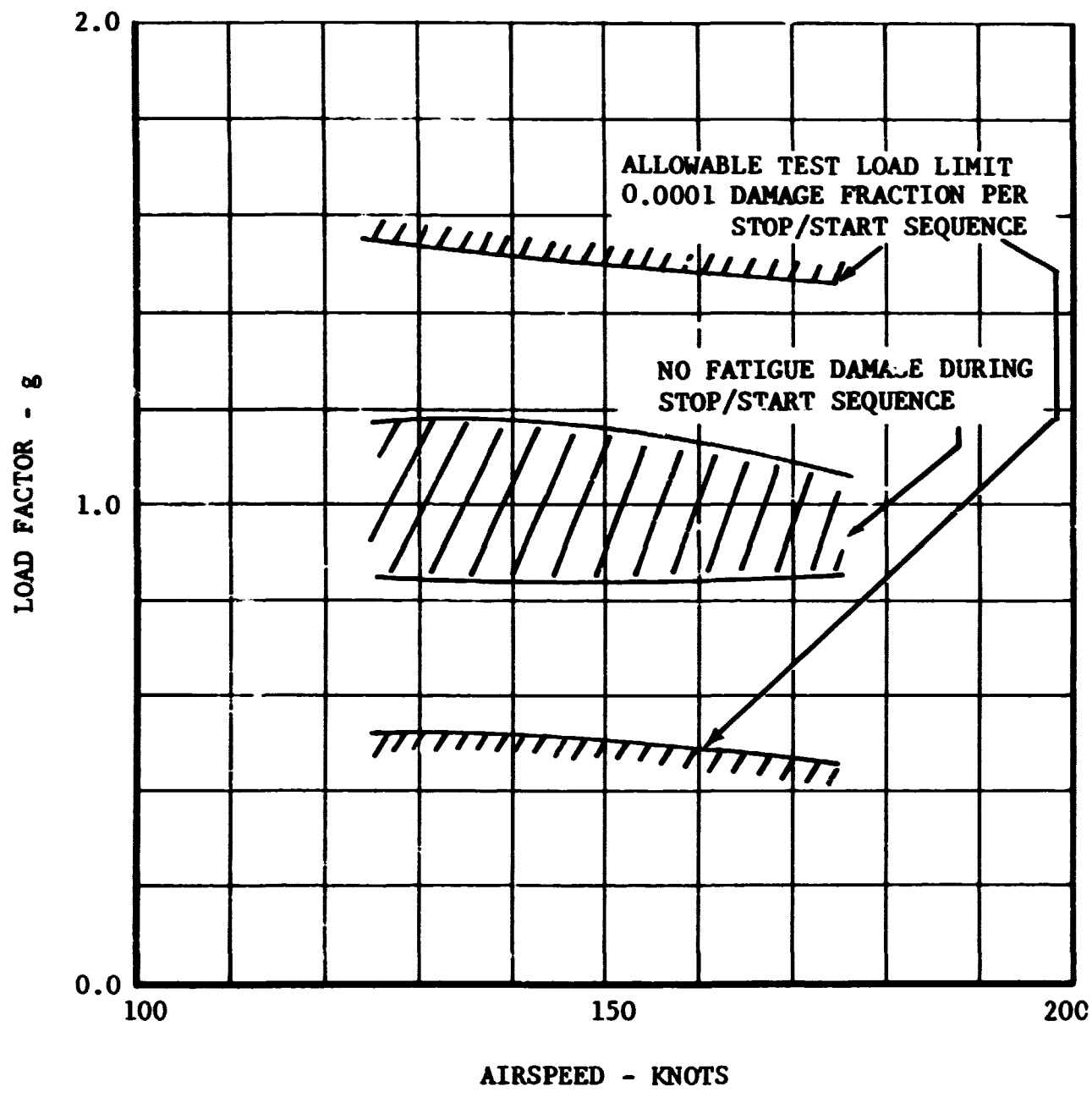


Figure VI-52. Model 627 Folding Proprotor V-n Diagram, Based on the Allowable Test Load Limit at Blade Fold Hinge.

Use or disclosure of data on this page is subject to the restriction on the title page.

VII. FOLDING PROPROTOR CONVERSION CRITERIA CONSIDERATIONS

A. SEQUENCE PROBLEMS INVESTIGATED

1. Rotor Speed Programming

Some events involved when transitioning between proprotor mode and airplane mode with the proprotors folded and stowed require rotor speed to be held or brought to a specific rpm quickly and precisely. The events are:

(a) Initial hub lockout

(b) Mast index and lock

(c) Hub unlock

(d) Prop cruise

To aid in attaining a given rpm condition quickly during the test, an electronic circuit sensing rpm with a photocell encoder was used to stop the collective actuator when the specific rpm was reached. Because of the mechanical lag of the actuator and the overall time required to actuate, the sensor has to "lead" the specific rpm point by a considerable margin. This presented problems because the amount of "lead" required depended on the particular collective rate and airspeed considered. The above method was satisfactory for the purpose of the wind-tunnel test but would have to be refined for use in an aircraft.

2. Mast Index and Lock

The mast index and lock sequence function of this test was accomplished by a positive mechanical detent stop and lock device as discussed in Section V, paragraph A.8. This device produced sudden mast torsional peak loads at the instant of index and lock which would be undesirable for an aircraft. This is shown in Figure VII-1. The high peak transient loads are caused by the uneven rpm of the rotor during the mast index phase of the sequence. The uneven rpm results from the wing-rotor interference effect which makes the rotor slow down as each blade passes the front of the wing and then immediately speed up as the blade moves away from the wing as shown in Figure VII-2. The azimuth for index and lockout was programmed by the design configuration requirements of the rotor-engine pod to occur at either the 65, 185, or 305 degree rotor azimuth positions. These points occur near the peaks in the rpm variation in rotational speed near the stopped condition. The general way the rotor rpm responds to the blade tip collective setting near feather is shown in Figure VII-3.

It was also evident from the test that if index and lock occurred with hydraulic pressure below 2500 psig, or at a rotor speed above an average of 8 rpm, the lock safety device did not always become positively engaged. This problem is further discussed under recommended future work of Section VIII, paragraph E.3. The method discussed above was satisfactory for the purpose of the wind-tunnel test, but would require refinement before being used in an aircraft.

Use or disclosure of data on this page is subject to the restriction on the title page.

B. RESULTING CRITERIA FOR AIRCRAFT DESIGN

The folding proprotor sequence for aircraft operation must be precise, smooth, repeatable, and highly reliable. It is also desirable for the sequence control to be automatic on command due to normal flying pilot work load during the time period of the conversion sequence. Most of the sequence investigated in this test was accomplished in a manner which would meet this criterion. For the most part, the approach taken in the folding proprotor conversion sequence of this test is applicable to an aircraft since the steps were performed in the appropriate order and within allowable loads and were smooth and repeatable. However, problems mentioned above do indicate a need for updating and improving the control criteria in these areas of the sequence. The pertinent points of design criteria for an aircraft as derived from this test are as follows:

1. Rotor Speed Control

The method employed to hold or bring rpm to a specified speed during the sequence ideally would drive the collective pitch at a pitch change rate proportional to the rpm change required, and would also avoid sudden thrust changes that could produce uncomfortable accelerations. This means collective pitch and rpm will change slowly initially when reducing from a high rpm to avoid large changes in thrust, then speed up for the main portion of the rpm change and will again slow down as the specified rpm is approached to prevent collective pitch overshoot as shown in Figure VII-4. For the case of changing from a lower to a higher rpm, the initial collective change rate is not as critical since rotor thrust is proportional to the square of the tip speed; however, a slow down is again necessary as the higher rpm is approached for the same reason as previously discussed. The system devised must also be sufficiently redundant so that it is extremely reliable and that the rpm control will always function.

2. Mast Index and Lock

The function of indexing and locking the mast must be accomplished at a steady rotor speed, and preferable between two and three rpm so that the rotational energy is low at lockout. The lock or unlock safety device must be positive regardless of hydraulic pressure or rotational speed at lockout. An indexing motor which would engage the mast at index command to rotate the rotor at a uniform rate to smooth out the peaks and valleys would be desirable. Aerodynamic rotor indexing based on rotor azimuth feedback at low rpm may provide the lightest solution.

3. Rotor Stop/Start Rate

Small-scale model investigations of the folding proprotor were conducted by Bell Helicopter during 1970 and 1971 (see Section II, paragraph C). During those tests, the stop/start rate was varied over a wide range. These investigations explored stopping and starting at full-scale values from less than one second to over ten seconds. The 1970 and 1971 investigations are discussed in detail in References 11 and 14. From those test programs, a range of feather rates was selected for exploration with the full-scale Model 627 rotor. Stop/start times from 2.0 to 4.0 seconds were picked based on

Use or disclosure of data on this page is subject to the restriction on the title page.

prior work. Most of the stopping and starting during the test was done at about 2.0 seconds. This rate is considered to be good from a dynamic standpoint based upon the very brief number of high oscillatory rotor and wing loads experienced and the very short time vibrations from the pylon were transmitted to the fuselage during the stop-start cycles of the full-scale test.

The stop/start rate criterion discussion of Reference 11 is briefly summarized here as further basis of this stop-start rate range mentioned above. Figures VII-5 and VII-6 show the calculated vibratory response during blade feathering at the pylon conversion axis and at the crew station, respectively, as a function of feathering rate. Also shown in Figure VII-6 is the longitudinal acceleration caused by the transient thrust generated by blade feathering. This, in combination with the vibratory response characteristics, suggests that a feathering time somewhere between 2.0 to 4.0 seconds is desirable as shown by the envelope lines selected for the Model 627 range. Small-scale model tests showed a valley in the wing chordwise moment as the only indicator of an "optimum feathering rate." Based on the chordwise moment valley, the optimum feather time would be about 2.75 to 3 seconds. However, the crew station response at the wing beam frequency indicates a potential human factors problem. At the beam frequency, the acceleration level is close to the level established as being alarming in Reference 18 which indicates the stopping time needs to be short. The transient nature may reduce the significance of this observation, but a requirement for a study of the crew acceptance of this type of response is indicated.

A second problem area is the acceptability of the crew station vibration during blade feathering. The largest response occurs at a frequency of approximately 2.5 cycles per second which is the wing beam bending natural frequency. At this frequency, the peak accelerations may reach ±0.60g, with higher angles of attack which exceed the "alarming" subjective discomfort level. However, the reference subject discomfort level was established for sinusoidal vibration whereas the response during feathering is a damped transient. A requirement for a human tolerance criterion for an acceptable level of crew station response is evident. Based on response studies for 25-, 38.5-, and 50-foot proprotors, an optimum feathering time may be approximated by

$$\Delta T = 2.75\sqrt{\frac{D}{38.5}} \text{ seconds}$$

where D is the proprotor diameter in feet

This optimum is not extremely sensitive and may be varied over a considerable range. For the 25-foot rotor of the full-scale test, this would indicate a $\Delta T = 2.2$ seconds.

Later information on stop/start rates given in Reference 14 which is based on a one-fifth-scale model of the Model 627 rotor. These data, as shown in Figures IV-12, IV-13, and IV-14 of Reference 14, indicate that 2.5 to 4.0 second stop/start is optimum.

Use or disclosure of data on this page is subject to the restriction on the title page.

4. Hub Flapping Lockout

Prior to the small-scale model work it was thought that flapping could be locked out during the feather/stop sequence at about 25-30 percent of the hover rpm. The effect of feathering rate on the dynamic flapping response and practical considerations, however, indicate flapping should be locked out at a higher rpm, or prior to feathering. The large-scale tests were run with flapping locked out at approximately 80 percent of hover rpm prior to feathering. This rotor speed is from 425 to 458 rpm which is the normal prop mode rpm at the start of the folding proprotor conversion sequence. Locking out flapping at these rotor speeds was accomplished with no difficulty. Hub flapping was reduced to near 0 in about 2.6 seconds. (About 0.25 degree flapping remained after lockout due to the slight structural deflection in the lockout mechanism.)

The hub flapping lockout moment load can be closely approximated from full-scale mast bending data since the energy expended to lock the hub is directly applied to the mast as a couple. This is shown in Figure VII-7 and appears to be fairly linear over the angle-of-attack range of the test. The reduction in flapping caused by the hub lockout is shown in Figure VII-8.

Locking out flapping did not significantly influence the wing and pylon dynamic response. Both test data and calculated pylon responses show the acceleration to be close to that with the flapping free.

The principal influence of locking out flapping freedom is a mast angle-of-attack limit resulting from blade loads. (Locking out the flapping freedom increases the one-per-rev out-of-plane loads since flapping acts to relieve the one-per-rev airloads.) Note that this limit would only apply during the feather/stop sequence. The angle-of-attack limit with the gimbal free is much higher.

The most significant conclusions are that flapping freedom must be sufficiently constrained prior to feathering the blades. During small-scale model tests with the gimbal flapping only lightly restrained, large flapping amplitudes were encountered even near zero shaft angle of attack. As the blade feathering rate was increased, the peak flapping excursion increased. At a model shaft angle of attack of 5.6 degrees, the blades contacted the mechanical flapping stops set at 12 degrees. Furthermore, a flapping instability was encountered at low rpm in the transition mode airspeed range. When the gimbal flapping freedom was locked out during both the small-scale and large-scale tests, the blade tip deflections were observed to be small and the flapping instability eliminated.

From a criteria standpoint, a proprotor type which combines stiff blades with the capability to constrain flapping freedom is desirable. Highly flexible, freely flapping, or even blades lightly restrained in flapping are susceptible to instability at low rotor speeds and can contribute to higher response levels during feathering. The fast-acting mechanical hub lockout mechanism of the Model 627 rotor performed well and appears to be a good design approach for an aircraft However, a slightly softer hub lockout device of the Model 627 design may be desirable to reduce blade loads and allow slightly more flapping after lockout.

Use or disclosure of data on this page is subject to the restriction on the title page.

5. Angle of Attack

Shaft angle of attack has a significant influence on the dynamic response. A time history of blade feathering at a shaft angle of attack of four degrees differs from the zero angle-of-attack history most markedly in the area of impulsive response at the wing beam natural frequency. This is shown in Figure VI-1 for the wing beam data channel at four degrees angle of attack which is greater response than shown in Figure VI-42 for data channel No. 1 at zero angle of attack. This is the result of the sudden buildup in normal force as the proprotor stops since the normal force is essentially proportional to the inflow angle. The feather/stop sequence should be made with the shaft angle of attack near zero degrees for lower wing response.

The blade load buildup on the other hand remains moderate during feathering even at the four- to six-degree shaft angle of attack. During blade folding, mast angle of attack may be varied over a much larger range than for feathering since static limit loads are now the criterion for blade or wing loads. Airspeed has a major effect on the allowable mast angle of attack. It can be seen from the test data that an airspeed for conversion at 140 to 160 knots allows 50- to 60-percent more angle-of-attack flight range than does flight at 175 knots.

6. Airspeed

From the test data it appears that the response amplitude increased essentially linearly with airspeed for a constant wing lift coefficient. This is logical since the system damping is proportional to velocity, whereas the airload forcing function is proportional to the velocity squared. At resonance, the response amplitude is proportional to the ratio of the forcing function divided by the damping. Hence, the response would be expected to be proportional to velocity. At the lower wing lift coefficients associated with increased airspeeds, the wing upwash is reduced and the net effect is a negligible influence of airspeed on response.

From the standpoint of loads and other dynamic response data, an airspeed of 150 knots for the stop/fold conversion appears preferable since it provides the broadest maneuver envelope.

Use or disclosure of data on this page is subject to the restriction on the title page.

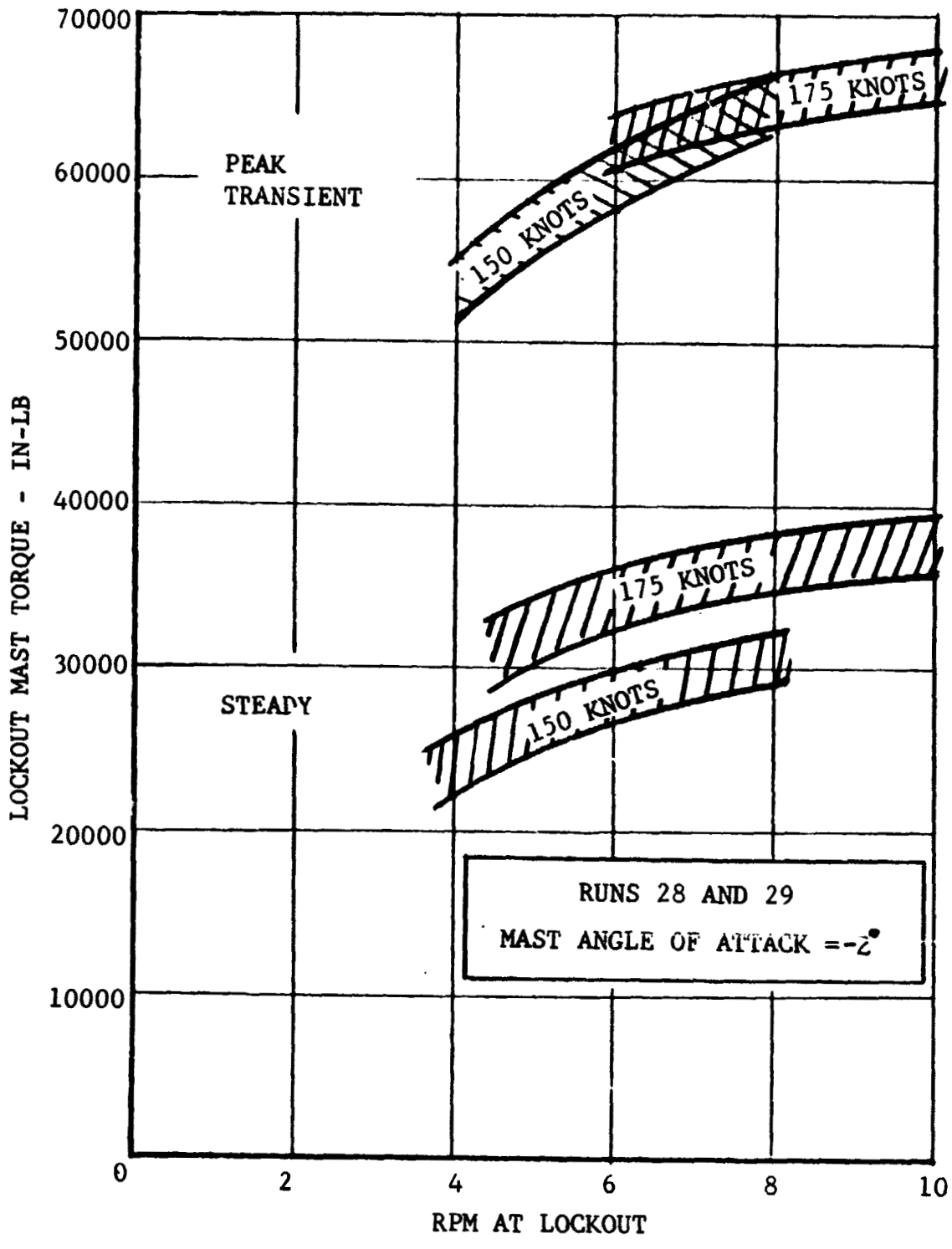


Figure VII-1. Mast Index and Lockout Loads.

Use or disclosure of data on this page is subject to the restriction on the title page.

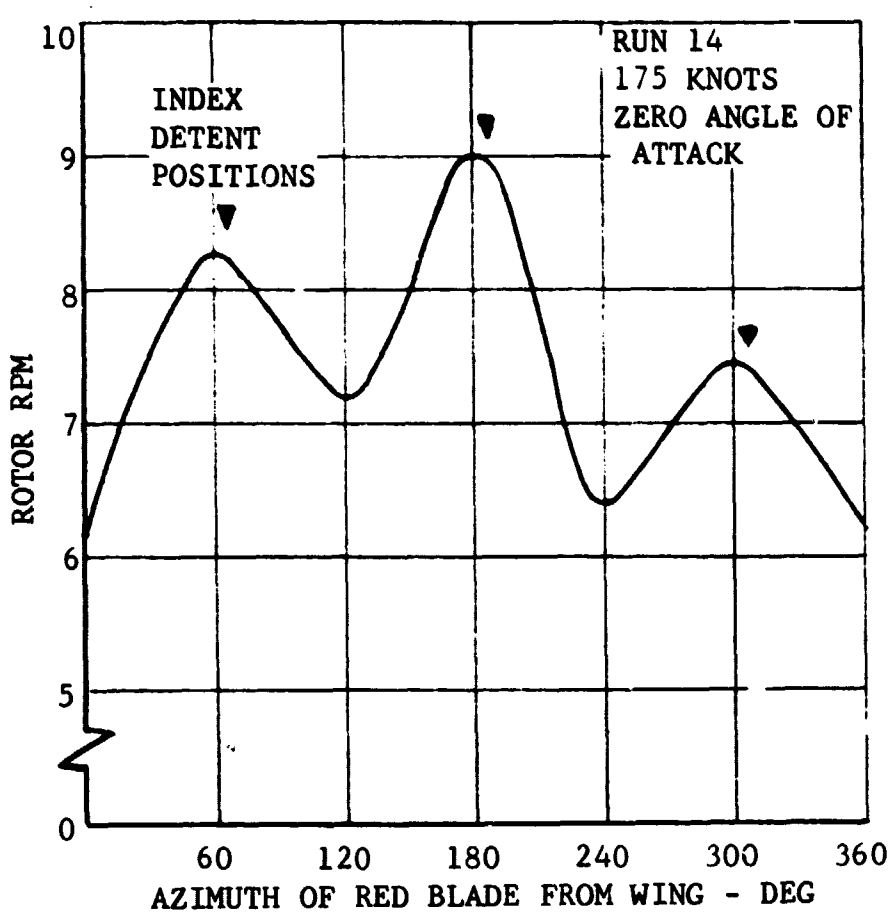


Figure VII-2. Rotor RPM Variation Prior to Mast Index.

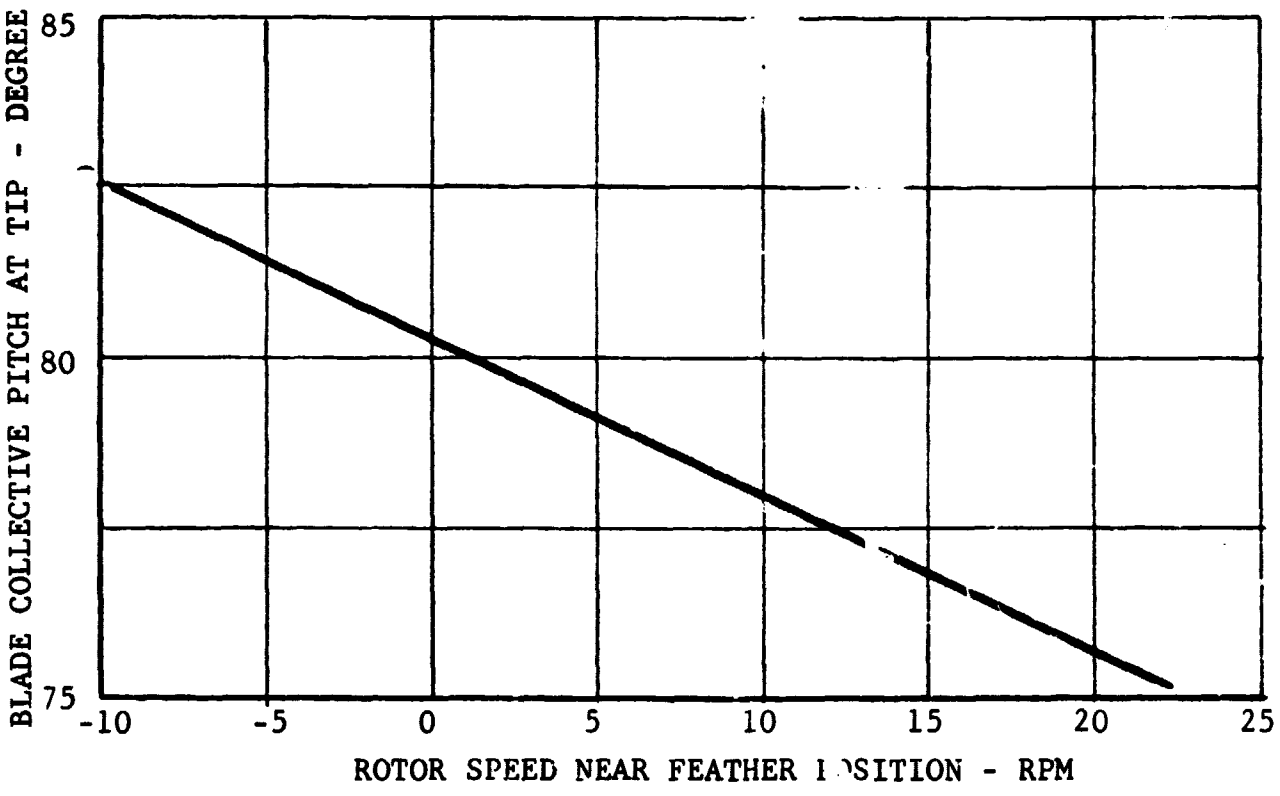


Figure VII-3. Rotor RPM Response to Collective Near Feather.

Use or disclosure of data on this page is subject to the restriction on the title page.

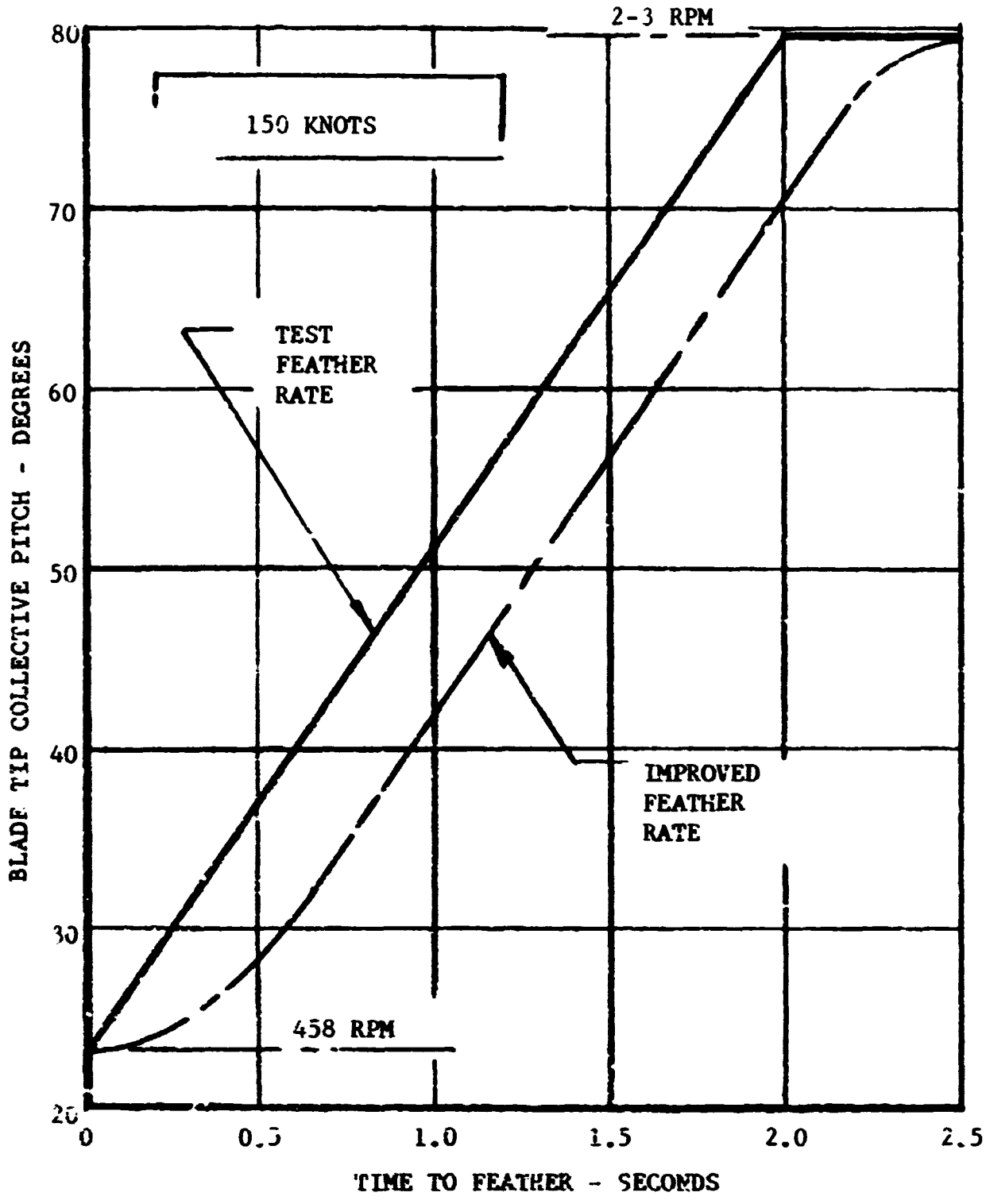


Figure VII-4. Collective Pitch - Feather Schedule.

Use or disclosure of data on this page is subject to the restriction on the title page

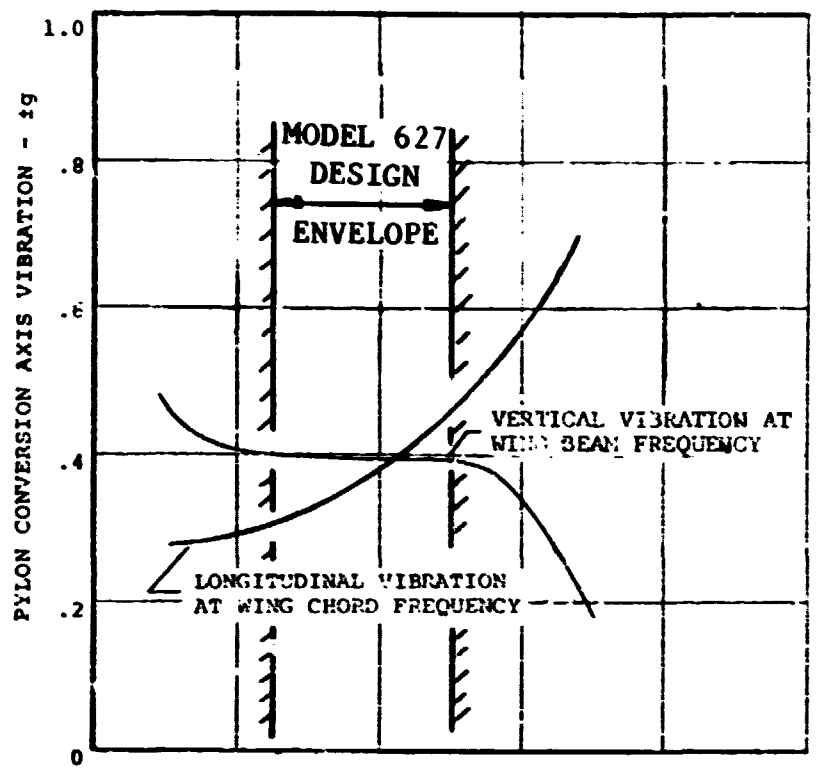


Figure VII-5. Peak Vibration at Pylon Conversion Axis During Blade Feathering, Calculated.

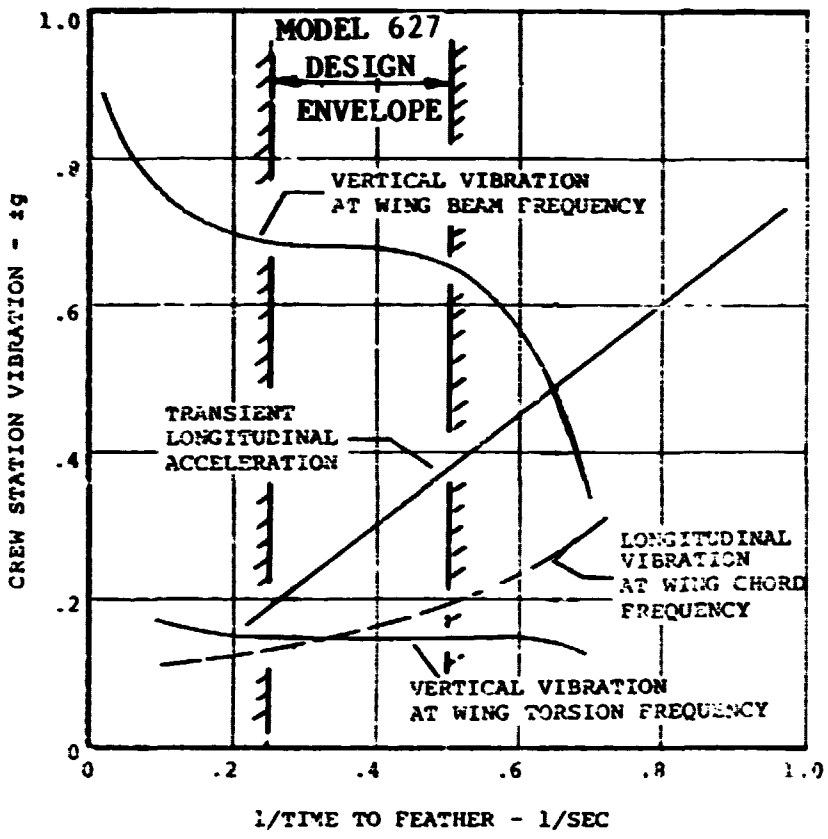


Figure VII-6. Peak Vibration at Crew Station During Blade Feathering, Calculated.

Use or disclosure of data on this page is subject to the restriction on the title page.

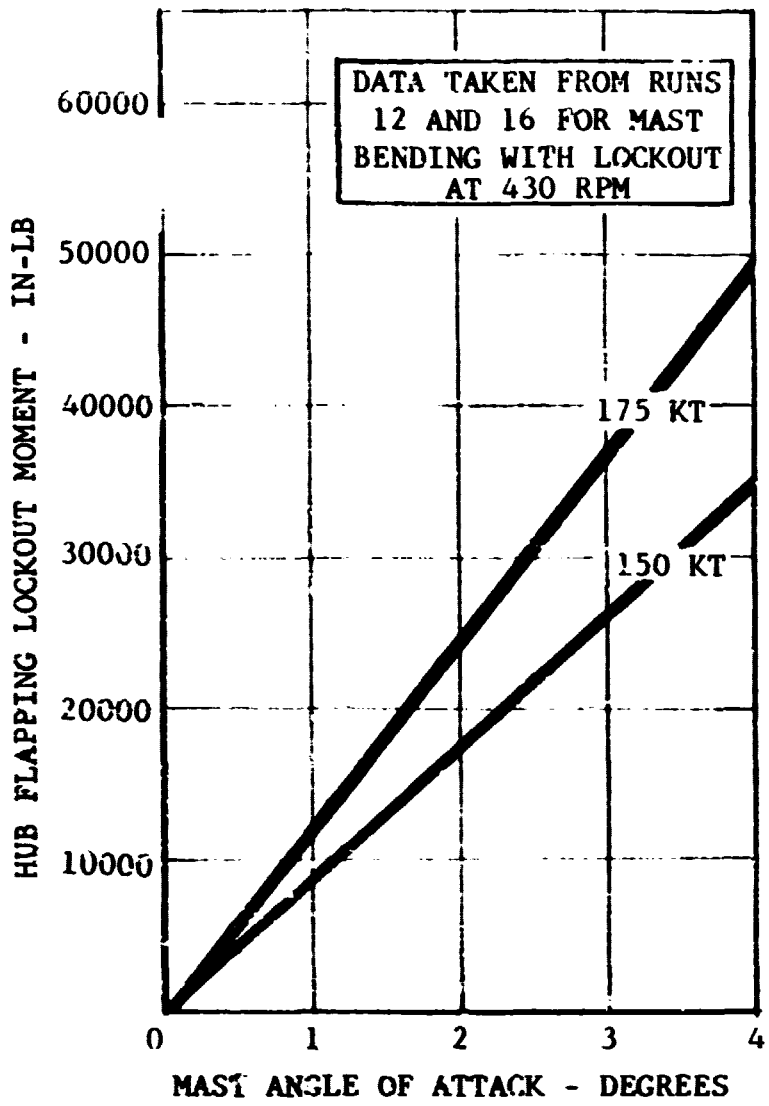


Figure VII-7. Hub Flapping Lockout Moment

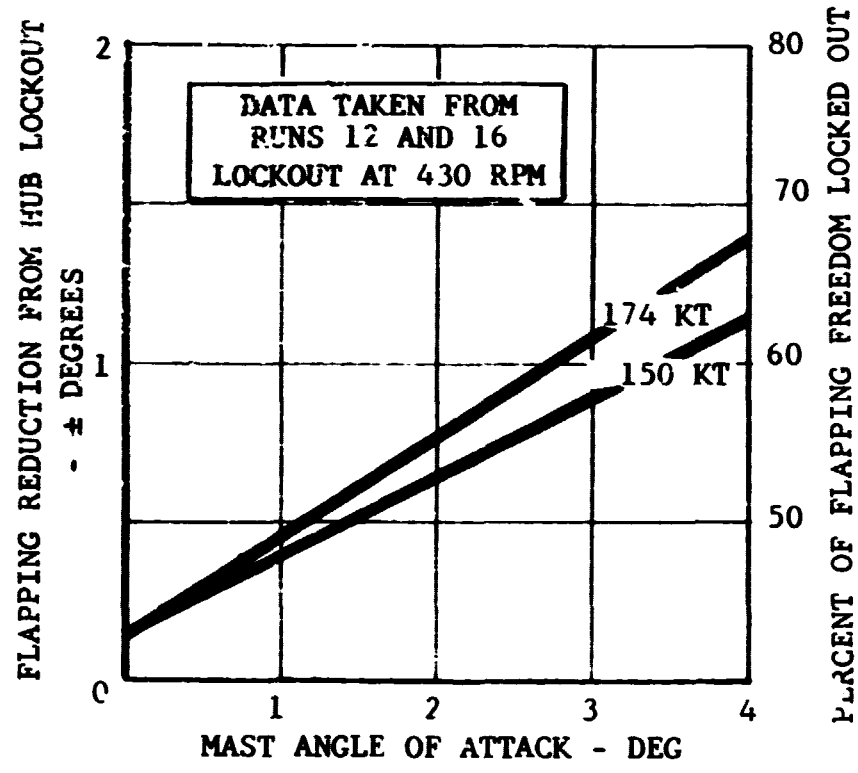


Figure VII-8. Flapping Reduction Caused by Hub Lockout Actuation.

Use or disclosure of data on this page is subject to the restriction on the title page

VIII. RECOMMENDED FUTURE WORK

A. GENERAL

The Model 627 folding proprotor design embodied many new concepts which were initially evaluated during this wind-tunnel test. The majority of the systems performed well and appear directly applicable to a research vehicle. Some systems have not been adequately evaluated or have shown undesirable characteristics which need improvement for flight. These are the systems which need further redesign work or further testing.

It is recommended that following the suggested additional tests and design improvements listed in the following paragraphs, the next phase in the future work be a preflight ground test program. This program could be conducted with flightworthy rotors installed on a research flight vehicle, or on a winged propulsion system for wind-tunnel tests to assure orderly progress into research flight.

B. FULL-SCALE LIFT AND DRAG INVESTIGATION

Since the Model 627 folding proprotor was designed for a dynamic wind-tunnel investigation, minimum attention was paid to aerodynamic considerations. For this reason, no blade root cuffs were provided.

It is recommended that the Model 627 folding proprotor fold hinge area and nacelle pod be improved aerodynamically, and that lift and drag wind-tunnel tests on the dynamic wing stand be conducted. The rotor blade roots should incorporate a flight-type cuff fairing with afterbody similar to the design depicted in Reference 2, Figure IV-70. This would provide full-scale data to predict more accurately the performance of a research aircraft.

C. AUTOMATIC CONVERSION SEQUENCE CONTROL

In Section III of this report the full conversion sequence of a folding proprotor aircraft is described. Since the folding proprotor requires many more sequence steps than the proprotor, it is important to investigate an automatic sequence control through design and manufacture of a prototype unit which could be applied to a model or a full-size rotor such as the Model 627.

D. ROTOR FATIGUE EVALUATION

For the wind-tunnel evaluation of the Model 627 folding proprotor, the loads for the fold hinge lugs during stopping and starting were limited to the 3.0-hour fatigue life load. This limit was established conservatively from contractor and other fatigue test data of a standard lug without clamp up or anti-fretting protection and with a stress concentration factor equal to 2.5 and a 25 percent reduction. For this test load condition, the oscillatory endurance limit is critical rather than static strength.

It is recommended that this test criterion be evaluated by a fatigue test to describe an actual fatigue strength S-N curve of the Model 627 hub and blade with complete fold mechanism. This is advisable to establish a reasonable criterion for research flight which is completely safe and yet does not penalize the rotor with additional weight at the blade root. This test could

Use or disclosure of data on this page is subject to the restriction on the title page.

be accomplished in the following manner. The test specimen would be set up within a lab test fixture to apply beam, chord, torsion, and centrifugal loads in directions to simulate design flight loads with each of the three blades receiving a different load level to failure. From the load-time data point for each blade fold joint, an S-N curve could be described to determine a reasonable fatigue life for the Model 627 blade and fold joint. This recommended fatigue test can probably be accomplished on the existing Model 627 test hardware since the cycle count indicates that less than one percent of the fatigue life was expended during the wind-tunnel test.

Since a test of this type results in structural failure, it is recommended this test be run after all other possible programs with the existing Model 627 hardware are complete.

E. DESIGN IMPROVEMENT OF FOLDING PROPROTOR FOR FLIGHT

1. Elimination of Hydraulics from Rotating System

The Model 627 wind-tunnel test design criterion required that the Model 300 control system be retained for cost and engineering hour economy purposes. With this control system, space did not exist to bring mechanical power into the rotating system for folding and pitch locking. Hydraulic power was employed through a hydraulic slip ring into the rotating system of the rotor for this purpose.

The use of a hydraulic slip ring and high pressure lines on the rotor hub is not considered an optimum flight service life design. During the wind-tunnel test, the hydraulic slip ring developed a major leak at the rear face seal which required teardown and seal replacement.

It is recommended, therefore, that the hydraulic system on the rotor be eliminated in favor of an all-mechanical drive through the mast from a hydraulic power system in the nonrotating pylon. An initial predesign layout of this system indicates a mechanical system to be feasible and desirable for a flight rotor. An emergency fold power system should also be investigated as part of this predesign which would restore the rotor to the proprotor mode in event of aircraft hydraulic failure. An alternate to this could be a complete dual hydraulic power system. The redesigned system should be evaluated during the recommended preflight research ground-test program.

2. Full-Collective Pitch Range

In Section V, Paragraph A.3, the Model 627 full collective pitch range mechanism for flight was discussed. This was a planetary gear system in the root of the blades and was evaluated during the contractor whirl test and found to possess undesirable characteristics. Since the basic rotor control system without the planetary system provided adequate control range for the wind-tunnel test, this mechanism was locked out.

It is recommended that a new mechanism or control system for flight collective pitch range be designed, manufactured, and evaluated by a whirl test prior to incorporating into the suggested preflight research ground-test program.

Use or disclosure of data on this page is subject to the restriction on the title page

3. Mast Index and Lock

This system, which is described in Section V, paragraph A.8, locked the mast without good low rpm control since only collective was used to control rpm. This resulted in excessive rotational energy absorbed at the instant of lockout which excited the first wing beam natural frequency. Using collective for low rpm index control was more difficult than anticipated due to the wing/rotor interference effect causing the rotor to slow down and then speed up three times each revolution at each blade passage. This is shown in Figure VII-2 from an actual low rpm test run.

It is recommended that this system be improved to incorporate an index rpm control motor or a rotor azimuth-collective feedback system which would control speed during indexing to two to three rpm without fluctuation. This would provide a smoother engagement of the lock without the mast torsional jolt experienced during the wind-tunnel test. Also, a more positive lock holding device is needed so inadvertent unlock is not possible regardless of hydraulic pressure. The redesigned system should be evaluated during the preflight research ground-test program recommended previously.

4. Rotor Weight Reduction

Based on the loads and operational characteristics from the wind-tunnel test program, a review of all components of the rotor, controls, and pylon should be made to determine possible weight reductions for the flight hardware. This is primarily in the area of the blade root and grips, the hub spring and hub lockout actuator, and the fold drive system.

IX. REFERENCES

1. Large-Scale Wind-Tunnel Investigation of a Folding Tilt Rotor, NASA Contract NAS2-5461, 18 June 1969.

2. Summary Report - Task I, Preliminary Design Studies NASA Folding Proprotor Program NAS2-5461, Bell Report D272-099-001, 27 April 1970.

3. Advancement of Proprotor Technology, Task II - Wind-Tunnel Test Results, NASA Contractor Report CR 114363, September 1971.

4. DeTore, J. A. and Sambell, K. W., Preliminary Investigation of the Folding Proprotor V/STOL Aircraft, Bell Helicopter Company Report 599-189-900, November 1968.

5. DeTore, J. A. and Gaffey, T. M., The Stopped-Rotor Variant of the Proprotor VTOL Aircraft, presented at the AIAA/AHS, VTOL Conference at Georgia Institute of Technology, February 1969.

6. Fry, B. L. and Schneider, J. L., Design Optimization of Stoppable-Rotor V/STOL Aircraft Systems, presented at the National Aerospace-Electronics Conference, Dayton, Ohio, May 1969.

7. Vibration in V/STOL Aircraft, Air Force Systems Command Contract F33615-69-C-1339, 1 February 1969.

8. Stability and Control Prediction Methods for Stopped Rotor Aircraft, Air Force Systems Command Contract F33615-69-C-1121, 15 December 1968.

9. Wing/Rotor Aerodynamic Interference, Air Force Systems Command Contract F33615-70-C-1133, 3 November 1969.

10. Design Studies of Folding Proprotor VTOL Aircraft (USAF Contract F33615-69-C-1578), Bell Helicopter Company Interim Report D270-099-001, October 1969.

11. Yen, Dr. Jing G., et al, A Study of Folding Proprotor VTOL Dynamics, AFFDL-TR-71-7, September 1971.

12. DeTore, J. A., Lift/Propulsion System Size-Selection Considerations for Stoppable Rotor VTOL Aircraft, presented at the Air Force V/STOL Technology and Planning Conference, Las Vegas, Nevada, September 23-25, 1969.

13. Design Studies and Model Tests of the Stoppable Rotor Concept (Program Definition Report, Phase II), USAF Contract F33615-69-C-1578, Bell Helicopter Company Interim Report 299-099-464.

14. Summary of Design Studies and Results of Model Tests of the Folding Proprotor Aircraft Concept, Bell Helicopter Company Report D270-099-003,

15. Advancement of Proprotor Technology Task I - Design Study Summary, NASA Contractor Report CR 114363, September 1969.

Use or disclosure of data on this page is subject to the restriction on the title page

IX. REFERENCES - Concluded

16. Advancement of Proprotor Technology, NASA Contract NAS2-5386, 7 May 1969.

17. Sambell, K. W. and Smith, M. E., Performance Analysis of the D272B Folding Proprotor, Bell Helicopter Company Report 599-189-042, November 1970.

18. Parks, D. L. and Synder, F. W., Human Reaction to Low Frequency Vibration, The Boeing Company, Wichita Division, Document D3-3512-1, July 1961.

Use or disclosure of data on this page is subject to the restriction on the title page.

APPENDIX

LIFT AND DRAG INVESTIGATION

A. GENERAL

During the course of the wind-tunnel test, tunnel balance force data were taken to determine the drag differences between the blades fully folded and the blades fully unfolded but feathered. The model was designed for dynamics investigations and only minor consideration was given to the detailed aerodynamics of the pod or rotor blade grip area. Of particular concern in regard to the rotor was the fact that no cuffs or blade grip fairings were provided for this model. Also, the wing structure is faired, but does not possess the correct aircraft airfoil. In view of these aerodynamic differences between the model and full scale, the lift and drag differences between various configurations can be used, but the absolute values are not considered accurate. It has been recommended in Section VIII, paragraph B, however, that a future wind-tunnel force and moment investigation be performed to properly assess lift, drag, and pitching moment of the full-scale rotor model with flight type grip cuffs and fairings.

A full discussion of the performance gains expected in an operational folding proprotor aircraft based on the D272 configuration with convertible fan-shaft engines is given in Reference 17.

B. LIFT

Lift of the semispan model was determined up to wing stall at 16-18 degrees of turntable angle of attack. It was determined early in the wind-tunnel test that the angle of attack of the turntable and wing, α_W, that resulted in zero rotor flapping and minimum loads occurred at α_W equal to -2 degrees. At this angle of attack the rotor tip path plane is approximately normal to the mast centerline by virtue of the swashplate control rigging.

The data of particular interest from the test is that a lift increase occurs with the blades folded over a pod without blades. Figure 1 shows the lift coefficient (C_L) of the model with respect to angle of attack. The lift and drag test data reduced and plotted by NASA were based on a wing semispan reference area (S_W) equal to 65.8 square feet. (This is the same reference area used for the Model 300 test program of Reference 3). It can be seen from Figure 1 that for an angle of attack of four degrees, the lift coefficient for blades folded is 0.04 greater than for blades removed. An aircraft flying with blades folded at this angle of attack and at 150 knots true airspeed at sea level would have a lift increase of nearly 400 pounds over the same aircraft without stowed blades based on the following expression:

Use or disclosure of data on this page is subject to the restriction on the title page.

$$\text{Lift increase} = \Delta C_L S_W \ \ 1/2\ \rho V^2$$

which with the following values:

$$\Delta C_L = 0.04$$

$$S_W = 131.6\ ft^2$$

$$\rho = 0.00237\ lb\ sec^2/ft^4$$

$$V = 253\ ft/sec$$

yields:

$$\text{Lift increase} = 400\ lb$$

Note: No consideration is given here to blade root cuffs since cuffs are not expected to affect the lift change.

C. DRAG

Drag of the semispan model was determined over the same angle-of-attack range as for lift. For the purpose of this discussion, the drag difference between blades unfolded and blades folded is examined at the point where the lift coefficient is equal to zero. Figure 2 shows a plot of lift coefficient versus drag coefficient (C_D) for various fold angles from blades fully unfolded but feathered to blades fully folded. From Figure 2 it can be seen that at C_L equal 0 the drag coefficient of the rotor and test stand with blades folded is 0.037 less than for the blades fully unfolded; this represents a 35-percent reduction. The 15-degree increments of fold angle show fairly equal increments of drag reduction except that beyond 75 degrees of fold, the drag reduction is very small. Figure 3 shows drag coefficient (C_D) with respect to angle of attack, and it can be seen that for a moderate range of angles of attack (-4 degrees to +4 degrees), the reduction in drag coefficient for the model with blades folded as compared to blades unfolded remains at about 0.037. The increase in drag coefficient for the same angle of attack range for blades folded over blades completely removed is about 0.003.

Based on the same analogy as given in the above paragraph on lift, an aircraft flying with blades folded at a 4-degree angle of attack at a true airspeed of 150 knots at sea level would have a drag decrease of about 370 pounds as compared to the same aircraft with blades unfolded and feathered based on the following expression:

Use or disclosure of data on this page is subject to the restriction on the title page.

$$\text{Drag change} = \Delta C_D S_W \; 1/2 \; \rho V^2$$

which with the following values:

$$\Delta C_D = 0.037$$

$$S_W = 65.8 \times 2_{wings} = 131.6 \text{ ft}^2$$

$$\rho = 0.00237 \text{ lb sec}^2/\text{ft}^4$$

$$V = 253 \text{ ft/sec}$$

yields:

$$\text{Drag change} = -370 \text{ lb}$$

The assessment of drag reduction with folded blades in terms of square feet of frontal area (f) can be shown as follows: Based on the drag coefficient (C_D) change of 0.037, as shown in Figure 2, and the reference wing area for the semispan model of 65.8 square feet, the reduction in frontal area $\Delta f = 0.037 \times 65.8 = 2.44 \times 2_{wings} = 4.88$ square feet for the aircraft.

Use or disclosure of data on this page is subject to the restriction on the title page.

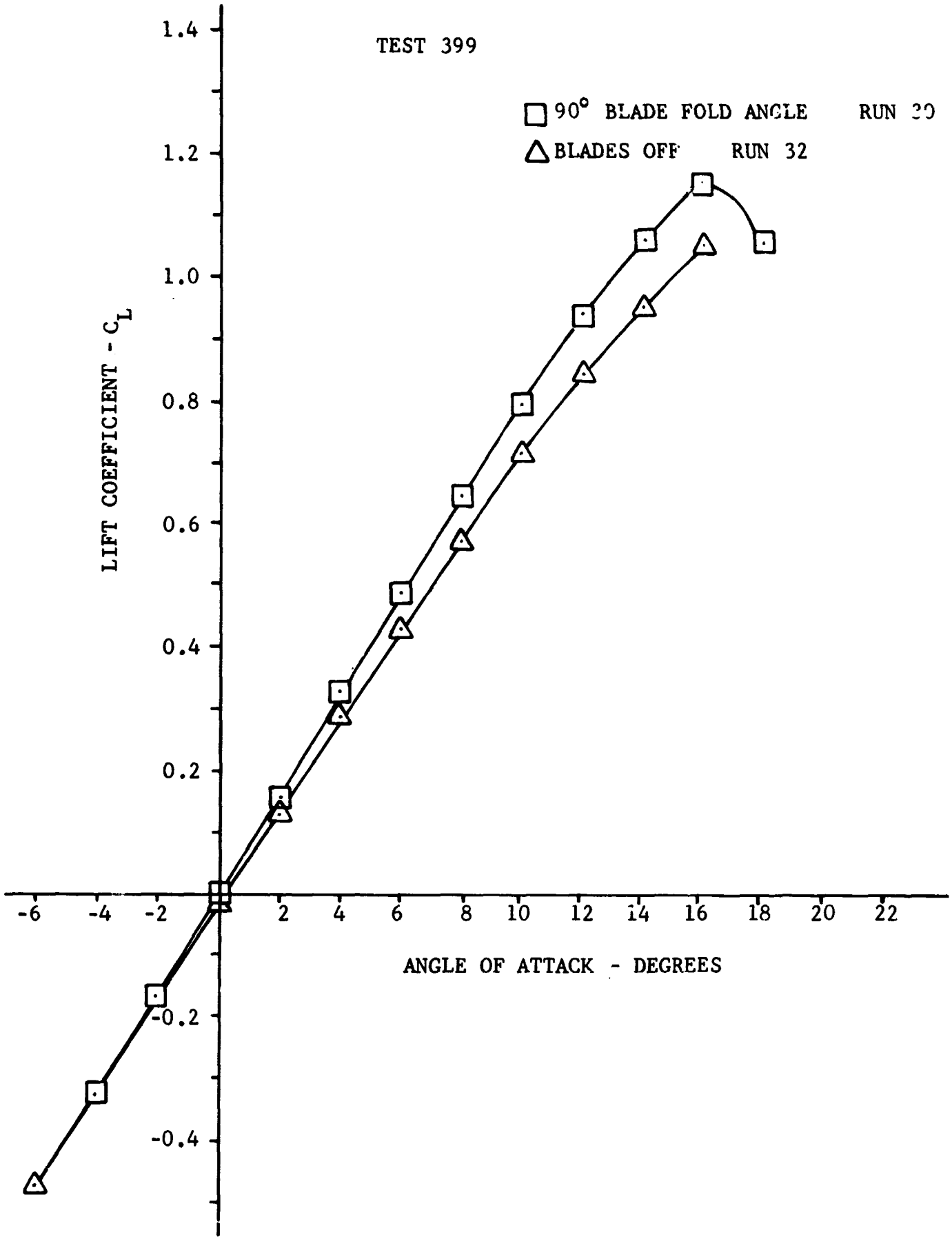


Figure 1. Model 627 Folding Proprotor Lift Coefficient Versus Angle of Attack.

Use or disclosure of data on this page is subject to the restriction on the title page.

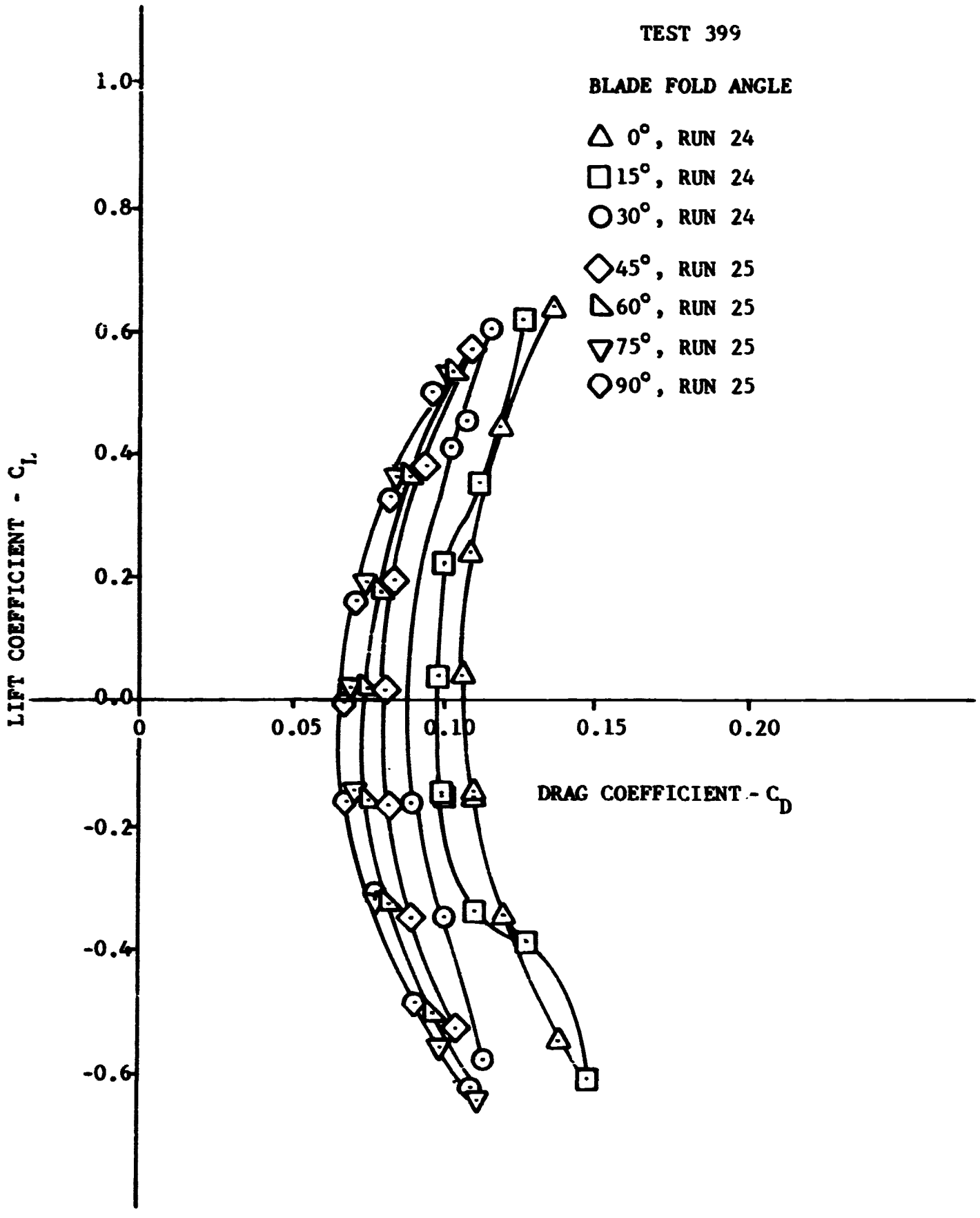


Figure 2. Model 627 Folding Proprotor Lift Versus Drag Coefficient at Various Fold Angles.

c-4

Use or disclosure of data on this page is subject to the restriction on the title page.

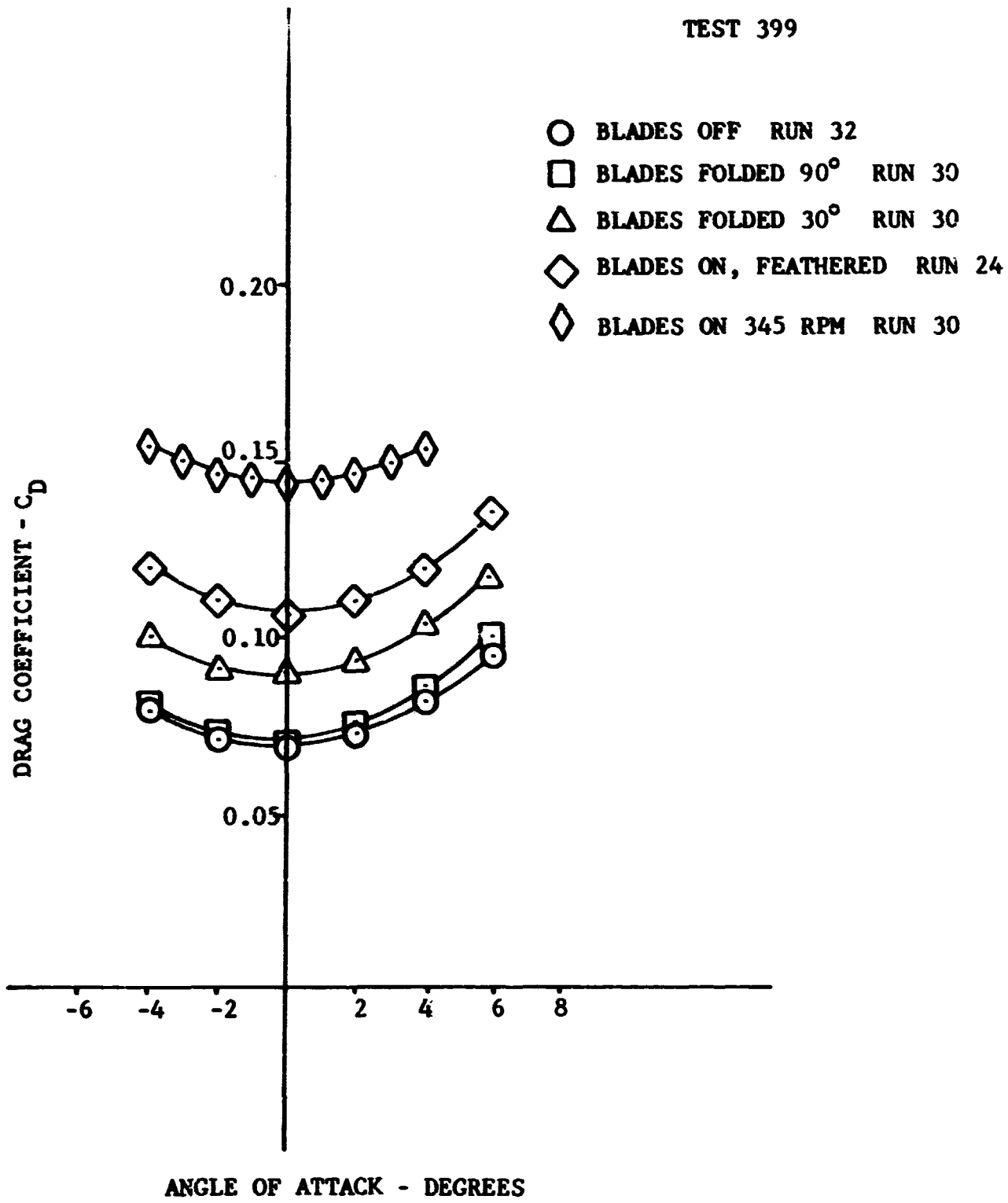


Figure 3. Model 627 Folding Proprotor Drag Summary.

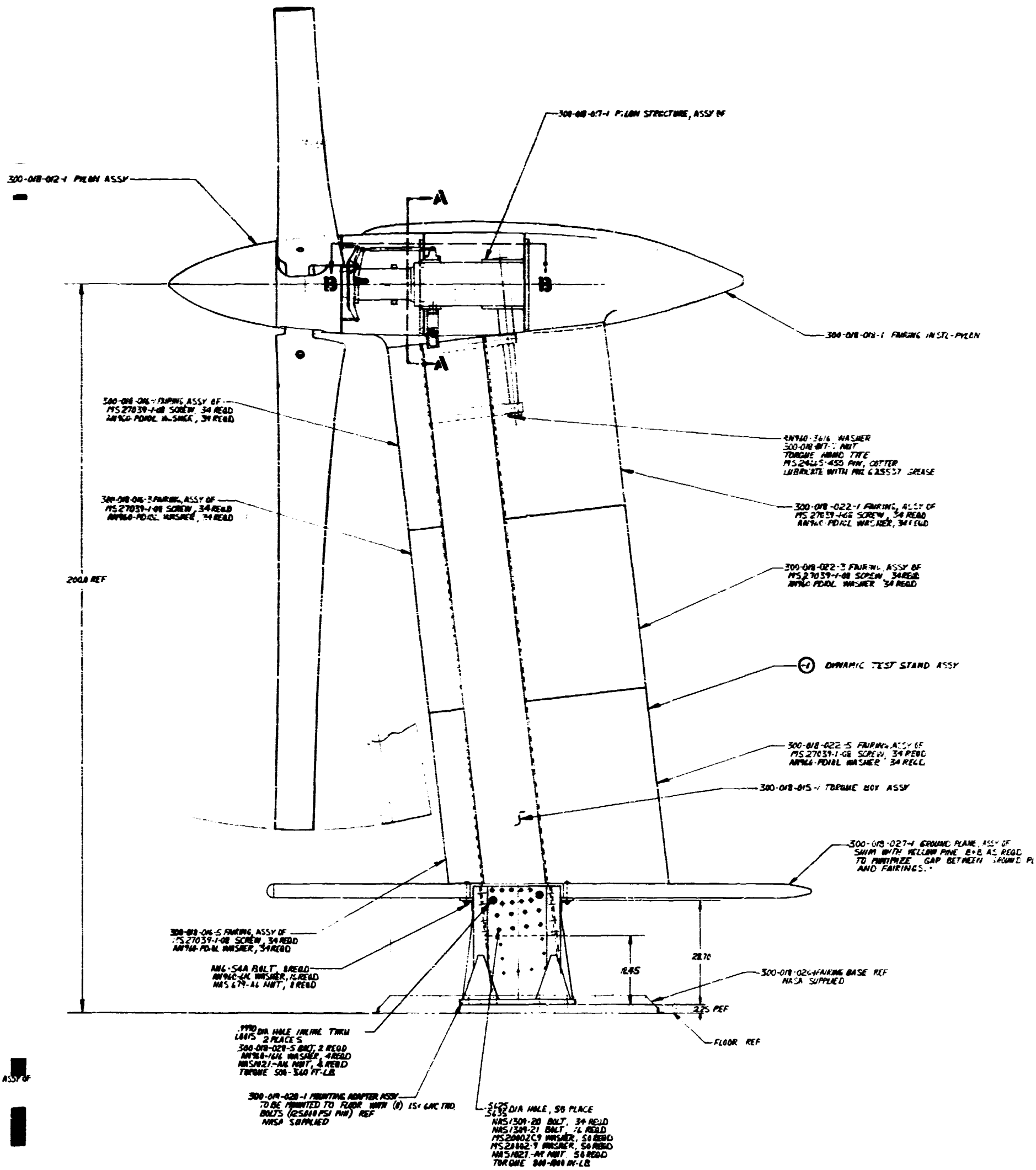
Use or disclosure of data on this page is subject to the restriction on the title page.

DRAWING LIST

DRAWINGS

300-018-014	Dynamic Wing Test Stand
627-018-100	Rotor and Controls Installation
627-010-101	Yoke Assembly
627-018-102	Fold Mechanism
627-018-103	Blade Assembly

REPRODUCIBILITY OF THE ORIGINAL PAGE IS POOR



FOLDOUT FRAME 1

REPRODUCIBILITY OF THE ORIGINAL PAGE IS POOR

DF

300-018-018-1 FAIRING INSTL-PYLON

AN960-3616 WASHER
300-018-017-7 NUT
TORQUE HAND TITE
MS24665-450 PIN, COTTER
LUBRICATE WITH MIL G25537 GREASE

300-018-022-1 FAIRING, ASSY OF
MS 27039-1-08 SCREW, 34 REQD
AN960-PD8L WASHER, 34 REQD

300-018-022-3 FAIRING, ASSY OF
MS 27039-1-08 SCREW, 34 REQD
AN960-PD8L WASHER 34 REQD

(-1) DYNAMIC TEST STAND ASSY

300-018-022-5 FAIRING ASSY OF
MS 27039-1-08 SCREW, 34 REQD
AN960-PD8L WASHER 34 REQD

300-018-015-1 TORQUE BOX ASSY

300-018-027-1 GROUND PLANE, ASSY OF
SHIM WITH YELLOW PINE B+B AS REQD
TO MINIMIZE GAP BETWEEN GROUND PLANE
AND FAIRINGS.*

300-018-026 FAIRING BASE REF
NASA SUPPLIED

REF

FLOOR REF

NOTE:
1. TORQUE PER BPS-FW4018 EXCEPT AS NOTED

300-018-024-1 SPAR ASSY

(-3) DYNAMIC TEST STAND ASSY
1/4 STIFFNESS
SAME AS -1 ASSY EXCEPT AS
SHOWN.

SHIM WITH YELLOW PINE B+B AS
REQD TO MINIMIZE GAP BETWEEN GROUND
PLANE & FAIRINGS.

2.70
5.85
83°45'
83°15'
8.00
300-018-024-7 BEAM
REF

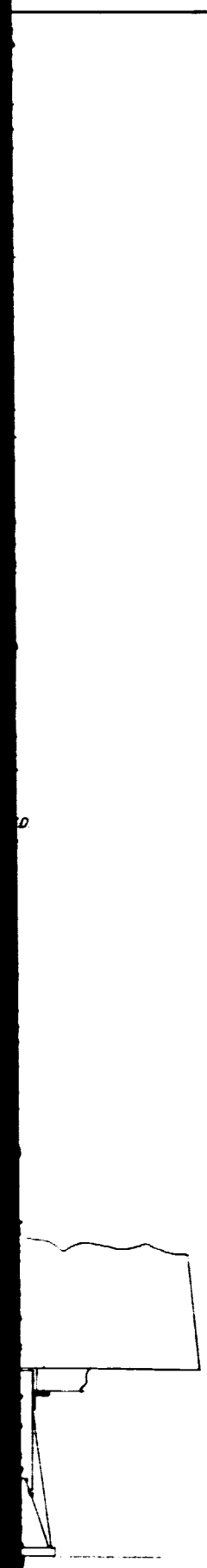
300-018-028-3 BOLT, 12 REQD
MS20002-9 WASHER, 24 REQD
NAS 1021-A9 NUT, 24 REQD
TORQUE 800-1000 IN-LB

300-018-028-5 BOLT, 2 REQD
AN960-1616 WASHER, 4 REQD
NAS 1021-A14 NUT, 4 REQD
TORQUE 500-560 FT-LB

4	4	NAS 1304
2	2	NAS 1306
	16	NAS 1309
	34	NAS 1309
		NAS 1308
		NAS 1305
		NAS 1305-2
4	4	NAS 1021
24	50	NAS 1021
12	13	NAS 1021-A
4	4	NAS 679-A
14	14	NAS 679-A
		NAS 679-A
12	12	NAS 1303
6	6	MS 20002
6	6	MS 20002
204	204	MS 27039
		MS 24665
		MS 24665
2	2	MS 24665
24	50	MS 20002
		MS 20002
18	18	MS 20002
2	2	MS 20002
1	1	MS 17-25
2	2	MS 7825
2	2	SK
1	1	AN3
1	1	AN960
9	9	AN960
4	4	AN960
22	22	AN960
6	6	AN 960
204	204	AN960-PD
6	8	ANL-59A
2	2	NAS 1307
2	2	NAS 1307-2
		300-018
		300-018
		300-018
		300-018
2	2	
12		300-018-02
		300-018-02
		300-018
		300-018
		-02
		300-018-02
		300-018-02
		300-018
		300-018-0
		300-018-02
		300-018-02
		300-018-02
		300-018-02
		300-018-02
-3	1	

FOLDOUT FRAME 2

REPRODUCIBILITY OF THE ORIGINAL PAGE IS POOR



1	4	NAS 1306-23	BOLT
2	2	NAS 1306-25	BOLT
	14	NAS 1309-21	BOLT
	34	NAS 1309-20	BOLT
	1	NAS 1308-300	BOLT
1	1	NAS 1305-250	BOLT
1	1	NAS 1305-210	BOLT
4	4	NAS 1021-A16	NUT
24	50	NAS 1021 A9	NUT
13	13	NAS 1021-A8	NUT
4	4	NAS 679-A7	NUT
14	14	NAS 679-A6	NUT
2	2	NAS 679-A5	NUT
12	12	NAS 1308-36	BOLT
6	6	MS 20002C7	WASHER
6	6	MS 20002C6	WASHER
204	204	MS 21039-108	SCREW
1	1	MS 24665-450	PIN COTTER
1	1	MS 24665-304	PIN COTTER
2	2	MS 24665-153	PIN COTTER
24	50	MS 20002-9	WASHER
	50	MS 20002C 9	WASHER
18	18	MS 20002C 8	WASHER
2	2	MS 20002C 5	WASHER
1	1	MS 17825-8	NUT
2	2	MS 17825-5	NUT
2	2	AN 175-12A	BOLT
1	1	AN 315-8	NUT
1	1	AN 960-3416	WASHER
19	19	AN 960-616	WASHER
4	4	AN 960-716	WASHER
22	22	AN 960-616	WASHER
6	6	AN 960-516	WASHER
204	204	AN 960-PD10L	WASHER
8	8	AN 6-9A	BOLT
2	2	NAS 1307-36	BOLT
2	2	NAS 1307-27	BOLT
1	1	300-018-020-3	LINK
1	1	-1	LINK
1	1	-9	TUBE ASSY
1	1	-7	LINK ASSY
2	2	-5	BOLT
12		300-018-020-3	BOLT
1	1	300-018-027-1	GROUND PLANE ASSY OF
1		300-018-024-1	SPAR ASSY W/ STIFFNESS
1	1	300-018-022-5	FAIRING ASSY OF
1	1	-022-3	FAIRING ASSY OF
1	1	300-018-022-1	FAIRING ASSY OF
1	1	300-018-020-1	MOUNTING ADAPTER ASSY
1	1	300-018-018-1	FAIRING INSTL PYLON
1	1	-9	BRACKET
1	1	-7	NUT
1	1	300-018-017-1	PYLON STRUCTURE ASSY OF
1	1	-5	FAIRING ASSY
1	1	-3	FAIRING ASSY
1	1	300-018-016-1	FAIRING ASSY
1	1	300-018-015-1	TRUNNION BOX
1	1	300-018-012-1	PYLON ASSY
1	1	300-018-010-5	CYLINDER ASSY (COLLECTIVE)
		-3	DYNAMIC TEST STAND ASSY & INSTALLATION (W/ STIFFNESS)
		300-018-014-1	DYNAMIC TEST STAND ASSY & INSTALLATION
-3	1		

BELL Helicopter CORP. FORT WORTH TEXAS

FABRICATION LAYOUT

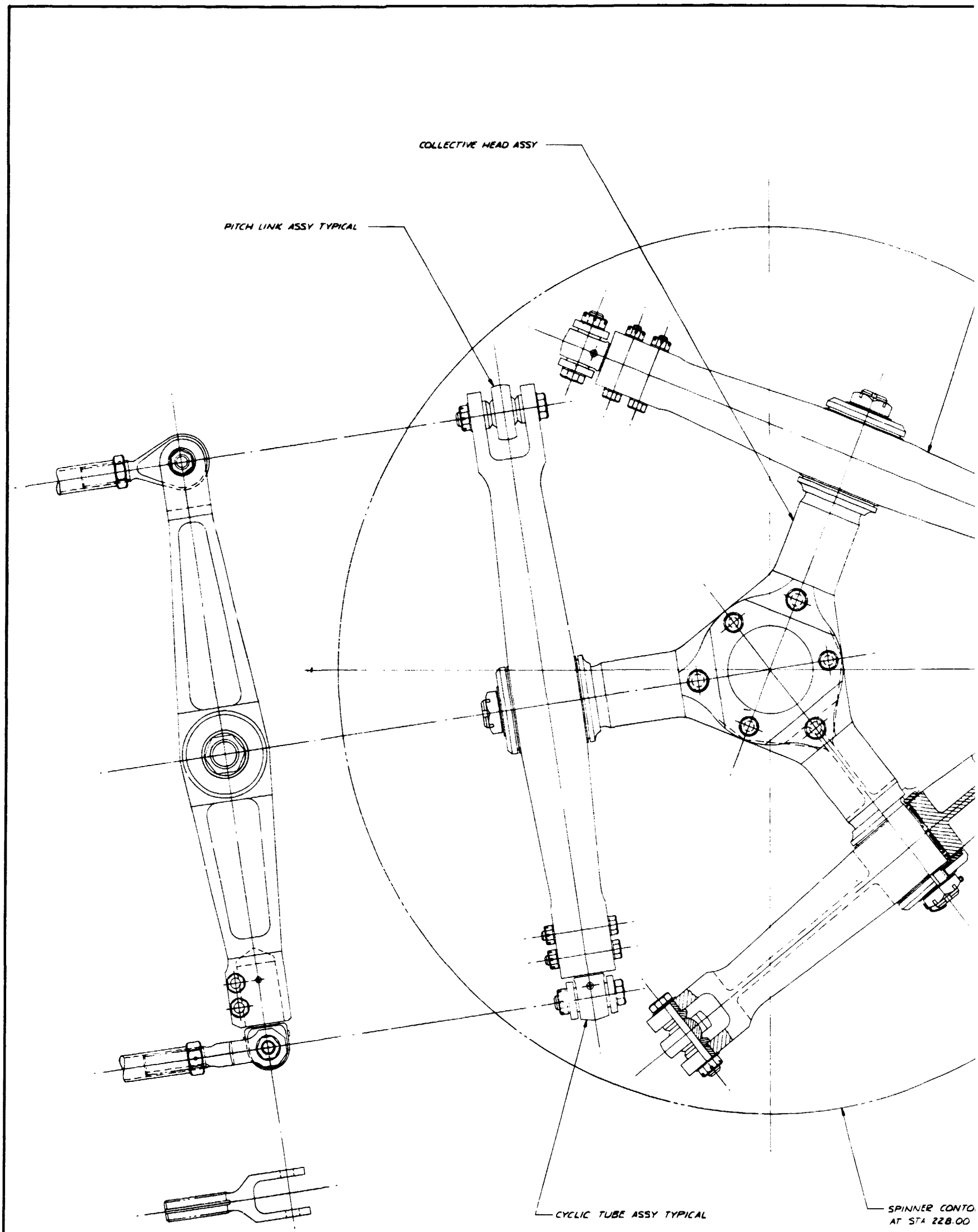
TITLE: DYNAMIC TEST STAND ASSY & INSTALLATION

DESIGNED: SCHELLHASE 12-1-69 | SCALE: 1/10

APPROVED: ACE [illegible] | 300-018-014

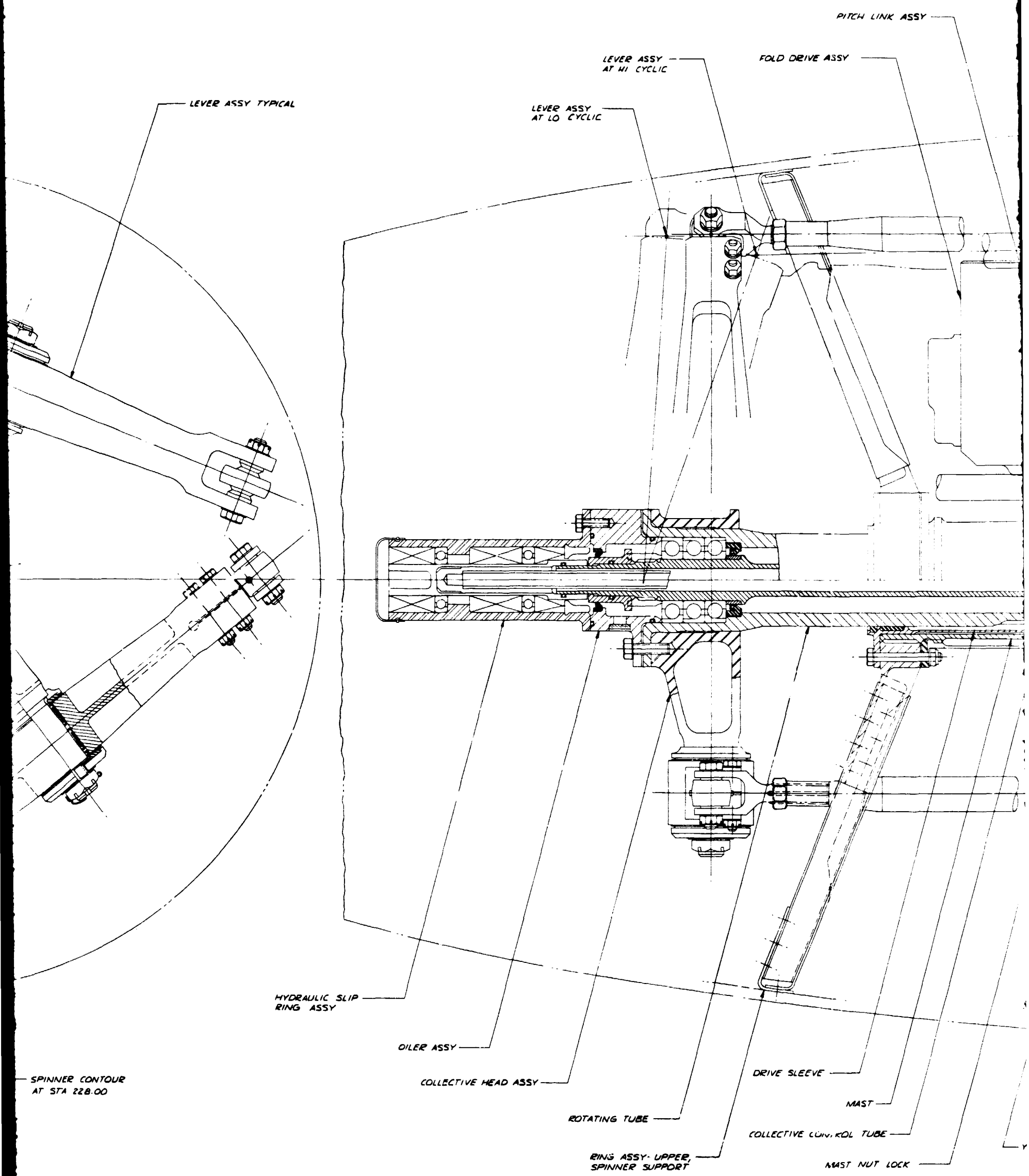
FOLDOUT FRAME 3

REPRODUCIBILITY OF THE ORIGINAL PAGE IS POOR



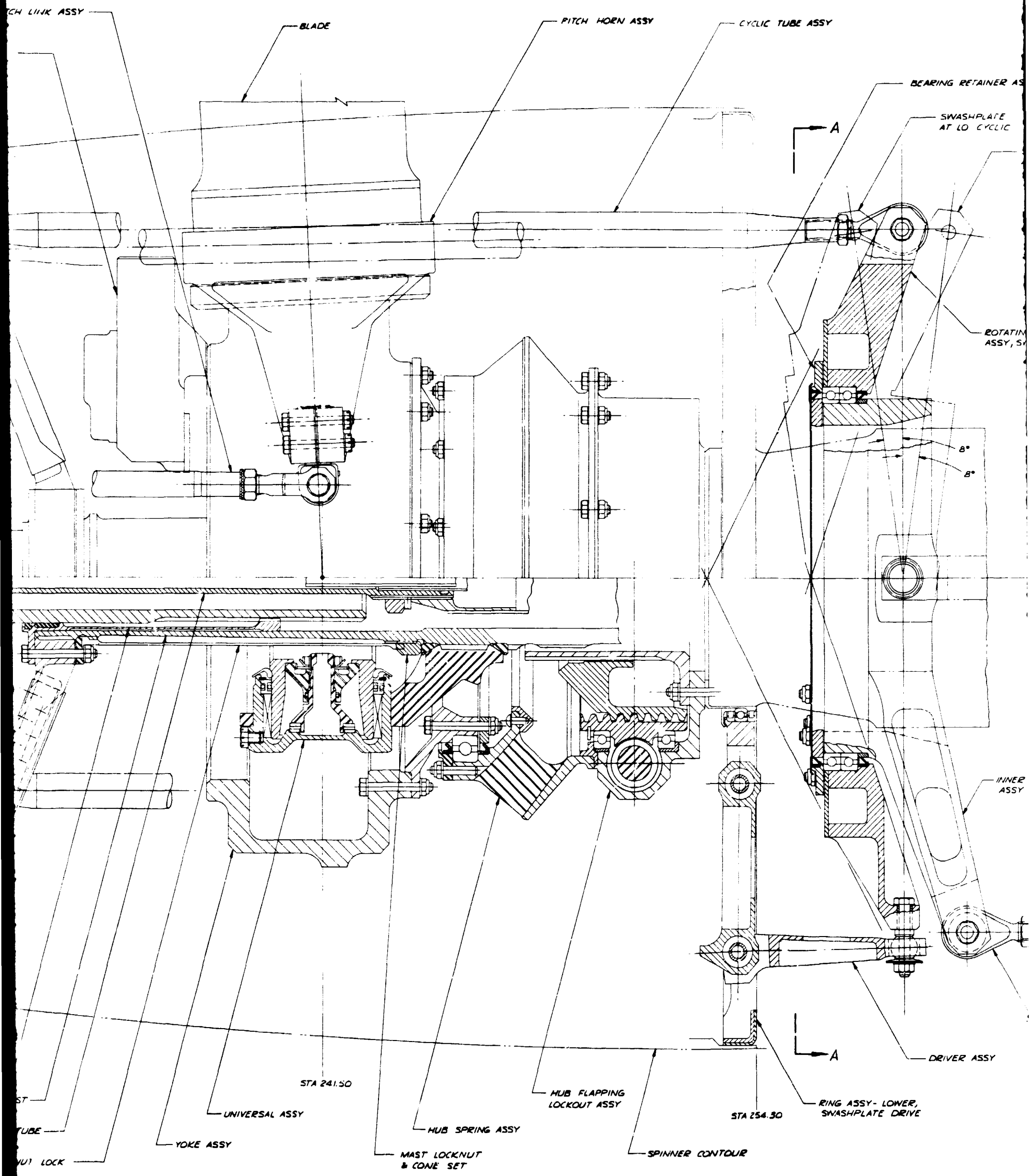
FOLDOUT FRAME

REPRODUCIBILITY OF THE ORIGINAL PAGE IS POOR



FOLDOUT FRAME 2

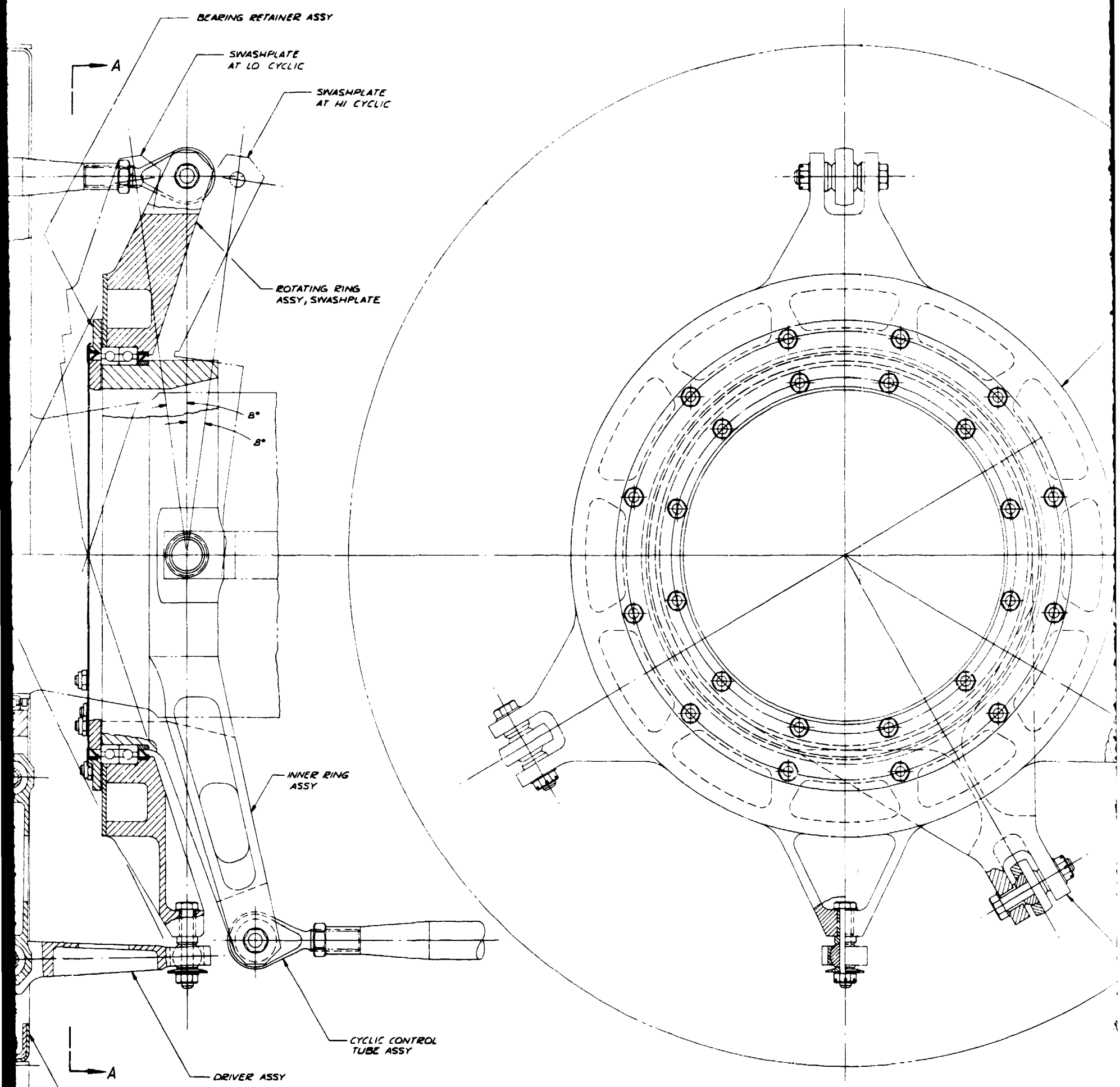
REPRODUCIBILITY OF THE ORIGINAL PAGE IS POOR



FOLDOUT FRAME 3

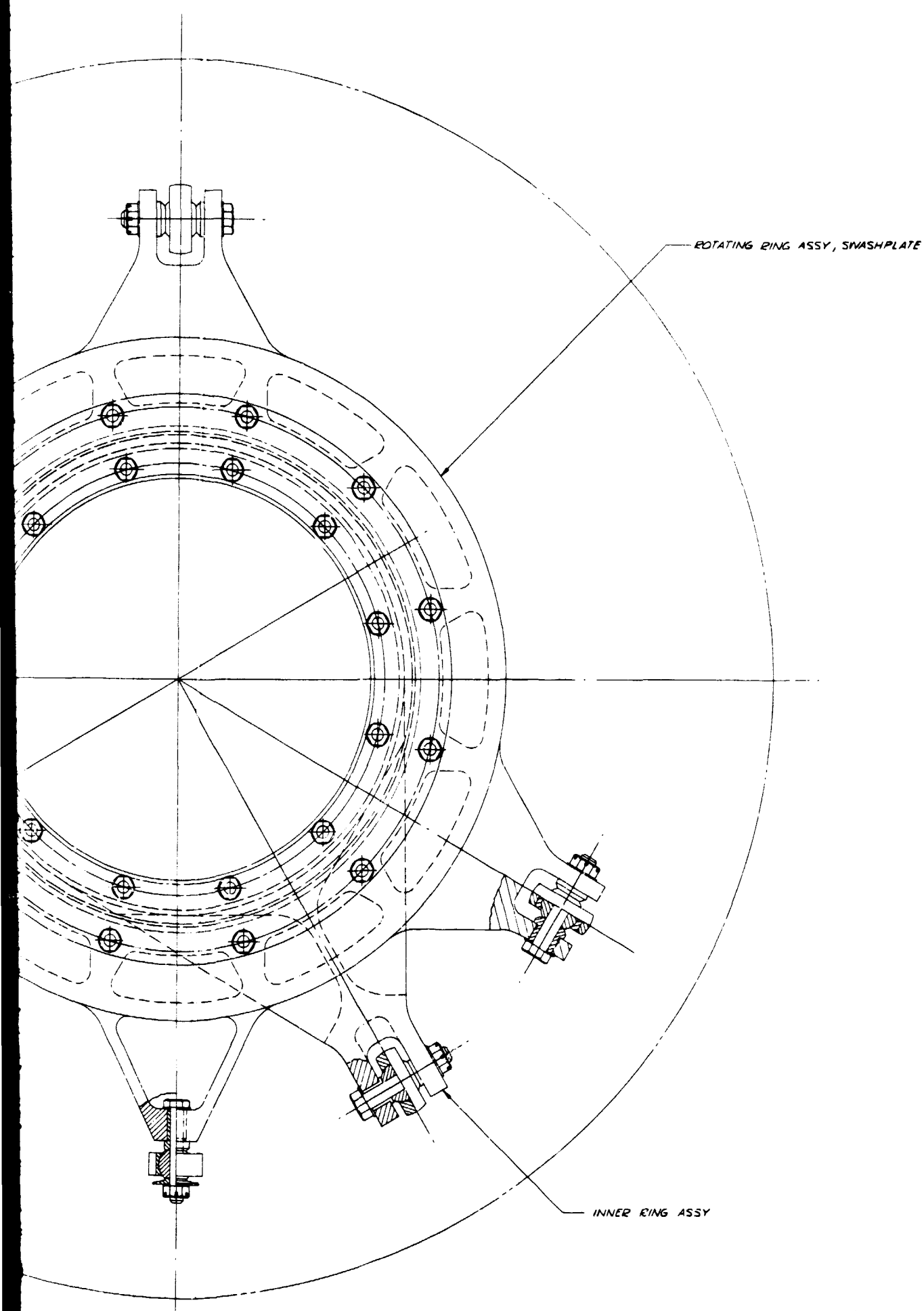
REPRODUCIBILITY OF THE ORIGINAL PAGE IS POOR

CYCLIC TUBE ASSY



FOLDOUT FRAME 4

REPRODUCIBILITY OF THE ORIGINAL PAGE IS POOR



SECTION A-A

NAS 2-5701

DESIGN LAYOUT

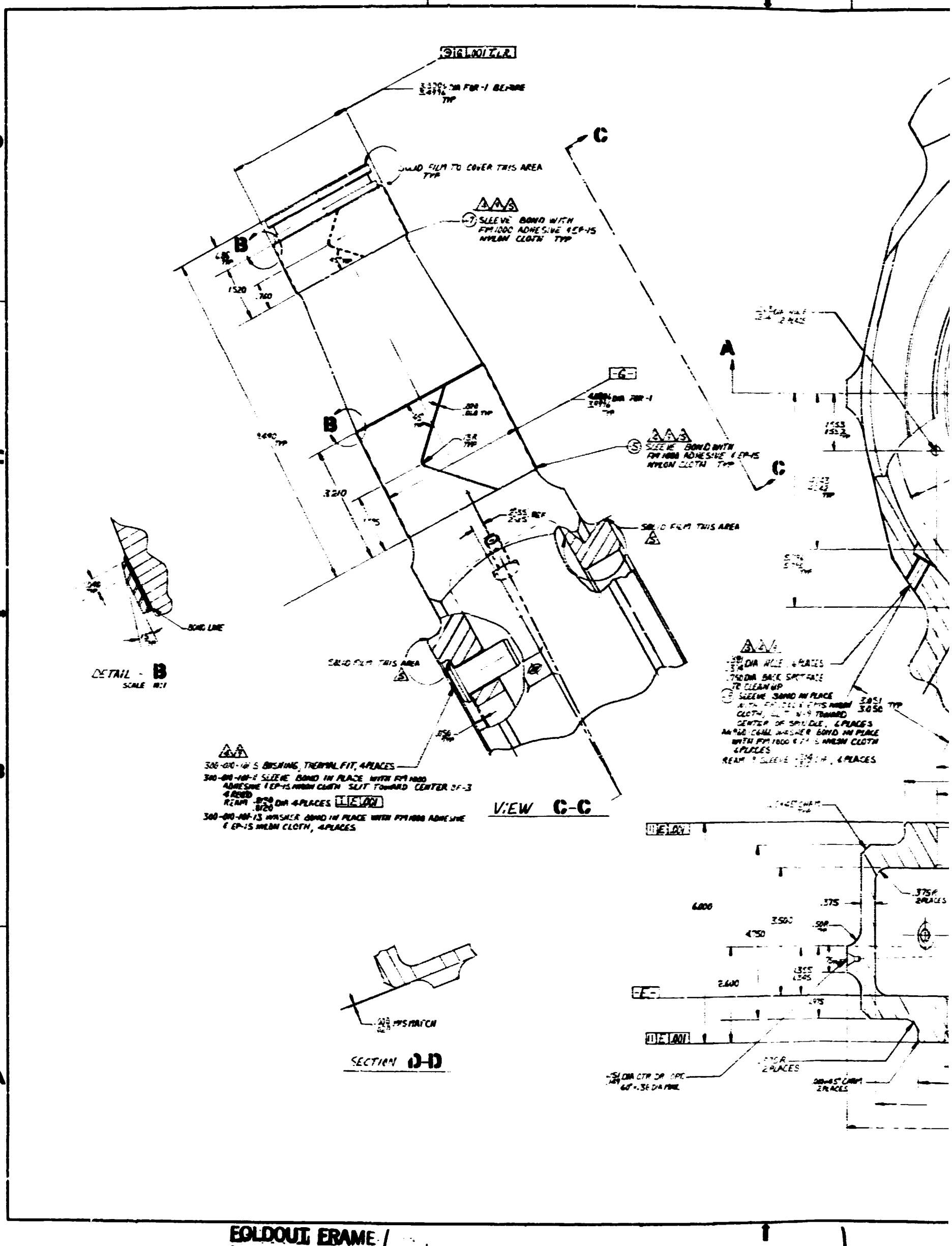
TITLE ROTOR & CONTROLS INSTL-FOLDING PROPROTOR

SIZE 11

627-018-100

FOLDOUT FRAME 5

"REPRODUCIBILITY OF THE ORIGINAL PAGE IS POOR"



FOLDOUT FRAME 1

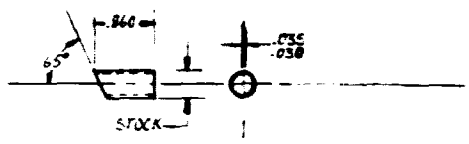
REPRODUCIBILITY OF THE ORIGINAL PAGE IS POOR

SECTION A-A

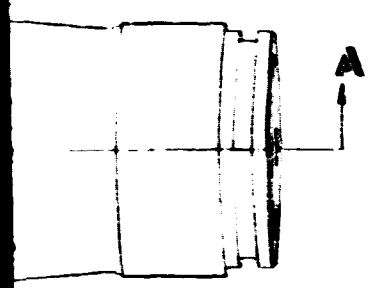
627 - 010 - 101

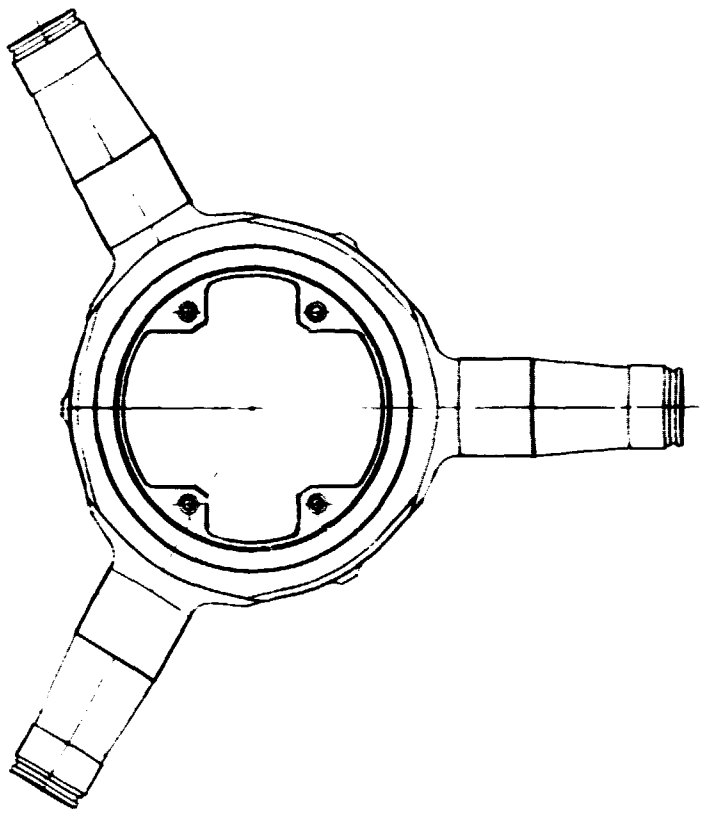
FOLDOUT FRAME 2

REPRODUCIBILITY OF THE ORIGINAL PAGE IS POOR

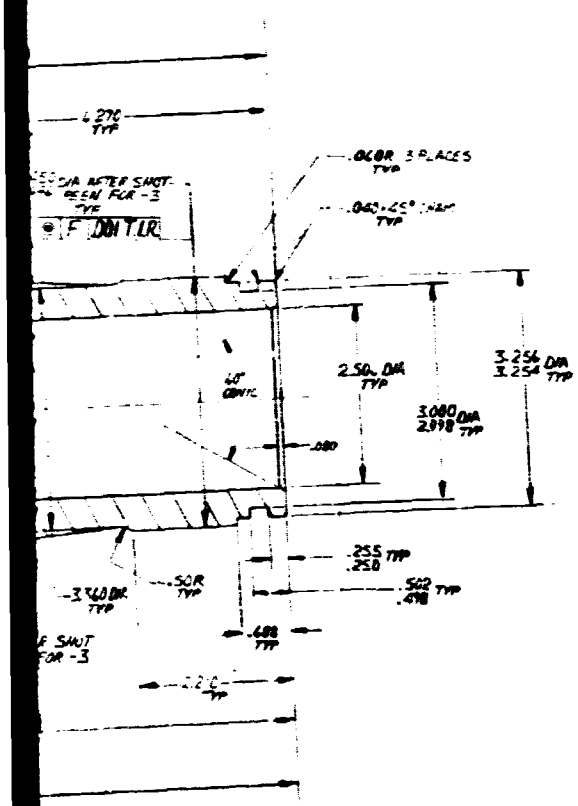


DETAIL - 9 SLEEVE





FULL VIEW - 1 YOKE ASSY
SCALE 1/3



NAS 2-5481

FOLDOUT FRAME 3

REPRODUCIBILITY OF THE ORIGINAL PAGE IS POOR

REVISIONS					REVISIONS					REVISIONS				
ZONE	LTR	DESCRIPTION	DATE	APPROVED	ZONE	LTR	DESCRIPTION	DATE	APPROVED	ZONE	LTR	DESCRIPTION	DATE	APPROVED

11. ASSEMBLY PER BPS FW4012. DO NOT HEAT THE YOKE

10. SOLID FILM LUBRICANT PER BPS FW4310 S4. EXCEPT BAKE 200°F MAX TEMPERATURE

9. PREPARE FOR BONDING PER BPS FW4352 SECTION I PAR 4 METHOD II WET ABRASIVE BLAST OR ACID ETCH PER SECTION V

8. PHOSPHATE FLUORIDE TREATMENT PER BPS FW4352 REF EO FW4352D-4 SECTION VI PARAGRAPHS THRU .015 INCLUSIVE.

7. FLUORESCENT PENETRANT INSPECT PER BPS FW4085

6. SHOT PEEN ALL EXTERNAL SURFACES PER MIL-S-13165 (AUTOMATIC CONTROLS) TO .010-.012 A2 INTENSITY 200% MIN COVERAGE USING S-330 (.033) SHOT. SHOT PEEN ALL INTERNAL SURFACES AS ABOVE USING INTERNAL NOZZLES. AFTER PEENING DECONTAMINATE USING GLASS BEADS PER SPECIFICATION.

5. DURING BAKING OF SOLID FILM LUB -5 & -7 SLEEVES MUST BE STRAPED IN PLACE

4. BOND PER BPS-FW4408.

3. CENTER LINE OF SPINDLE AND HOLES TO BE IN-LINE WITHIN .001.

2. BREAK EDGES .030R OR .030×45° CHAM.

1. MARK PER BPS FW4050 DO NOT STEEL STAMP OR VIBRO ETCH

NOTES:

AR	NARMCO 250	ADHESIVE						
AR	EP-15	NYLON FABRIC						
AR	EM-1000	ADHESIVE						
6	AIRTEC CELL	WASHER						
3	300-010-101-5	WASHER						
4	-13	WASHER						
4	-11	SLEEVE						
4	300-010-101-5	BUSHING						

LAST SECTION LETTER USED

627-010-101

QTY REQD	PART OR IDENTIFYING NO	NOMENCLATURE OR DESCRIPTION	STOCK SIZE	MATERIAL	MATERIAL SPEC			ZONE
6	627-010-101-9	SLEEVE	.375DIA×.035	CRES 321	MIL-T-8808 TM		L	
3	-7	SLEEVE	.040×2.0×1.56	CRES 301	MIL-S-5059 H		L	
3	-5	SLEEVE	.040×3.5×.70	CRES 301	MIL-S-5059 H		L	
1	-3	YOKE AS MACH	627EPM 4	6AL4V TITANIUM	AMS 4928			
-1	627-010-101-1	YOKE ASSY OF						

LIST OF MATERIAL OR PARTS

HC 6164

CONTRACT NUMBER NAS 2-5461

DASH NO	NEXT ASSY	USED ON
-1	627-010-100	627

APPLICATION

RIVET CODE PER NAS 523

HEAT TREAT FINISH SPEC 204-947-402

DRAWN SCHELLHASE 2-70

CHECKED

STRESS W. [illegible] 3-9-70

GROUP ENG COVINGTON 3-19-70

[illegible] 3-9-70

PROJECT W.E. [illegible] 3-18-70

BELL HELICOPTER COMPANY

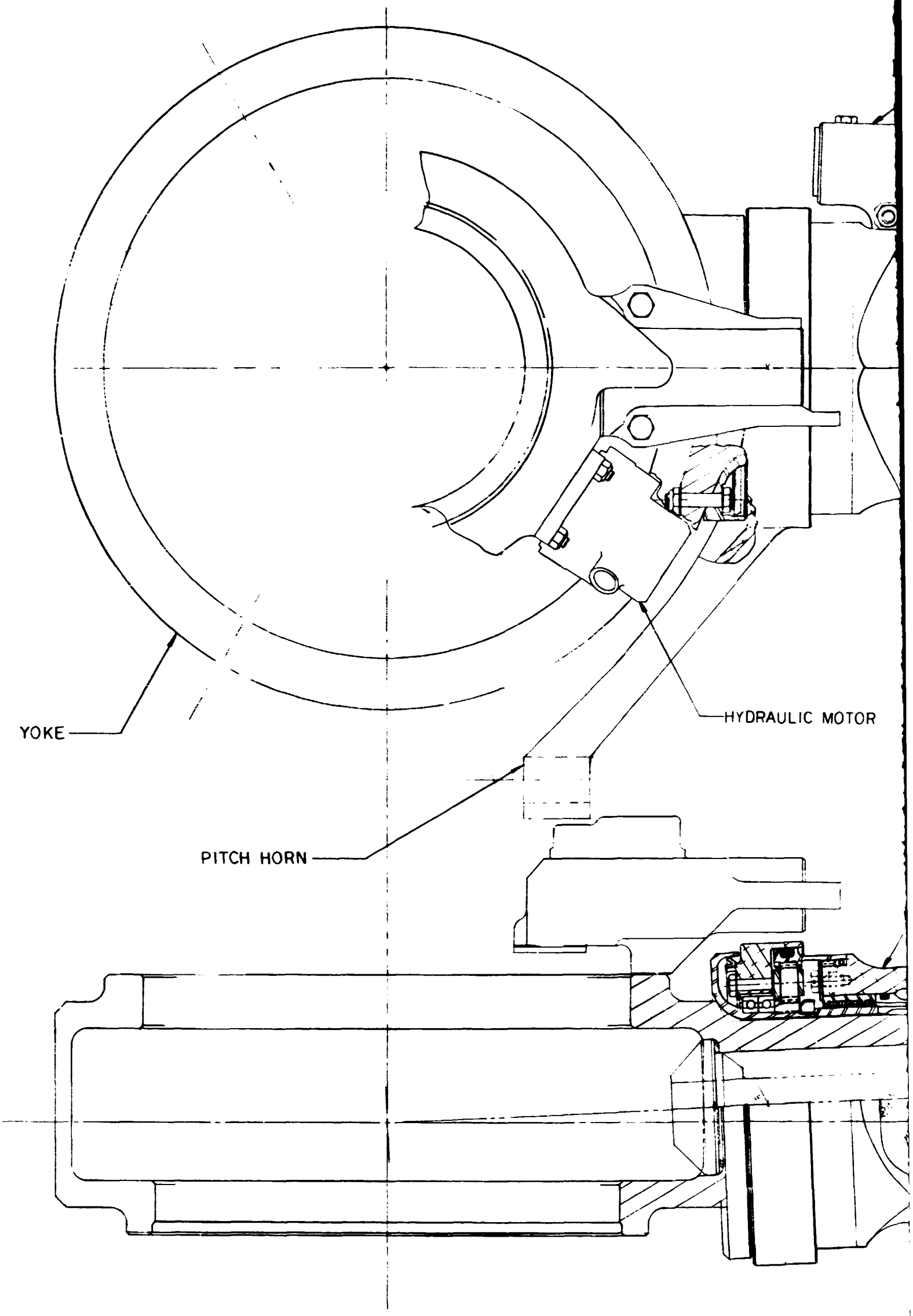
TITLE YOKE ASSY OF FOLDING PROPROTOR

SIZE J8 CODE IDENT NO 97499 DWG NO 627-010-101

SCALE FULL SHEET 1 OF 1

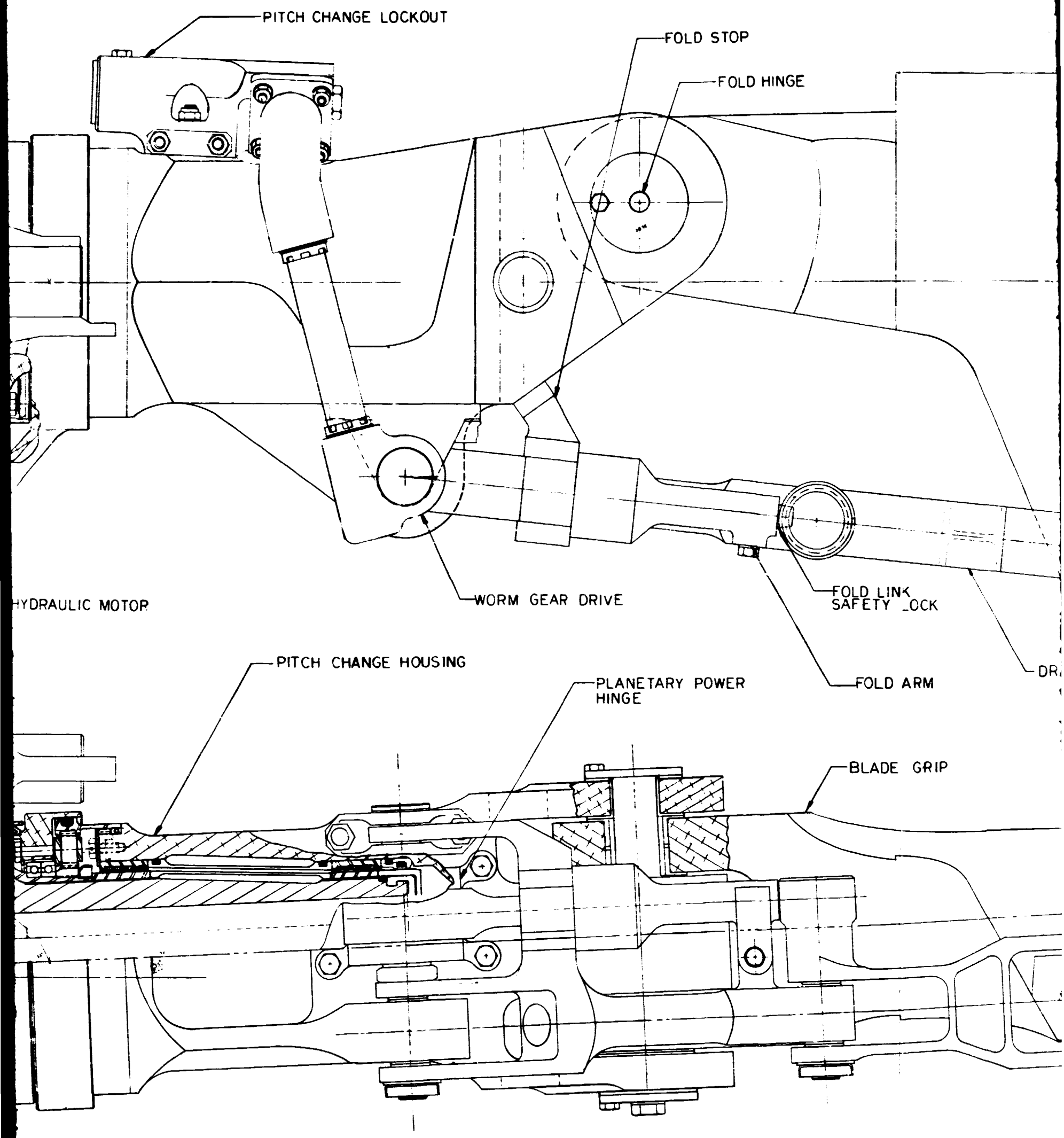
FOLDOUT FRAME 4

REPRODUCIBILITY OF THE ORIGINAL PAGE IS POOR



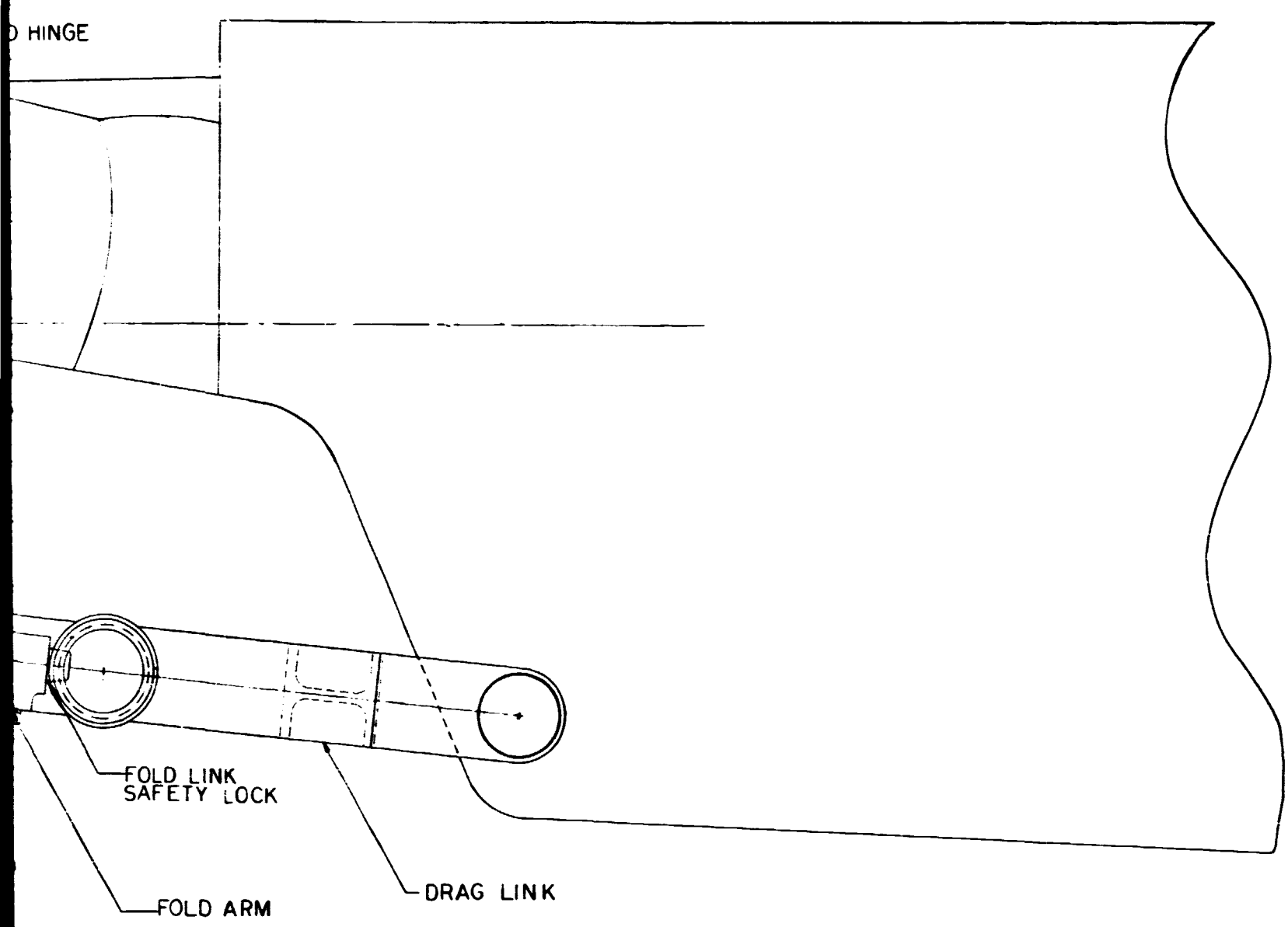
FOLDOUT FRAME

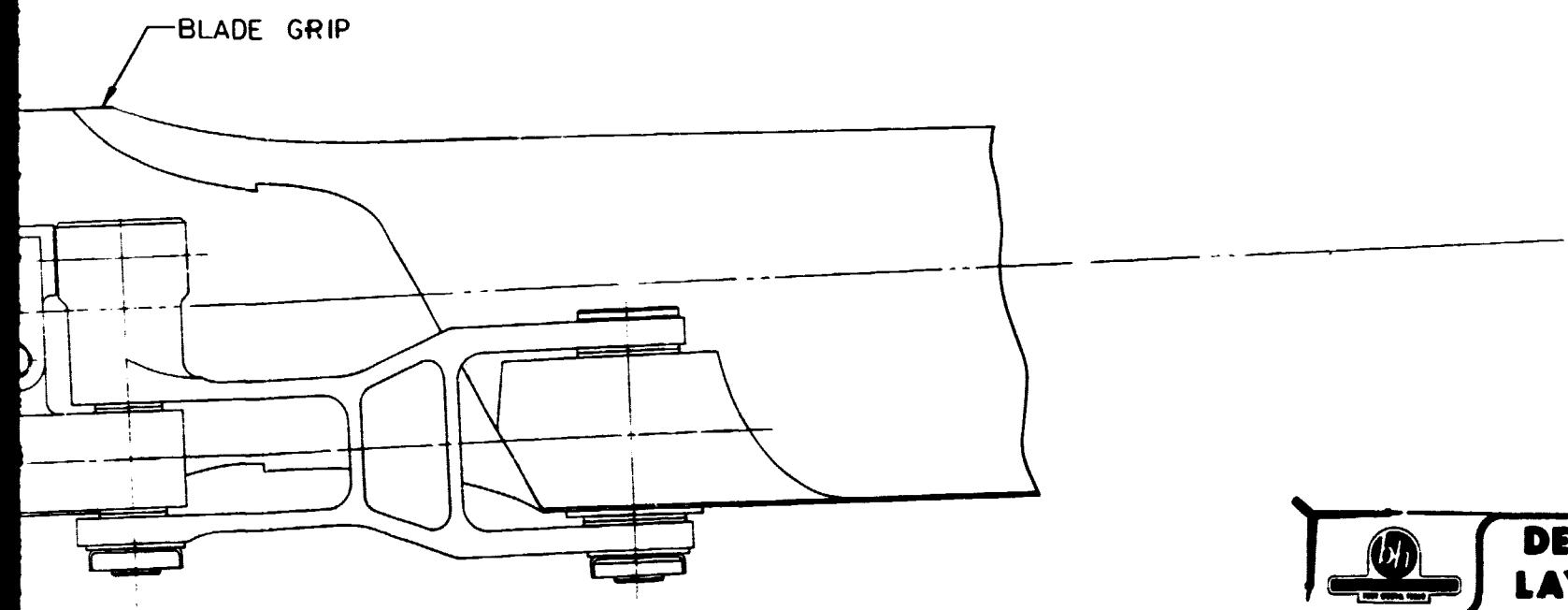
REPRODUCIBILITY OF THE ORIGINAL PAGE IS POOR



FOLD MECHANISM

REPRODUCIBILITY OF THE ORIGINAL PAGE IS POOR





NISM

NAS 2-5461

DESIGN LAYOUT

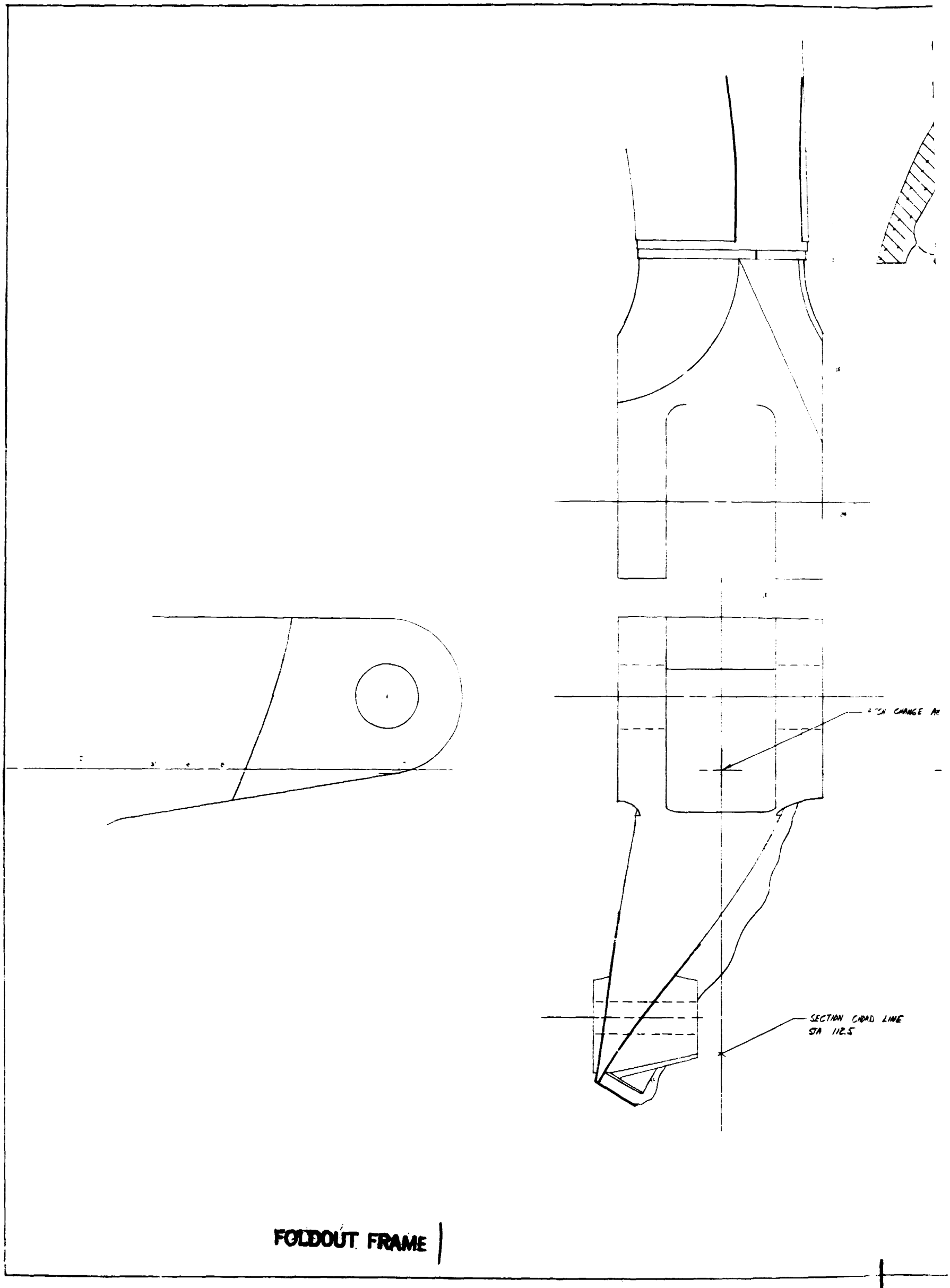
TITLE: FOLD MECHANISM UNFOLDED LOCK POSITION

N. WHITE | 2-24-71 | SCALE 1/1

627-018-102

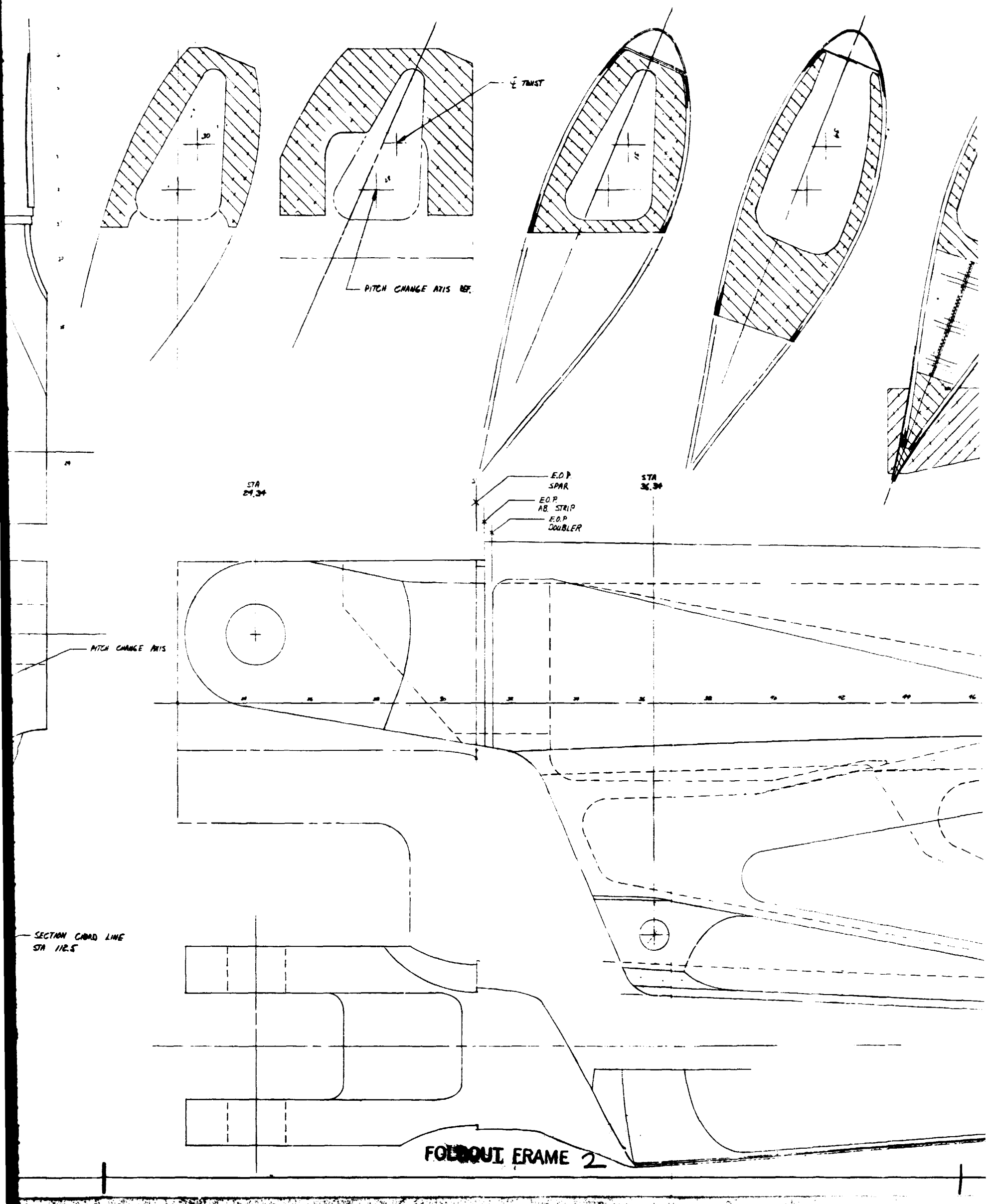
FOLDOUT FRAME 3

REPRODUCIBILITY OF THE ORIGINAL PAGE IS POOR



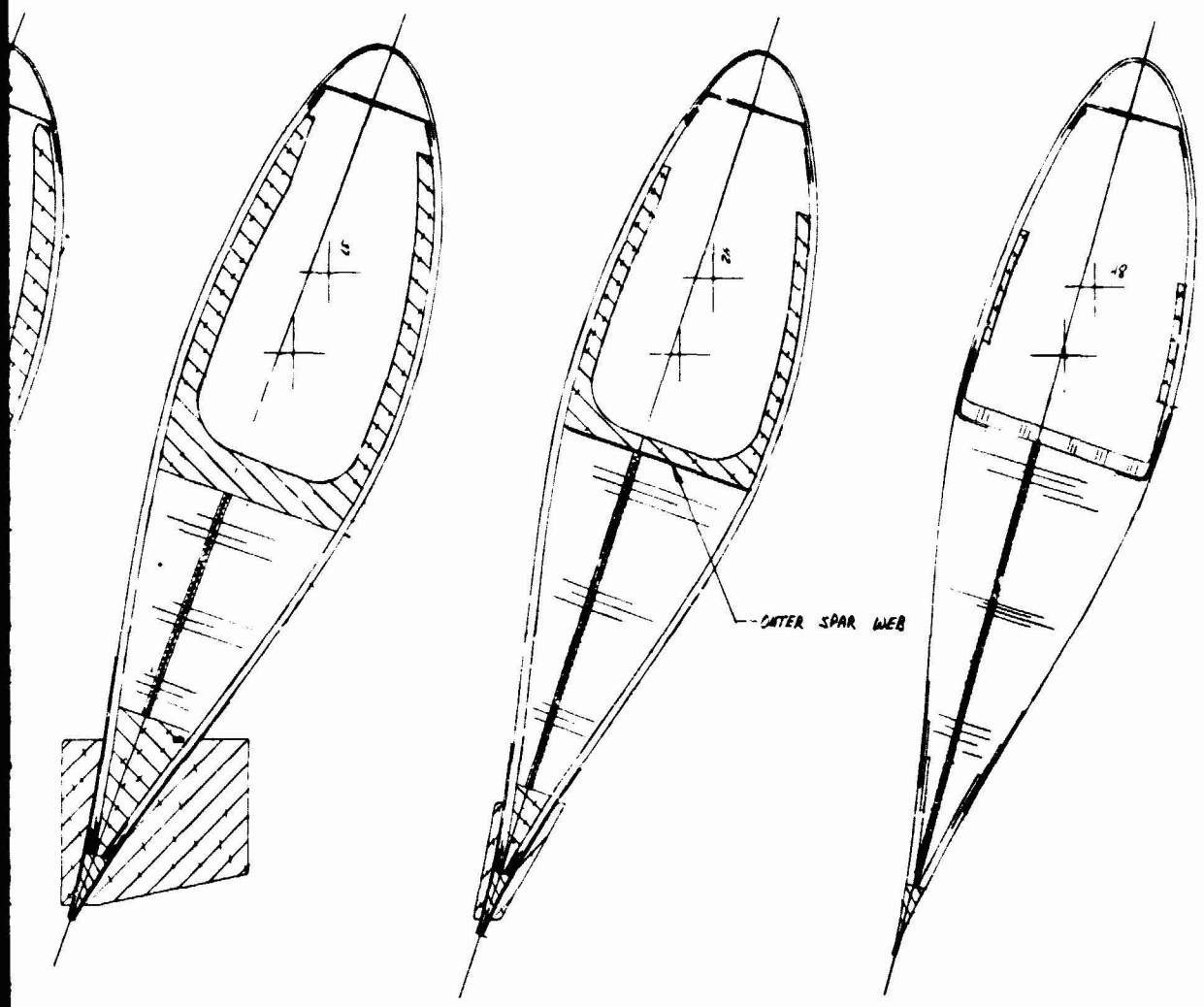
FOLDOUT FRAME

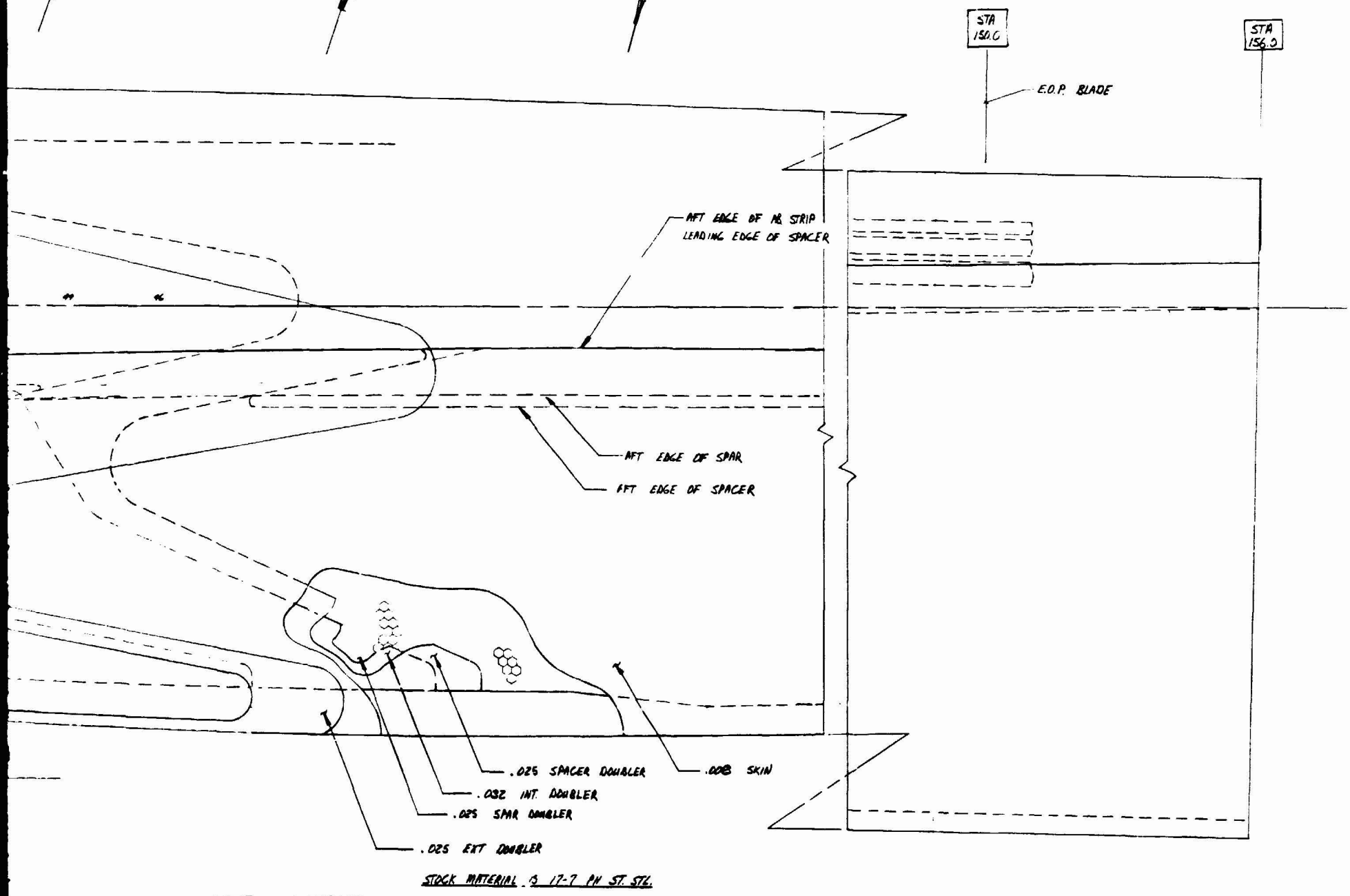
REPRODUCIBILITY OF THE ORIGINAL PAGE IS POOR



FOLDOUT FRAME 2

REPRODUCIBILITY OF THE ORIGINAL PAGE IS POOR.

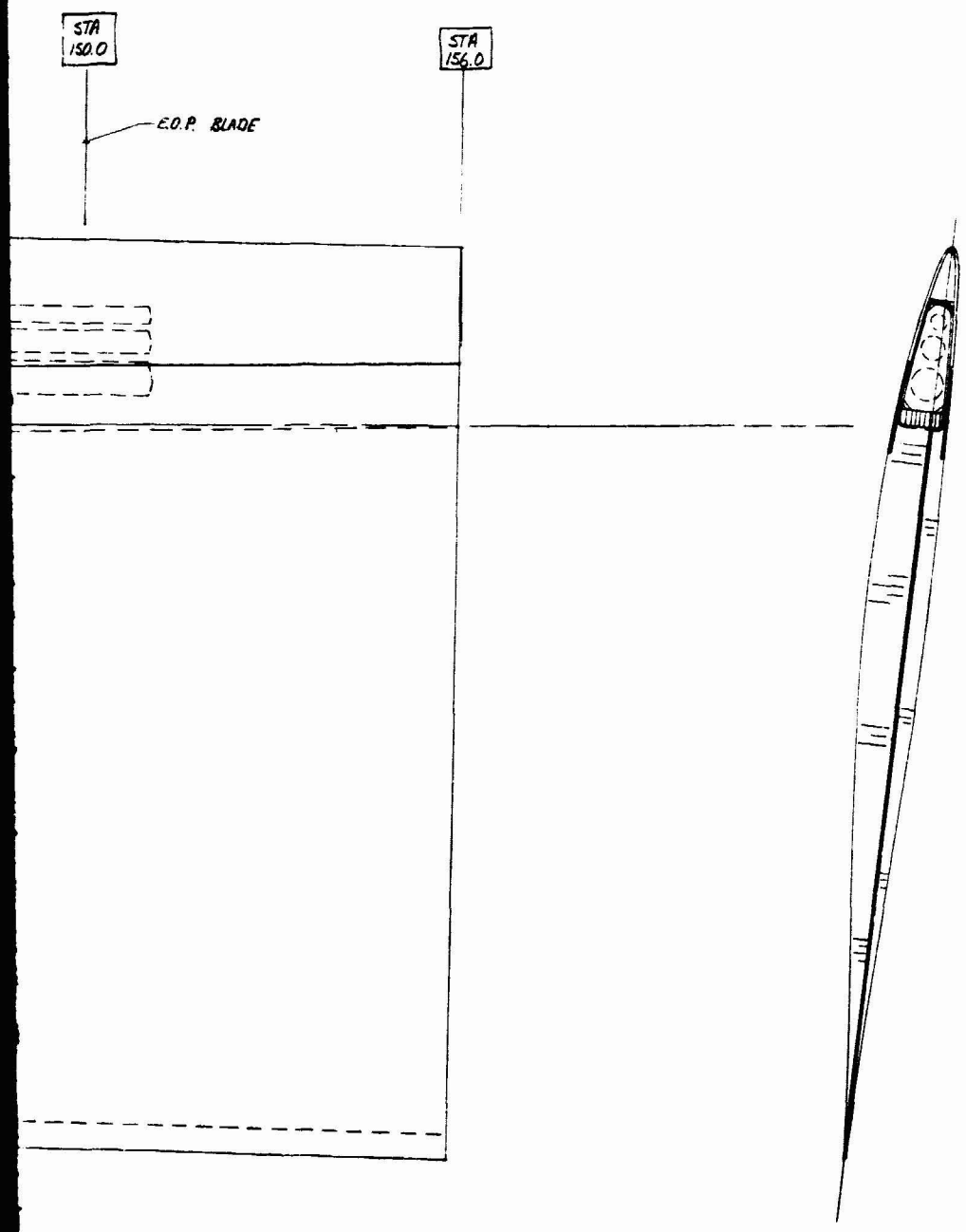




STOCK MATERIAL IS 17-7 PH ST. STL.

FOLDOUT FRAME 3

REPRODUCIBILITY OF THE ORIGINAL PAGE IS POOR.



NOTICE

THIS DATA IS PROPRIETARY TO BELL HELICOPTER AND ANY DISCLOSURE, REPRODUCTION OR USE OF THIS DATA FOR ANY PURPOSE IS FORBIDDEN WITHOUT WRITTEN AUTHORIZATION FROM BELL HELICOPTER COMPANY.

THIS DATA IS FURNISHED WITH DATA RIGHTS AS REQUIRED BY CONTRACT NO. NAS 2-5961

THIS DATA IS "RESTRICTED" UNDER UNITED STATES GOVERNMENT CONTRACT NO. _____ AND SHALL NOT BE EITHER RELEASED OUTSIDE THE U.S. GOVERNMENT OR USED, DUPLICATED, OR DISCLOSED IN WHOLE OR IN PART FOR MANUFACTURE OR PROCUREMENT, WITHOUT THE WRITTEN PERMISSION OF BELL HELICOPTER COMPANY, EXCEPT FOR:

(1) EMERGENCY REPAIR OR OVERHAUL WORK BY OR FOR THE GOVERNMENT WHERE THE ITEM OR PROCESS CONCERNED IS NOT OTHERWISE REASONABLY AVAILABLE TO ENABLE TIMELY PERFORMANCE OF THE WORK, OR

(2) A LICENSE OR A FOREIGN GOVERNMENT OR THE INTERNATIONAL MONETARY FUND PURSUANT TO AN APPLICABLE TREATY OR AGREEMENT, EXCEPT FOR THE RELEASE OR DISCLOSURE OF PROPRIETARY, OR COPYRIGHTED DATA SUBJECT TO THE FOREGOING RESTRICTIONS. THESE MARKINGS SHALL BE ERASED ON ANY REPRODUCTIONS MADE OF THESE DATA IN WHOLE OR IN PART.

DESIGN LAYOUT

TITLE	BLADE ASSEMBLY FOLDING PROPROTOR		
DESIGNED	JAY CARTER	DATE 2/24/70	SCALE FULL
DRAWN	D.E. Brannon	627-018-103	

EOLDOUT FRAME 4